



UNIVERSITÀ DEGLI STUDI DI MILANO
FACOLTÀ DI SCIENZE E TECNOLOGIE

Dipartimento di Chimica

Corso di Dottorato in Chimica - XXXV ciclo

New NCN-platinum(II) complexes with luminescent properties

Francesco Fagnani

R12748

Tutor: prof.ssa Claudia Dragonetti

Co-tutor: prof.ssa Alessia Colombo

Coordinatore del Corso di Dottorato: prof. Daniele Passarella

A.A. 2021/2022

CONTENTS

AIM OF THE THESIS.....	8
I - PHOTOLUMINESCENCE AND RELATED APPLICATIONS.....	9
1. Introduction to luminescence.....	9
1.1 Absorption.....	9
1.2 Photoluminescence.....	9
1.3 Fluorescence vs phosphorescence.....	11
1.4 Luminescence of transition metal complexes.....	11
2. OLEDs.....	12
2.1 Working mechanism.....	13
2.2 CIE coordinates.....	13
2.3 Transition metal complexes for OLEDs.....	14
2.3.1 Green emitters.....	15
2.3.2 Red emitters.....	16
2.3.3 Blue emitters.....	17
3. Bio-imaging.....	18
3.1 Transition metal complexes for bio-imaging.....	18
4. Photodynamic therapy.....	20
4.1 Transition metal complexes for PDT.....	22
II - NCN-Pt(II) COMPLEXES AND THEIR APPLICATIONS.....	24
1. 1,3-di(2-pyridyl)benzene ligand and related complexes.....	24
1.1 Complexes of nickel(II) and palladium(II).....	24
1.2 Platinum(II) complexes having an ancillary Cl ligand.....	26
1.3 Platinum(II) complexes having other ancillary ligands.....	31
1.3.1 Alkynes.....	31
1.3.2 Isocyanides.....	33
1.3.3 Thiolates and phenolates.....	34
1.3.4 Nitrogen-based ligands.....	35
1.3.5 Other types of ancillary ligands.....	36
2. Applications of NCN-Pt(II) complexes.....	37
2.1 NCN-Pt(II) complexes for OLEDs.....	37
2.2 NCN-Pt(II) complexes for bio-imaging.....	40
2.3 NCN-Pt(II) complexes for PDT.....	41

III – SYNTHESIS OF THE COMPLEXES.....	43
1. Synthesis of ligands L1-L7 and of complexes PtCl1-PtCl7.....	43
1.1 Synthesis of intermediate compounds I1-I6.....	44
1.1.1 Synthesis of I1-I4	44
1.1.2 Synthesis of I5.....	44
1.1.3 Synthesis of I6.....	44
1.2 Synthesis of ligands L1-L7.....	45
1.3 Synthesis of complexes PtCl1-PtCl7.....	45
2. Synthesis of complexes Pt1-Pt15	46
2.1 Aim of the tested ancillary ligands	46
2.2 Future possibilities.....	46
2.2.1 Isothiocyanate	47
2.2.2 Azide.....	47
2.3 Derivatives of PtCl1.....	48
2.4 Derivatives of PtCl2.....	49
2.5 Derivatives of PtCl6.....	50
2.6 Derivatives of PtCl7.....	51
3. Synthesis of ligands L8-L13 and of complexes PtCl8-PtCl13.....	52
3.1 Synthesis of intermediate compounds I7-I8	53
3.2 Synthesis of boronic esters B1-B5.....	53
3.2.1 Synthesis of B1-B4	53
3.2.2 Synthesis of B5.....	54
3.3 Synthesis of ligands L8-L13.....	54
3.3.1 Synthesis of ligands L8-L10	54
3.3.2 Synthesis of ligand L11.....	55
3.3.3 Synthesis of ligands L12-L13	55
3.4 Synthesis of complexes PtCl8-PtCl13.....	56
3.4.1 Synthesis of complexes PtCl8-PtCl10	56
3.4.2 Synthesis of complex PtCl11	56
3.4.3 Synthesis of complexes PtCl12-PtCl13	56
IV – CHARACTERIZATION OF THE COMPLEXES.....	57
1. General comments.....	57
1.1 UV-Vis absorption spectra and molar extinction coefficients.....	57
1.2 Excitation and emission measurements.....	57

1.3 Absolute Quantum Yield measurements	58
1.4 Lifetime measurements	60
2. Photophysical characterization of complexes PtCl1-PtCl7.....	60
2.1 UV-Vis absorption spectra of complexes PtCl3-PtCl5.....	60
2.2 Molar extinction coefficients of complexes PtCl1-PtCl7	62
3. Photophysical characterization of complexes Pt1-Pt15	63
3.1 UV-Vis absorption spectra of complexes Pt1-Pt15	63
3.2 Molar extinction coefficients of complexes Pt1-Pt15.....	71
3.3 Excitation and emission spectra of complexes Pt1-Pt15	73
3.4 Absolute Quantum Yields and lifetimes	80
3.5 Comparison with parent compounds PtCl1-PtCl2 and PtCl6-PtCl7.....	82
3.6 Solid state characterization of Pt1	84
3.7 Solid state characterization of Pt5.....	85
4. Photophysical characterization of complexes PtCl8-PtCl13.....	88
4.1 UV-Vis absorption spectra of complexes PtCl8-PtCl13.....	88
4.2 Molar extinction coefficients of complexes PtCl8-PtCl13	91
4.3 Excitation and emission spectra of complexes PtCl8, PtCl10, PtCl12 and PtCl13	92
4.4 Absolute Quantum Yields and lifetimes	94
4.5 Comparison with related compounds PtCl1, PtCl2 and PtCl6.....	95
5. Crystal structure of Pt1	96
6. OLEDs produced with the Pt(II) complexes	98
6.1 OLEDs produced with Pt1	98
6.2 OLED produced with Pt9.....	102
6.3 Comments about the prepared OLEDs.....	103
V – EXPERIMENTAL SECTION	104
1. General comments.....	104
1.1 Synthesis of I1.....	105
1.2 Synthesis of L1	106
1.3 Synthesis of PtCl1.....	107
1.4 Synthesis of Pt1.....	108
1.5 Synthesis of Pt2.....	109
1.6 Synthesis of Pt3.....	110
1.7 Synthesis of Pt4.....	111

1.8 Synthesis of Pt5.....	112
1.9 Synthesis of Pt6.....	113
1.10 Synthesis of I2.....	114
1.11 Synthesis of L2.....	115
1.12 Synthesis of PtCl2.....	116
1.13 Synthesis of Pt7.....	117
1.14 Synthesis of I3.....	118
1.15 Synthesis of L3.....	119
1.16 Synthesis of PtCl3.....	120
1.17 Synthesis of I4.....	121
1.18 Synthesis of L4.....	122
1.19 Synthesis of PtCl4.....	123
1.20 Synthesis of I5.....	124
1.21 Synthesis of L5.....	125
1.22 Synthesis of PtCl5.....	126
1.23 Synthesis of I6.....	127
1.24 Synthesis of L6.....	128
1.25 Synthesis of PtCl6.....	129
1.26 Synthesis of Pt8.....	130
1.27 Synthesis of Pt9.....	131
1.28 Synthesis of Pt10.....	132
1.29 Synthesis of Pt11.....	133
1.30 Synthesis of L7.....	134
1.31 Synthesis of PtCl7.....	135
1.32 Synthesis of Pt12.....	136
1.33 Synthesis of Pt13.....	137
1.34 Synthesis of Pt14.....	138
1.35 Synthesis of Pt15.....	139
1.36 Synthesis of I7.....	140
1.37 Synthesis of B1.....	141
1.38 Synthesis of L8.....	142
1.39 Synthesis of PtCl8.....	143
1.40 Synthesis of B2.....	144

1.41 Synthesis of B3.....	145
1.42 Synthesis of L9.....	146
1.43 Synthesis of PtCl9.....	147
1.44 Synthesis of B4.....	148
1.45 Synthesis of L10.....	149
1.46 Synthesis of PtCl10.....	150
1.47 Synthesis of B5.....	151
1.48 Synthesis of L11.....	152
1.49 Synthesis of PtCl11.....	153
1.50 Synthesis of I8.....	154
1.51 Synthesis of L12.....	155
1.52 Synthesis of PtCl12.....	156
1.53 Synthesis of L13.....	157
1.54 Synthesis of PtCl13.....	158
VI – CONCLUSIONS.....	159
VII – BIBLIOGRAPHY.....	161
APPENDIX.....	172
NMR spectra.....	173
Lifetime measurements.....	221

AIM OF THE THESIS

Luminescent complexes of transition metals are characterized by appealing features which make them interesting for different applications, with the possibility to play an important role in everyday life.

Among the wide variety of metals, ligands, coordination environments and oxidation states which these complexes can present, platinum(II) compounds are particularly important because of their remarkable photophysical properties due to the presence of the heavy metal atom; moreover, complexes characterized by a rigid terdentate ligand, such as a 1,3-di(2-pyridyl)benzene, show high phosphorescence Quantum Yield and an intense luminescence emission which can be tuned through the introduction of the proper substituents on the aromatic rings and with the appropriate choice of the ancillary ligands on the platinum center.

In this PhD project, different pathways were followed to explore the possibility to improve the mentioned properties: i) maintaining the typical scaffold of the NCN ligand and introducing new aromatic moieties (*e.g.* carbazole, pyrene, etc.) on the benzene ring; ii) starting from already known ligands and the corresponding Pt-Cl complexes but replacing the chloride with other anionic species such as thiolates and azides; iii) expanding the aromatic system of the terdentate ligand with the introduction of new substituents (2-thienyl, *p*-NPh₂-phenyl) on the pyridines.

As a result, almost thirty NCN-Pt(II) complexes were synthesized, and the majority of them was also fully characterized from the luminescence point of view. The possible applications of these compounds, as reported more in detail in the following chapters, range from the preparation of OLED devices to the testing in the field of cellular biology, both as dyes for bio-imaging and as sensitizers for anticancer therapies.

I - PHOTOLUMINESCENCE AND RELATED APPLICATIONS

1. Introduction to luminescence

The phenomenon of luminescence is the spontaneous emission of ultraviolet, visible or infrared light from an excited state of a molecule; differently from incandescence, light is not emitted as a consequence of an increase of temperature.

Several kinds of luminescence can be distinguished on the basis of the source of excitation:

- *Photoluminescence*, if excitation comes from light;
- *Electroluminescence*, if from current or electric field;
- *Triboluminescence*, in the case of mechanical energy;
- *Chemiluminescence* or *bioluminescence*, if excitation is caused by a chemical reaction.

1.1 Absorption

In order for a molecule to reach one of its possible excited states, at first light must be absorbed; the absorption of radiation is generally quantified by referring to the *transmittance* or to the *absorbance* of a sample. The transmittance (T) is defined as the ratio between the intensity of the transmitted and of the incident light:

$$T = \frac{I}{I_0}$$

where I and I_0 represent the transmitted and the incident light intensities, respectively.

By calculating the negative decimal logarithm of T , the absorbance (A) value is obtained:

$$A = -\log_{10} T$$

Absorbance and concentration of a solution are related through the *Lambert-Beer law*, stating a direct proportionality between them:

$$A = \epsilon cl$$

in which ϵ is the molar extinction coefficient (in $\text{cm}^{-1} \text{M}^{-1}$), c is the molar concentration of the sample, l is the optical path length (in cm). This law is obeyed only for dilute solutions, since at higher concentrations different optical phenomena (such as scattering) can occur, leading to a deviation from the linearity described by the Lambert-Beer relationship.

1.2 Photoluminescence

In the case of photoluminescence, a photon with proper energy interacts with a molecule A, promoting it from its fundamental state to an excited state, thus producing a new chemical species with different properties and reactivity. The excited state (indicated as *A) can lead a product (P) or can go back to the fundamental state, following many possible photophysical pathways, both radiative and non-radiative (**Figure 1**).

The population of the excited state is possible only if the energy of the incident photon equals the energetic gap between the two electronic states involved in the transition, according to Bohr's equation:

$$E_{\text{photon}} = h\nu = \Delta E_{\text{transition}} = E_f - E_i$$

E_f and E_i being the energies of the final and of the starting states, respectively.

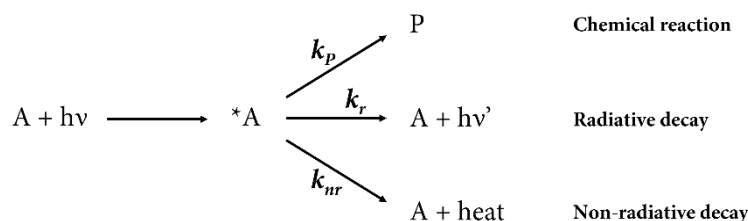


Figure 1. General scheme of the possible deactivation pathways for an excited molecule *A .

All processes leading to the decay from the excited state of a molecule compete with each other and can occur simultaneously; each of them is characterized by a kinetic constant k , from which the probability associated to a photophysical pathway can be obtained.

From the kinetic constants k_i it is possible to calculate the lifetime of an excited state, defined as the time required to reduce the number of molecules in the excited state to $1/e$ times the initial value (e is Neper's constant):

$$\tau({}^*A) = \frac{1}{k_p + k_r + k_{nr}} = \frac{1}{\sum k_j}$$

where p refers to a chemical reaction of the excited molecule, r to a radiative process, nr to a non-radiative process.

The probability n_i of each process i is expressed as follows:

$$n_i = \frac{k_i}{\sum k_j} = k_i \tau({}^*A)$$

In the case of processes involving light absorption, we can define a Quantum Yield (Φ_i):

$$\Phi_i = \frac{n_{\text{ex}, i}}{n_{\text{ph}, A}}$$

in which $n_{\text{ex}, i}$ is the number of excited molecules *A following that pathway and $n_{\text{ph}, A}$ is the number of photons absorbed by molecule A .

The possible deactivation processes are reported in the so-called Jablonski diagram, proposed by Aleksander Jablonski in 1933 [1] (**Figure 2**). Starting from the fundamental singlet state S_0 , the molecule absorbs radiation and higher excited states are populated; from the higher vibrational levels of an excited state (for example S_1), the excess energy can be lost through *vibrational relaxation* and the lower level of S_1 is therefore reached. The same level can also be reached by *internal conversion*, this being a radiationless transition from a higher to a lower excited state (in this case from S_2 to S_1). From S_1 , different processes can occur: if radiation is emitted, we observe the phenomenon of *fluorescence*, conserving the spin between the starting and final states of the molecule.

If a triplet excited state is close enough in energy, it can be populated through another type of radiationless transition, *i.e.* by *intersystem crossing*, involving a change in spin and consequently being formally forbidden. If emission of radiation occurs from a triplet state, the process is defined *phosphorescence*.

If the excited state lies at sufficiently low energy, the non-radiative decay can become favored, due to the so-called *energy gap law*. This law arises from the fact that the vibrational levels of the excited and fundamental states can be close enough to give an easy deactivation process not resulting in the emission of light.

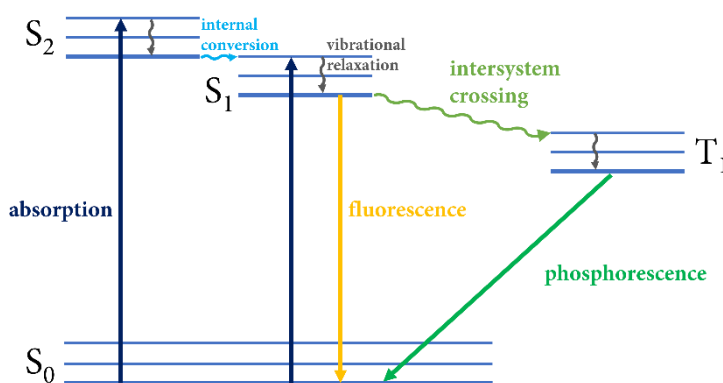


Figure 2. The Jablonski diagram, showing the possible photophysical processes.

1.3 Fluorescence vs phosphorescence

Fluorescence and phosphorescence are the two processes through which an excited state can decay in a radiative way. Fluorescence occurs between two states having the same spin multiplicity (singlet), so that $\Delta S=0$. Being an allowed transition, fluorescence is very rapid and has a timescale of 10^{-9} - 10^{-7} s; in most cases the emission comes from the lowest excited state, according to Kasha's rule [2]. This rule is generally obeyed and states that the excess energy provided upon excitation is dispersed until the lowest excited state is reached, having as a result that the emission is practically independent on the excitation energy and comes from the lowest excited state.

An important consequence of this process is the so-called Stokes shift: the emitted light has a lower energy with respect to the exciting radiation, since a part of the energy is always lost in vibrational and relaxational processes or is dispersed to the surrounding environment.

On the other hand, phosphorescence has a much wider timescale, from 10^{-3} to 10^2 s, with the emission of light able to continue even after the exciting source is removed. This can happen because the intersystem crossing (and so the triplet population) is formally forbidden, involving a change in spin multiplicity and a $\Delta S \neq 0$. Since the T_1 - S_0 transition is kinetically disfavored, the lifetime of the excited triplet state is long and so this radiative decay occurs for longer time.

1.4 Luminescence of transition metal complexes

Even if it is a formally forbidden mechanism, intersystem crossing can occur if the molecule presents a strong spin-orbit coupling, in general thanks to the presence of a heavy atom such a transition metal. In this case, an efficient population of the excited triplet state is likely, and phosphorescence becomes the favored process of radiative decay.

Nevertheless, since the emitting state is a long-living triplet and molecular oxygen has a fundamental triplet state, this molecule can very efficiently quench the emission of compounds such as Pt and Ir complexes. The energy transfer from the excited state of the complex to O₂ is so favored that the Φ_{lum} can have very low values, limiting the applications of such compounds. Therefore, to obtain meaningful luminescence spectra and valid Quantum Yield values in solution, measurements must be performed on deaerated solutions, in which this type of quenching is strongly limited or absent.

Metal complexes show important features making them very useful for different purposes:

- the emission from triplet states allows for a wide Stokes shift, hampering the phenomenon of self-absorption;
- the proper choice of ligands helps the tuning of the emission color;
- they have high stability towards photo- and chemical degradation;
- they have long-living excited states;
- they have a wide range of excited states, depending on the metal and on the ligands.

The most common states populated by excitation of a transition metal complex include MC (metal-centered), metal-to-ligand charge-transfer (MLCT) and ligand-to-ligand charge-transfer (LLCT) transitions. These states are reached depending on numerous factors: the metal center, the structure and the electronic levels of the ligands, the environment, the intramolecular and intermolecular interactions.

2. OLEDs

Organic Light-Emitting Diodes (OLEDs) are multi-layer electronic devices born as a development of the already widespread LEDs, based on inorganic semiconductors such as GaN or GaAs. Like their parent devices, OLEDs are able to emit light when a voltage is applied to the electrodes.

Compared to traditional LCD technology, this kind of displays are self-luminescent and so they do not require backlighting, thus allowing the devices to be thinner and lighter; consequently, only the needed pixels are lit up, leading to a decrease of the energy consumption ranging from 20 to 80%. As a further advantage, OLED displays are characterized by truer colors and wider viewing angles.

The first device based on organic thin films, and showing light emission with a voltage as low as 2.5 V, was published in 1987 by Tang and Val Slyke [3]; in their work, the organic component was sandwiched between an ITO anode and a cathode made up of a Mg:Ag alloy; it was obtained *via* vapor deposition and presented two different layers: the former containing the fluorescent Al(III) complex Alq₃ (structure in **Figure 3**), the latter being made of a diamine (**Figure 3**). The mentioned device emitted in the green region with a maximum at 550 nm, an External Quantum Efficiency (EQE) of 1% and a brightness of over 1000 cd m⁻¹.

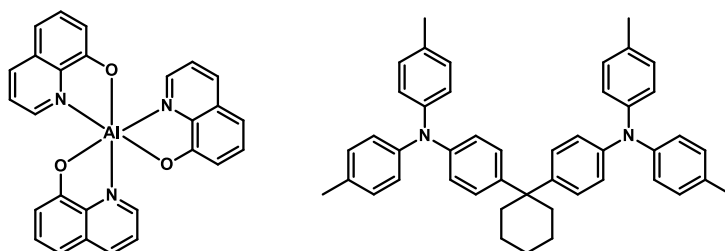


Figure 3. Structure of the Al(III) complex and of the diamine employed in 1987 by Tang and Van Slyke.

When dealing with the development of OLEDs, their history is generally divided into three “generations” [4], depending on the mechanism through which the emission of light occurs. The first generation is that of fluorescent OLEDs, the second refers to phosphorescent devices, while the third is related to OLEDs based on the phenomenon of the *thermally activated delayed fluorescence* (TADF). The different generations and working principles are discussed in detail in the following sections.

2.1 Working mechanism

The external components of an OLED are typically a transparent anode (generally ITO) and a metallic cathode (made of Mg-Ag, Li-Al, *etc.*); between them, two charge-carrying organic layers are present, namely an electron-transporting layer (ETL) and a hole-transporting layer (HTL), whose function is to allow the generated charges to migrate through the layers and to reach the central emissive layer (EL). Once reached the emissive layer (consisting in a dopant emissive compound dispersed in an organic host material), holes and electrons can recombine, generating neutral excited species called *excitons*; the radiative decay of the produced excitons leads to the emission of light from the device. **Figure 4** reports the simplified general structure of an OLED.

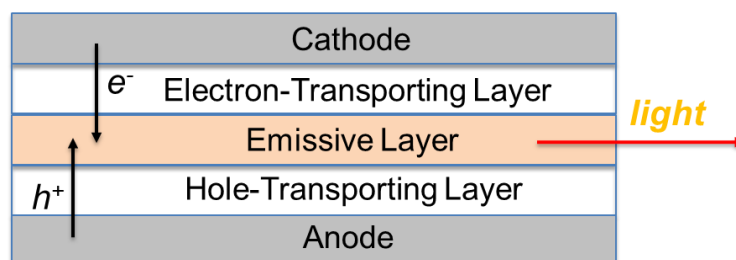


Figure 4. Simplified general structure of an OLED device.

A more detailed discussion of the theoretical efficiency of an OLED device and of the advantages arising from the use of transition metals will be presented in **Chapter I – Section 2.3**, while some representative examples of compounds used as HTL and/or ETL will be discussed in **Chapter II – Section 2.1**.

2.2 CIE coordinates

In order to have a precise description of the color of the light emitted by a device, the CIE chromaticity diagram (shown in **Figure 5**) is generally used. This diagram was adopted in 1931 [5] by the *Commission Internationale de l'Éclairage* (CIE) and finds application in identifying the exact color of a visible radiation.

Every point of the diagram corresponds to a color visible to humans and is represented by a couple of (x, y) coordinates; while pure white is identified by (0.33, 0.33), saturated colors are located on the border of the scheme and are defined by the corresponding wavelength values.

By referring to this standardized method of color identification and description, the comparison between the light produced by different devices becomes possible.

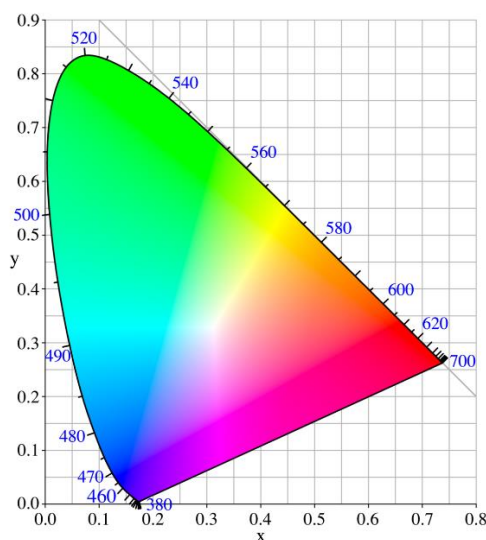


Figure 5. CIE chromaticity diagram.

2.3 Transition metal complexes for OLEDs

As previously mentioned in **Chapter I - Section 2.1**, the emission of light in an OLED occurs from the radiative decay of excitons, originating from the recombination of positive holes with electrons. Up to 1997, only fluorescent organic compounds were employed in the organic layers (first generation), thus limiting the theoretical maximum efficiency of the device, since the statistical singlet:triplet ratio for excitons is 25:75 and only the singlet ones could be exploited. If a compound having a heavy atom (such as a transition metal complex) is used as dopant in the emissive layer, also the triplet excitons can transfer their energy to the complex; in this way, the theoretical maximum efficiency is increased up to 100% and all produced excitons can be exploited if the dopant has an efficient and fast intersystem crossing populating its excited triplet states.

As already stated when presenting the basic notions about luminescence (**Chapter I - Sections 1.2 and 1.3**), emission from triplet excited states is formally forbidden by quantummechanic rules, but nevertheless the phenomenon of phosphorescence can occur due to the high spin-orbit coupling of the heavy metal atom. Consequently, the research in this field has led to the so-called *triplet-harvesting OLEDs* (*i.e.* phosphorescent OLEDs or PHOLEDs, second generation), based on the use of transition metal complexes [6–10].

The first examples of phosphorescent compounds employed in OLEDs were independently published in 1998 by Ma and Che et al. [11] and by Baldo and coworkers [12].

In the first case, the phosphorescent compound was an octahedral complex of Os(II) bearing a 4,4'-diphenyl-2,2'-bipyridine, two triphenylphosphines and two cyanides; in the second paper, the emitting complex was a Pt(II) octaethyl-porphyrin.

Figure 6 shows the structure of the mentioned molecules.

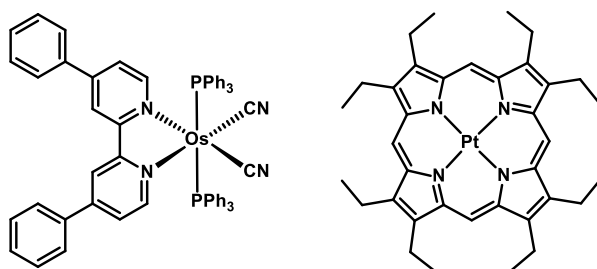


Figure 6. Structure of the emitting complexes employed in the first examples of 1998.

A different approach is that of the so-called third generation of OLEDs, based on the use of molecules whose excited singlet states can be populated through a *reverse intersystem crossing*, namely a process in which the energetic gap between the involved states is sufficiently small to allow for a thermal activation at room temperature. Therefore, a thermally activated delayed fluorescence (TADF) can occur, resulting in the theoretical use of 100% of the excitons, with a radiative emission arising from the singlet excited states.

When designing phosphorescent compounds with potential use for OLEDs, some parameters should be carefully taken into account:

- *emission wavelength* (λ_{em}). In order to have full-color devices, the emitted light should cover all the visible region, with the primary colors blue (450-470 nm), green (500-550 nm) and red (650-700 nm). While red and green emitters are diffused, blue emitters are much rarer, since they require a large energy gap, this increasing the probability of non-radiative decay from the excited state.
- *lifetimes* (τ). If the compound remains in the excited triplet state for a long period, the repopulation of the excited states becomes slow and the conversion of electricity into light becomes a limiting factor.
- *Quantum Yields* (QY). Ideally, at room temperature the phosphorescence QY should approach unity, to achieve a good efficiency of the device.

Up to now, a remarkable variety of phosphorescent compounds has been published and tested in OLEDs [4]; in the following sections, only few selected examples of Ir(III) and Pt(II) complexes will be presented: these compounds belong to the second generation and can be divided into different categories on the basis of the emission color they provide.

2.3.1 Green emitters

In 1999 Forrest and coworkers [13] tested the already known complex *fac*-[Ir(ppy)₃] (where ppy = 2-phenylpyridine) in a phosphorescent OLED device, resulting in a green emission with a peak at 510 nm and a EQE of 8%. Two years later, Thompson et al. [14] used the similar compound [Ir(ppy)₂(acac)], with a ppy substituted by an acetylacetonate (acac) bidentate ligand; by means of this replacement, the fabricated device presented an EQE of 12.3% and a $\lambda_{em} = 525$ nm.

A different dendrimer-based structure was at the basis of the work of 2006 by Wang et al. [15], in which the [Ir(C[^]N)₃] complex **G2** gave an EQE of 16.6% and brightness above 20000 cd m⁻², showing an emission at 528 nm.

Figure 7 shows the structure of the three Ir(III) green emitters.

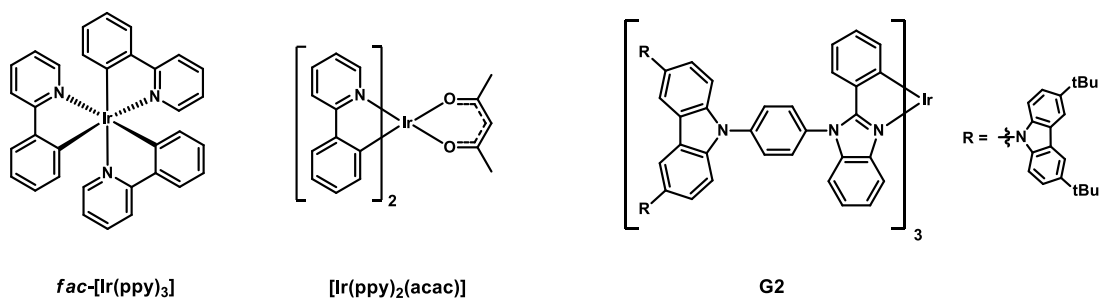


Figure 7. Examples of green Ir(III) emitters.

Moving to Pt(II), in 2007 Williams and coworkers reported the use of the cyclometalated $[Pt(Me-NCN)Cl]$, having a terdentate NCN ligand [16]; this dopant exhibited an EQE of 10% and an emission at 510 nm. In 2015, Che et al. published a series of CNN-based platinum(II) complexes [17], among whom the best compound was $[Pt(tBuPh-CNN-Qu)(CC-PhF_5)]$, providing an efficiency of 22.8% and a green emission with CIE coordinates (0.368, 0.598). These two complexes are shown in **Figure 8**.

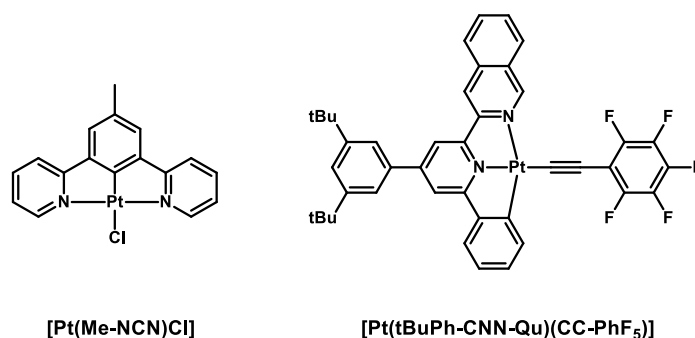


Figure 8. Examples of green Pt(II) emitters.

2.3.2 Red emitters

In the already discussed work of Thompson et al. of 2001 [14], the simple acetylacetonate ligand was tested for Ir(III) not only with the simple ppy but also together a C^N bidentate ligand being a pyridyl-substituted benzothiophene, giving complex $[Ir(btp)_2(acac)]$; the corresponding OLED emitted in the red region (616 nm) with a EQE of around 7%. In 2003, Hoshino and coworkers published complex $[Ir(piq)_3]$ [18] in which the iridium cation was bound to three 1-phenyl-isoquinolines; the device doped with this compound emitted at 620 nm and had a EQE of 12.3%.

Another Pt(II) complex with an NCN-terdentate ligand ($[Pt(COOMePh-NCN)Cl]$) was published by Williams et al. in 2008 [19]; in this case, the central benzene ring presented a 4-COOMe-phenyl moiety, and the corresponding OLED device exhibited a λ_{em} of 700 nm, with an EQE of 14.5%.

A different bidentate anionic ligand was chosen by Chi and coworkers, whose paper from 2016 [20] reported complex $[Pt(fprpz)_2]$, which emitted in the NIR (at 740 nm) and provided the produced OLED with an efficiency of 24%. **Figure 9** shows the structure of the discussed red emitters of iridium(III) and platinum(II).

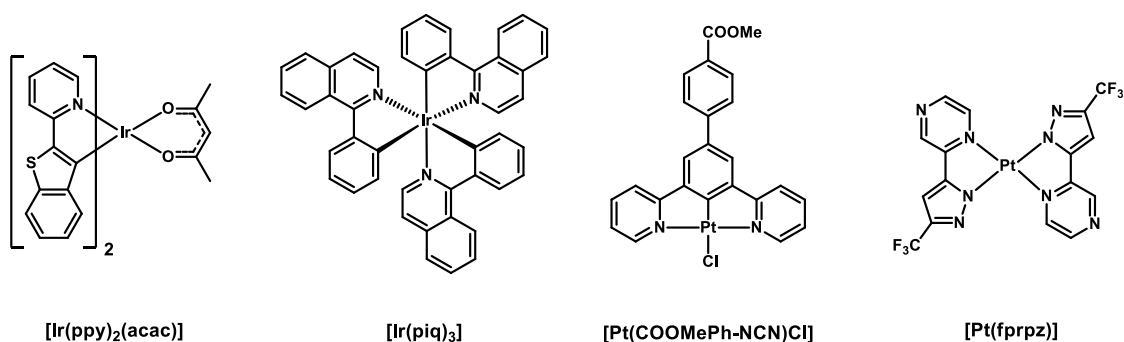


Figure 9. Examples of red Ir(III) and Pt(II) emitters.

2.3.3 Blue emitters

One of the first examples of blue-emitting phosphorescent OLEDs was published in 2001 by Forrest and coworkers [21] and consisted in the $[\text{Ir}(\text{dFppy})_2(\text{picolinate})]$ dopant, having two dFppy ligands (dFppy = 2-(2,4-difluorophenyl)pyridine) and a chelating picolinate; the obtained device had an efficiency of 5.7% and an emission at 475 nm (CIE coordinates: 0.16, 0.29). After ten years, Lee and Yook presented the very similar complex $[\text{Ir}(\text{CN-dFppy})_2(\text{picolinate})]$ [22], having the only difference of an additional CN substituent between the fluorine atoms on the phenyl ring; this structural modification led to an important increase in the triplet energy, reaching a value of 2.74 eV and a λ_{em} of 466 nm; the EQE of the fabricated device was 22.1%. An additional development of the same family was that of Kim and coworkers of 2019 [23]: besides the picolinate, in compound $[\text{Ir}(\text{dF-SiMe}_3\text{-ppy})_2(\text{picolinate})]$ the other ligands were two 2,3'-bipyridines bearing two fluorine atoms and a SiMe₃ moiety. The emission energy was furtherly increased with an emission around 445 nm and a remarkable OLED efficiency of 31.9%.

Considering the Pt(II) dopants, an important example was that of Li et al. of 2014 [24], in which a rigid tetradentate ligand in complex $[\text{Pt}(\text{ON1-tBu})]$ provided an efficiency of 24.8% and an emission maximum at 451 nm.

Figure 10 presents the structure of the discussed blue emitters based on iridium and platinum.

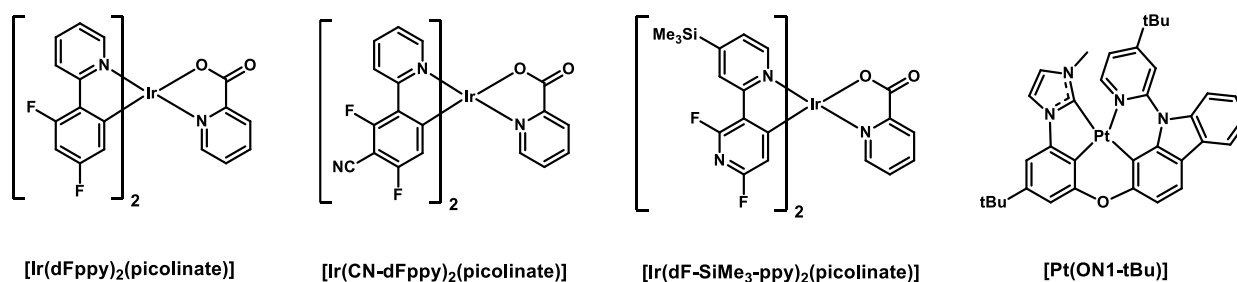


Figure 10. Examples of blue Ir(III) and Pt(II) emitters.

3. Bio-imaging

Luminescent compounds can be employed in the field of biological imaging, in which their features result useful in order to have a good vision inside cells and to study biologically relevant mechanisms occurring inside living organisms.

This technique consists in the injection of a solution containing the dye inside the cell or tissue under study, and in the consequent detection of the radiative emission arising from the excitation of the fluorophore, induced by an external source of radiation having the proper energy. In that way, also the pathway followed by the molecule inside the cell can be observed, as well as the parts of the cell in which the molecule accumulates due to the structure and to the lipophilic/lipophobic substituents it is characterized by.

On the basis of the charge, of the hydrophilicity, of the size and of the conjugation with biologically active molecules (biotin, estradiol, folates, peptides, *etc.*), the sensitizer can reach different parts of the cell or tissue under exam and can bind to the aimed organelles, cellular structures or nucleic acids, enabling their detection.

3.1 Transition metal complexes for bio-imaging

Complexes of transition metals are particularly appealing for bio-imaging, because of many features providing advantages for their use. For instance, the heavy metal atom brings about a long-living luminescence, some orders of magnitude longer than that of most classical organic fluorophores; this represents the main difference with purely organic dyes and allows for the removal of background fluorescence from biological compounds on the basis of time, thus improving the quality of the images: by measuring the emission at longer times, a differentiation of the emitting species can be easily obtained, together with a time-resolved mapping of cells or tissues [25–27].

As previously discussed, such transition metal complexes show a wide Stokes shift, allowing for the detection of the emitted light in a different spectral region with respect to the exciting radiation, hence limiting the overlap between the exciting and detected light. Moreover, these compounds can be excited using low-energy red or near-infrared light, able to deeply penetrate in tissues without interfering with their normal autofluorescence.

Moreover, other remarkable advantages are:

- a large emission color tunability, easily controlled by a suitable choice of the ligands;
- a larger range of excited states when compared to organic molecules;
- a high stability towards photo- and chemical degradation;
- convenient synthetic strategies involving the step-by-step introduction of substituents, whereas the modification of various fluorescent organic compounds can be more difficult.

Among the transition metals employed in the field of bio-imaging, a key role is played by Ru(II), Ir(III) and Pt(II), characterized by a d^6 or d^8 electronic configuration [28–33].

One of the most important transition metal compounds applied as dye for bio-imaging is $[\text{Ru}(\text{bipy})_3]^{2+}$ (bipy = 2,2'-bipyridine), in which the metal presents an octahedral coordination and a d^6 configuration. Thanks to the Ru(II) cation and the π -accepting ligands, the lowest excited state has a MLCT character, with a triplet emitting state having a lifetime of around 500 ns, two orders of magnitude longer than the commonly used fluorescent organic dyes.

Starting from 1990 [34], many examples of differently substituted $[\text{Ru}(\text{bipy})_2(\text{dppz})]^{2+}$ (dppz = dipyrido[3,2-a:2',3'-c]phenazine) complexes have been published and tested [35–37], replacing the simple bipy with differently substituted N^N ligands. The dppz chelating ligand is able to intercalate into DNA, causing a variation in the luminescence properties of the compounds and also providing cytotoxicity to the target cell.

The discussed Ru(II) complexes are shown in **Figure 11**.

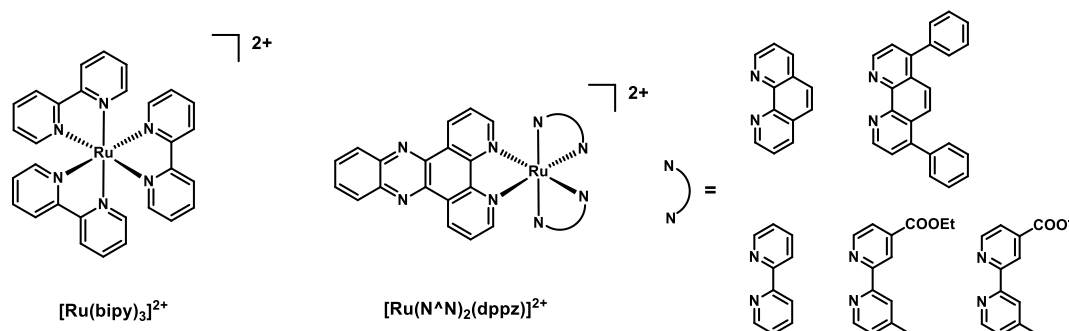


Figure 11. Structure of $[\text{Ru}(\text{bipy})_3]^{2+}$ and of $[\text{Ru}(\text{N}^{\wedge}\text{N})_2(\text{dppz})]^{2+}$ derivatives.

Moving to iridium(III) complexes, the first examples were reported in 2008 by Li et al. [38] and by Lo and coworkers [39], and consisted in cyclometalated compounds with general formula $[\text{Ir}(\text{C}^{\wedge}\text{N})_2(\text{N}^{\wedge}\text{N})][\text{PF}_6]$, with C^N and N^N bearing various substituents. **Figure 12** resumes some examples of such dyes.

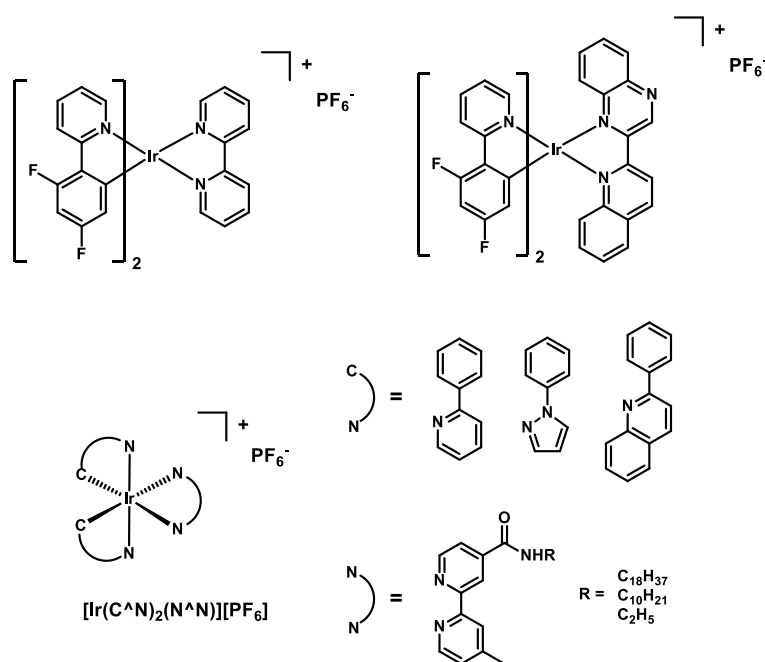


Figure 12. Structure of some examples of $[\text{Ir}(\text{C}^{\wedge}\text{N})_2(\text{N}^{\wedge}\text{N})][\text{PF}_6]$ complexes.

Important examples of platinum(II) complexes tested for bio-imaging were presented in 2005 by Che et al. [40] and by Nair and coworkers [41]. In the former paper, the Pt(II) cation was bound to a cyclometalating 2-(2-thienyl)pyridine and to an O^N-coordinating amino acid (glycine, phenylalanine and tryptophan); in the latter, the metal was chelated by a terdentate NNN bzimpy ligand (bzimpy = 2,6-bis(benzimidazo-2-yl)pyridine).

Figure 13 shows the structure of complexes Pt-AA and [Pt(bzimpy)Cl][PF₆].

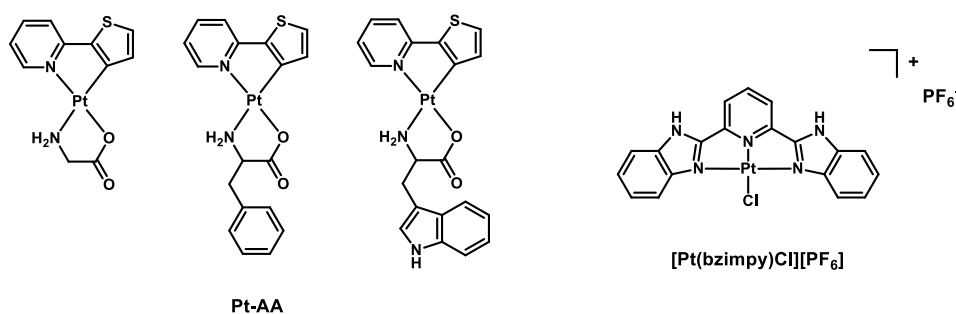


Figure 13. Structure of complexes Pt-AA and [Pt(bzimpy)Cl][PF₆].

More examples of Pt(II) compounds, based on NCN terdentate ligands, will be discussed in **Chapter II – Section 2.2**.

4. Photodynamic therapy

Organic or organometallic compounds able to be excited by an external source of radiation can be tested for anticancer treatments such as the so-called *photodynamic therapy* (PDT). In this kind of therapy, luminophores are activated by light and cause cytotoxic reactions leading to severe damages (or even the death) of the cells hit by the exciting radiation, without involving cells and tissues not exposed to the radiation [42–44].

In the presence of the activated photosensitizer, the excess energy of the excited state can be transferred to molecular oxygen, generating cytotoxic species through different processes: in this way, both *reactive oxygen species* (ROS, such as OH·, O₂⁻, H₂O₂, etc.; type I mechanism) or singlet oxygen (¹O₂, type II mechanism) can be produced. A third mechanism is independent on the presence of oxygen, since the excited state of the active compound directly reacts with cellular biomolecules, causing the death of the cell.

Figure 14 shows the mentioned mechanisms.

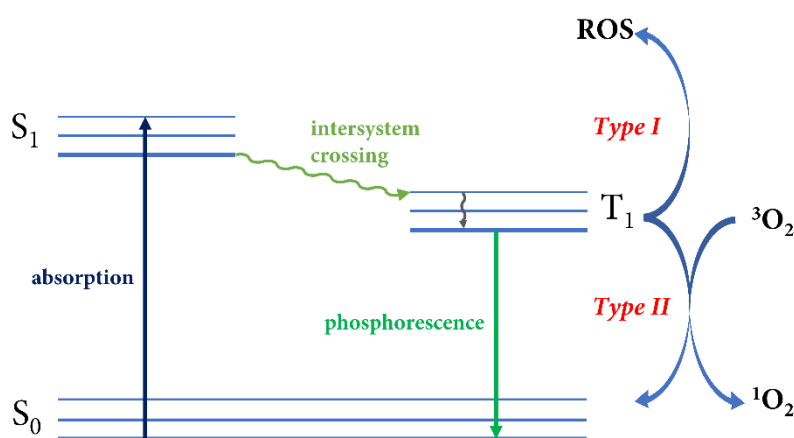


Figure 14. Photophysical mechanisms of PDT.

Up to now hundreds of compounds have been designed and tested for the purpose of photodynamic therapy [45, 46], even if only few have reached a clinical trial due to many difficulties arising from the requested characteristics these molecules should have. Ideally, the best compound for application in PDT should:

- have a high Quantum Yield of triplet formation;
- for mechanisms I and II, efficiently react with oxygen;
- not to be toxic in the absence of exciting radiation;
- be soluble and stable in the biological medium;
- accumulate preferentially in the target cells or tissues;
- absorb light at long wavelengths, at which photons can penetrate more in depth in tissues.

Up to now, the oligomeric porphyrin-based compound **Photofrin**[®] [47] (structure in **Figure 15**) is the only photosensitizer which has received approval for anticancer therapy all over the world; this molecule shares a common scaffold with an important quantity of the other compounds actually tested for PDT, namely a tetrapyrrolic core. This structure is at the basis of both their photophysical properties and drawbacks; the main problems associated with the use of such sensitizers are represented by their poor solubility in water, low photostability, quite difficult synthesis and low selectivity towards cancer.

A further step in this field is the coordination of this kind of molecules to different metals, such as tin, aluminum, or various transition metals (for them, see **Chapter I – Section 4.1**).

The tin- and aluminum-based sensitizers **Purlytin**[®] and **Photosens**[®], which have received approval for certain types of cancer or are undergoing clinical trials [48] are reported in **Figure 15**.

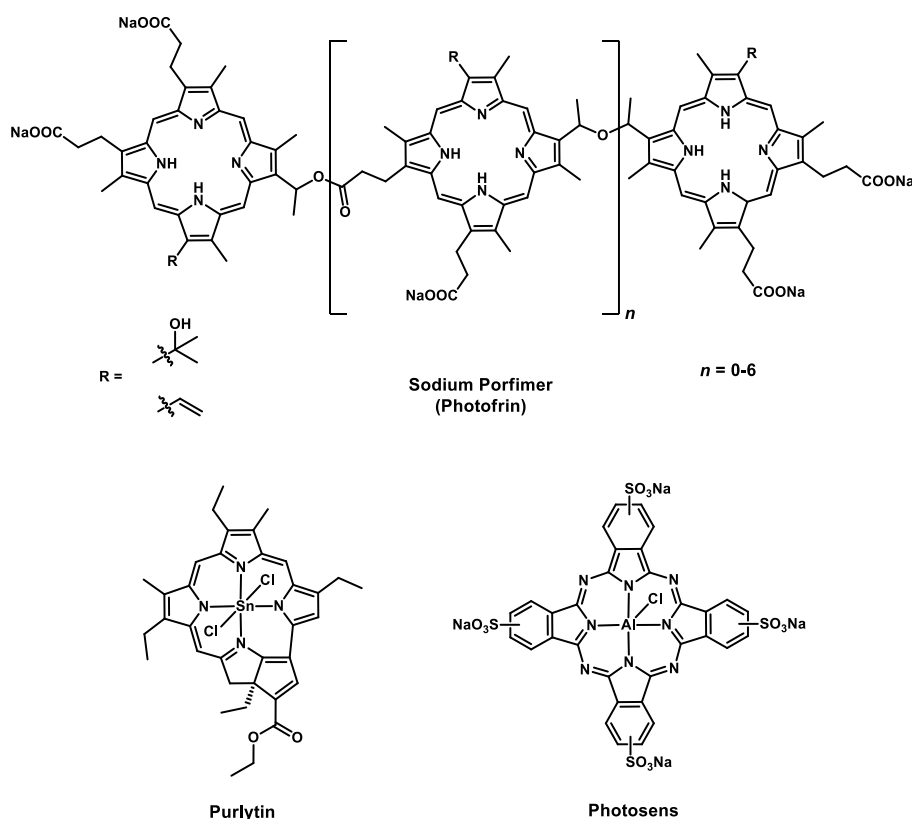


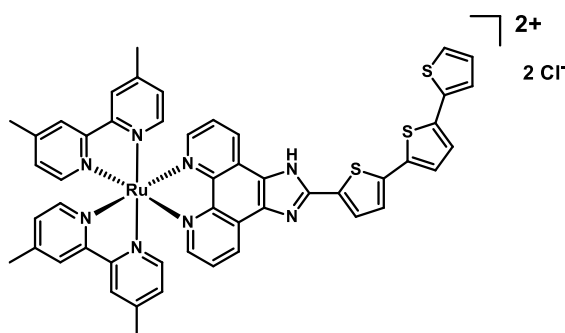
Figure 15. Structure of **Photofrin**[®], **Purlytin**[®] and **Photosens**[®].

The main challenges associated with the research of new candidates for PDT are related to different aspects of the therapy itself: the compound must accumulate only (or at least preferentially) in tumor cells, the local environment should be rich of oxygen, the exciting radiation must reach the sensitizer at the appropriate depth in cells and tissues, the water solubility should be increased in order to use lower doses of sensitizers (to reduce side effects in other parts of the body), the compound should have high molar extinction coefficient in the low-energy range (~700-900 nm).

4.1 Transition metal complexes for PDT

Considering transition metal compounds, a lot of effort has been devoted to test the different elements belonging to these periods of the periodic table [48, 49]; the most investigated family is certainly that of diimine complexes of ruthenium(II), based on parent compound $[\text{Ru}(\text{bipy})_3]^{2+}$. As already discussed in **Chapter I – Section 3.1** about bio-imaging, many dppz-based Ru(II) complexes have been checked up to now. These molecules show long-living triplet states and an efficient production of singlet oxygen; moreover, the careful design of the chelating ligands allows for a tuning of the possible excited states, and consequently of the associated photophysical properties.

The first Ru(II) photosensitizer to enter a human clinical trial was compound **TLD1433** (**Figure 16**), being a racemic Δ/Λ mixture of an octahedral complex presenting two 4,4'-dimethyl-bipyridines and a phenanthrolic ligand bearing a terthiophene moiety [50].



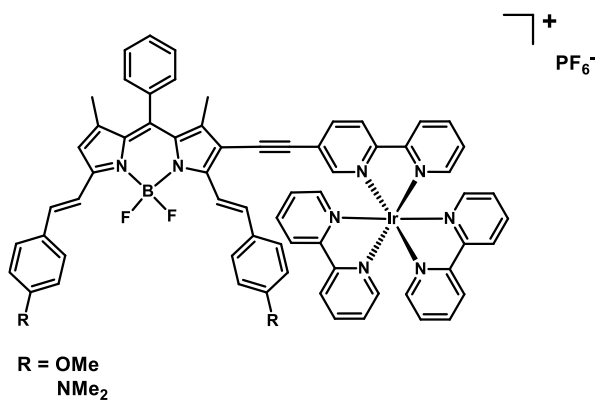
TLD1433

Figure 16. Structure of the Ru(II) sensitizer TLD1443.

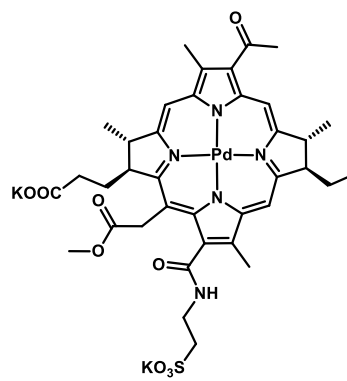
Moving to other groups of the periodic table, also compounds of Ir(III), Pd(II) and Pd(II) have been proposed as PDT sensitizers.

Figure 17 shows some representative examples of complexes based on such metals: the **Ir-BODIPY** family [51] consists of a BODIPY unit linked to the iridium-bearing core in which the metal is bound to three chelating bipyridines; a porphyrin-based ligand is employed with palladium in the case of **Padeliporfin** [52], while another metal-free porphyrinic core is used as linker for four Pt(II) moieties in the case of the **Pt-PORF** series [53].

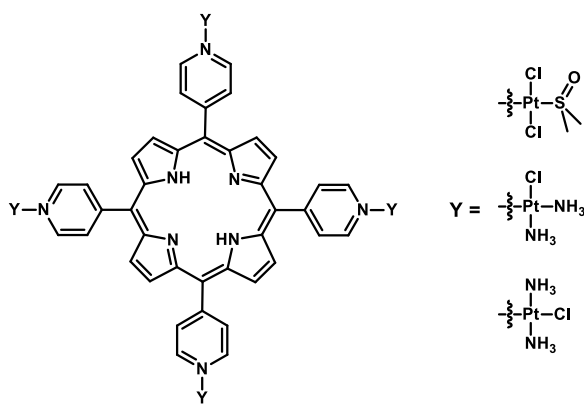
Other platinum(II) candidates for photodynamic therapy will be discussed in **Chapter II – Section 2.3**.



Ir-BODIPY



Padeliporfin, WST11



Pt-PORF

Figure 17. Structure of Ir-BODIPY, Padeliporfin and Pt-PORF.

II - NCN-Pt(II) COMPLEXES AND THEIR APPLICATIONS

1. 1,3-di(2-pyridyl)benzene ligand and related complexes

Complexes based on an NCN ligand like 1,3-di(2-pyridyl)benzene (dpby, structure in **Figure 18**) show numerous advantages and useful features, such as:

- they present a terdentate chelating ligand, binding the metal *via* two nitrogen atoms and a cyclometallating carbon atom, providing a rigid coordination environment around the metal center and hence reducing non-radiative decays from the excited states;
- the synthesis is quite simple, involving Pd-catalyzed cross-coupling reactions (such as Suzuki-Miyaura and/or Stille) for a step-by-step introduction of the pyridine rings and other moieties directly on the benzene core;
- the substituents on the aromatic rings (like the possible R_n shown in **Figure 18**) can be aimed at the tuning of important features of the complex, resulting in a wide range of possibilities: the solubility in water, the introduction of chirality through the presence of the suitable moieties, the increase or the reduction of aggregation and/or excimer formation on the basis of intramolecular interactions, the possibility to bind the molecule to other compounds, the sensing of particular species, *etc.*;
- the HOMO and the LUMO levels are located on different parts of the complex: the former on the benzene-platinum region and the latter on the pyridines, allowing for a fine modulation of the electronic features. In this way, the emissive properties of the complex can be modified by introducing the proper substituents on the ligand.

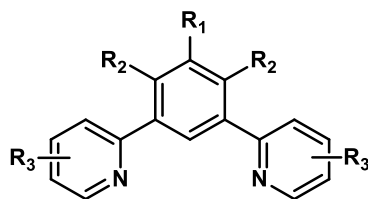


Figure 18. General structure of dpby, with the possible substitution positions on the rings.

This type of NCN ligand has been tested for many transition metals, belonging to different groups of the periodic table; in particular, complexes of Au(III) [54], Ru(II) [55, 56], Os(II)[57], Fe(III) [58], Ni(II), Pd(II) and Pt(II) have been synthesized.

Compounds of metals of group 10 will be discussed in detail in **Chapter II – Section 1.1** (for Ni and Pd) and **Chapter II – Sections 1.2-1.3** (for Pt).

1.1 Complexes of nickel(II) and palladium(II)

A first example of (dpby)Ni complex was published in 2020 by Yam and coworkers [59], with the aim of exploiting the useful features of this class of ligands by binding it to an earth-abundant metal such as nickel. The synthesis was performed by firstly binding the cyclometallating carbon atom to mercury(II) and then transmetallating to nickel, to give [Ni(dpby)Cl]. From this compound, by reacting it with carbazole in the presence of NaH, the corresponding carbazolyl complex was also obtained.

It was pointed out that the chlorido complex was not luminescent, neither at room temperature nor at 77 K, while the carbazolyl compound showed emissive properties also at rt.

In the same year Hörner and Klein [60] achieved the synthesis of this type of complexes without the need of transmetalation from the highly toxic Hg; the $[\text{Ni}(\text{dpyb})\text{X}]$ ($\text{X} = \text{Cl}, \text{Br}, \text{I}$) family of compounds was obtained from NiX_2 through a base-assisted C-H activation in a high-boiling nonpolar solvent such as *p*-xylene.

The synthetic pathways reported by the two papers are shown in **Figure 19**.

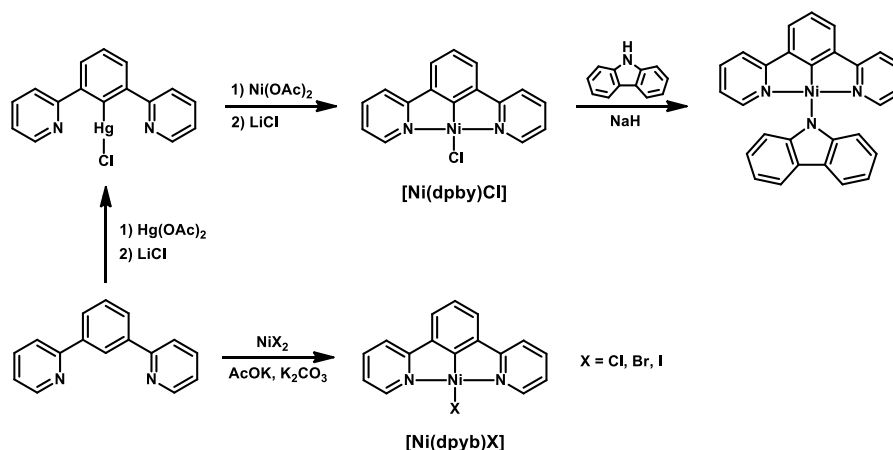


Figure 19. The synthetic pathways followed by Yam and by Klein to obtain the (dpyb)Ni complexes.

Concerning the homologous Pd complexes, a first attempt was made by Cardenas et al. in 1999 [61], by testing the same procedure already known for the obtaining of the similar platinum(II) compound, *i.e.* by using a salt of the metal and refluxing the reaction mixture in glacial AcOH. As a result, only dimers were obtained: in the case of $\text{Pd}(\text{OAc})_2$, the terdentate ligand behaved as a simple 2-phenylpyridine, cyclometallating with the carbon atoms in positions 4 and 6 of the benzene ring and having bridging acetates connecting two ligand molecules. The use of Li_2PdCl_4 as a source of the metal did not result in cyclometallation, but in a dimer with the NCN ligand binding only through the nitrogen atoms.

The desired complex with the ligand binding *via* the carbon atom in position 2 was synthesized only in 2005 by Soro and coworkers [62], by obtaining at first the Hg-Cl compound, then transmetalating with $\text{Pd}(\text{OAc})_2$ and finally adding the lithium salt of the desired halide (the same procedure at the basis of Yam's work of 2020, previously discussed). The mentioned syntheses are shown in **Figure 20**.

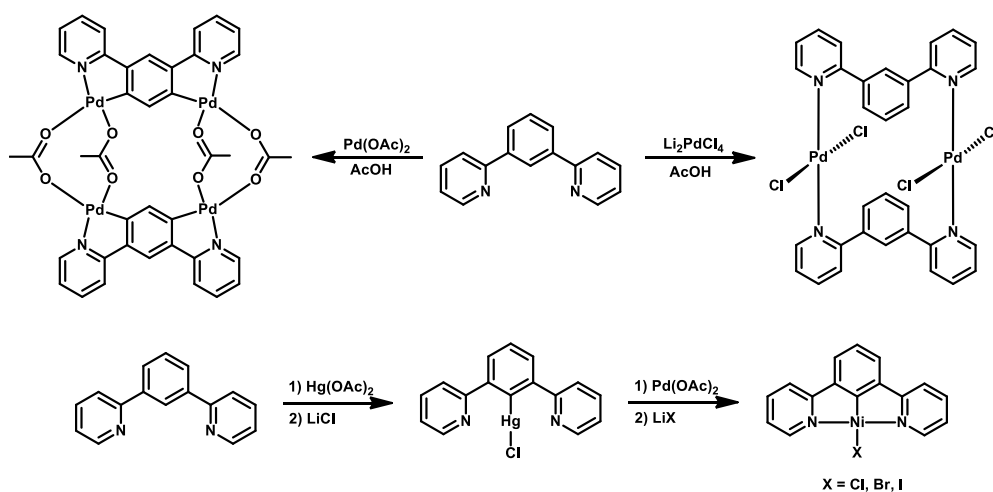


Figure 20. The synthetic strategies reported by Cardenas and Soro.

1.2 Platinum(II) complexes having an ancillary Cl ligand

Besides the already discussed paper of Cardenas of 1999 [61], being the first to report the synthesis of simple [Pt(dpyb)Cl] (**1**), a pioneering article was published in 2003 by Williams and Weinstein [63]. In this work, other two ligands of the same family were synthesized, having a -Me (**2**) and a -COOMe (**3**) substituent in position 5 on the benzene ring; the corresponding complexes were obtained by refluxing the ligand and K₂PtCl₄ in acetic acid or acetonitrile. In the following years, a very wide range of aromatic substituents were tested on the benzene ring, starting from the important works of Williams et al. of 2005 [64] and 2009 [65]; the structure of the new NCN-based complexes **4-15** is reported in **Figure 21**, together with compounds **1-3**. The introduction of differently substituted aryl or heteroaryl groups was meant to explore their influence on the luminescence properties of the complexes, and in fact the emission maxima of the compounds was found to be dependent on the effect of the substituent on the HOMO of the molecule. In the case of **12** and **15**, the azacrown and benzo-18-crown-6 moieties were used to observe the change in luminescence in the presence of different cations of group I and II.

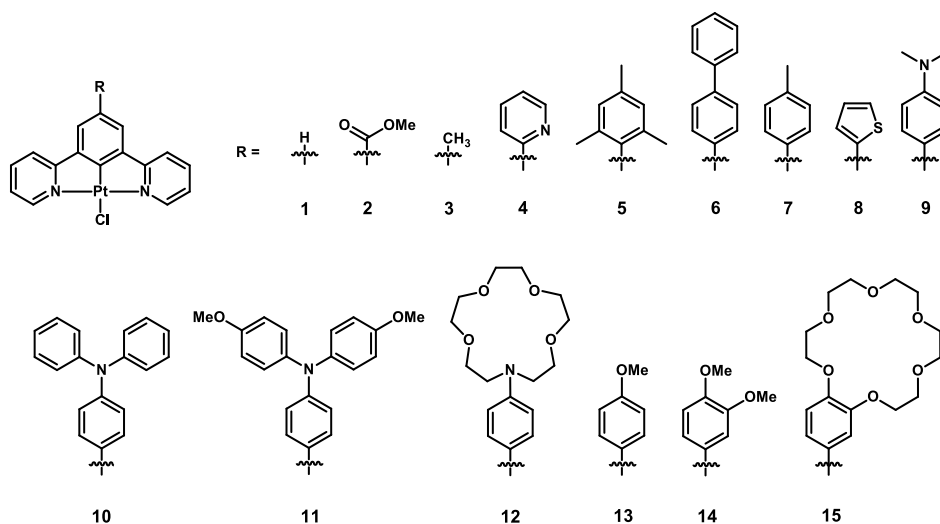


Figure 21. Structure of compounds **1-15**.

In 2009 Cocchi, Kalinowski and coworkers published a paper [66] reporting the first complexes (**16-18**) bearing fluorine atoms on the benzene ring, a scaffold which will give inspiration for other works in the following years, such as that of Cocchi and Williams of 2012 (complex **19**, [67]), that of Li et al. of 2010 (compounds **20-24**, [68]), the paper of Roberto and Williams of 2011 (**25-27**, [69]) and the article by Kozhevnikov and Bruce in 2014 (**28-29**, [70]).

The main feature shared by the majority of the presented Pt(II) complexes is the presence of fluorine atoms (or other electron-withdrawing groups like -CF₃) on the terdentate ligand, aiming at the understanding of the effect exerted by these moieties on the position of the HOMO and the LUMO levels of the compounds, and consequently on the emissive properties of the molecule.

The structure of compounds **16-29** is shown in **Figure 22**.

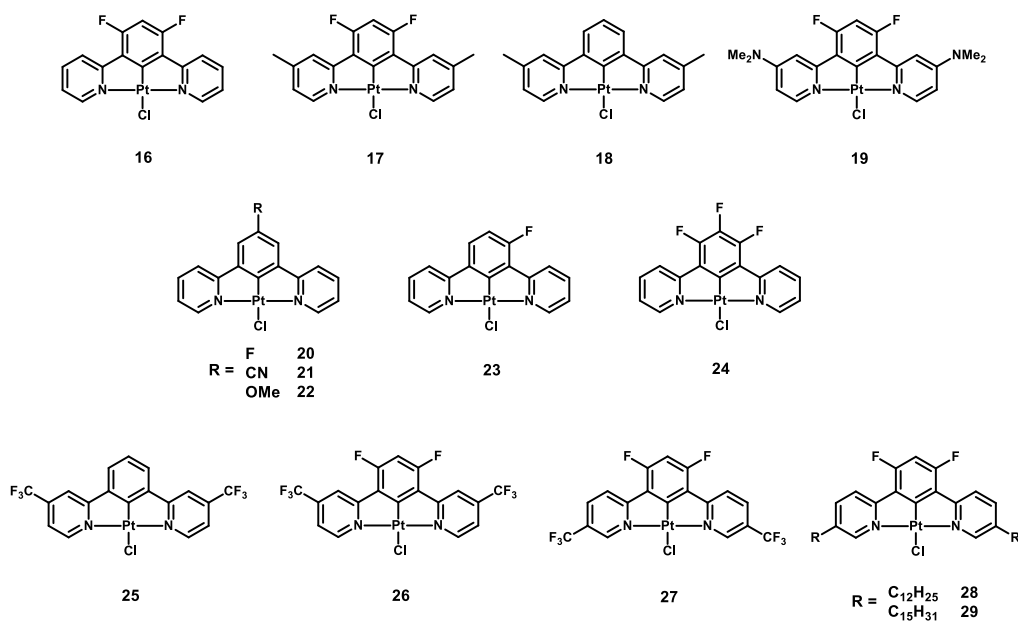


Figure 22. Structure of compounds 16-29.

In 2014 Roberto, Cocchi and Williams published [71] the first two Pt(II) complexes having an NCN ligand with an alkynyl (**30**) or alkenyl (**31**) spacer between the cyclometallating benzene ring and a triphenylamine substituent; this scaffold was employed also in the works of Fantacci and Roberto of 2017 [72] for compounds **32** and **33**, and in the paper of Colombo, Guerchais and Fantacci [73] of 2018 (complex **34**). In this way, a simple phenyl, a pyrene and a terthiophene were introduced as -R substituent on the central ring of the ligand.

A similar moiety, but with a guaiazulene group (compound **40**), was present in the article of Colombo and Fantacci of 2019 [74], together with other five complexes having a 2-thienyl directly bound to the benzene ring: complexes **35-39** bear respectively a methyl, a hexyl-thiophene, a triphenylamine, a *p*-CN-phenyl and a pyrene in position 5 of the mentioned thiophene ring. Furthermore, a Mes₂B-substituted complex (**41**) was presented by Kang and Wang in 2012 [75], to be tested for the production of OLED devices together with other Pt(II) complexes to explore the effect of the boron-based group on the emission properties. All discussed complexes are shown in **Figure 23**.

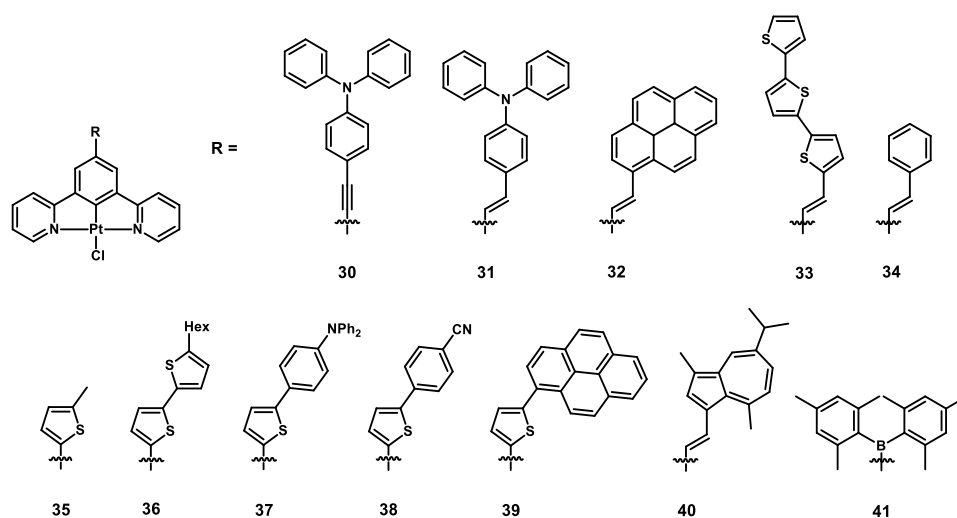


Figure 23. Structure of compounds 30-41.

In 2014 an NCN platinum(II) complex bearing a $-\text{CH}_2\text{NH}_3\text{Cl}$ chain (**42**) was published by Botchway, Haycock, Williams and Weinstein [76], and was employed as water-soluble probe in cellular bio-imaging studies. A similar purpose was presented in the paper by Dragonetti, Mauro and De Cola of 2015 [77], in which the complexes (**43** and **44**) had two hydrophilic chains with different length, and in that of Sarli of 2017 [78], in which compounds **2**, **42**, **45** and **46** were tested in studies about their efficacy in photodynamic treatment of cancer. In particular, in complex **45** the NCN scaffold was linked to oligopeptide c(RGDyK), whose function was to guide the compound to the targeted cancer cells.

Figure 24 shows the structure of compounds **42-46**.

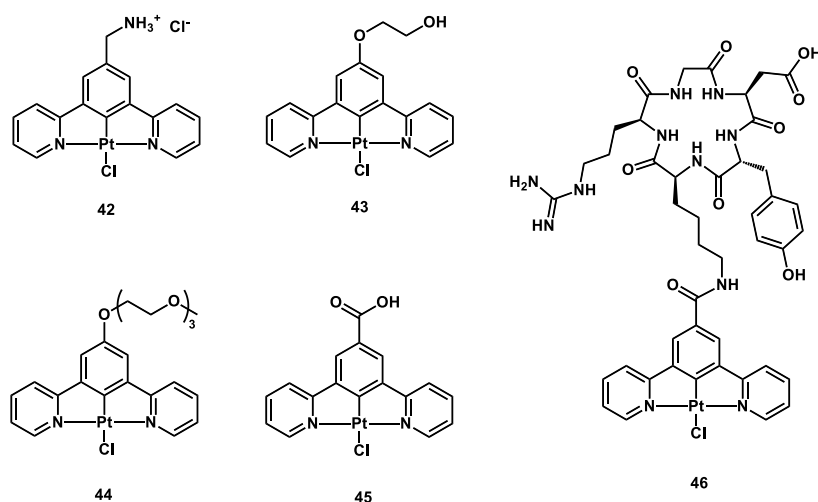


Figure 24. Structure of compounds **42-46**.

In the field of non-linear optics (NLO), NCN-Pt(II) complexes have attracted remarkable interest in the past years and new compounds have been designed for this purpose; for example the two new complexes **47** and **48**, bearing a strongly electron-withdrawing group and presenting a “push-pull” structure, were published by Odobel and coworkers in 2009 [79].

Moreover, in 2018 Dragonetti, Jacquemin and Boixel reported other two compounds [80] in which a dithienylethene (DTE) moiety was bound to the NCN scaffold in different ways: directly in position 5 of the benzene ring in the case of complex **49**, and *via* a $-\text{O}-\text{CH}_2\text{CH}_2-\text{O}-\text{C}_6\text{H}_4-$ linker for **50**.

The DTE group is known for the ability of switching its structure from the open to the closed form depending on the applied light; this feature causes an important variation of the NLO properties of the compounds.

Complexes **47-50** are presented in **Figure 25**.

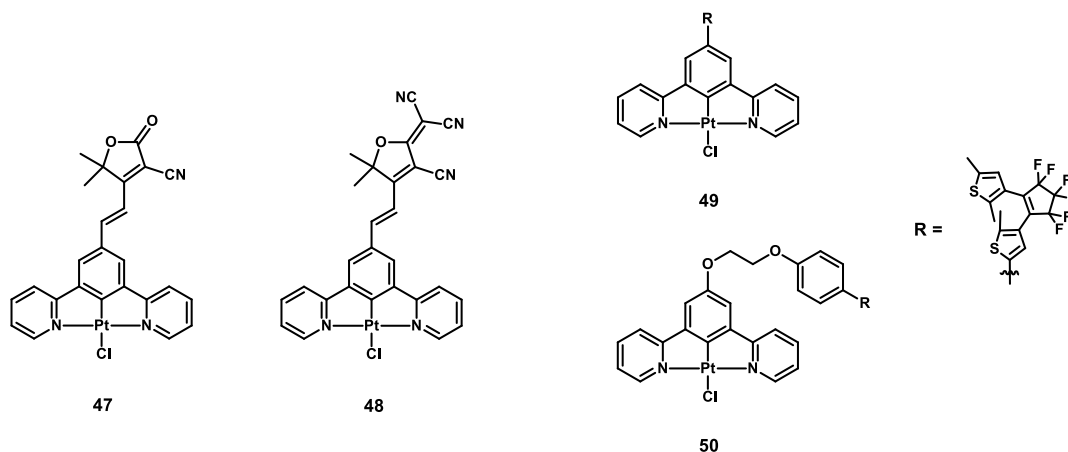


Figure 25. Structure of compounds 47-50.

A particular substituent meant to hamper the π -stacking between complex molecules, and consequently to improve their photoluminescence properties, is the pentaptycene, *i.e.* a rigid H-shaped scaffold introduced in compound **51** [81] by linking it to the NCN core through a C-C triple bond, also bearing an octyloxy chain. In that way, the resulting molecule showed both mechanochromism and vapochromism, with a switchable emission from the excimeric to the monomeric form.

A further development of this strategy was published by Yang and coworkers in 2020 [82], by adding a *-t*Bu group in position 4 of the pyridine rings (compound **52**) to introduce the proper steric hindrance on the ligand, able to increase the luminescence performance of the compound. Together with the new complex **52**, also a reference compound **53** was presented, being a simple NCN-PtCl with the mentioned *terz*-butyl groups.

A different aim was at the basis of the work of Takata and coworkers of 2020 [83], who published two complexes tested as active catalysts in the hydrosilylation reaction; while complex **54** had an open structure, with a 4-OMe-phenyl ring in α position on each pyridine, in **55** the corresponding oxygen atoms were connected by a triethylene glycol chain, thus obtaining a macrocycle.

Figure 26 reports the structure of complexes **51-55**.

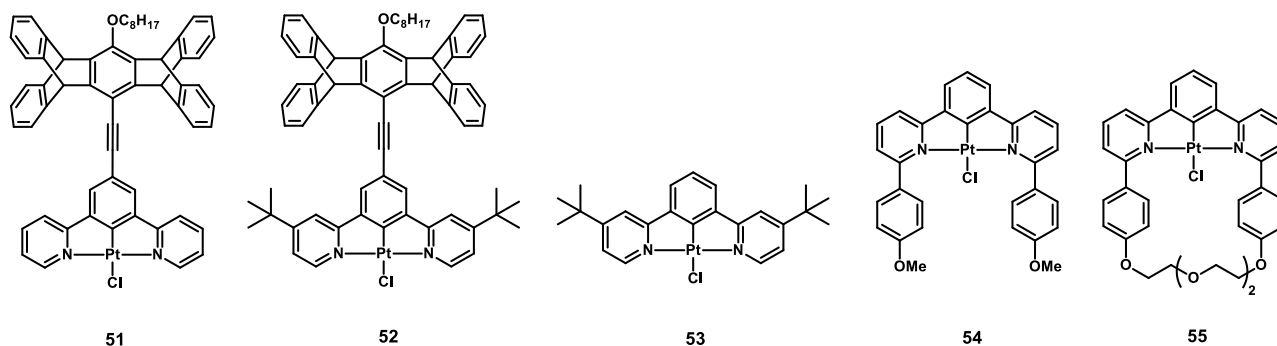


Figure 26. Structure of compounds 51-55.

Besides the monomeric compounds discussed up to now, some dimeric species were synthesized by choosing the proper manner to connect two NCN-PtCl units. Taking inspiration from the paper of Tanaka and coworkers of 2004 [84], in 2008 Williams et al. [85] employed a xanthene scaffold to obtain a ligand (and the related complexes **56-57**) in which two 1,3-di(2-pyridyl)benzenes lied parallel in a face-to-face manner. The short distance between the two metal centers allowed for the formation of intramolecular excimers, having as a result the shift of the emission maximum to the deep red (690 nm). By varying the reaction time, complex **56** or **57** was preferentially obtained, since the introduction of the second Pt atom required much longer time (11 vs 3 days).

A similar monometallic complex was published in 2010 by Chan and coworkers [86]: the same xanthene core was used to obtain an amino acid-sensitive compound having the NCN-PtCl moiety parallel to a $-C_6H_4-COOR$ group (R = H for **58** and CH_3 for **59**). By testing them with numerous amino acids, complex **58** was found to be effective in the preferential binding of cysteine to the Pt center, also exploiting the stabilizing interaction between the carboxylic group of the complex and the amine moiety of the amino acid.

In 2017 a dimer (**60**) was obtained by Zhong et al. [87] by using a *N,N*-dimethyl urea as bridging unit between two di(pyridyl)benzene scaffolds. In that way, the authors synthesized a U-shaped compound, whose crystal structure and photophysical properties were explored in deep.

In the work of Jacquemin and Guerchais of 2018 [88], another dimeric structure was obtained *via* a tetraethylene glycol chain connecting the NCN-PtCl moieties from positions 5 of the benzene rings. Interestingly, compound **61** showed the ability to self-associate with both an intra- and an intermolecular arrangement. Moreover, complex **62** was synthesized and studied as a reference for luminescence measurements and DFT calculations.

Figure 27 presents compounds **56-62**.

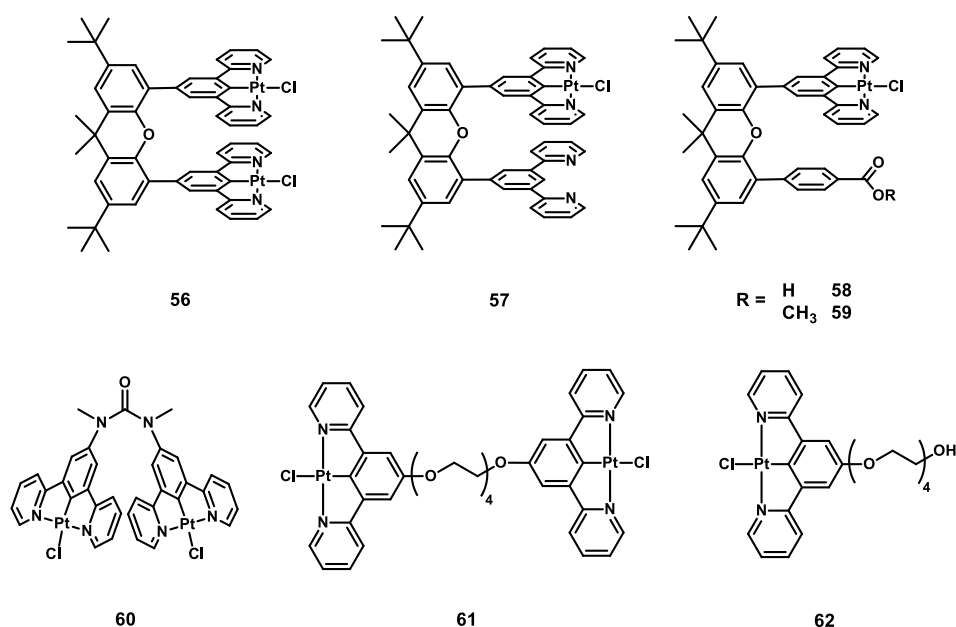


Figure 27. Structure of compounds **56-62**.

1.3 Platinum(II) complexes having other ancillary ligands

Different species have been tested as ancillary ligand on the Pt(II) center, by replacing the chloride with acetylides, isocyanides, phenolates, thiolates, azides, isothiocyanates, *etc.* The following sections discuss the numerous complexes obtained through the substitution of the -Cl, presenting the obtained Pt(II) compounds on the basis of the nature of the new ancillary ligand.

1.3.1 Alkynes

In the last paper discussed in the previous section [88], also a dimeric bimetallic compound was synthesized and studied, namely complex **63** (Figure 28). In this case, a bis(alkynyl) ligand with a glycol chain linking two phenylacetylenes was bound to both Pt(II) atoms, giving a structure able to form excimers in a very efficient manner through intramolecular interactions.

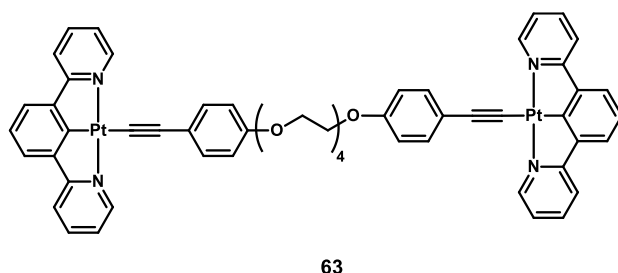


Figure 28. Structure of compound 63.

Another example was reported in the already mentioned work of Odobel of 2009 [79], by reacting compound **47** with 4-NHex₂-phenylacetylene, to give complex **64**. Similarly in 2012 Roberto, Cocchi and Williams [89] synthesized two complexes having a 3,5-difluorophenylacetylene ligand on the metal and a methyl or mesityl substituent on the benzene (compounds **65** and **66**, respectively).

Figure 29 shows the discussed compounds.

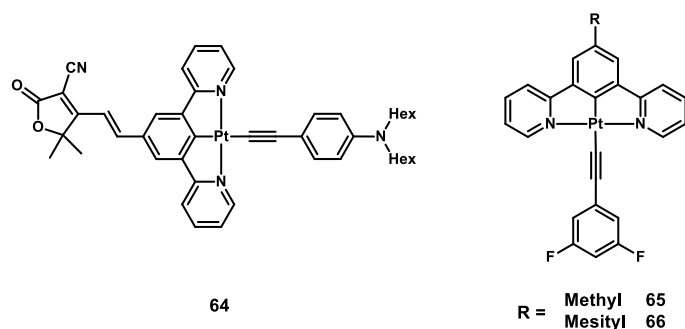


Figure 29. Structure of compounds 64-66.

In their papers of 2017 [90] and 2020 [91] Yang et al. had shown not only compounds **51** and **52**, but also the alkynyl-substituted analogues **67** and **69**, together with reference compound **68**. With these molecules the authors aimed at the study of the effect of different grades of steric hindrance, provided by the presence of the big pentiptycene moiety, but also by the *t*Bu groups on the NCN-pyridines. In particular, complex **67** had pentiptycene substituents both on the terdentate ligand and on the Pt(II), in both cases linked by a C-C triple bond.

The structure of complexes **67-69** is reported in **Figure 30**.

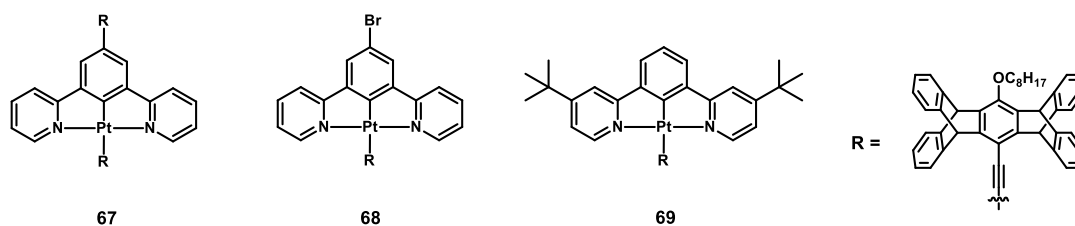


Figure 30. Structure of compounds **67-69**.

In 2019 Li, Yam and coworkers [92] proposed some new Pt(II) complexes to be tested as building blocks for molecular motion. In fact, compounds **70-72** represented a “molecular hinge” with a diyne axis connecting two NCN-Pt structures: upon excitation under the proper radiation, they observed a motion around the axis, which could be monitored through changes in the phosphorescence properties of the compound.

The mentioned switch between an open and a closed form was an important development towards future application in the field of molecular machines; as reference compounds, alkynyl-based complexes **73-75** were also obtained and studied.

Figure 31 presents the structure of complexes **70-75**.

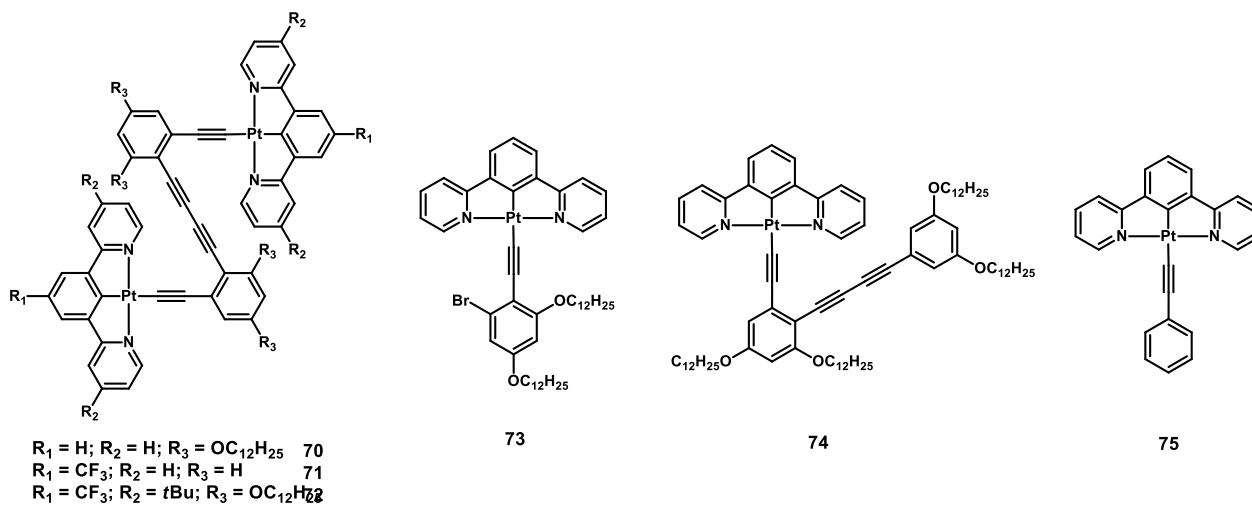


Figure 31. Structure of compounds **70-75**.

Also in 2021 Yam and Li published a paper [93] dealing with alkynyl NCN-Pt(II) complexes, this time having a terdentate ligand bearing two methyl groups on the central benzene ring and a 4-R-phenylacetylene on the metal, with R being a formyl in the case of **76** and different imines in compounds **77-80**. In particular, complexes **79** and **80** presented a chiral moiety, *i.e.* a methyl-benzylamine.

All mentioned compounds are shown in **Figure 32**.

Interestingly, the S and the R enantiomeric complexes did not have the same solid-state structure: the former (**79**) formed nanospheres, while the latter (**80**) leaf-like lamellae; in that way, the chirality of the substituent was transferred to the whole complex and exerted a remarkable influence on the luminescence, on the packing and on chiroptical properties of the synthesized compounds.

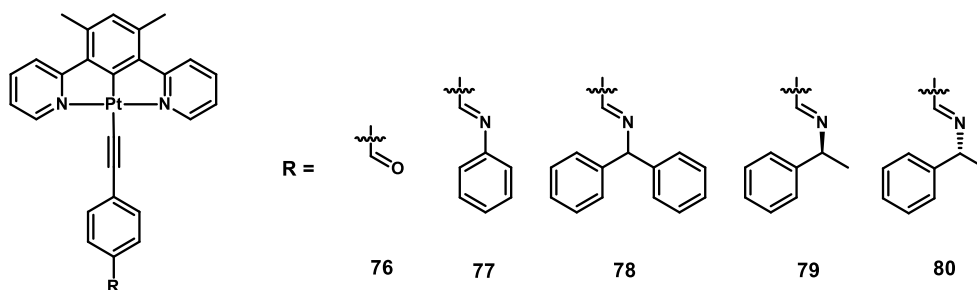


Figure 32. Structure of compounds 76-80.

1.3.2 Isocyanides

A neutral species which can be bound to the platinum center, resulting in cationic complexes, is the isocyanide. The first paper to deal with this monodentate ligand was that of Che and coworkers of 2013 [94], in which the compounds differed on the basis of the substituent on the chelating ligand, being a simple -H for **81**, a -CF₃ for **82** and a -CH₃ in **83**; in all cases the ancillary ligand was a 2,6-dimethylphenyl isocyanide and the counterion a hexafluorophosphate.

Later, the same ancillary ligand was employed by Kuwabara and Kanbara in their works of 2017 [95] and 2018 [96], even if together with a much more substituted NCN ligand having a benzenamide on the two pyridines, each of them bearing dodecyloxy chains. The counteranions were a B(C₆F₄)₄⁻, a Cl⁻ and a PF₆⁻ for **84**, **85** and **86**, respectively. Thanks to the structure of the ligands and to the chosen anions, different emission colors of the complexes could be achieved through molecular interactions, hydrogen bonding and solvophobic effects, ranging from blue to yellow to orange.

The structure of complexes **81-86** is shown in Figure 33.

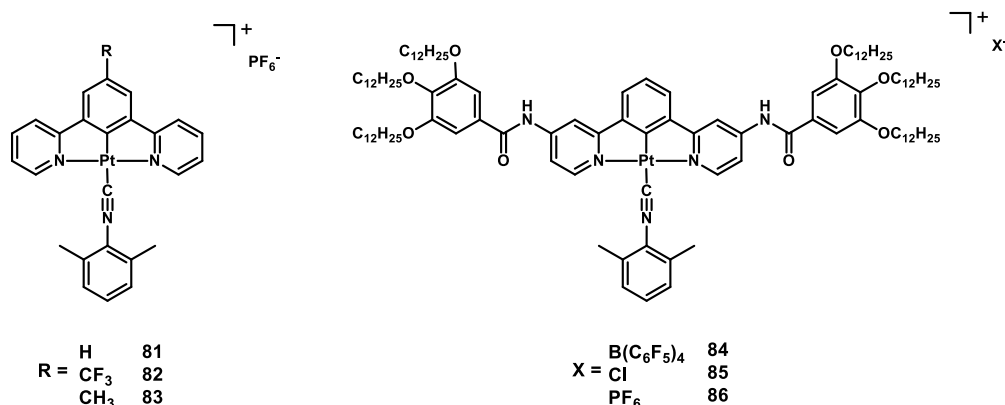


Figure 33. Structure of compounds 81-86.

1.3.3 Thiolates and phenolates

An important first attempt to bind sulfur-based ligands to the platinum center was made by Williams and coworkers in 2014 [97]; in their paper, the authors employed the simple NCN ligand without substituents and the corresponding ligand bearing a COOMe group on the benzene. For both Pt(II) complexes, five different thiolates were tested, namely the simple CH₃SH (for compounds **87** and **88**) and four 4-R-thiophenols (R being -H, -CH₃, -OCH₃ and -NO₂ for **89-96**). The structures of the mentioned complexes are presented in **Figure 34**. From the luminescence point of view, the result of the substitution on the platinum center was a red-shift of the emission, reaching maxima between 634 and 714 nm, even if with a remarkable decrease of the Quantum Yield.

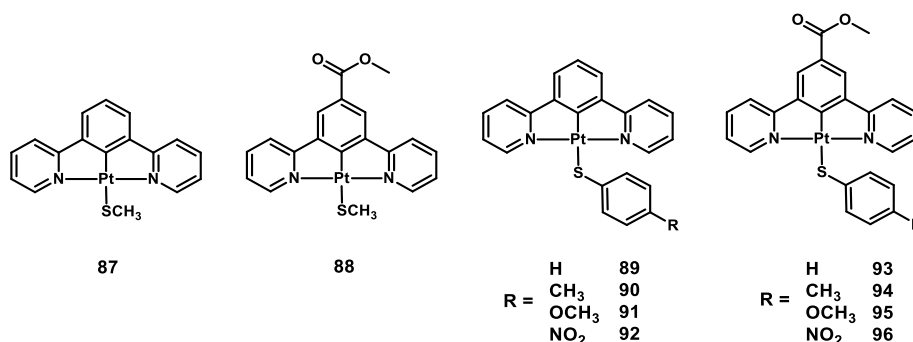


Figure 34. Structure of compounds **87-96**.

In the work of Cockroft of 2019 [98] other thiolates (anionic forms of thiophene-2-thiol and 5-methyl-1,3,4-thiadiazole-2-thiol) were introduced on the Pt(II) by replacement of the Cl ligand, obtaining complexes **97** and **98**. These two compounds, also having hexyloxy chains in position 5 of the pyridines, were used as model compounds to test metallophilic interactions, which were found to be sufficiently weak in most common solvents to play a noticeable role in intermolecular interactions.

Starting from **98**, in their paper of 2020 [99] the same authors explored the photophysical properties of a dimeric compound formed by the chosen thiolate, which was able to bind a second platinum center *via* one of its nitrogen atoms: in that way, from two molecules of **98**, the new cationic compound **99** was obtained, having the second thiolate molecule as counteranion.

Considering phenolates, or more in general alkoxides, as ancillary ligands, it appears that the only published complex (among those having a terdentate di(pyridyl)benzene) is **100**; this complex is in the already discussed paper of Li from 2010 [68], in which the synthesis and the luminescence characterization of many new NCN-Pt complexes were reported. Compounds **97-100** are shown in **Figure 35**.

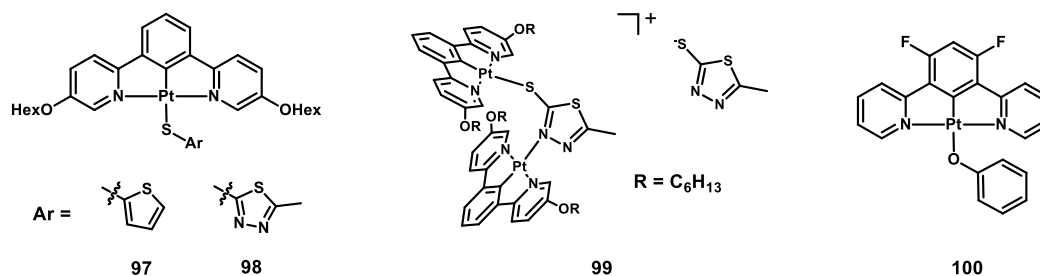


Figure 35. Structure of compounds **97-100**.

1.3.4 Nitrogen-based ligands

Moving to monodentate nitrogen-based ligands, an isothiocyanate, an azide and a pirazolate have been introduced on the Pt(II).

In 2011 Mróz, Roberto and Williams [100] presented various NCN-complexes and among them also compound **101**, synthesized from parent complex **3** (**Figure 21**) by reacting it in the presence of an excess of NaNCS. Similarly did Roberto, Cocchi and Williams both in 2012 [101] for complex **102** (from **5**, **Figure 21**) and in 2014 [71] for compound **103** (from **30**, **Figure 23**); finally in 2015 Dragonetti, Mauro and De Cola [77] obtained compound **104** from **43** (**Figure 24**).

While complexes **101**, **102** and **103** were aimed to be employed in OLED devices, compound **104** was tested for bio-imaging application in cells.

Figure 36 shows compounds **101-104**.

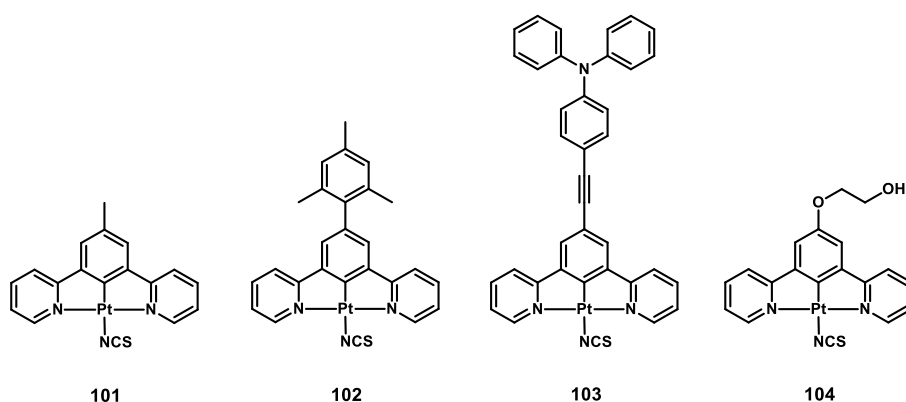


Figure 36. Structure of compounds **101-104**.

The other anionic ligand was the azide, used in the work of Sadler et al. of 2019 [102]; in that paper, the authors obtained the simple unsubstituted NCN-Pt(II) complex **105** with the N_3 ligand directly bound to the metal, to test it in the field of photochemotherapeutics. In fact, the mentioned ligand could be photoreleased by applying the proper radiation, producing reactive species with a detrimental effect on cancer cells.

In the same year Slinker and coworkers [103] employed a 3,5-diphenylpyrazole to bridge two NCN-Pt units, binding the metal with both nitrogen atoms and resulting in the cationic dimeric species **105**. This compound was studied from the point of view of the electrochemical and photophysical properties, also testing it in a light-emitting cell (LEEC). **Figure 37** reports the structure of compounds **105** and **106**.

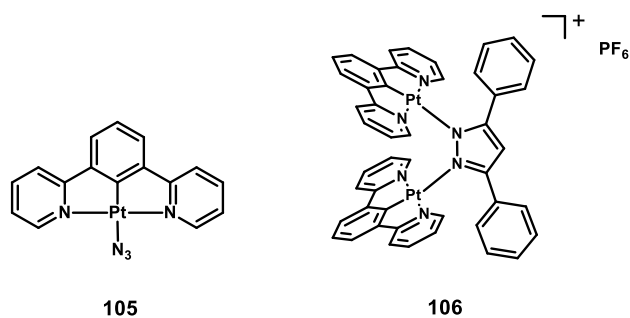


Figure 37. Structure of compounds **105** and **106**.

1.3.5 Other types of ancillary ligands

A different ligand was employed by Che et al. in 2011 [104]: starting from the simple unsubstituted NCN-PtCl complex and the corresponding compound with a -CF₃ group, the chloride was replaced by a carbene ligand with *n*Bu chains on the two nitrogen atoms of the five-membered ring. The resulting complexes (**107** and **108**, structure in **Figure 38**) were effective as solid-state sensors for acidic vapors, in the presence of whom the intensity of the emitted radiation was reversibly increased.

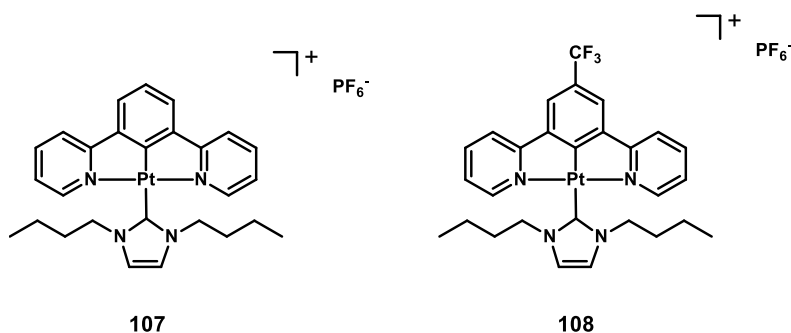


Figure 38. Structure of compounds **107** and **108**.

Finally, two classes of heterobimetallic compounds were published in 2017 and had the NCN-Pt moiety connected to another transition metal complex.

In the work of Yam and Amouri [105], the sulfur- or seleno-based 1,4-benzoquinone was bound to a Cp*Ir unit (Cp* being pentamethylcyclopentadienide) and to two NCN-Pt scaffolds, giving dicationic complexes **109-113**, having triflates or hexafluoroantimonates as counterions. The self-aggregation, the structure and the luminescence of these compounds were investigated in the mentioned work.

In the article of Hirva, Tunik and Koshevoy [106], a bidentate ligand made up of a pyridine presenting a -*p*-(CH₂)_{*n*}NH₂ chain (*n* = 1 for **114** and *n* = 2 for **115**) was used to link the NCN-Pt unit to a Rhenium(I) center, also bearing a 1,10-phenanthroline and three CO ligands.

Figure 39 reports the structure of complexes **109-115**.

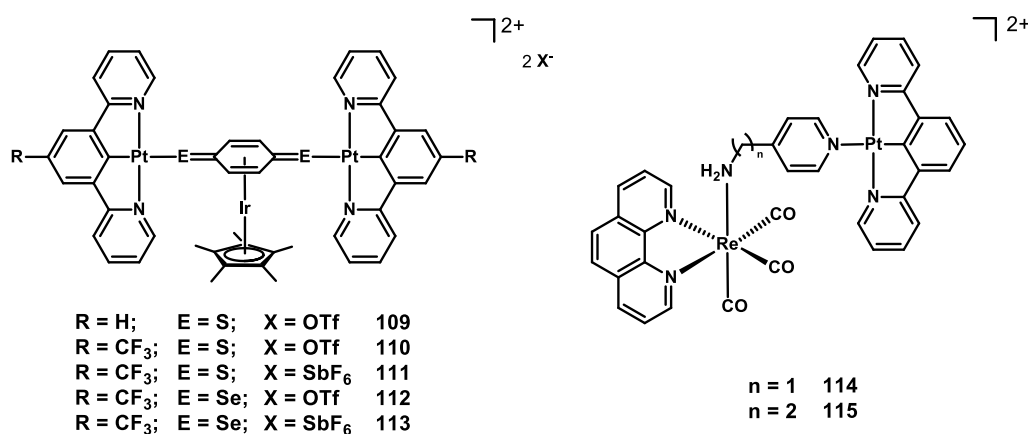


Figure 39. Structure of compounds **109-115**.

2. Applications of NCN-Pt(II) complexes

NCN complexes of Platinum(II) have found applications in various fields in the last decades, from the production of electrochemical devices to biological imaging and sensing. The following sections will present the main results concerning these possibilities.

2.1 NCN-Pt(II) complexes for OLEDs

Because of the good phosphorescent properties of Pt(II) complexes provided by the presence of the heavy metal atom and of its high spin-orbit coupling, these kinds of compounds can find useful application in the field of OLED production [9, 10].

Up to now, many of the already presented NCN-Pt(II) compounds (shown in **Figure 40**) were tested as dopants in OLED devices. **Tables 1** and **2** resume the composition, the CIE coordinates and the External Quantum Efficiency (EQE) of the OLEDs produced with the mentioned Pt(II) complexes; the EQE values refer to the current density j (expressed in $A\ cm^{-2}$).

The main organic compounds usually employed as hole-transporting layers, emitting layers and electron-transporting layers are shown in **Figure 41**.

The following abbreviations are used in **Tables 1** and **2**, and they stand for:

CBP = 4,4'-*N,N'*-dicarbazole-biphenyl;

TPD = *N,N'*-bis(3-methylphenyl)-*N,N'*-diphenylbenzidine;

PC = bisphenol-A polycarbonate;

TCTA = tris(4-carbazoyl-9-ylphenyl)amine;

TBPi = 2,2',2''-(1,3,5-benzinetriyl)-tris(1-phenyl-1-*H*-benzimidazole);

TAZ = 3-(4-biphenyl)-4-phenyl-5-tert-butylphenyl-1,2,4-triazole;

OXA = 3,5-bis[5-(4-tert-butylphenyl)-1,3,4-oxadiazol-2-yl]benzene;

HTL: hole-transporting layer;

EL: emissive layer;

ETL: electron-transporting layer;

EQE: external quantum efficiency.

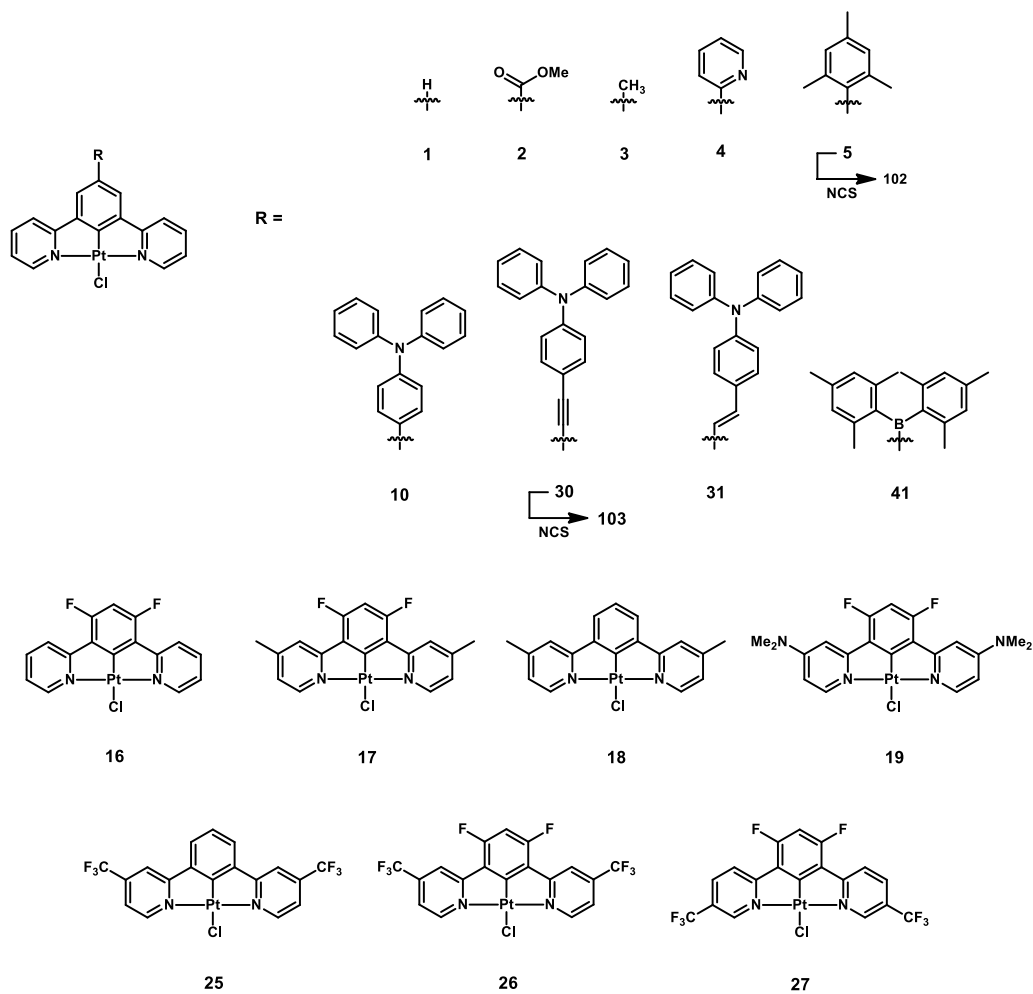


Figure 40. Structure of some NCN-Pt(II) tested in OLED devices.

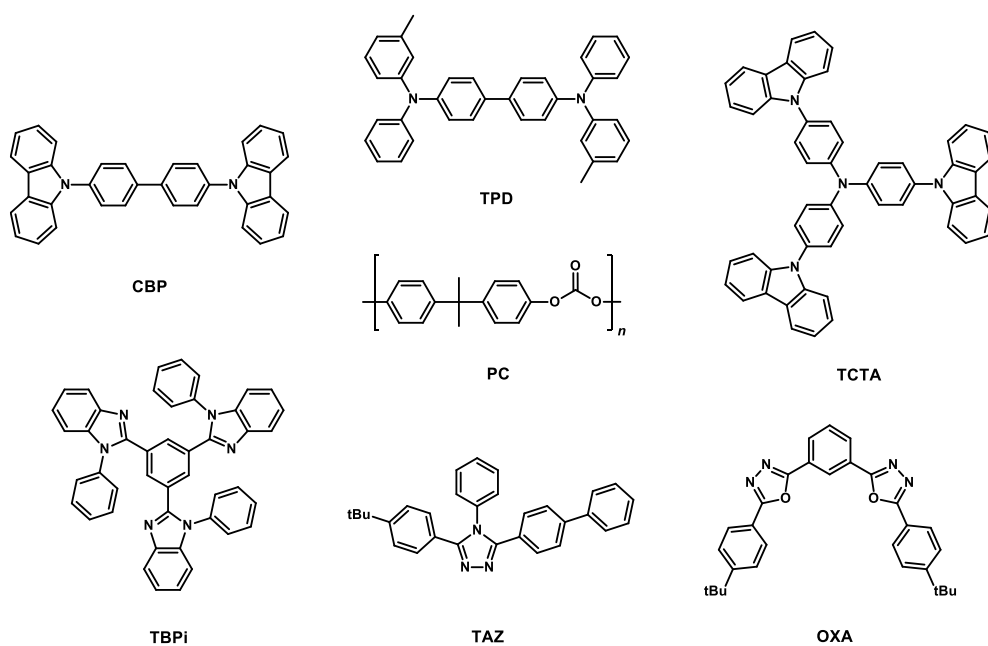


Figure 41. Structure of some organic compounds employed in HTL, EL and ETL.

Table 1. Composition, CIE coordinates and EQE of the OLEDs produced with complexes **1-5, 10, 30-31, 41, 102-103**.

Complex	HTL	EL	%Pt	ETL	CIE	EQE	ref
1	TPD:PC	CBP	6%	OXA	-	~10%	[16]
1	TPD:PC	CBP:OXA	6%	OXA	(0.23, 0.57)	~10.5%	[16]
2	TPD:PC	CBP:OXA	6%	OXA	(0.14, 0.46)	~9%	[16]
3	TPD:PC	CBP:OXA	6%	OXA	(0.31, 0.61)	~10%	[16]
4	TPD:PC	CBP:OXA	6%	OXA	(0.20, 0.76)	~9%	[16]
5	TPD:PC	CBP:OXA	6%	OXA	(0.24, 0.63)	~5%	[16]
10	TPD:PC	CBP:OXA	6%	OXA	(0.48, 0.51)	~10%	[16]
30	TCTA	-	100%	TBPI	-	~0.2%	[71]
31	TCTA	-	100%	TBPI	(0.673, 0.315)	~1%	[71]
31	TCTA	TCTA	5%	TBPI	(0.302, 0.203)	~1%	[71]
31	TCTA	CBP	5%	TBPI	(0.537, 0.203)	~0.3%	[71]
41	CBP	CBP	12%	TBPI	(0.34, 0.56)	30%	[75]
102	TPD:PC	-	100%	TAZ	-	~1%	[101]
103	TCTA	-	100%	TBPI	-	~0.1%	[37]

Table 2. Composition, CIE coordinates and EQE of the OLEDs produced with complexes **16-19** and **25-27**.

Complex	HTL	EL	%Pt	ETL	CIE	EQE	ref
16	TPD:PC	TCTA	5%	TAZ	(0.19, 0.42)	7.8%	[66]
16	TPD:PC	-	100%	TAZ	(0.63, 0.35)	5.3%	[66]
17	TPD:PC	TCTA	5%	TAZ	(0.18, 0.35)	13.0%	[66]
17	TPD:PC	TCTA	10%	TAZ	(0.27, 0.37)	18.3%	[66]
17	TPD:PC	TCTA	15%	TAZ	(0.33, 0.38)	18.1%	[66]
17	TPD:PC	TCTA	20%	TAZ	(0.45, 0.38)	14.9%	[66]
17	TPD:PC	TCTA	25%	TAZ	(0.53, 0.38)	16.8%	[66]
17	TPD:PC	-	100%	TAZ	(0.61, 0.38)	14.7%	[66]
18	TPD:PC	TCTA	5%	TAZ	(0.24, 0.57)	15.5%	[66]
18	TPD:PC	-	100%	TAZ	(0.57, 0.40)	0.1%	[66]
19	TPD:PC	TCTA:TCP	3%	TAZ	(0.20, 0.30)	3.9%	[67]
19	TPD:PC	TCTA:TCP	6%	TAZ	(0.26, 0.34)	11.3%	[67]
19	TPD:PC	TCTA:TCP	12%	TAZ	(0.32, 0.37)	7.1%	[67]
19	TPD:PC	TCTA:TCP	20%	TAZ	(0.36, 0.37)	3.7%	[67]
19	TPD:PC	TCTA:TCP	25%	TAZ	(0.37, 0.39)	2.7%	[67]
19	TPD:PC	TCTA:TCP	100%	TAZ	(0.52, 0.47)	6.4%	[67]
25	TPD:PC	TCTA	5%	TAZ	(0.35, 0.62)	7.0%	[69]
25	TPD:PC	TCTA	100%	TAZ	(0.65, 0.33)	0.3%	[69]
26	TPD:PC	TCTA	5%	TAZ	(0.30, 0.59)	4.9%	[69]
26	TPD:PC	TCTA	100%	TAZ	(0.65, 0.35)	0.4%	[69]
27	TPD:PC	TCTA	5%	TAZ	(0.31, 0.54)	4.9%	[69]
27	TPD:PC	TCTA	100%	TAZ	(0.67, 0.32)	1.2%	[69]

By observing the collected data, it can be noticed that very often the best efficiencies were reached in the case of “dilute” Emitting Layers, having a low amount of Pt(II) complex in the organic matrix; this remarkable decrease in efficiency (*e.g.* for compounds **18**, **25-27**) is a consequence of the quenching of the emission caused by aggregates and/or excimers, whose formation in the layer is favored by the high concentration of the molecules in the solid state. In other cases, such as for complexes **17** and **19**, the trend is not regular, and a general conclusion cannot be achieved by simply comparing the %Pt and EQE values.

2.2 NCN-Pt(II) complexes for bio-imaging

NCN platinum complexes can find convenient application for bio-imaging, since they possess the ability to interact with nucleic acids, to intercalate in DNA (due to the planar structure) and/or to bind to nucleobases by replacement of the ancillary Cl ligand by nitrogen atoms. Another possible bonding manner could be that with thiols (*e.g.* with cysteine or glutathione), because of the thiophilic nature of the soft platinum(II) center.

Furthermore, by taking advantage of the quenching of luminescence brought about by molecular oxygen, it can be possible to develop lifetime maps which give a good approximation of the O₂ concentration in the different parts of the cells (membrane, cytoplasm, nucleus, *etc.*), as a consequence of the different degree of exposition to oxygen.

Up to now, many of the previously presented Pt(II) complexes based on an NCN scaffold (structure in **Figure 42**) have been tested as dyes in biological imaging [107].

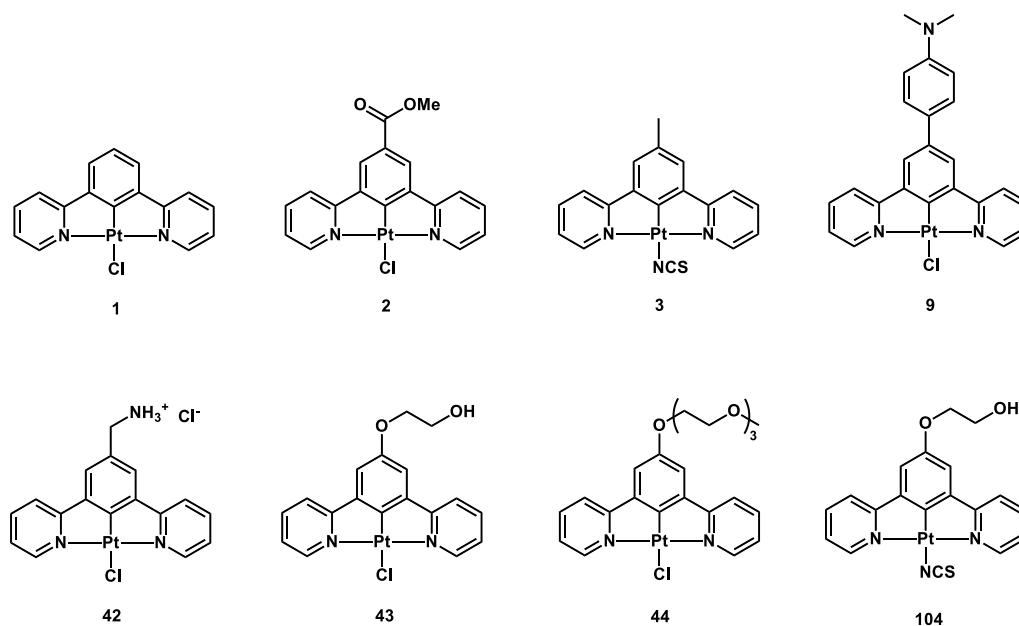


Figure 42. Structure of the NCN-Pt(II) complexes tested for bio-imaging.

Compounds **1-4** were presented by Haycock, Weinstein, Williams et al. [25] and employed in cells using two-photon excitation (TPE) and time-resolved emission imaging microscopy (TREM); the TREM technique implies longer time scales, which allow for a better discrimination between wide changes in lifetimes, and time-gated experiments, able to distinguish the emitted radiation from the biological autofluorescence.

Particularly interesting are the results of **1**: after an MTT assay, performed to determine the cytotoxicity of the compounds, the luminescence properties of this complex were studied by incubating the cells using a 100 μM solution of the dye in phosphate buffer solution (PBS) containing 1% of DMSO. The maximum intensity of emission was reached after only 5 minutes, suggesting that the small neutral complex could easily permeate through the membrane of the cell by diffusion, without the need of specific transport mechanisms such as endocytosis or activated channels.

Further experiments involved cell co-staining, employing the standard dye 4',6-diamidine-2'-phenylindole dihydrochloride (DAPI), whose emission did not overlap with that of **1**, allowing for a clear view of the localization of the two compounds inside the cell; this test confirmed that **1** preferentially accumulated in the nucleus of the cell.

Dyes **42-44** and **104** were designed with the aim of testing the effect of different substituents on the central benzene ring on cellular diffusion and on the photophysical properties. In fact, complex **42** [27, 108], water-soluble thanks to the $-\text{CH}_2\text{NH}_3^+\text{Cl}^-$ chain, could be tested without the need to be pre-solubilized in an organic solvent that can be toxic for cells.

Moreover, in **43-44** and **104** [77] glycol chains with different length were introduced to achieve a higher solubility in water. They were tested in HeLa cells, stained with a 50 μM solution of platinum complex in PBS containing less than 1% of DMSO; for all the three complexes the internalization into the cells was very rapid, being complete within 10 minutes and without negative effects arising from the presence of the hydrophilic chain or of the ancillary NCS ligand.

2.3 NCN-Pt(II) complexes for PDT

Besides bio-imaging in cells and tissues, NCN complexes of Pt(II) can be employed in the field of PDT [107]. A first application of this family of complexes for photodynamic therapy was presented in 2016 by Weinstein et al. [109]: in their paper the simple compound **3**, bearing a methyl group on the benzene ring (**Figure 21**), was tested in HeLa cancer cells, working with various concentrations of the complex and monitoring the effect at different time points during a period of 12 days. Remarkably, no dark toxicity was observed up to a concentration of 1 μM . Later, the same complex was applied to colorectal cancer cell line SW480 and to bladder cancer cell line EJ, showing very important effects, since the exposure to light led to cell death even in tumor cells resistant to the well-known *cis*-platin agent.

A similar approach was reported by Sarli and coworkers in 2017 [78] with compound **46**, bearing a c(RGDyK) oligopeptide coupled to the NCN scaffold. This substituent was meant to target integrin receptors, typically overexpressed in some cancer types (such as melanoma, glioblastoma, *etc.*). Complex **45**, having a carboxylic group, was used as reference compound for cellular studies. After having confirmed the efficient targeting of the RGD fragment towards $\alpha_v\beta_3$ receptors, a cytotoxicity investigation was performed, pointing out the effective cellular death caused by the compound, even if it was due to cytostatic rather than cytotoxic properties.

Figure 43 shows the structure of complexes **45** and **46**.

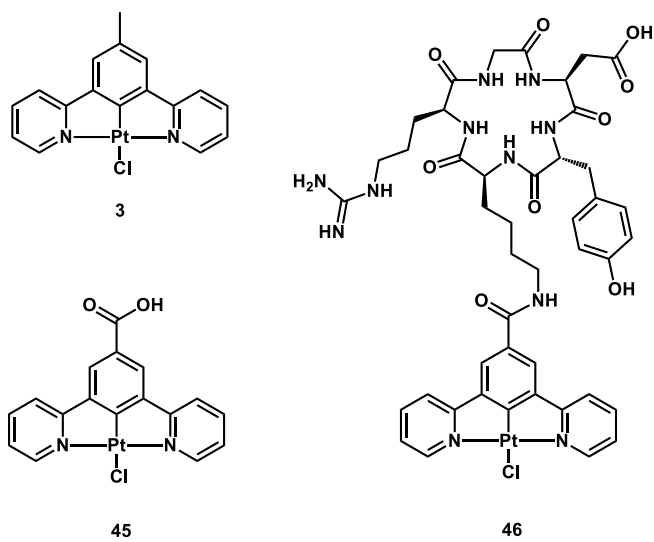


Figure 43. Structure of complexes 3, 45 and 46.

III – SYNTHESIS OF THE COMPLEXES

1. Synthesis of ligands L1-L7 and of complexes PtCl1-PtCl7

In this section the synthetic strategies for NCN-PtCl complexes **PtCl1-PtCl7** are briefly presented, while all details and procedures are reported in **Chapter V**, together with NMR spectra in the **Appendix**.

All compounds present the NCN terdentate chelating ligand, with a monodentate ancillary chloride ligand on the platinum center.

Complexes **PtCl1**, **PtCl2**, **PtCl6** and **PtCl7** were already known and published (being the same as compounds **5**, **10**, **8** and **3** respectively, reported in **Figure 21**), but were re-synthesized in order to use them as starting materials for the derivatives which will be presented and discussed in **Chapter II – Sections 2.3-2.6**. On the contrary, complexes **PtCl3-PtCl5** are new and never appeared in published papers.

The pyrenyl group in **PtCl3** was introduced with the aim of testing the luminescence properties of an NCN-Pt complex bearing this kind of polycyclic aromatic moiety, which could provide an interesting emission region.

Considering **PtCl4** and **PtCl5**, the purpose was to observe the effect of the expansion of the aromatic system and of the presence of an amino group directly bound to the NCN scaffold (in the case of **PtCl5**), to be compared with the analogue **PtCl4** having a phenylene spacer between the two parts of the ligand.

Figure 44 shows the structure of complexes **PtCl1-PtCl7**.

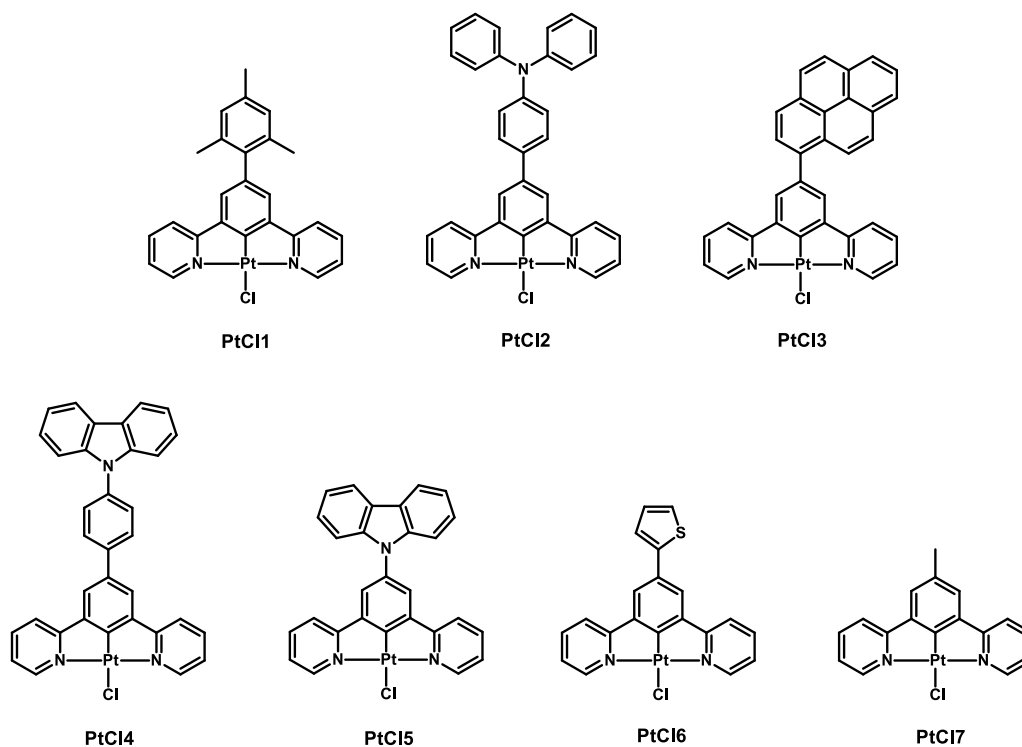


Figure 44. Structure of the synthesized NCN-Pt(II) complexes **PtCl1-PtCl7**.

1.1 Synthesis of intermediate compounds I1-I6

To achieve the NCN ligands and the corresponding platinum(II) complexes, some intermediate compounds had to be synthesized, starting from the central benzene ring and the adding the suitable substituent and the two pyridines.

1.1.1 Synthesis of I1-I4

For complexes **PtCl1-PtCl4**, the synthesis started from 1,3,5-tribromobenzene, being the core ring of the NCN terdentate ligand. The substrate underwent a Suzuki-Miyaura Pd-catalyzed cross-coupling reaction with the suitable arylboronic acid to give intermediates **I1-I4**; the synthetic pathway is reported in **Figure 45**.

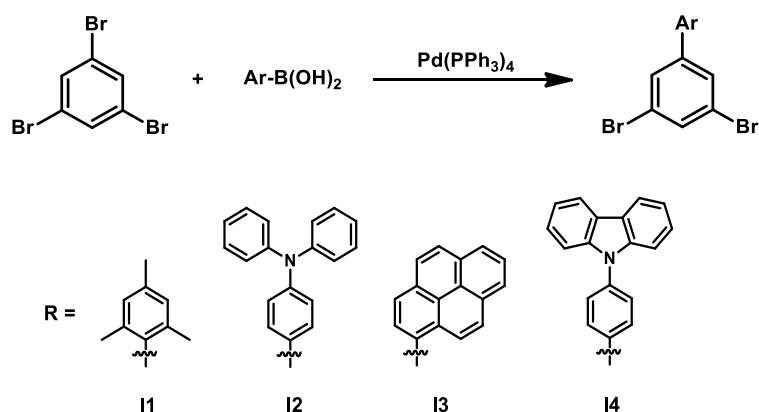


Figure 45. Synthesis of intermediate compounds **I1-I4**, obtained through Suzuki-Miyaura cross-coupling.

1.1.2 Synthesis of I5

Unlike the other dibromo-aryl-benzene intermediates presented in this section, **I6** was not obtained from a boronic acid or ester, but *via* the direct N-arylation of carbazole [110]; this nucleophilic aromatic substitution was performed in the presence of a strong base (KOH) and without the need of a transition metal catalyst (**Figure 46**).

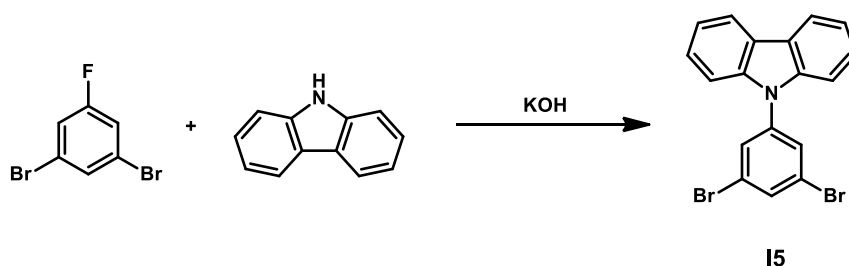


Figure 46. Synthesis of intermediate compound **I5**.

1.1.3 Synthesis of I6

Compound **I6** was obtained reacting 1,3,5-tribromobenzene with 2-(tributylstannyl)thiophene, by means of a Stille coupling (**Figure 47**) catalyzed by $\text{Pd(PPh}_3)_4$.

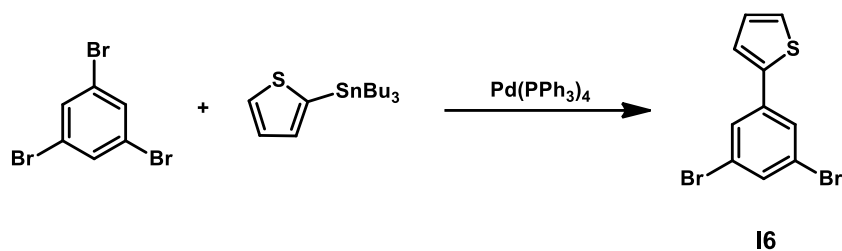


Figure 47. Synthesis of intermediate compound I6, obtained through Stille cross-coupling.

1.2 Synthesis of ligands L1-L7

Once intermediates **I1-I6** were obtained, the synthesis of the NCN ligands continued by reacting them (or the commercially available 3,5-dibromotoluene in the case of **L7**) *via* a Stille cross-coupling with 2-(tributylstannyl)pyridine in the presence of Pd(PPh₃)₂Cl₂ as catalyst. In that way the introduction of the pyridyl rings was performed and gave ligands **L1-L7**. **Figure 48** shows the general synthesis of the mentioned ligands.

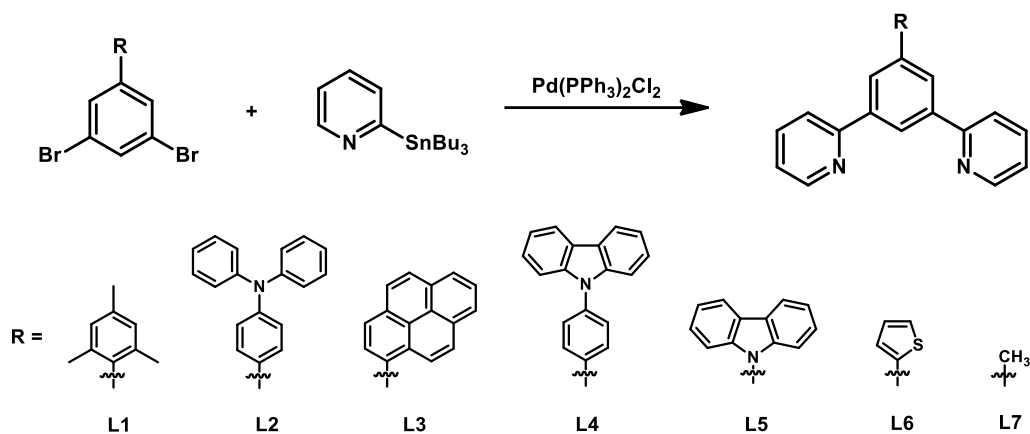


Figure 48. Synthesis of ligands L1-L7, obtained through Stille cross-coupling.

1.3 Synthesis of complexes PtCl1-PtCl7

For all ligands the complexation procedure was the same, *i.e.* using K₂PtCl₄ as source of the metal and refluxing the reagents in glacial acetic acid under argon atmosphere [61] (**Figure 49**).

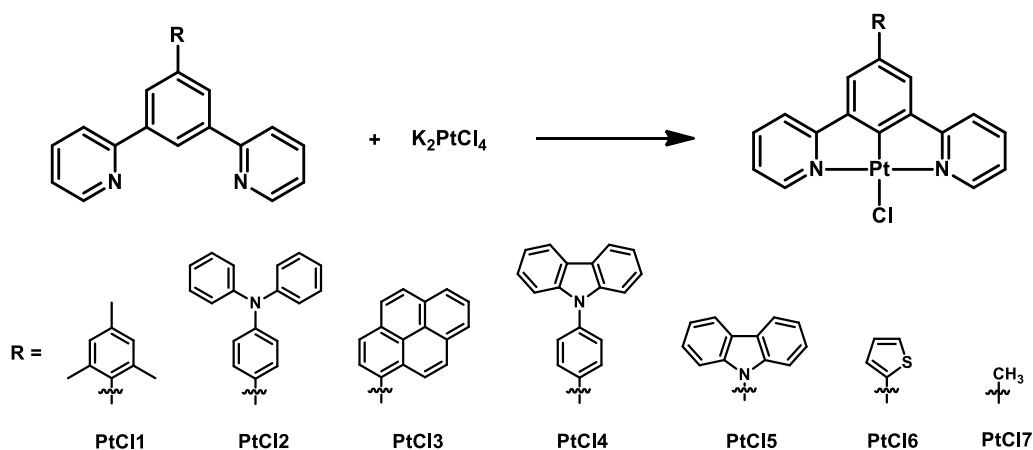


Figure 49. Synthesis of complexes PtCl1-PtCl7.

2. Synthesis of complexes Pt1-Pt15

As extensively discussed in **Chapter II – Section 1.3**, the chloride ligand can be quite easily replaced by other species, to give new complexes from the parent NCN-PtCl compounds.

Here is reported the synthesis of fifteen derivatives, having as ancillary ligand three different thiolates (*i.e.* 1-phenyl-1*H*-tetrazole-5-thiolate, 4-phenylthiazole-2-thiolate, thioacetate), an azide, a phthalimide and an isothiocyanate. **Figure 50** shows the structure of the sodium or potassium salt of the employed species; except for the NCS-substituted compound **Pt6** (being the same as **102**, see **Figure 36**), all complexes are new.

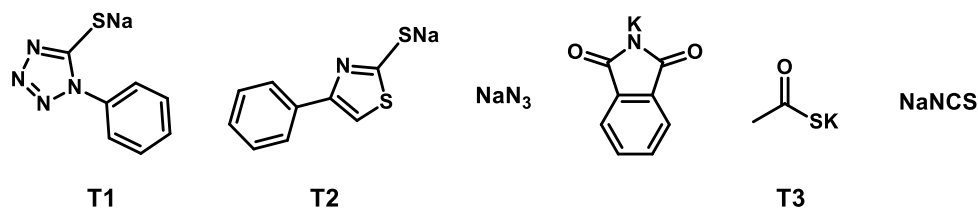


Figure 50. The salts employed as source of the anionic ancillary ligands.

The synthetic details and procedures are reported in **Chapter V**, while the NMR spectra in the **Appendix**.

As a general remark, one should be careful when using azides and should work on a small scale; heavy metal azides can be heat- and shock-sensitive, and can explosively decompose with little input of external energy. However, during this work, no problems were encountered.

2.1 Aim of the tested ancillary ligands

Phenyl-substituted heteroaromatic thiolates **T1** and **T2** were chosen with the purpose of testing the effect of new sulfur-based aromatic ligands on the Pt(II) center, in order to make a comparison with luminescence data of compounds **87-96** ([97], **Figure 34**), in which the ancillary ligand was a simple CH₃S⁻ or a 4-R-thiophenolate (R being -H, -Me, -OMe, -NO₂).

Moving to **T3**, this species was employed to test the possibility of replacing the chloride of the parent compound with a non-aromatic thiol such as the thioacetate.

In the case of the azide and the phthalimide, these common reagents were tested as representative examples of N-based ligands, being commercially available compounds that can easily bind a variety of transition metals.

Finally, the isothiocyanate ligand was expected to bind the Pt(II) with the sulfur atom (according to the thiophilic nature of the soft platinum cation), but through the X-ray analysis of the crystals it was found that this bidentate anion binds the metal *via* the nitrogen atom.

2.2 Future possibilities

Up to now, only few derivatives of the NCN-Pt complexes presenting the -NCS or -N₃ ligand have been synthesized and characterized, but in the future it will be surely interesting to develop new compounds, since various biological applications of these complexes can be tested.

2.2.1 Isothiocyanate

The presence of the NCS on the metal can open new possibilities in the field of this family of NCN-Pt complexes, since this class of molecules could act as sensors for thiol-bearing biologically active species, such as cysteine. In fact, isothiocyanates can rapidly react with cysteine to form an adduct which undergoes intermolecular cyclization to give a 5-membered ring, that can produce further species by releasing an amine or H_2S [111] (see **Figure 51** for the proposed mechanisms).

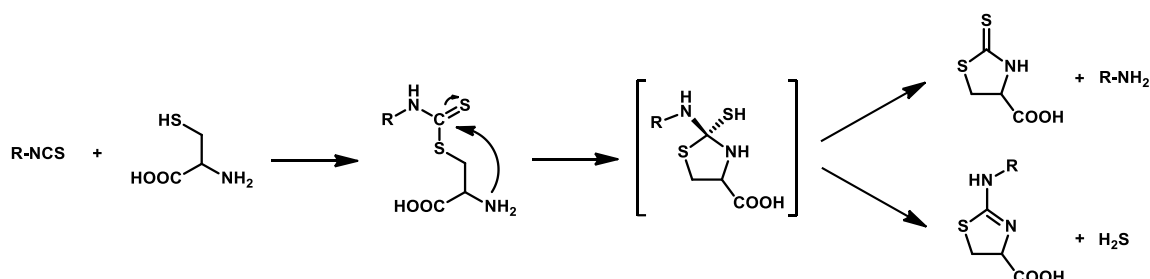


Figure 51. Proposed general mechanism for the reaction of an isothiocyanate with cysteine.

This reaction can be not only a sensing technique for thiolates (by monitoring the process through luminescence variations) or a useful method for the labelling of proteins (as shown by Chudasama and Keserú [112]), but also a synthetic procedure to develop new ligands by adding moieties to the simple NCS.

2.2.2 Azide

The use of an azide as ancillary ligand is particularly appealing because azido complexes of Pt(II) can find application in photoactivated chemotherapy, due to their ability to intercalate in DNA (because of the planar coordination environment) and to photorelease azidyl radicals that can attack and damage cancer cells [102, 113–115].

Furthermore, this ancillary ligand can be the starting point for the well-known *click reaction* with an alkyne. As shown in the papers of Schatzschneider and coworkers of 2019 [116] and 2021 [117], square planar platinum(II) complexes can easily react at room temperature and without the need of a catalyst with an electron-poor alkyne, to give triazolite complexes. Once formed, such complexes can undergo isomerization to change the nitrogen atom they bind the metal with (see **Figure 52**), passing from a N1- to a N2-triazole; obviously, if the employed alkyne is not symmetrical, different products can be obtained, with a different structure depending on the position of the electron-withdrawing groups.

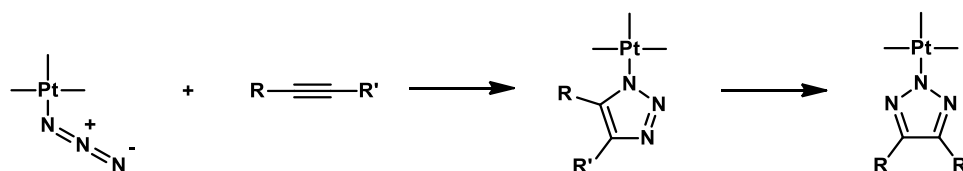


Figure 52. General example of reaction between an azido complex and an alkyne.

2.3 Derivatives of PtCl1

Complex **PtCl1** has been used as parent compound to react with all the six species presented in **Figure 50**, to give complexes **Pt1-Pt6** (**Figure 53**):

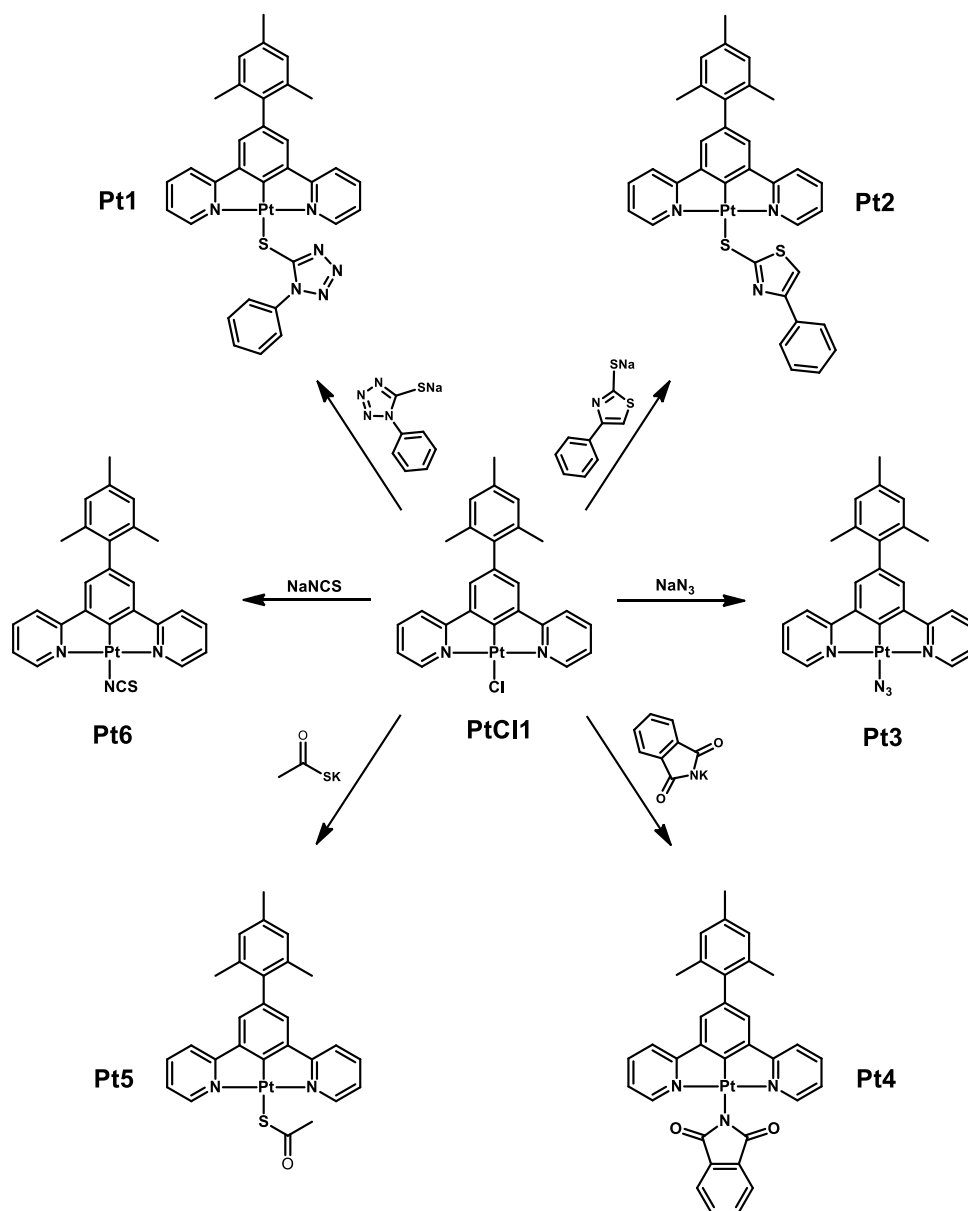


Figure 53. Synthesis of complexes **Pt1-Pt6**, starting from parent compound **PtCl1**.

2.4 Derivatives of PtCl₂

Complex **Pt7** has been obtained by reaction of **PtCl₂** with sodium 4-phenylthiazole-2-thiolate (**Figure 54**):

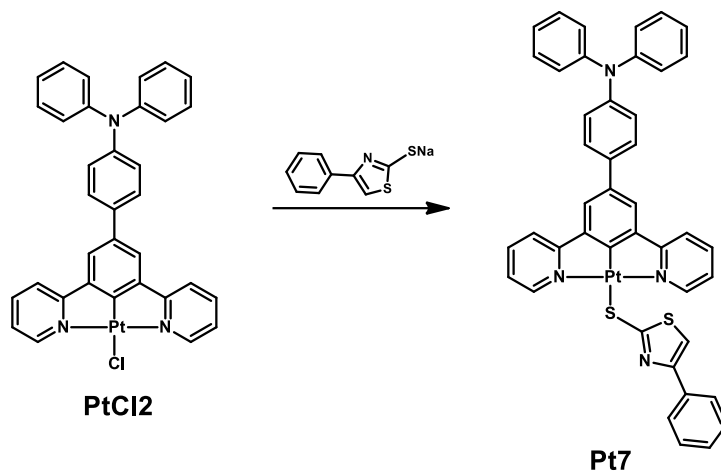


Figure 54. Synthesis of complex **Pt7**, starting from parent compound **PtCl₂**.

Up to now, this is the only example of derivative of **PtCl₂**, obtained by replacement of the chloride with another anionic species.

2.5 Derivatives of PtCl6

Complexes **Pt8-Pt11** (structure in **Figure 55**) were obtained from parent compound **PtCl6** by reacting it with four of the salts shown in **Figure 50**.

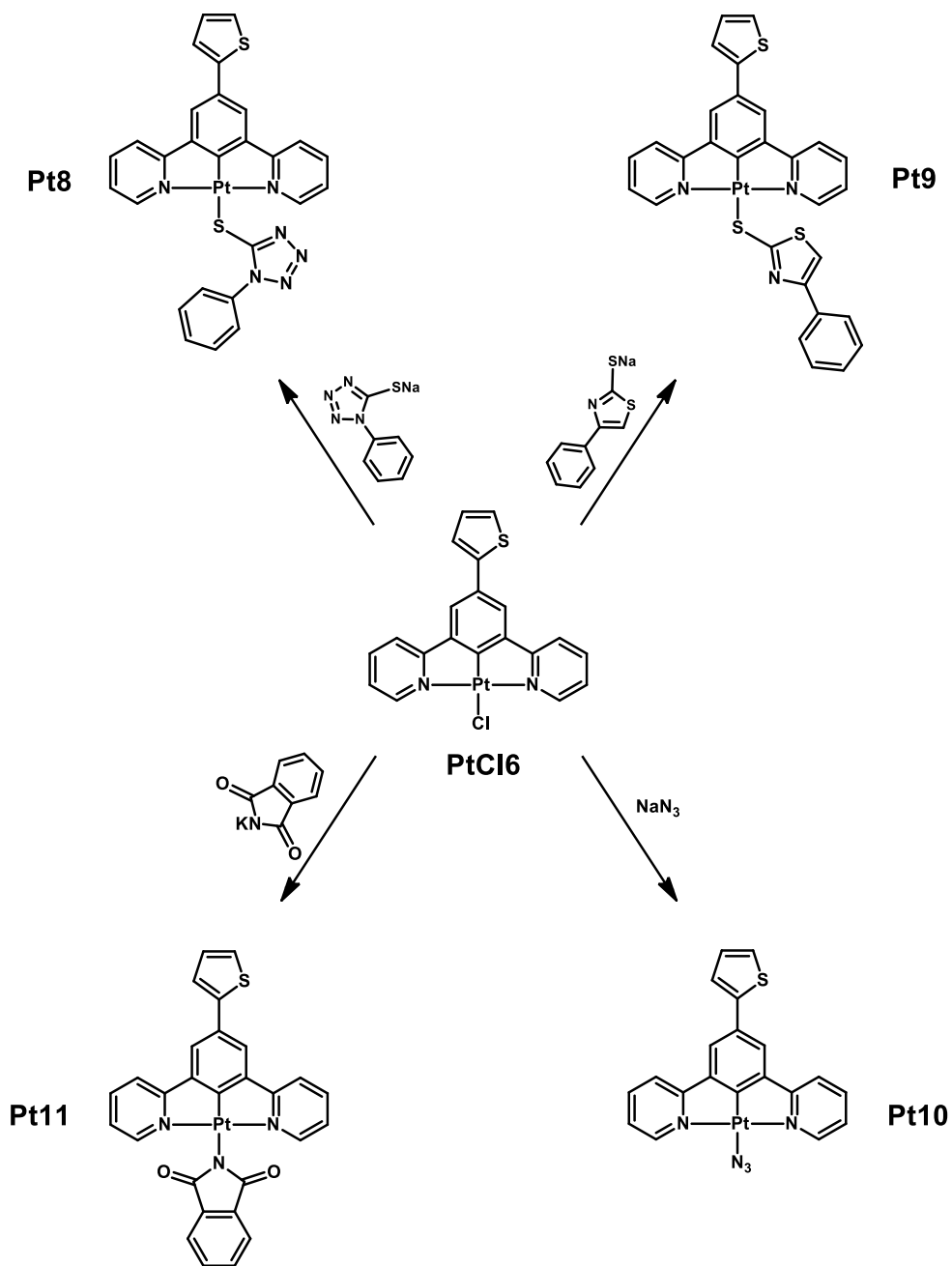


Figure 55. Synthesis of complexes **Pt8-Pt11**, starting from parent compound **PtCl6**.

2.6 Derivatives of PtCl7

Through the already presented reactions of the NCN-Pt(II) complex **PtCl8**, compounds **Pt12-Pt15** were obtained. Their structure is reported in **Figure 56**.

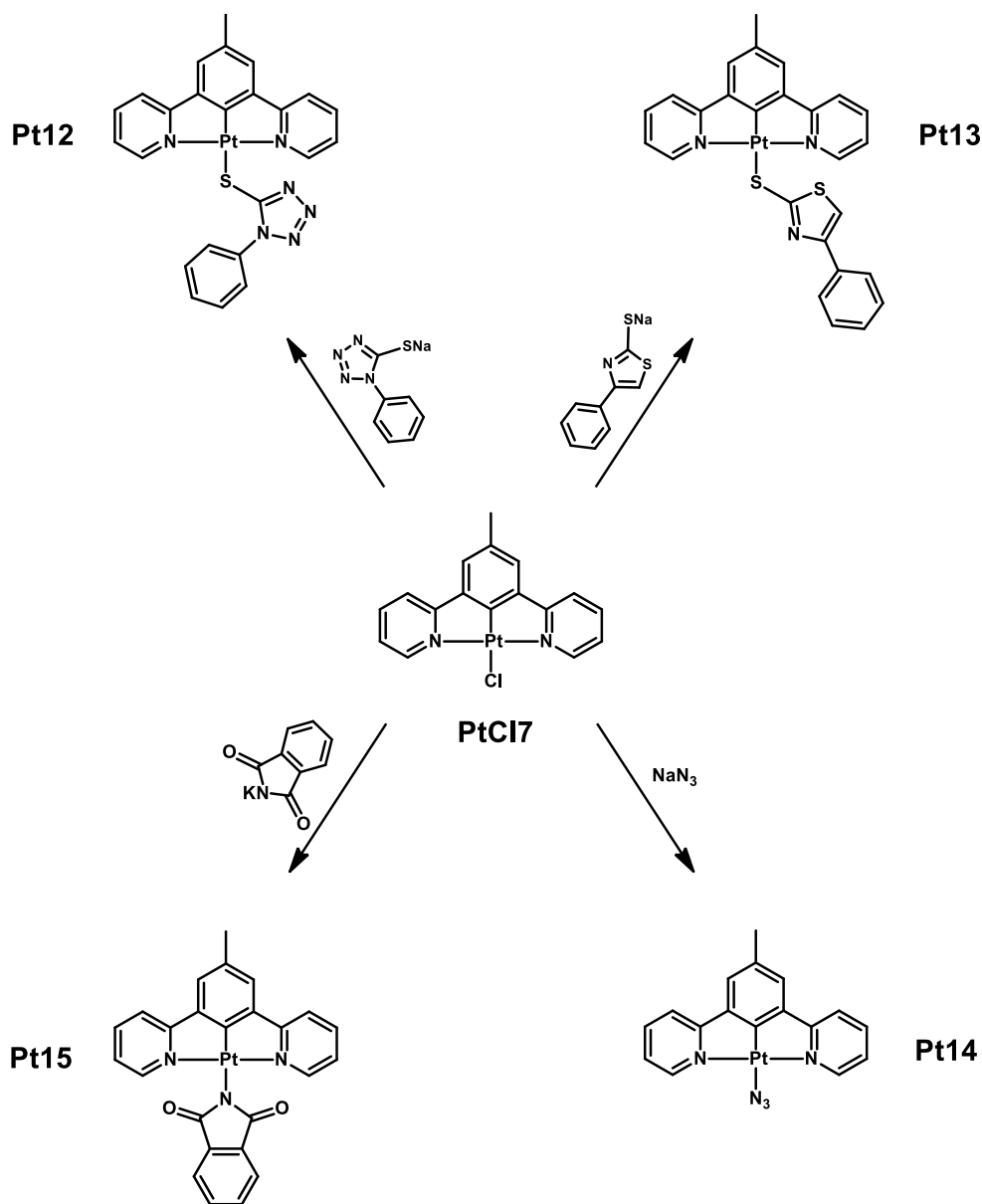


Figure 56. Synthesis of complexes **Pt12-Pt15**, starting from parent compound **PtCl7**.

3. Synthesis of ligands L8-L13 and of complexes PtCl8-PtCl13

Since complexes **PtCl8-PtCl13** present aryl substituents also on the pyridine rings, their synthesis started from the introduction of such moieties *via* Suzuki-Miyaura coupling, employing the suitable aryl bromide (2-Br-4-hexylthiophene for **PtCl8-PtCl11** and 4-Br-triphenylamine for **PtCl12-PtCl13**) together with 2-Cl-pyridine-4-boronic acid. The long hexyl chains on the thienyl rings aimed at the increase of the solubility of the related complexes and resulted very effective in this.

In the meanwhile, the already presented intermediates **I1**, **I2**, **I3**, **I6** and 1,3-dibromo-4,6-difluorobenzene were used to synthesize the corresponding boronic pinacol esters, to be reacted in another Suzuki-Miyaura coupling with the mentioned 2-Cl-4-arylpiperidines, to give ligands **L8-L13**.

Finally, as shown before in **Chapter III – Section 1.3**, the usual complexation reactions gave compounds **PtCl8-PtCl13**, whose structure is here reported in **Figure 57**.

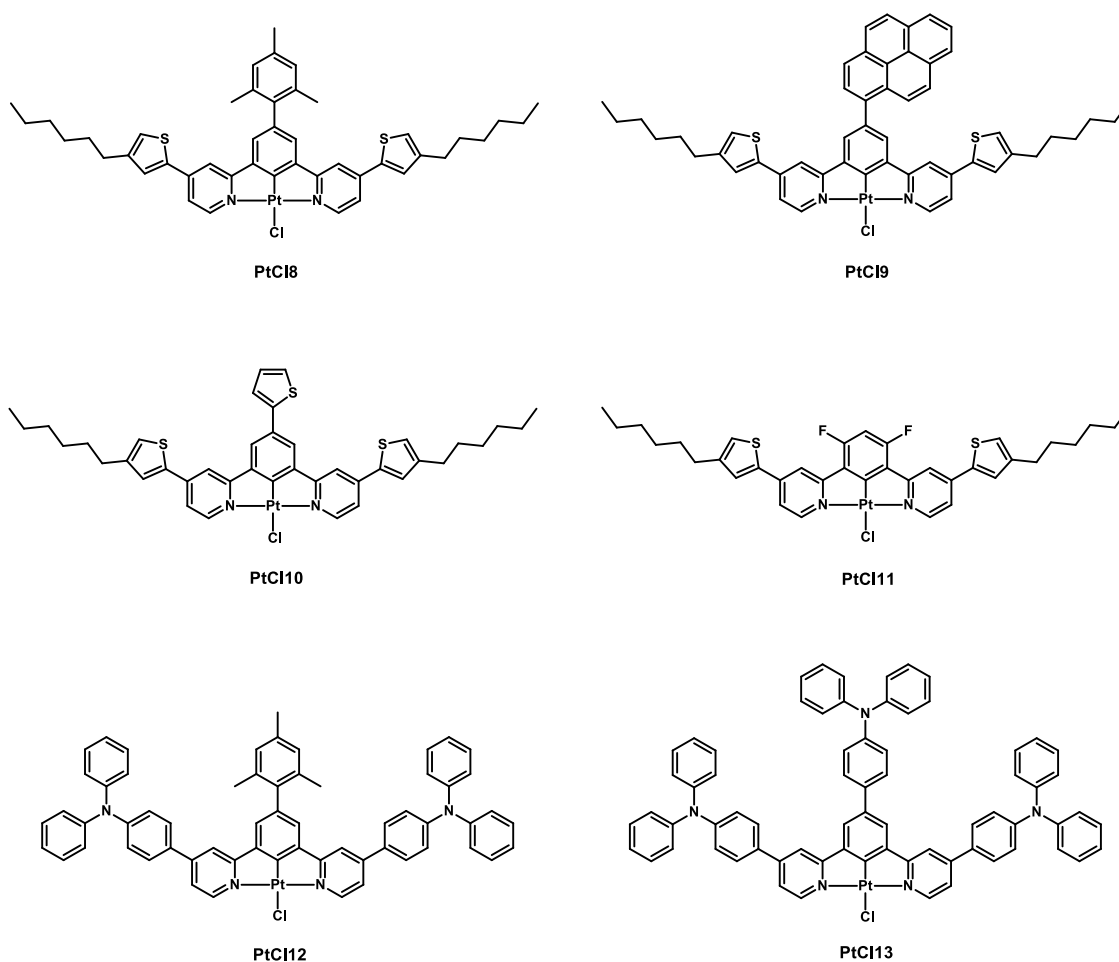


Figure 57. Structure of the synthesized NCN-Pt(II) complexes **PtCl8-PtCl13**.

3.1 Synthesis of intermediate compounds I7-I8

Intermediates **I7** and **I8** were 2-chloro-pyridines bearing an aryl substituent in position 4, namely a 4-hexyl-2-thienyl for the former compound and a 4-diphenylamino-phenyl for the latter. The compounds were obtained with a Suzuki-Miyaura coupling, as shown in **Figure 58**.

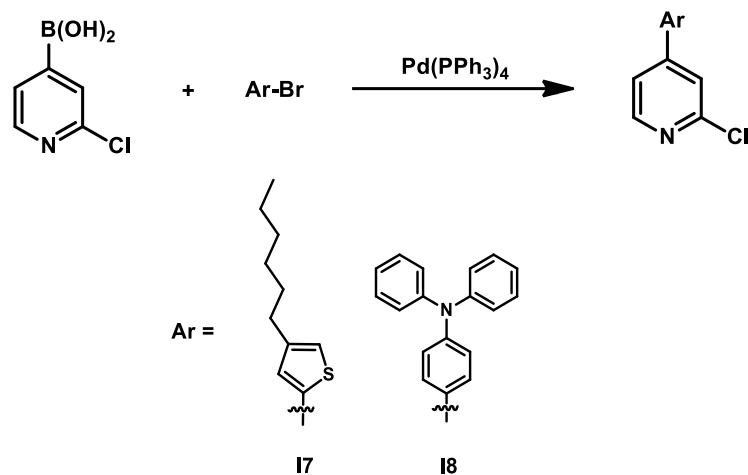


Figure 58. Synthesis of intermediates **I7** and **I8**.

3.2 Synthesis of boronic esters B1-B5

The other reagents needed to perform the Suzuki-Miyaura cross-coupling, to give the NCN ligands, were the diboronic esters of the differently substituted benzene core; these compounds were obtained through a Miyaura coupling catalyzed by $\text{Pd}(\text{dppf})\text{Cl}_2$.

3.2.1 Synthesis of B1-B4

Using intermediates **I1-I3** and **I6**, boronic esters **B1-B4** were achieved. The general synthesis is shown in **Figure 59**.

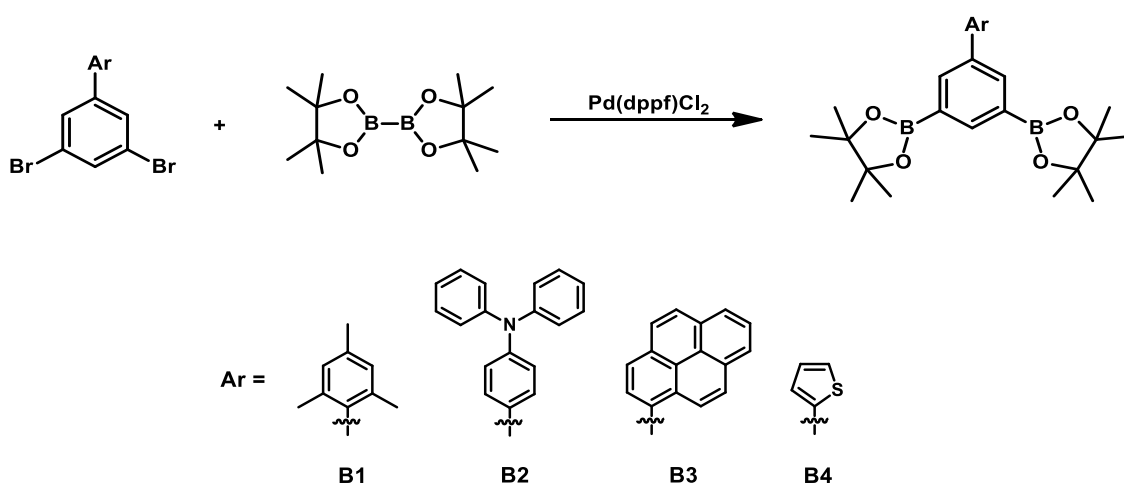


Figure 59. Synthesis of boronic esters **B1-B4**.

3.2.2 Synthesis of B5

Compound **B5** was synthesized starting from the commercially available 1,3-dibromo-4,6-difluorobenzene (**Figure 60**), through a Miyaura Pd-catalyzed reaction.

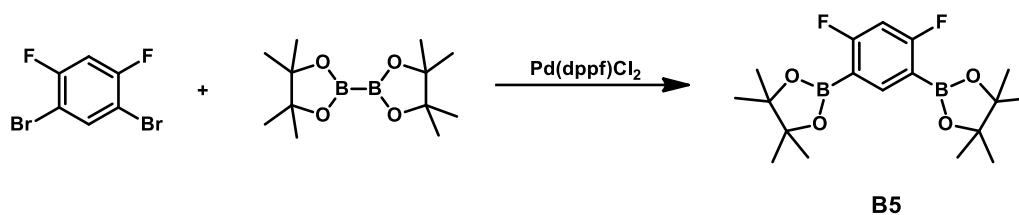


Figure 60. Synthesis of boronic ester **B5**.

3.3 Synthesis of ligands L8-L13

By combining pyridines **I7-I8** with boronic esters **B1-B5**, six new NCN ligands were synthesized through Suzuki-Miyaura cross coupling reactions.

3.3.1 Synthesis of ligands L8-L10

The synthetic pathway for ligands **L8-L10** is shown in **Figure 61**.

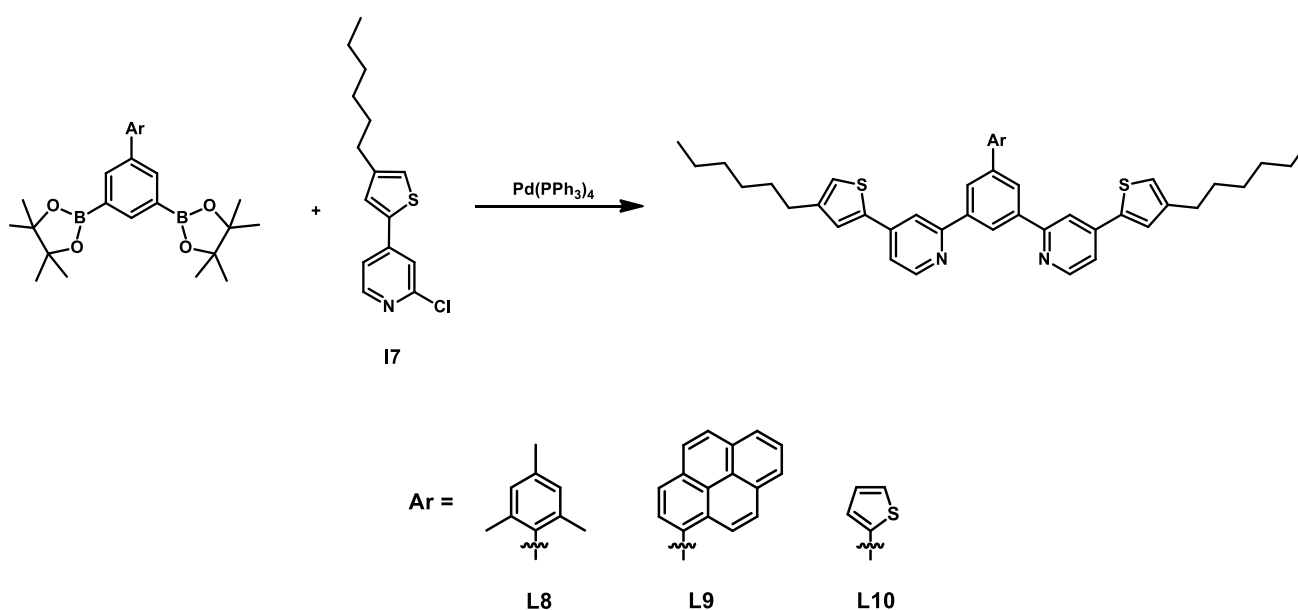


Figure 61. Synthesis of ligands **L8-L10**.

3.3.2 Synthesis of ligand L11

Ligand L11 was obtained by reacting B5 with I7, as reported in Figure 62.

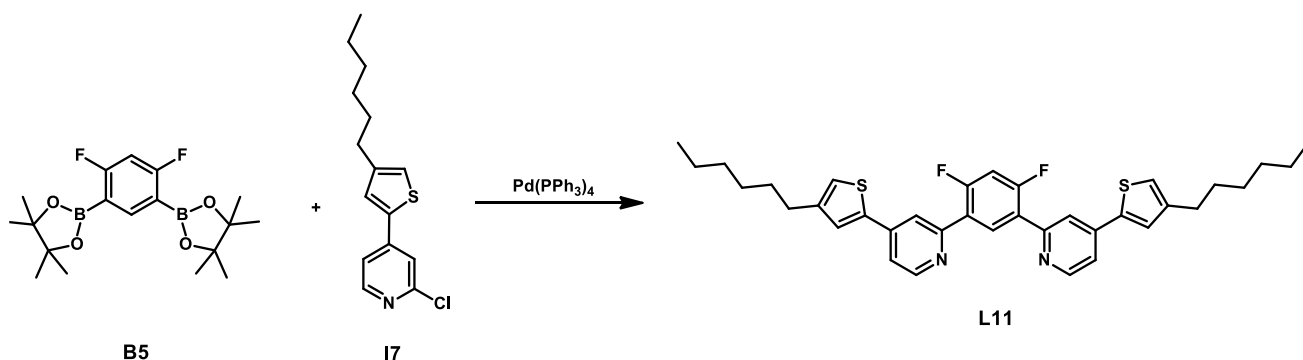


Figure 62. Synthesis of ligand L11.

3.3.3 Synthesis of ligands L12-L13

Through the same procedure presented for ligands L8-L10 (Figure 61), also compounds L12 and L13 were obtained, by using intermediate I8 together with boronic esters B1 and B2 (Figure 63).

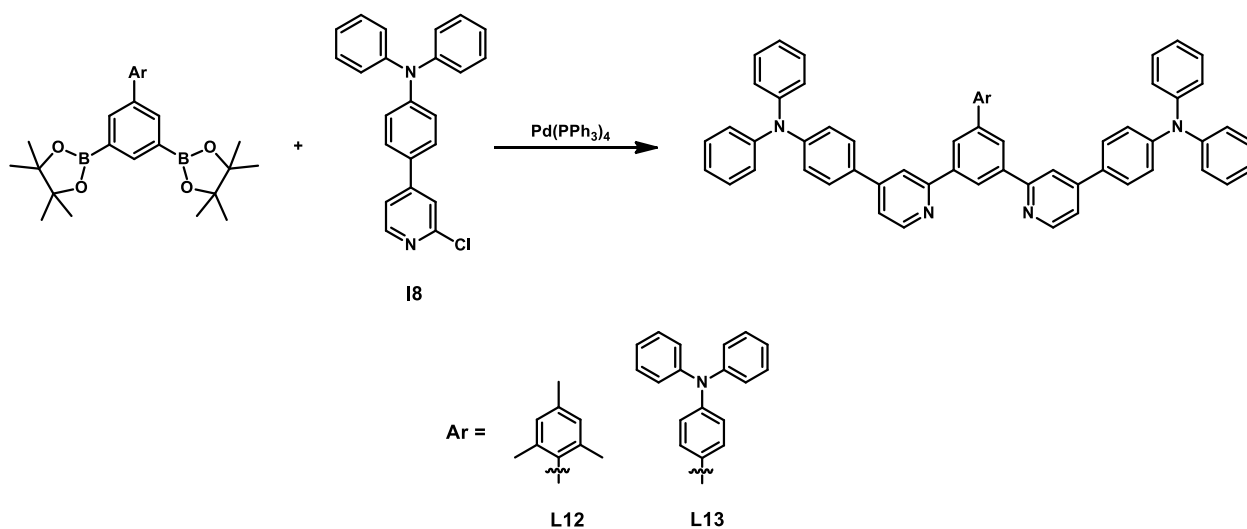


Figure 63. Synthesis of ligands L12-L13.

3.4 Synthesis of complexes PtCl8-PtCl13

The synthesis of the corresponding platinum(II) complexes was the same for all ligands **L8-L13** and involved the reaction with K_2PtCl_4 in glacial acetic acid at reflux under argon atmosphere, as discussed for compounds **PtCl1-PtCl7** (Figure 49).

3.4.1 Synthesis of complexes PtCl8-PtCl10

The synthesis of complexes **PtCl8-PtCl10** is presented in Figure 64.

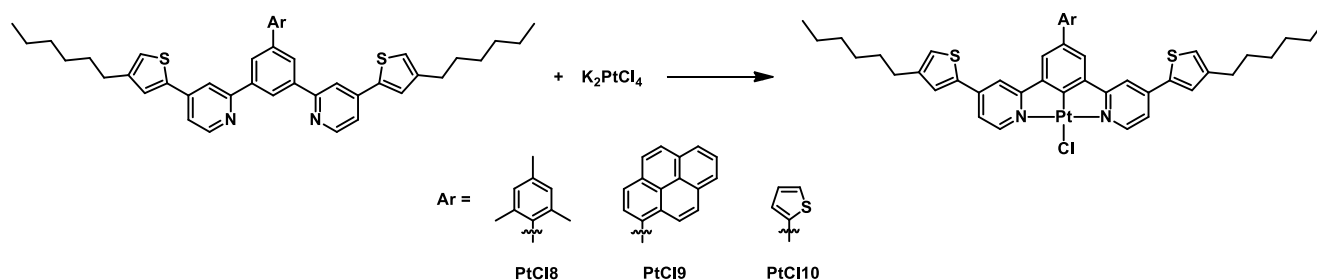


Figure 64. Synthesis of complexes **PtCl8-PtCl10**, starting from ligands **L8-L10**.

3.4.2 Synthesis of complex PtCl11

Complex **PtCl11** was obtained from ligand **L11**, as shown in Figure 65.

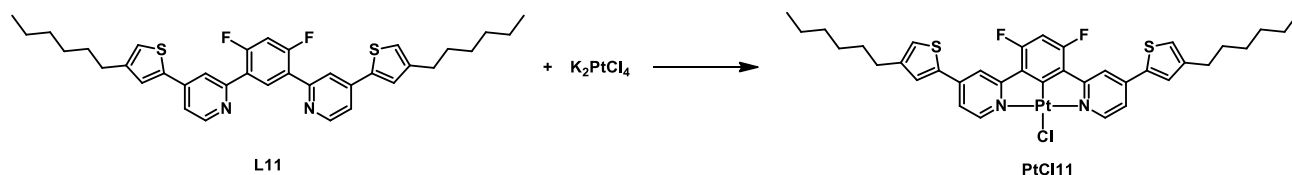


Figure 65. Synthesis of complex **PtCl11**, starting from ligand **L11**.

3.4.3 Synthesis of complexes PtCl12-PtCl13

Figure 66 reports the synthesis of complexes **PtCl12** and **PtCl13** from the corresponding ligands **L12** and **L13**.

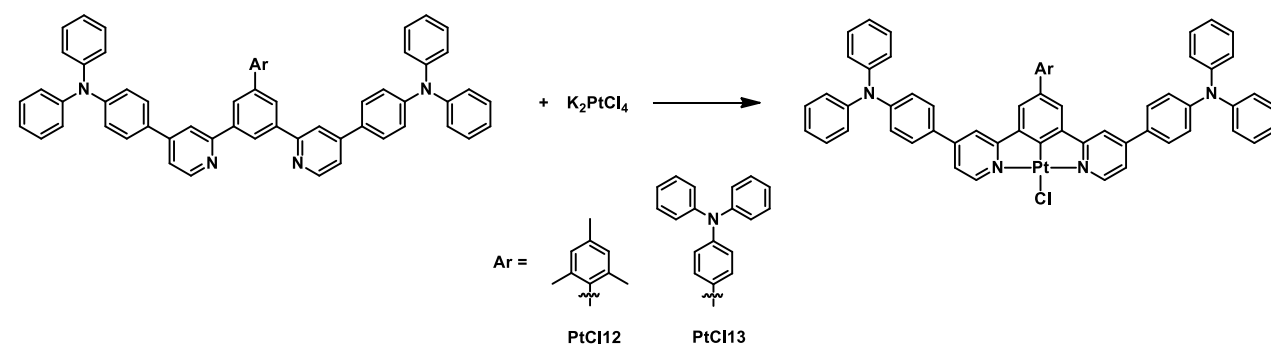


Figure 66. Synthesis of complexes **PtCl12** and **PtCl13**, starting from ligands **L12** and **L13**.

IV – CHARACTERIZATION OF THE COMPLEXES

1. General comments

The new platinum(II) complexes were characterized from the photophysical point of view by means of different techniques.

For a complete photophysical characterization, at first the UV-Visible absorption spectra were recorded, followed by emission and excitation spectra and by measurements of the absolute Quantum Yield (QY) and of the lifetimes.

Luminescence measurements were carried out after three Freeze-Pump-Thaw (FPT) cycles, necessary to remove the oxygen present in the cuvette and in solution, as explained in **Chapter I – Section 1.4**.

The performed measurements will be presented in the following sections, together with a description of the employed instruments.

Luminescence data (*i.e.* emission wavelengths, Quantum Yields and lifetimes) for the already published complexes **PtCl1-PtCl2** and **PtCl6-PtCl7** were taken from literature [63–65] and listed in **Table 7** for a comparison with the new compounds. Among the presented Pt(II) complexes, up to now compounds **Pt1-Pt3**, **Pt5**, **Pt7-Pt10**, **Pt12-Pt14**, **PtCl8**, **PtCl10**, **PtCl12** and **PtCl13** have been studied from the luminescence point of view. The photophysical analysis of the other complexes will be carried out in the near future.

1.1 UV-Vis absorption spectra and molar extinction coefficients

For all complexes, the UV-Vis absorption spectra at different concentrations were registered with a Shimadzu UV3600 spectrophotometer, using quartz cuvettes with 1 cm optical path length.

Dichloromethane solutions at different concentrations were prepared, in order to calculate the molar extinction coefficients (ϵ) for wavelengths corresponding to the absorption maxima.

1.2 Excitation and emission measurements

The excitation and emission spectra of the Pt complexes were registered from dichloromethane solutions after three Freeze-Pump-Thaw (FPT) cycles, using a FLS980 spectrofluorimeter (Edinburg Instrument Ltd); emission spectra were corrected for background intensity and quantum efficiency of the photomultiplier tube, while excitation spectra were corrected for the intensity fluctuation of the 450 W Xenon arc lamp.

As already mentioned, the FPT procedure was necessary to remove the oxygen dissolved in the solution and present in the cuvette, since O₂ can efficiently quench the emission coming from the excited triplet states of the Pt(II) complexes; since these excited states are long-living and dioxygen molecule has a triplet fundamental state, the energy from the NCN complex can be easily transferred to O₂, being lost without emission of radiation.

For each mentioned complex, an excitation and an emission spectrum are reported for both a dilute and a concentrated dichloromethane solution; the dilute solution is in the range $1 \cdot 10^{-6}$ – $5 \cdot 10^{-6}$ M, while the concentrated one in the range $6 \cdot 10^{-5}$ – $2 \cdot 10^{-4}$ M.

The concentrations were not always the same since different aspects had to be taken into account for each compound, as a consequence of the specific behavior and features of the complex molecules in solution.

In the case of the dilute solution, the chosen concentration not only had to ensure the detection of just the monomeric species, but had to be chosen also on the basis of the corresponding absorbance value; in fact, the absorbance of the solution employed for the determination of the absolute QY must be in the proper range (not exceeding 0.1, but also not being too low for the detection limit of the instrument) to have a meaningful value without notable errors coming from an incorrect measurement procedure.

Concerning the concentrated solutions, the concentration was the result of a balance between the minimum amount necessary to appropriately observe the aggregate species and the solubility limit of each complex. Moreover, even for the compounds characterized by a very high solubility in dichloromethane, too high concentrations were not employed, since the undesirable *inner filter effect* could be present and could lead to difficulties in the registration of valid spectra.

The so-called inner filter effect is a phenomenon arising from the fact that the radiation emitted from the first thin layers of solution is then re-absorbed by the other complex molecules in the cuvette, preventing the possibility to register a valid spectrum since only a limited amount of emitted light reaches the detector. This effect causes the deviation of the excitation spectra of the concentrated solutions with respect to the UV-Vis absorption spectra. When possible, a cuvette with an optical path length of only 2 mm was employed, but in that case without the possibility to perform the FPT cycles.

For all studied complexes, even if with different intensity, the presence of aggregate species (leading to the appearance of a new emissive band at longer wavelengths) could be clearly observed when a concentrated solution was analyzed. Depending on the molecular structure, and consequently on the ease to form aggregates (whose structure and origin are yet unclear), the intensity of the emission at lower energy could appear predominant with respect to the monomer emission.

The identification of the multinuclear species as aggregates was due to the evidence that the excitation spectra of the complexes varied depending on the exciting wavelength, this not being possible for excimers since that kind of dimeric species do not exist as fundamental state and therefore cannot be excited and give different spectra when different exciting energies are employed.

Nevertheless the presence of excimers, and consequently their contribution to the luminescence results, could be excluded, even if these species did not appear to be the predominant ones.

The emission region and the radiative features of the complexes will be discussed in the following sections.

1.3 Absolute Quantum Yield measurements

Absolute photoluminescence Quantum Yields (Φ_{lum}) were measured using a C11347 Quantaaurus Hamamatsu Photonics K.K spectrometer equipped with a 150 W Xenon lamp, an integrating sphere and a multichannel detector, both before and after the FPT cycles.

Φ_{lum} was calculated according to the following equation:

$$\Phi = \frac{PN(em)}{PN(abs)} = \frac{\int \frac{\lambda}{hc} [I_{em}^{sample}(\lambda) - I_{em}^{ref}(\lambda)] d\lambda}{\int \frac{\lambda}{hc} [I_{exc}^{sample}(\lambda) - I_{exc}^{ref}(\lambda)] d\lambda}$$

where $PN(em)$ is the number of emitted photons, $PN(abs)$ the number of absorbed photons, λ is the wavelength, h the Planck's constant, c the speed of light; I_{em}^{sample} and I_{em}^{ref} represent the photoluminescence intensities of the sample solution and of the pure CH_2Cl_2 used as reference, respectively, while I_{exc}^{sample} and I_{exc}^{ref} are the excitation light intensities of the sample solution and reference in dichloromethane. The error made was estimated at around 5%.

Table 6 resumes the values of Quantum Yield and lifetimes for complexes **Pt1-Pt3**, **Pt5**, **Pt7-Pt10**, **Pt12-Pt14**, with a dilute and a concentrated dichloromethane solution for each new compound. In the case of the absolute QY, the measure was performed both before and after the Freeze-Pump-Thaw procedure, to have a comparison between the data collected in the presence and in the absence of O_2 .

From the reported data, it can be observed that the Quantum Yield is characterized by a strong dependence on both the presence of oxygen and the concentration of the solution under study, since the formation of aggregates at higher concentrations causes a quenching of the emission.

As an illustrative example, **Figure 67** shows the QY values of complex **Pt1** at different intermediate concentrations, both before and after the FPT cycles: as a matter of fact, a dramatic decrease of the emission Quantum Yield is caused by the increase of concentration. This aggregation-caused quenching can be mainly attributed by the low-lying excited state of the aggregate species, favoring non-radiative decays according to the energy gap law (**Chapter I – Section 1.2**).

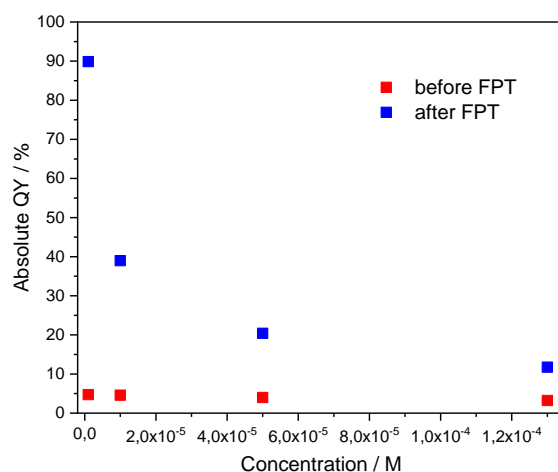


Figure 67. Absolute QY vs Concentration for dichloromethane solutions of **Pt1** at different concentrations.

A similar remarkable difference will be found also for lifetime values: the efficient quenching caused by the appearance of aggregates reduced the lifetime of the excited state, leading to an important decrease of the mentioned values.

1.4 Lifetime measurements

Time-resolved fluorescence data were obtained using a FLS980 spectrofluorometer (Edinburg Instrument Ltd) through the Time-Correlated Single Photon Counting (TCSPC) technique.

TCSPC is a common statistical technique employed to measure luminescence decays in the time domain. The sample is excited by a pulsed laser source with a high repetition rate, the time measure is started by the signal pulse and is then stopped by the arrival of the photon emitted by the sample. By counting many events, a histogram of the photon distribution over time is achieved. In order to have meaningful lifetime values, only a small fraction (generally <5%) of the emitted pulses must reach the sample, so that a maximum of one emitted photon is detected at a time; this is required since the simultaneous arrival of multiple photons would cause an important error in the attribution of the signal to the correct time slot: if for example two photons arrive at the detector in a short time range, the first one stops the time measurement, so that the second photon is not detected and an accumulation of low-time photons is produced, while many photons at larger times are neglected.

After the measurement, time-resolved fluorescence curves were reconvoluted using the following multi-exponential impulse response function:

$$I(\lambda, t) = \sum_{i=1}^n \alpha_i(\lambda) \exp\left(\frac{-t}{\tau_i}\right)$$

where n is the number of exponentials, $\alpha_i(\lambda)$ is the amplitude at wavelength λ and τ_i is the lifetime of the component i . The quality of the fit was evaluated through the reduced χ^2 values.

All registered decay graphs are reported in the **Appendix**.

2. Photophysical characterization of complexes PtCl1-PtCl7

In this section only UV-Vis spectra and molar extinction coefficients for complexes **PtCl3-PtCl5** are presented, since luminescence measurements for these compounds have still to be carried out. Emission maxima for **PtCl1-PtCl2** and **PtCl6-PtCl7**, together with Quantum Yield and lifetime values, are reported in **Table 7**, to give a comparison with the complexes derived from them by substitution of the chloride ligand.

2.1 UV-Vis absorption spectra of complexes PtCl3-PtCl5

Figures 68-70 report the UV-Visible absorption spectra of complexes **PtCl3-PtCl5**. Compounds **PtCl1-PtCl2** and **PtCl6-PtCl7** were already known in literature [63–65] and correspond to compounds **5**, **10**, **8** and **3**, respectively (**Figure 21**).

In the case of **PtCl3**, a small amount of DMSO (4% v/v) was added to the CH_2Cl_2 in order to fully dissolve the compound.

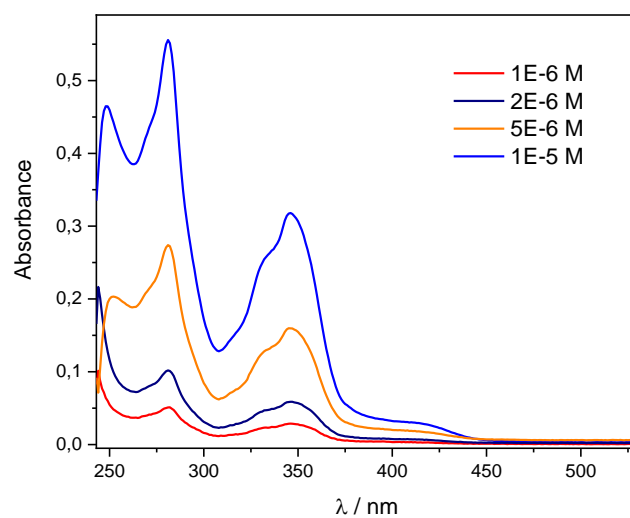


Figure 68. UV-Vis absorption spectra of complex **PtCl₃** in CH₂Cl₂ (containing 4% DMSO) at different concentrations.

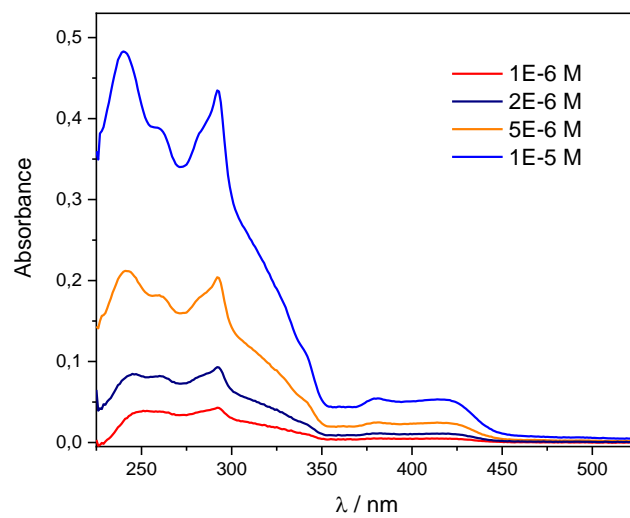


Figure 69. UV-Vis absorption spectra of complex **PtCl₄** in CH₂Cl₂ at different concentrations.

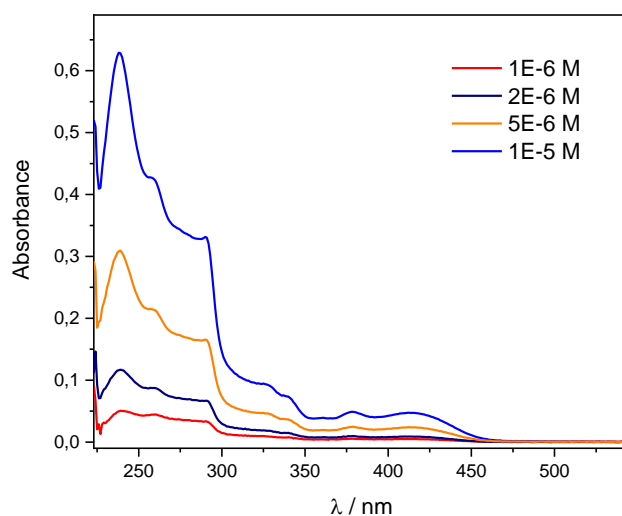
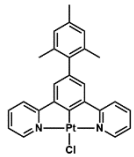
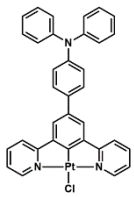
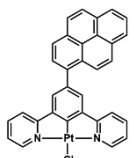
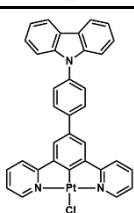


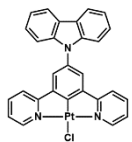
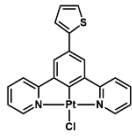
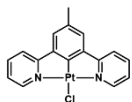
Figure 70. UV-Vis absorption spectra of complex **PtCl5** in CH_2Cl_2 at different concentrations.

2.2 Molar extinction coefficients of complexes PtCl1-PtCl7

Table 3 resumes the molar extinction coefficients (ϵ) for the absorption maxima of complexes **PtCl1-PtCl7**. Data for **PtCl1-PtCl2** and **PtCl6-PtCl7** are taken from literature.

Table 3. Absorption maxima and corresponding molar extinction coefficients for complexes **PtCl1-PtCl7**.

Complex		$\lambda_{\text{max, abs}} / \text{nm}$	$\epsilon / (10^3 \text{ cm}^{-1} \text{ M}^{-1})$
	PtCl1 ^a	332	5.6
		363	3.8
		381	5.4
		410	5.2
	PtCl2 ^b	380	7.2
		422	7.2
	PtCl3	250	48.6
		281	53.1
		346	31.9
	PtCl4	240	50.5
		292	43.1
		379	6.0
		420	5.8

Complex	$\lambda_{\text{max, abs}} / \text{nm}$	$\epsilon / (10^3 \text{ cm}^{-1} \text{ M}^{-1})$
	238	64.3
	290	34.9
	379	5.2
	413	5.1
	363	3.3
	380	4.7
	426	5.1
	335	5.7
	381	6.9
	412	6.8

^a From ref. [64]; ^b from ref. [65].

3. Photophysical characterization of complexes Pt1-Pt15

For all complexes **Pt1-Pt15** the UV-Vis spectra are reported in this section, together with the corresponding molar extinction coefficients. For compounds **Pt1-Pt3**, **Pt5**, **Pt7-Pt10** and **Pt12-Pt14**, also the complete luminescence data are listed in this section.

Compound **Pt6** was already known [101] and corresponds to compound **102** (Figure 36).

3.1 UV-Vis absorption spectra of complexes Pt1-Pt15

Figures 71-85 show the UV-Visible absorption spectra of complexes **Pt1-Pt15**.

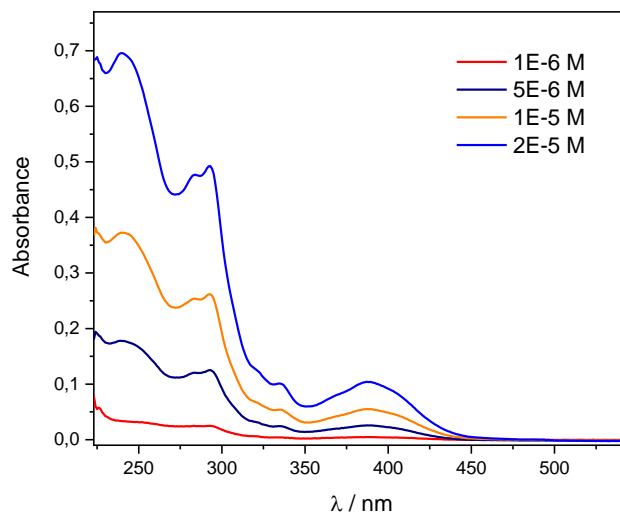


Figure 71. UV-Vis absorption spectra of complex **Pt1** in CH_2Cl_2 at different concentrations.

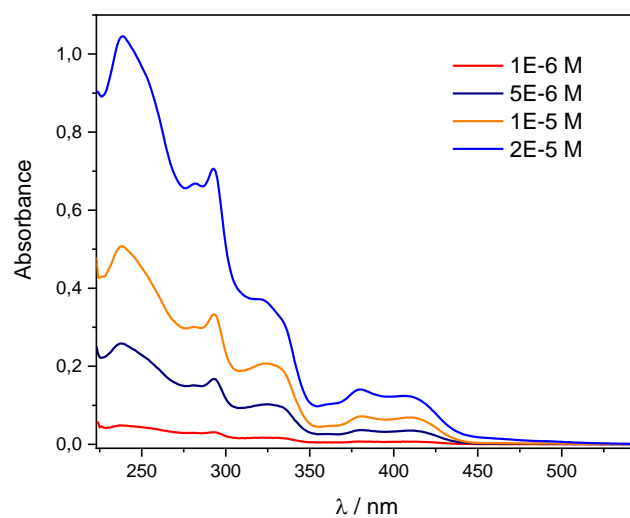


Figure 72. UV-Vis absorption spectra of complex **Pt2** in CH_2Cl_2 at different concentrations.

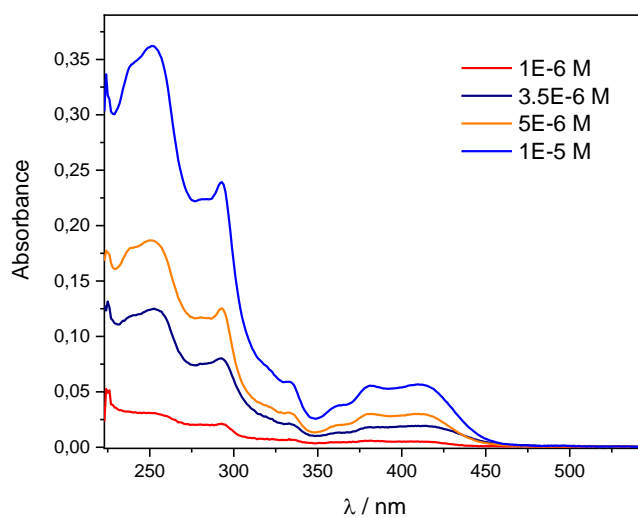


Figure 73. UV-Vis absorption spectra of complex **Pt3** in CH_2Cl_2 at different concentrations.

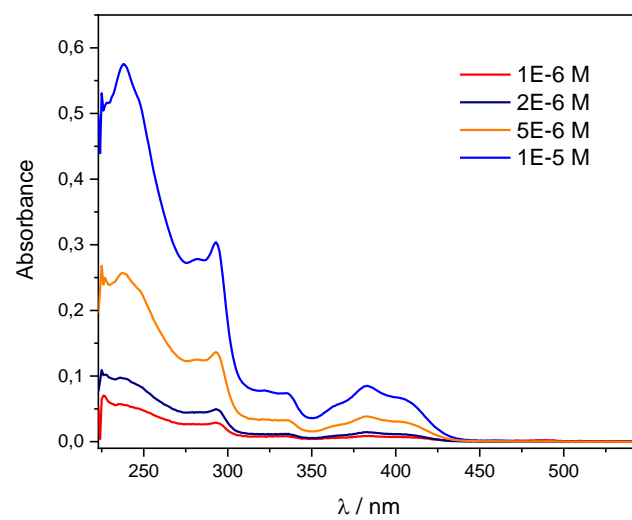


Figure 74. UV-Vis absorption spectra of complex **Pt4** in CH_2Cl_2 at different concentrations.

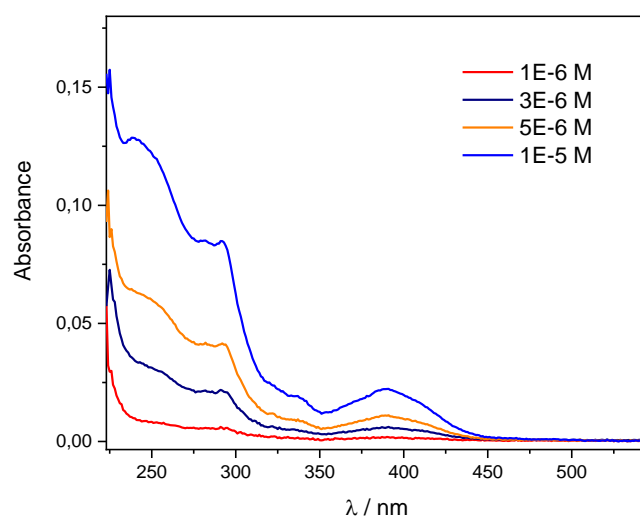


Figure 75. UV-Vis absorption spectra of complex **Pt5** in CH_2Cl_2 at different concentrations.

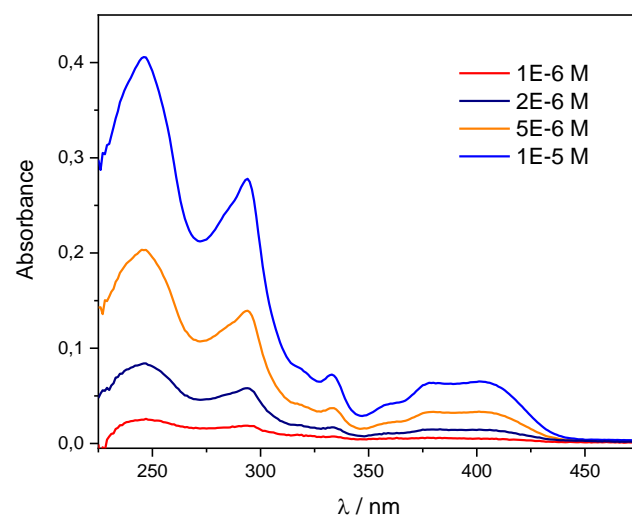


Figure 76. UV-Vis absorption spectra of complex **Pt6** in CH_2Cl_2 at different concentrations.

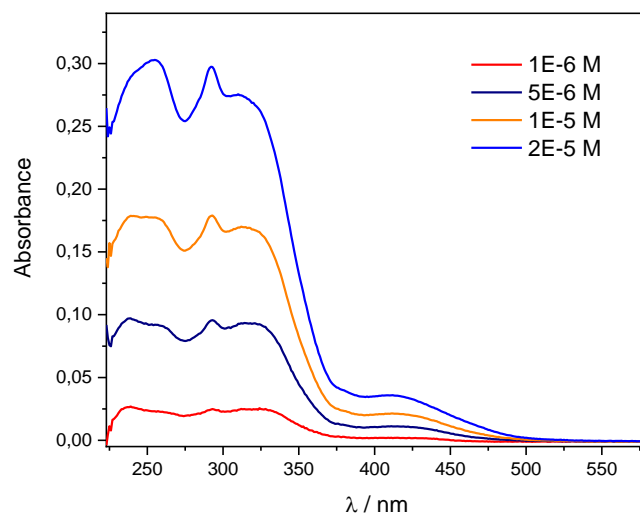


Figure 77. UV-Vis absorption spectra of complex **Pt7** in CH_2Cl_2 at different concentrations.

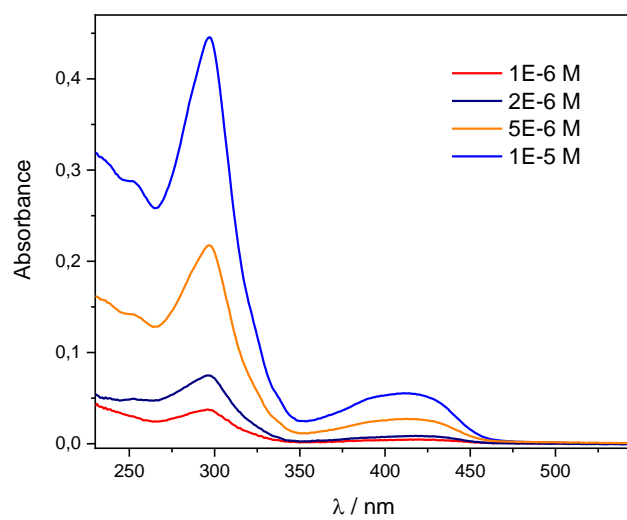


Figure 78. UV-Vis absorption spectra of complex **Pt8** in CH_2Cl_2 at different concentrations.

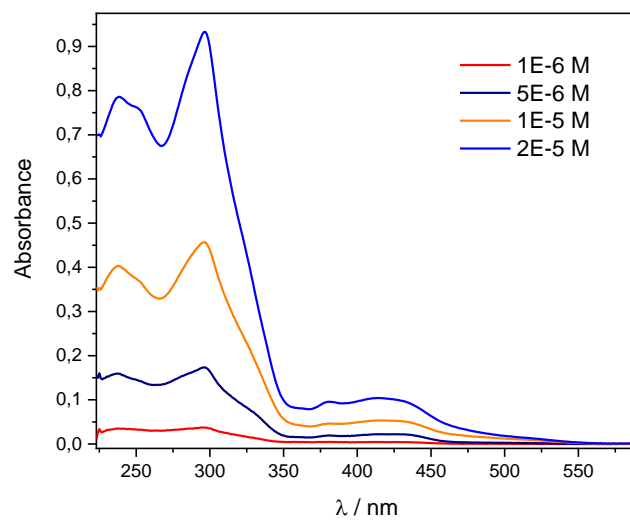


Figure 79. UV-Vis absorption spectra of complex **Pt9** in CH_2Cl_2 at different concentrations.

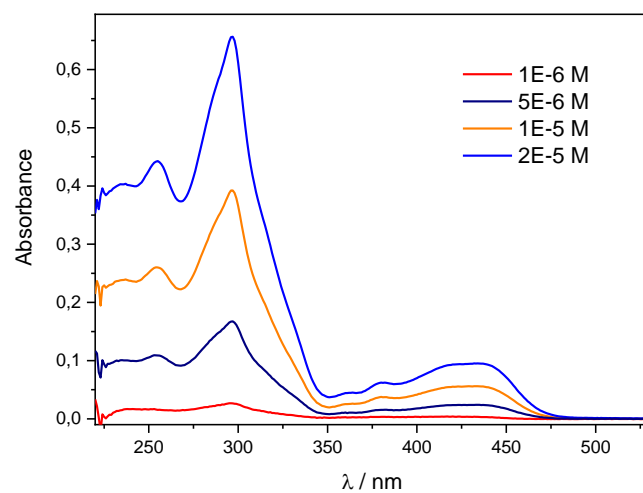


Figure 80. UV-Vis absorption spectra of complex **Pt10** in CH_2Cl_2 at different concentrations.

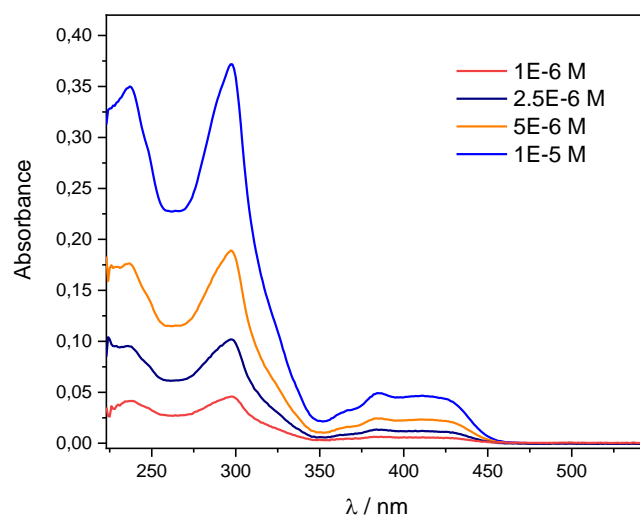


Figure 81. UV-Vis absorption spectra of complex **Pt11** in CH_2Cl_2 at different concentrations.

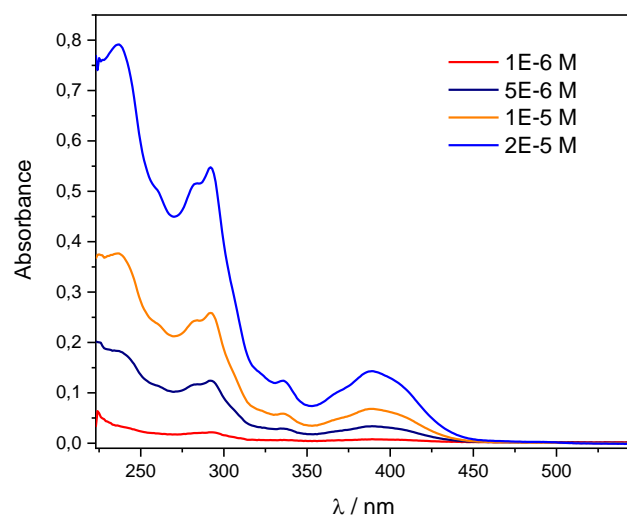


Figure 82. UV-Vis absorption spectra of complex **Pt12** in CH₂Cl₂ at different concentrations.

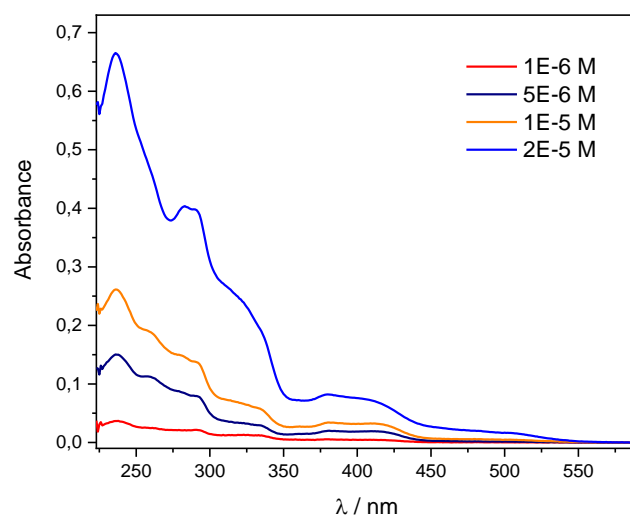


Figure 83. UV-Vis absorption spectra of complex **Pt13** in CH₂Cl₂ at different concentrations.

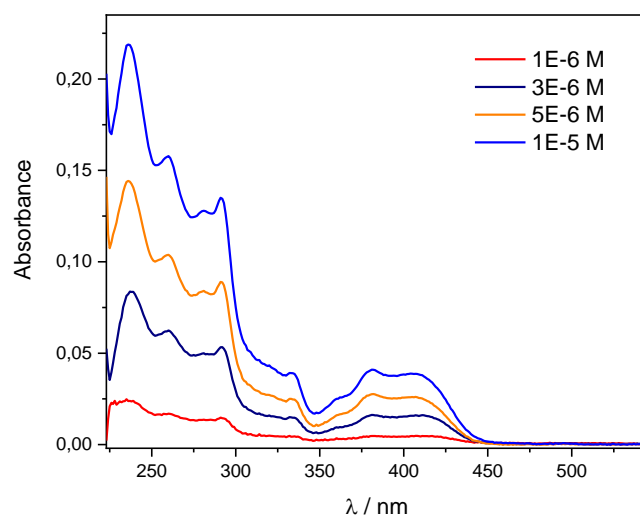


Figure 84. UV-Vis absorption spectra of complex **Pt14** in CH₂Cl₂ at different concentrations.

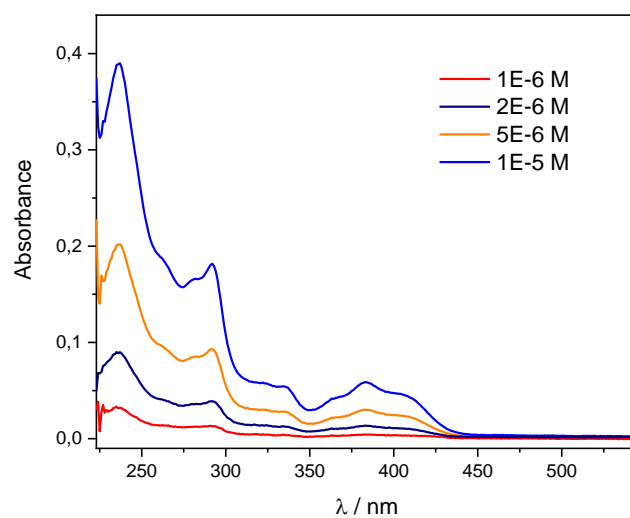
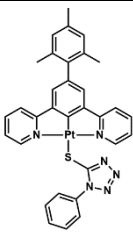
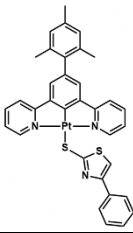
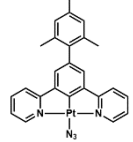
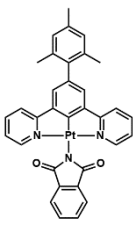
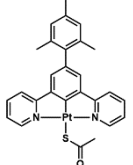
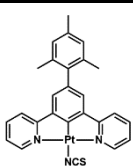
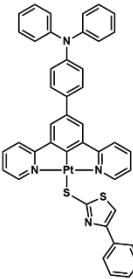


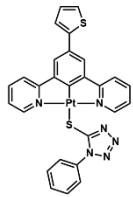
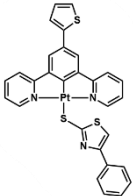
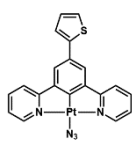
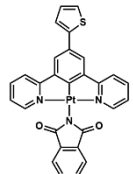
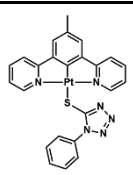
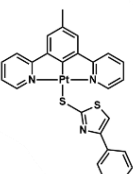
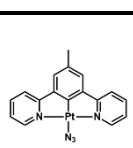
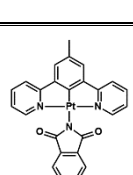
Figure 85. UV-Vis absorption spectra of complex **Pt15** in CH₂Cl₂ at different concentrations.

3.2 Molar extinction coefficients of complexes Pt1-Pt15

Table 4 resumes the molar extinction coefficients for the absorption maxima of complexes Pt1-Pt15.

Table 4. Absorption maxima and corresponding molar extinction coefficients for complexes Pt1-Pt15.

Complex	$\lambda_{\text{max, abs}} / \text{nm}$	$\epsilon / (10^3 \text{ cm}^{-1} \text{ M}^{-1})$
	Pt1 240 293 389	34.9 24.6 5.2
	Pt2 238 293 380 408	52.4 35.5 7.0 6.1
	Pt3 251 293 381 412	36.8 24.3 5.6 5.7
	Pt4 238 293 383	58.2 30.8 8.6
	Pt5 292 391	8.4 2.2
	Pt6 246 294 333 380 402	41.5 28.6 7.3 6.6 6.5
	Pt7 253 292 408	14.6 14.2 1.7

Complex	$\lambda_{\text{max, abs}} / \text{nm}$	$\epsilon / (10^3 \text{ cm}^{-1} \text{ M}^{-1})$
	Pt8 232 297 411	31.9 47.1 6.1
	Pt9 238 297 381 415	40.1 48.5 4.9 5.3
	Pt10 255 297 381 436	27.2 39.9 3.9 6.3
	Pt11 237 297 384 412	34.2 36.2 4.7 4.5
	Pt12 237 292 389	40.0 27.8 7.3
	Pt13 236 283 380 410	33.4 20.4 4.1 3.5
	Pt14 236 260 291 381 407	30.1 21.7 18.5 5.7 5.3
	Pt15 237 292 383	39.0 18.9 6.2

3.3 Excitation and emission spectra of complexes Pt1-Pt15

For each of the studied compounds (**Pt1-Pt3**, **Pt5**, **Pt7-Pt10**, **Pt12-Pt14**) representative excitation and emission spectra are reported in **Figures 86-96**, for a dilute and a concentrated solution in dichloromethane, after the FPT procedure.

Emission maxima for the mentioned complexes, with the values corresponding to both the monomeric species and the related aggregates appearing at higher concentrations, are listed in **Table 5**.

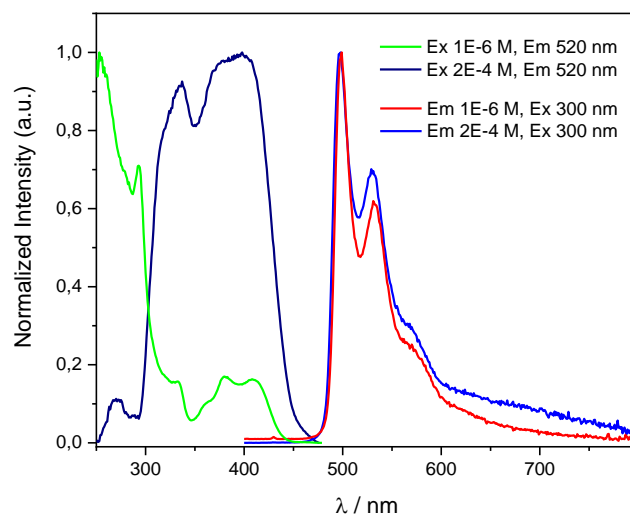


Figure 86. Normalized excitation and emission spectra of a dilute ($1 \cdot 10^{-6}$ M) and a concentrated ($2 \cdot 10^{-4}$ M) solution of complex **Pt1** in CH_2Cl_2 , after three Freeze-Pump-Thaw cycles

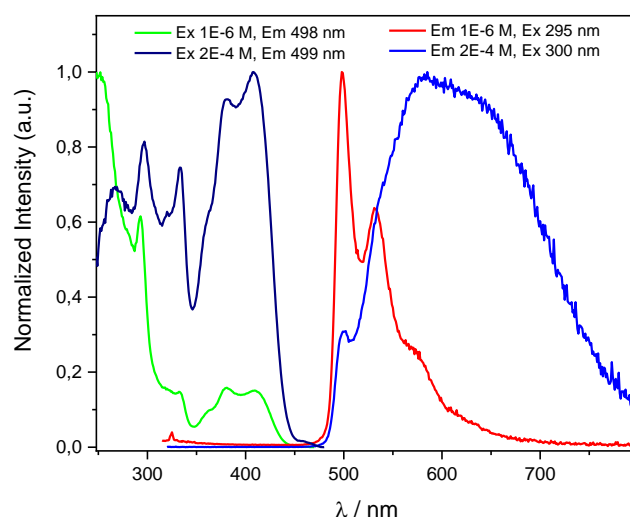


Figure 87. Normalized excitation and emission spectra of a dilute ($1 \cdot 10^{-6}$ M) and a concentrated ($2 \cdot 10^{-4}$ M) solution of complex **Pt2** in CH_2Cl_2 , after three Freeze-Pump-Thaw cycles.

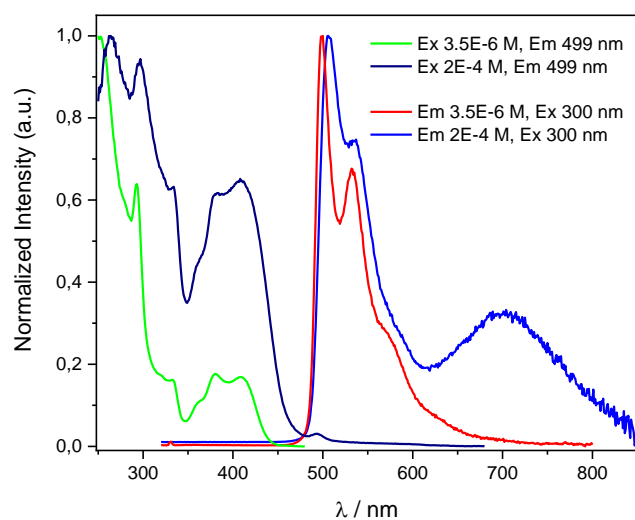


Figure 88. Normalized excitation and emission spectra of a dilute ($3.5 \cdot 10^{-6}$ M) and a concentrated ($2 \cdot 10^{-4}$ M) solution of complex **Pt3** in CH_2Cl_2 , after three Freeze-Pump-Thaw cycles.

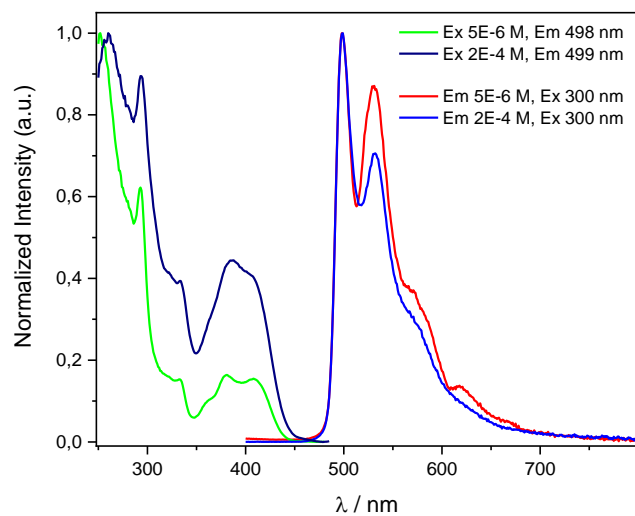


Figure 89. Normalized excitation and emission spectra of a dilute ($5 \cdot 10^{-6}$ M) and a concentrated ($2 \cdot 10^{-4}$ M) solution of complex **Pt5** in CH_2Cl_2 , after three Freeze-Pump-Thaw cycles.

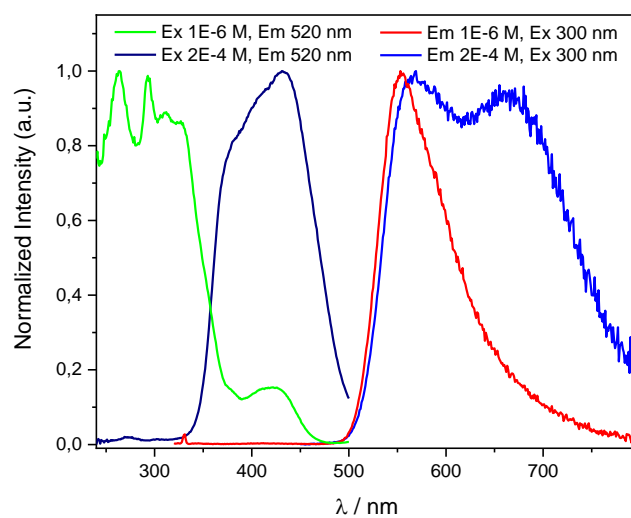


Figure 90. Normalized excitation and emission spectra of a dilute ($1 \cdot 10^{-6}$ M) and a concentrated ($2 \cdot 10^{-4}$ M) solution of complex **Pt7** in CH_2Cl_2 , after three Freeze-Pump-Thaw cycles.

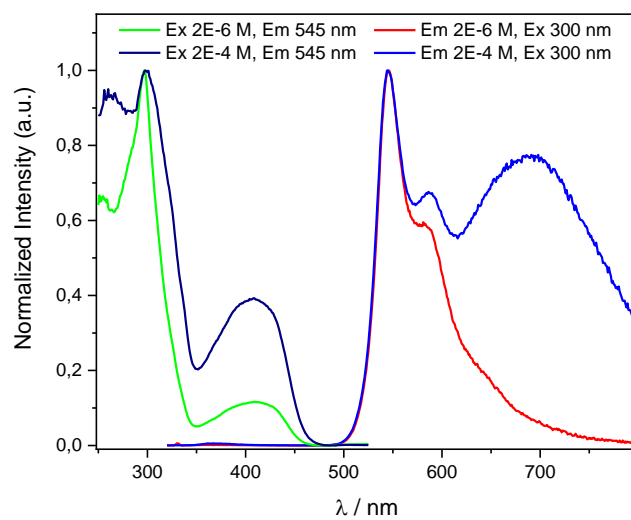


Figure 91. Normalized excitation and emission spectra of a dilute ($2 \cdot 10^{-6}$ M) and a concentrated ($2 \cdot 10^{-4}$ M) solution of complex **Pt8** in CH_2Cl_2 , after three Freeze-Pump-Thaw cycles.

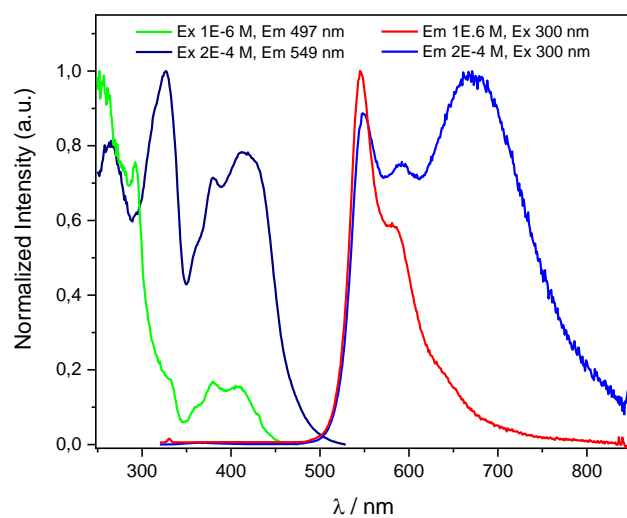


Figure 92. Normalized excitation and emission spectra of a dilute ($1 \cdot 10^{-6}$ M) and a concentrated ($2 \cdot 10^{-4}$ M) solution of complex **Pt9** in CH_2Cl_2 , after three Freeze-Pump-Thaw cycles.

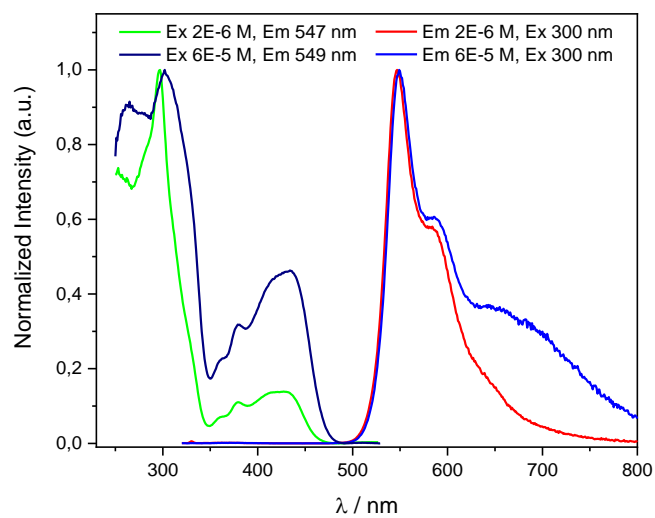


Figure 93. Normalized excitation and emission spectra of a dilute ($2 \cdot 10^{-6}$ M) and a concentrated ($6 \cdot 10^{-5}$ M) solution of complex **Pt10** in CH_2Cl_2 , after three Freeze-Pump-Thaw cycles.

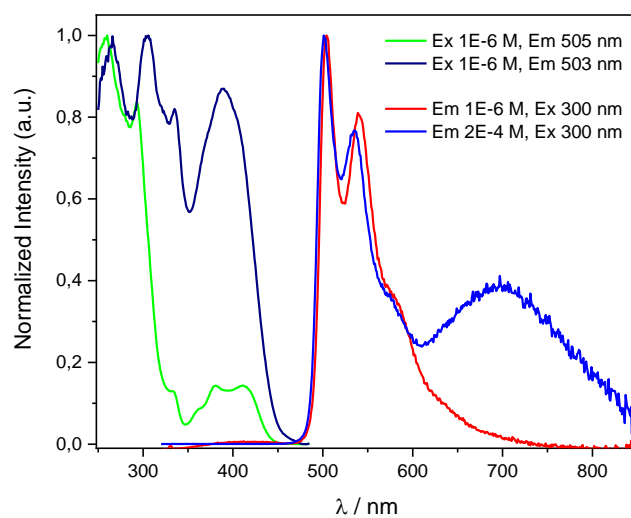


Figure 94. Normalized excitation and emission spectra of a dilute ($1 \cdot 10^{-6}$ M) and a concentrated ($2 \cdot 10^{-4}$ M) solution of complex **Pt12** in CH_2Cl_2 , after three Freeze-Pump-Thaw cycles.

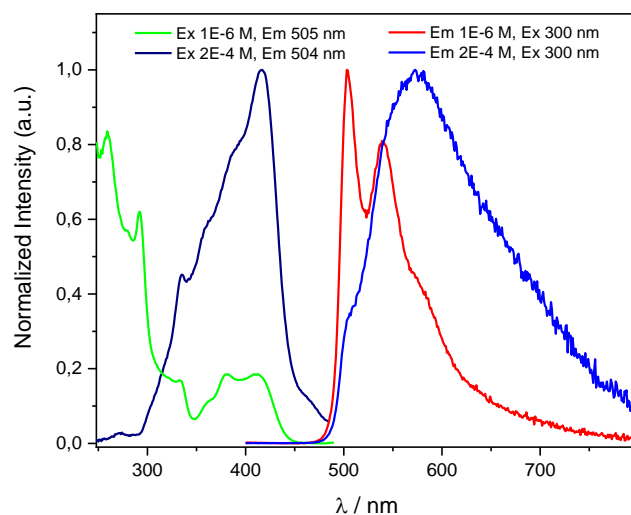


Figure 95. Normalized excitation and emission spectra of a dilute ($1 \cdot 10^{-6}$ M) and a concentrated ($2 \cdot 10^{-4}$ M) solution of complex **Pt13** in CH_2Cl_2 , after three Freeze-Pump-Thaw cycles.

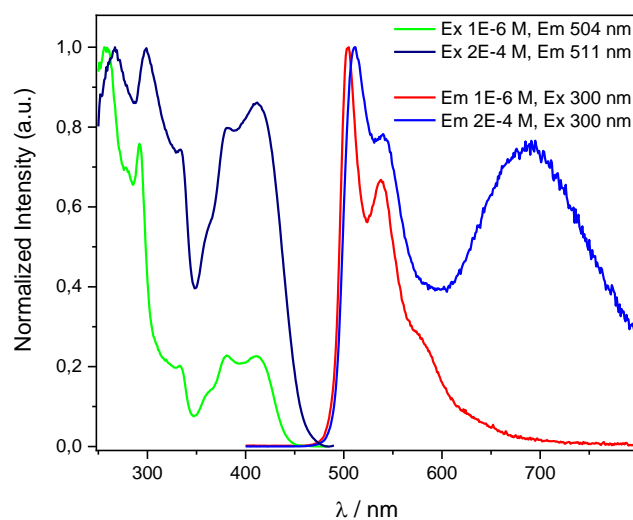
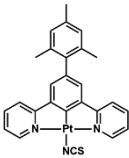
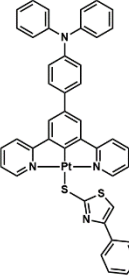
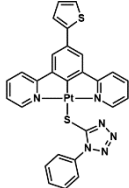
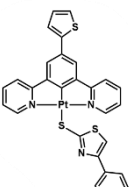
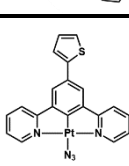
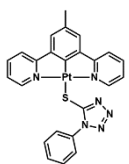
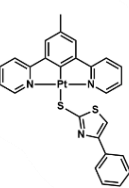
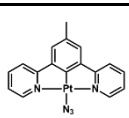


Figure 96. Normalized excitation and emission spectra of a dilute ($1 \cdot 10^{-6}$ M) and a concentrated ($2 \cdot 10^{-4}$ M) solution of complex **Pt14** in CH_2Cl_2 , after three Freeze-Pump-Thaw cycles.

Table 5. Emission maxima for complexes **Pt1-Pt3**, **Pt5**, **Pt7-Pt10**, **Pt12-Pt14**, for both the monomer and the aggregates.

Complex	$\lambda_{\text{max, em}} / \text{nm}$ (monomer)	$\lambda_{\text{max, em}} / \text{nm}$ (aggregates)
	498 531	~650
	498 531	~667
	500 532	~703
	499 532	~670

Complex	$\lambda_{\text{max, em}} / \text{nm}$ (monomer)	$\lambda_{\text{max, em}} / \text{nm}$ (aggregates)
	Pt6^a	496 530 ~670
	Pt7	556 ~681
	Pt8	545 583 ~661
	Pt9	545 582 ~684
	Pt10	547 582 ~660
	Pt12	504 540 ~663
	Pt13	503 539 ~683
	Pt14	504 538 ~671

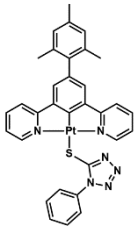
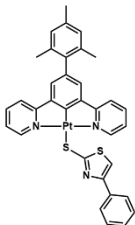
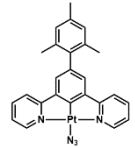
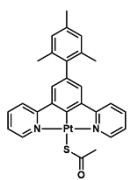
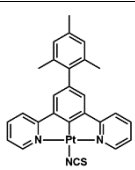
^aData from ref [101].

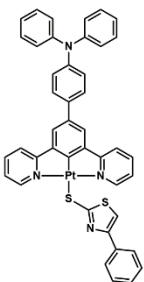
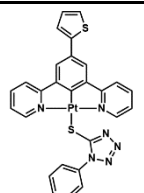
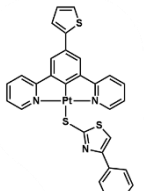
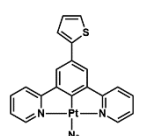
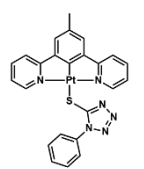
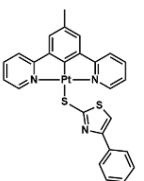
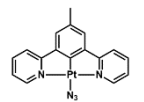
3.4 Absolute Quantum Yields and lifetimes

In **Table 6** all data about the absolute Quantum Yields are listed, for a dilute and a concentrated dichloromethane solution, both before and after the FPT procedure. Lifetime values are also reported, with the employed excitation and emission wavelength; in the case of non-monoexponential decays, the percentage relative to the different contributions is indicated.

Complete graphs about the excited state decay are reported in the **Appendix**.

Table 6. Quantum Yield and lifetime values for complexes **Pt1-Pt3, Pt5, Pt7-Pt10, Pt12-Pt14**.

Complex	c / M	QY _{after} (QY _{before})	τ / μ s	$\lambda_{ex}, \lambda_{em}$ / nm
	1·10 ⁻⁶	90% (5%)	7.39	374, 498
	2·10 ⁻⁴	12% (3%)	0.73 (72.11%) 2.43 (27.89%)	374, 498
	1·10 ⁻⁶	54.6% (3.5%)	7.7 7.5	374, 498 374, 532
	2·10 ⁻⁴	15.3% (3.1%)	1.1	374, 498
			0.31 (27.8%) 1.38 (72.2%)	374, 659
			0.33 (22.8%) 1.25 (77.2%)	442, 498
			0.28 (15.2%) 1.26 (84.8%)	442, 659
		3.5·10 ⁻⁶	86.5% (5.7%)	7.48
2.4·10 ⁻⁴		25.2% (3.0%)	1.38	374, 499
	5·10 ⁻⁶	22.2% (4.5%)	0.34 (2.1%) 7.61 (97.9%)	404, 498
			0.30 (2.7%) 7.97 (97.3%)	404, 620
	2·10 ⁻⁴	3.3% (1.4%)	0.24 (50.3%) 3.10 (49.7%)	404, 499
			0.24 (60.5%) 3.25 (39.5%)	404, 620
	-	60% (-)	8.6	374, 495

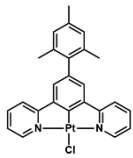
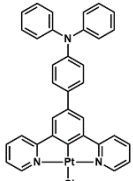
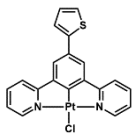
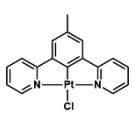
Complex	c / M	QY _{after} (QY _{before})	τ / μ s	$\lambda_{ex}, \lambda_{em}$ / nm
	1·10 ⁻⁶	69.0% (2.5%)	13.58	404, 520
			13.96	404, 555
			12.97	404, 663
	2·10 ⁻⁴	9.3% (2.0%)	0.38 (31.4%)	404, 520
			1.02 (68.6%)	
			0.42 (40.4%)	404, 550
1.08 (59.6%)				
0.23 (5.7%)			404, 670	
1.05 (94.3%)				
0.21 (4.7%)	442, 670			
1.05 (95.3%)				
	5·10 ⁻⁶	83.2% (3.0%)	19.16	404, 545
			19.04	404, 650
	2·10 ⁻⁴	18.5% (2.6%)	1.85	404, 545
			1.76	404, 650
	1·10 ⁻⁶	89.3% (3.0%)	19.09	374, 440
			19.20	374, 545
	2·10 ⁻⁴	9.5% (2.4%)	0.42 (26.4%)	440, 549
			1.28 (75.6%)	
0.29 (4.5%)	440, 670			
1.05 (95.5%)				
	2·10 ⁻⁶	78.5% (2.1%)	17.77	404, 547
			17.88	404, 586
	6·10 ⁻⁵	1.7%	6.58	404, 549
			6.80	404, 680
	5·10 ⁻⁶	41.6% (4.7%)	8.7	445, 505
			7.9	404, 505
	2·10 ⁻⁴	14% (2.2%)	0.72	404, 503
	1·10 ⁻⁶	65% (2.5%)	7.94	374, 495
			0.18 (10.9%)	374, 495
	0.69 (89.1%)			
	2·10 ⁻⁴	8.8% (2.1%)	0.27	442, 575
0.23 (24.2%)			442, 685	
0.82 (75.8%)				
	1·10 ⁻⁶	59.2% (4%)	8.07	374, 504
	2·10 ⁻⁴	18% (3%)	0.87	374, 495

^aData from ref. [101], missing values are not given in the paper.

3.5 Comparison with parent compounds PtCl1-PtCl2 and PtCl6-PtCl7

For comparison's sake, data of related parent NCN-PtCl compounds **PtCl1-PtCl2** and **PtCl6-PtCl7** are resumed in **Table 7**.

Table 7. Emission maxima, QY and lifetimes for complexes **PtCl1-PtCl2** and **PtCl6-PtCl7**; data are from reff. [64] and [65], and refer only to monomeric emission.

Complex	$\lambda_{\text{max, em}} / \text{nm}$ (monomer)	QY _{after} (QY _{before})	$\tau / \mu\text{s}$
	PtCl1 501 534	62% (4.5%)	7.9
	PtCl2 557	29% (-)	9.0
	PtCl6 505 539	54% (1.5%)	20.5
	PtCl7 548 584	68% (2.5%)	7.8

From data listed in **Tables 6-7**, it appears evident that the effect of the substitution of the chloride ligand with other anionic species does not bring about a variation in the emission wavelengths, since the emission maxima differ only for few nanometers (in any case the difference does not exceed 5 nm). As will be discussed later, the main effect was on the emission Quantum Yield.

The emission at lowest energy was provided by the thienyl-bearing NCN complexes, being around 40 nm more red-shifted with respect to the mesityl-, 4-NPh₂-phenyl- and methyl-substituted ones.

To have a better overview of the QY values, and to compare them with those of the parent complexes, data for dilute solutions were collected in a graph (**Figure 97**). The first column of each group stands for the Pt-Cl complex, with the values being taken from literature [63–65].

Considering the mesityl-bearing complexes, it is not possible to point out a general trend, since the replacement of the chloride ligand causes an important increase of the Quantum Yield only in the case of the phenyl-tetrazole-thiolate and of the azide (passing from 62% to 90% and 86.5%, respectively); the variation is limited in the case of the phenyl-thiazole-thiolate (54.6%) and of the isocyanate (60%), while a remarkable decrease is observed in the presence of the thioacetate (22.2%).

Moving to the 4-diphenylamino-phenyl moiety, the QY undergoes a large increase, passing from 29% to 69%; unfortunately, having only one example of such substitution of the ancillary ligand, no general conclusion can be achieved up to now.

Only in the case of the 2-thienyl substituent, for all derivatives **Pt8-Pt10** the Quantum Yield reaches very high values (up to 89.3%), so that the introduction of the aromatic thiolates and of the azide has a positive effect.

Finally, for the methyl group, the QY values do not change noticeably, remaining in the range 41-65% and without a large difference with respect to parent compound **PtCl7**.

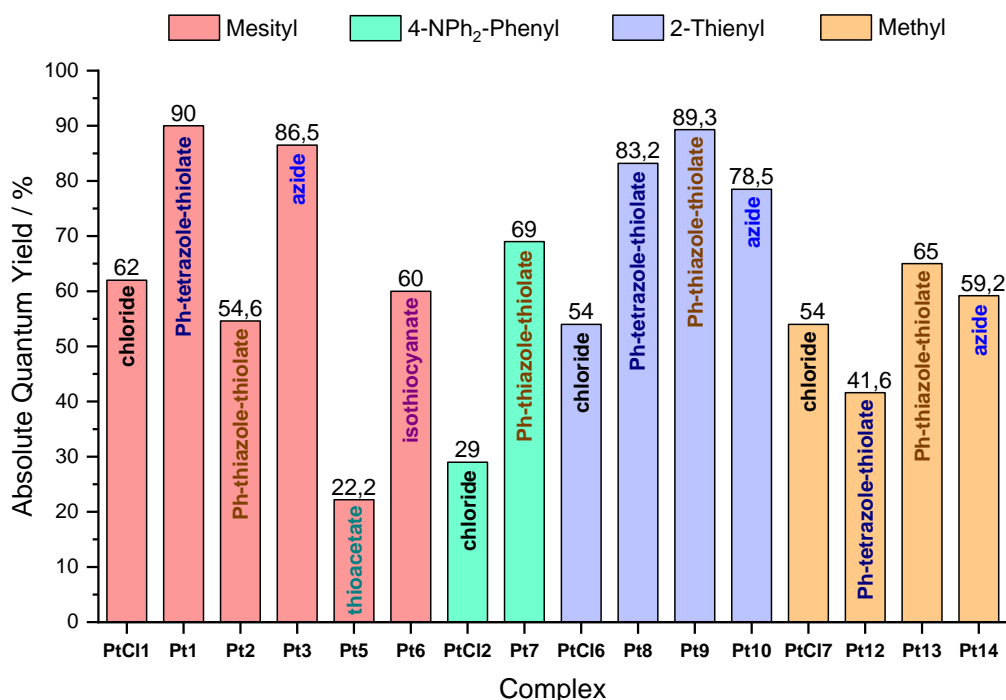


Figure 97. Graphical comparison of the QY values for the studied complexes, referring to deaerated diluted solutions.

Concerning the lifetimes, they can be grouped on the basis of the moiety present on the central benzene ring.

For complexes **Pt1-Pt3** and **Pt5**, the values range from 7.39 μ s to 7.6 μ s, not far from the parent compound **PtCl1**, whose lifetime is 7.9 μ s.

Pt7 shows a lifetime of 13.5 μ s, quite longer than that of **PtCl2** (9.0 μ s).

The longest lifetimes are those of the thienyl-bearing complexes, being in the range 17.82-19.20 μ s, close to the value reported for **PtCl6**, *i.e.* 20.5 μ s.

Finally, while **PtCl7** has a lifetime of 7.8 μ s, the methyl-substituted compounds **Pt12-14** have a lifetime going from 7.94 μ s to 8.3 μ s.

Consequently, the substitution of the ancillary ligand does not bring about a significant variation of the lifetimes, since the average values are in good agreement with those of the Pt-Cl complexes.

3.6 Solid state characterization of Pt1

Complex **Pt1** was studied from the luminescence point of view also at the solid state. The measurements were carried out on the powders both at Room Temperature (RT, 293 K) and at Low Temperature (LT, 77 K). **Figures 98** and **99** show the excitation and emission spectra of **Pt1** at RT and LT.

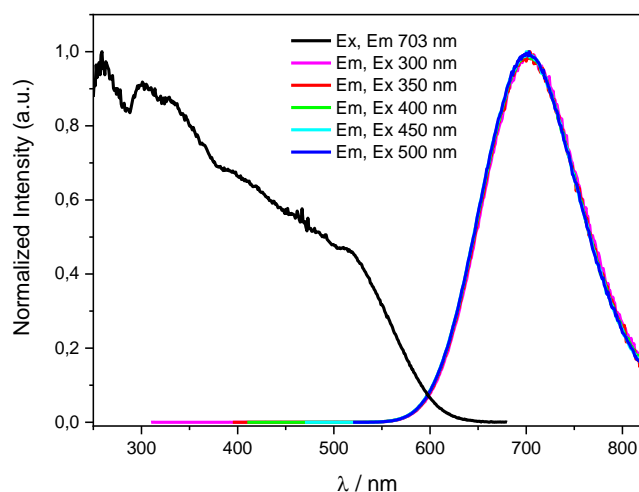


Figure 98. Normalized excitation and emission spectra of the powders of complex **Pt1**, at Room Temperature.

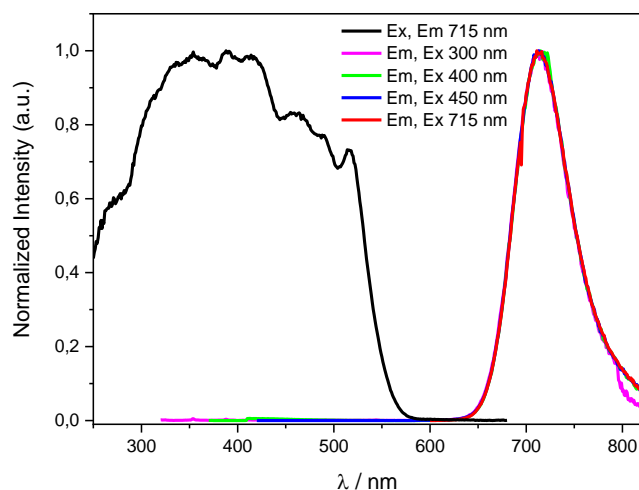


Figure 99. Normalized excitation and emission spectra of the powders of complex **Pt1**, at Low Temperature.

The emission of the powder is in the red region, with a maximum at 703 nm at RT and at 713 nm at LT, with a slight shift towards lower energies and a narrowing of the peak when the measurement was performed at 77 K. The effect of the temperature is particularly evident when considering the lifetimes, since the value increases from 1.24 μs at RT to 2.03 μs at LT, this being due to the reduced non-radiative transitions occurring at 77 K. The lifetime decays are reported in the **Appendix**.

The absolute Quantum Yield was measured at Room Temperature and it shows a remarkable value of 62%, being very high when compared to other members of the NCN-Pt(II) family.

Table 8 resumes and compares the registered data concerning **Pt5** at RT and LT.

Table 8. Emission maxima, QY and Lifetimes for complex **Pt1** as powder, at RT and LT.

Temperature	$\lambda_{\text{max, em}} / \text{nm}$	QY	$\tau / \mu\text{s}$	$\lambda_{\text{ex}}, \lambda_{\text{em}} / \text{nm}$
293 K (RT)	703	62%	1.24	374, 703
77 K (LT)	713	-	2.03	374, 713

3.7 Solid state characterization of Pt5

The photophysical properties of complex **Pt5** were studied also at the solid state at Room Temperature, both as powders and as thin films. Thin films were obtained through the spin-coating technique, starting from dichloromethane solutions, and were prepared as blend in PMMA at two different concentrations (7.5 % and 15% w/w). As for the solutions, also in the case of films and powders the sample was characterized with absorption, excitation and emission spectra, and measuring the Quantum Yield and the lifetimes.

Figure 100 shows the normalized UV-Vis absorption spectra of the 7.5% and 15% films in PMMA: they are quite similar to those observed for the solutions at high concentration, and in particular it is possible to notice more clearly the presence of an absorption band in the range between 450 and 600 nm, which is consistent with a solid-state aggregation behavior (due to the probable formation of dimers) typical of this kind of square-planar Pt(II) complexes.

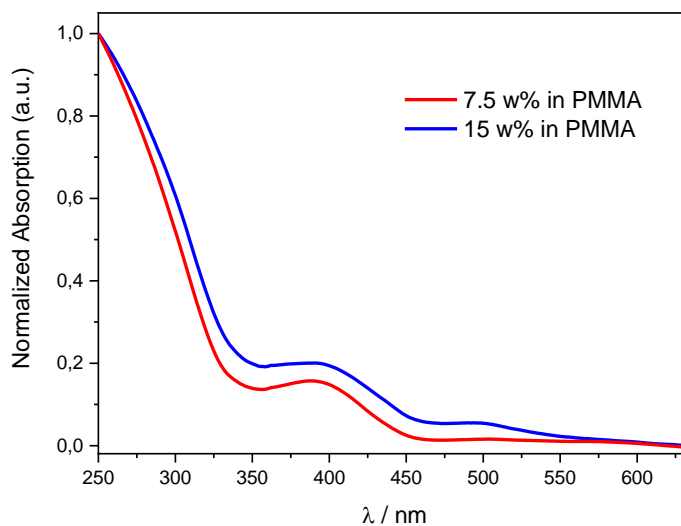


Figure 100. UV-Vis absorption spectra of complex **Pt5** in PMMA films.

The excitation and emission spectra of the thin films in PMMA, at both w/w concentrations, are reported in **Figures 101-102**, while the spectra relative to the powders are shown in **Figure 103**.

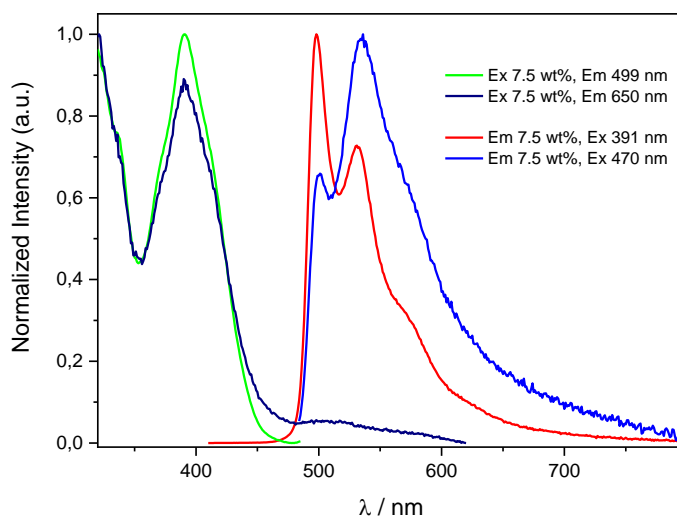


Figure 101. Normalized excitation and emission spectra of complex **Pt5** as thin film in PMMA (7.5% w/w).

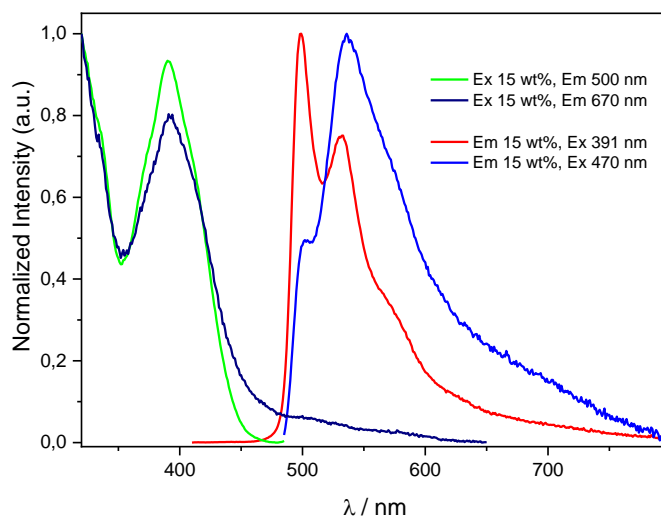


Figure 102. Normalized excitation and emission spectra of complex **Pt5** as thin film in PMMA (15% w/w).

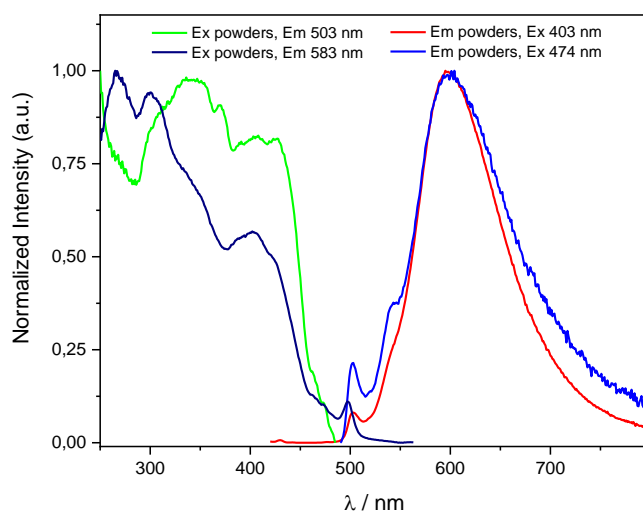


Figure 103. Normalized excitation and emission spectra of complex **Pt5** as powders.

Figure 104 reports the emission spectrum of the powders of **Pt5**, compared to the emission of the PMMA films. The different spectra are normalized at 532 nm, in order to present a comparison between them and to show the effect of increasing concentration on the emission maximum.

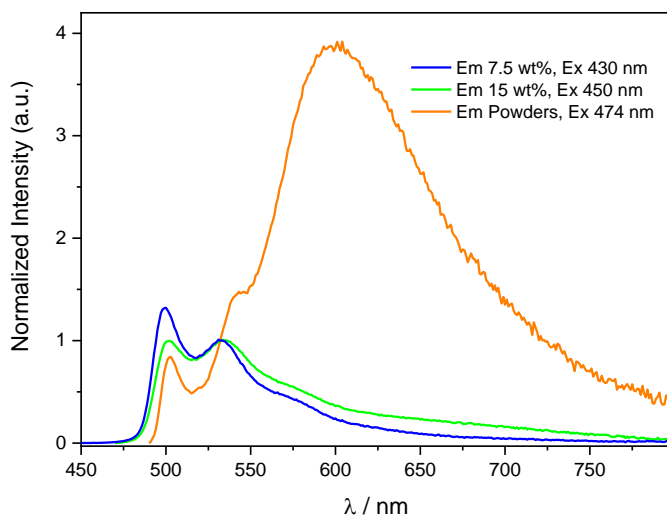


Figure 104. Normalized emission spectra of **Pt5** as thin films and as powder. Spectra are normalized at 532 nm.

As expected, the increase in concentration (from 7.5% to 15% to the powders) caused a red-shift of the emission, due to formation of aggregates in the solid state. These aggregates lie at lower energy, having as a result the shift of the emission maximum from 500 to 532 to ~601 nm.

Table 9 resumes the most relevant photophysical data for complex **Pt5**, including the emission maxima, the QY and the lifetime values.

Table 9. Emission maxima, QY and lifetimes for complex **Pt5** as film in PMMA and as powder.

Complex Pt5	$\lambda_{\text{max, em}} (\lambda_{\text{ex}}) / \text{nm}$	QY	$\tau / \mu\text{s}$	$\lambda_{\text{ex}}, \lambda_{\text{em}} / \text{nm}$
7.5% in PMMA	498 (391) 536 (470)	17%	1.08 (26.6%) 3.75 (73.4%)	404, 500
15% in PMMA	499 (391) 536 (470)	10%	0.66 (39.5%) 2.47 (60.5%)	404, 500
powder	601	1%	0.05 (9.4%) 0.99 (90.6%)	404, 507

As it was already pointed out by the spectra, the increase in concentration is at the basis of a red-shift in the emission and of a decrease in the absolute Quantum Yield, followed by a reduction of the lifetimes. The lifetime decays are reported in the **Appendix**.

4. Photophysical characterization of complexes PtCl8-PtCl13

For all complexes **Pt8-Pt13** the UV-Vis spectra are reported in this section, together with the corresponding molar extinction coefficients. For compounds **PtCl8**, **PtCl10**, **PtCl12** and **PtCl13** also the complete luminescence data are presented here.

4.1 UV-Vis absorption spectra of complexes PtCl8-PtCl13

Figures 105-110 report the UV-Visible absorption spectra of complexes **PtCl8-PtCl13**.

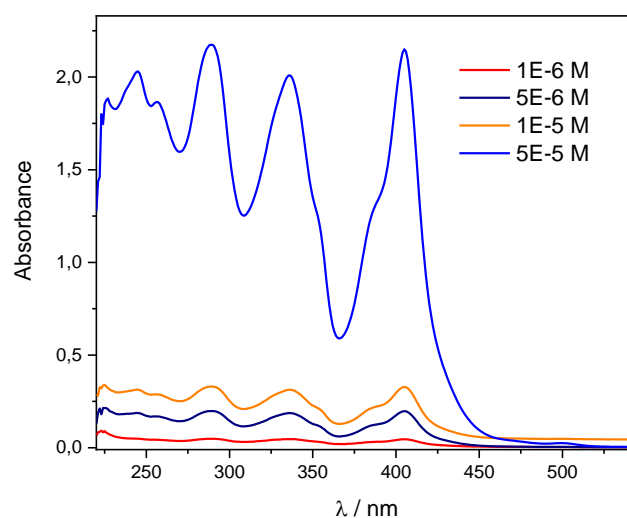


Figure 105. UV-Vis absorption spectra of complex **PtCl8** in CH_2Cl_2 at different concentrations.

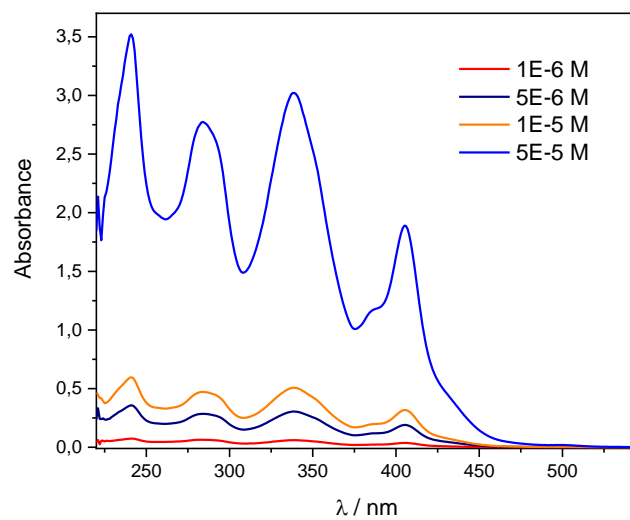


Figure 106. UV-Vis absorption spectra of complex **PtCl₉** in CH₂Cl₂ at different concentrations.

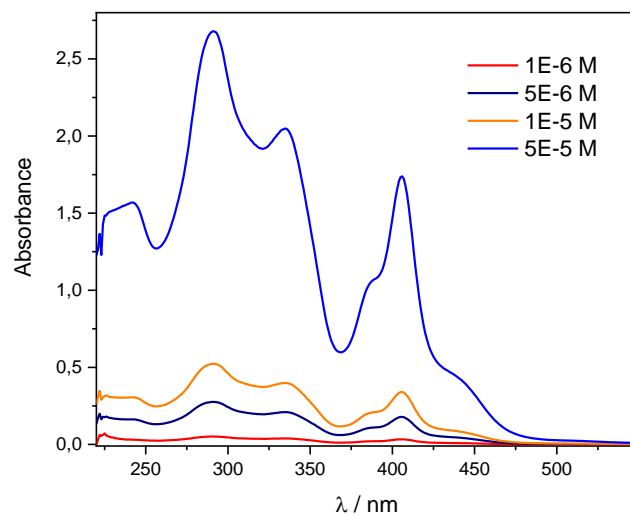


Figure 107. UV-Vis absorption spectra of complex **PtCl₁₀** in CH₂Cl₂ at different concentrations.

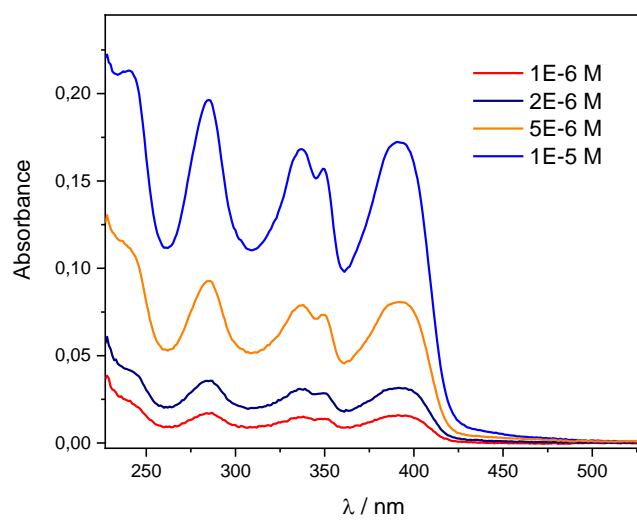


Figure 108. UV-Vis absorption spectra of complex **PtCl11** in CH_2Cl_2 at different concentrations.

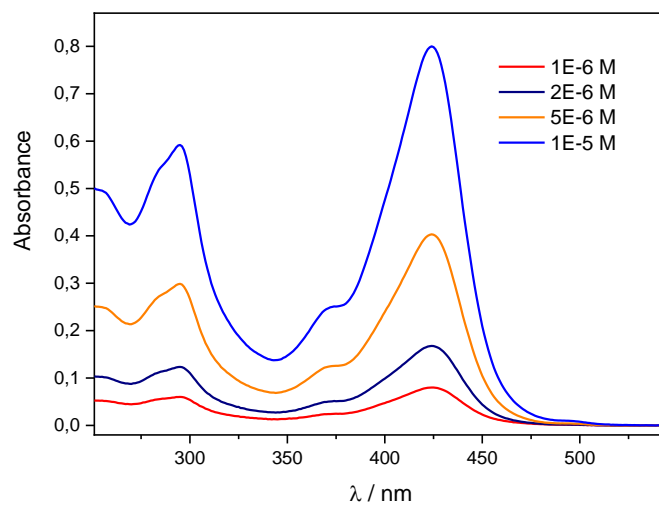


Figure 109. UV-Vis absorption spectra of complex **PtCl12** in CH_2Cl_2 at different concentrations.

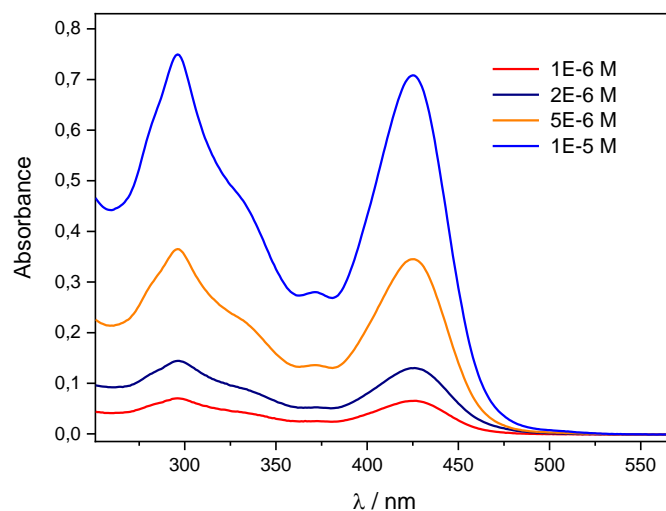
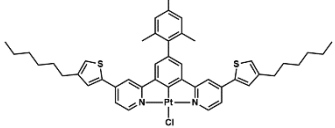
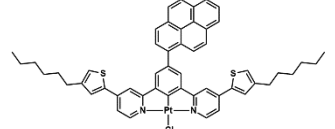
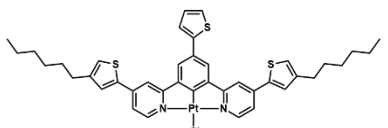
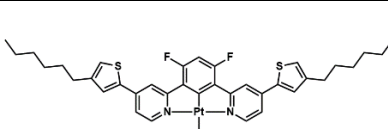
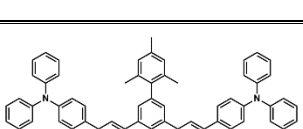
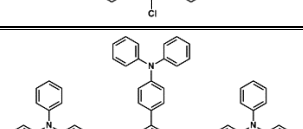


Figure 110. UV-Vis absorption spectra of complex **PtCl13** in CH_2Cl_2 at different concentrations.

4.2 Molar extinction coefficients of complexes PtCl8-PtCl13

Table 10 resumes the molar extinction coefficients for the absorption maxima of complexes **PtCl8-PtCl13**.

Table 10. Absorption maxima and corresponding molar extinction coefficients of complexes **PtCl8-PtCl13**.

Complex	$\lambda_{\text{max, abs}} / \text{nm}$	$\epsilon / (10^3 \text{ cm}^{-1} \text{ M}^{-1})$
	PtCl8 289 336 405	43.6 40.2 43.1
	PtCl9 241 284 338 405	70.8 55.7 60.8 38.0
	PtCl10 291 335 406	53.6 41.0 34.8
	PtCl11 243 285 337 349 392	20.0 20.6 17.7 16.5 18.0
	PtCl12 295 424	58.9 79.6
	PtCl13 296 425	75.1 71.1

4.3 Excitation and emission spectra of complexes PtCl8, PtCl10, PtCl12 and PtCl13

For each of the studied compounds (**PtCl8**, **PtCl10**, **PtCl12**, **PtCl13**), representative excitation and emission spectra are reported (**Figures 111-114**) for a dilute and a concentrated solution in dichloromethane, after the FPT procedure.

Emission maxima for the mentioned complexes, with the values corresponding to both the monomeric species and the related aggregates appearing at higher concentrations, are listed in **Table 11**.

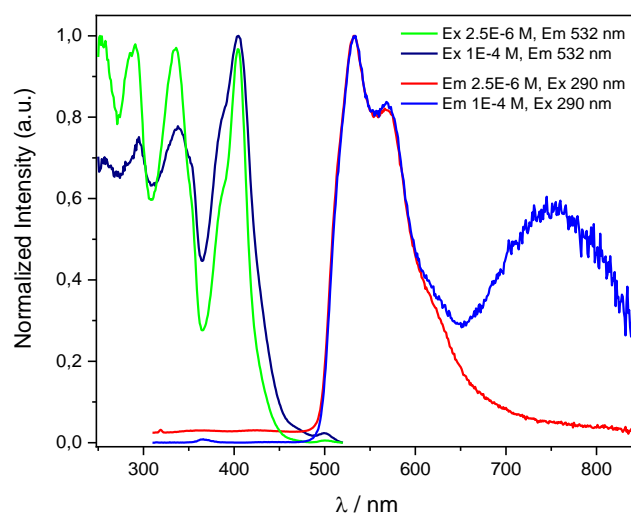


Figure 111. Normalized excitation and emission spectra of a dilute ($2.5 \cdot 10^{-6}$ M) and a concentrated ($1 \cdot 10^{-4}$ M) solution of complex **PtCl8** in CH_2Cl_2 , after three Freeze-Pump-Thaw cycles.

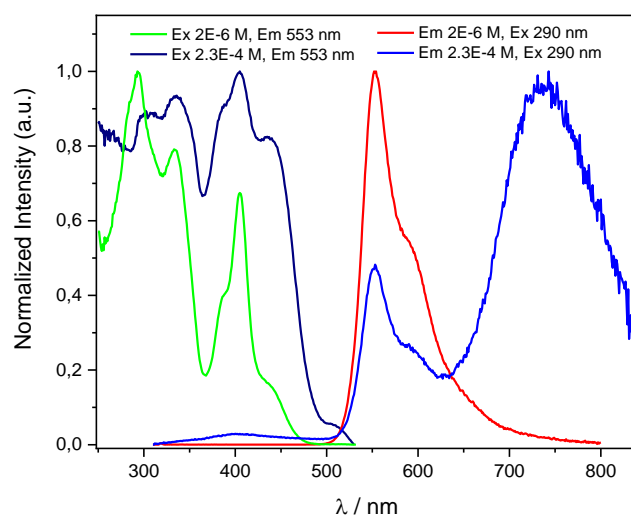


Figure 112. Normalized excitation and emission spectra of a dilute ($2 \cdot 10^{-6}$ M) and a concentrated ($2.3 \cdot 10^{-4}$ M) solution of complex **PtCl10** in CH_2Cl_2 , after three Freeze-Pump-Thaw cycles.

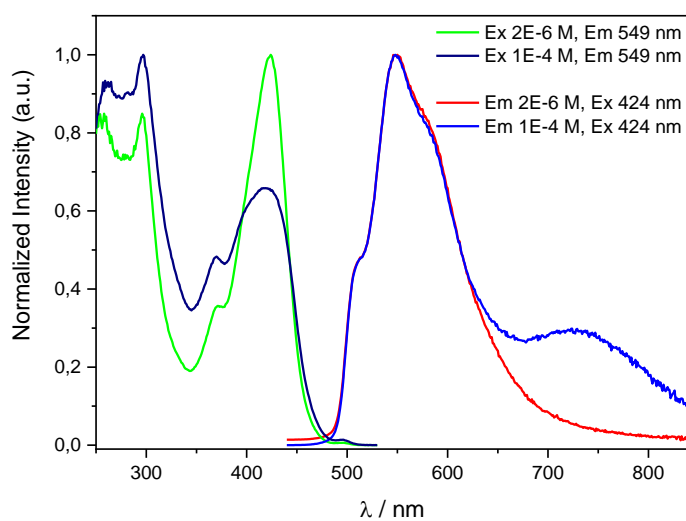


Figure 113. Normalized excitation and emission spectra of a dilute ($2 \cdot 10^{-6}$ M) and a concentrated ($1 \cdot 10^{-4}$ M) solution of complex **PtCl12** in CH_2Cl_2 , after three Freeze-Pump-Thaw cycles.

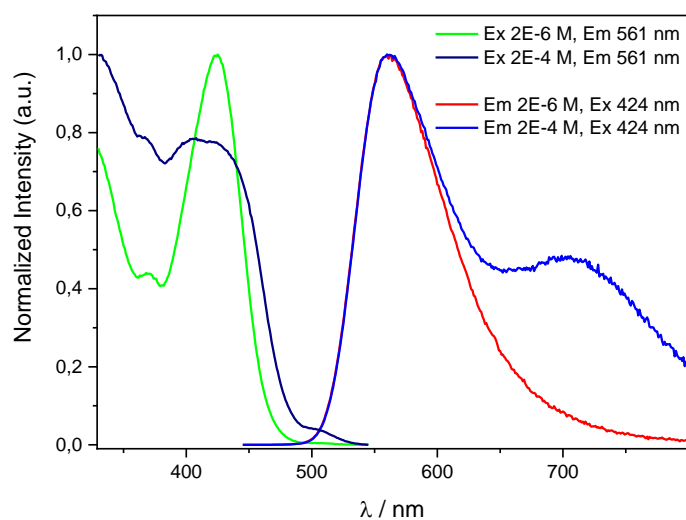
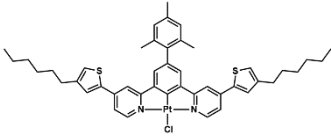
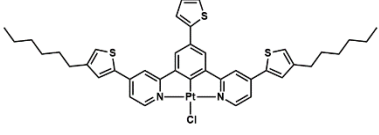
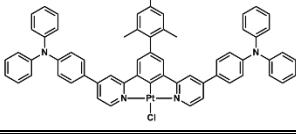
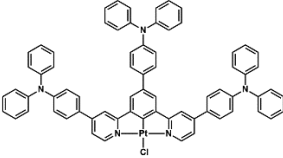


Figure 114. Normalized excitation and emission spectra of a dilute ($2 \cdot 10^{-6}$ M) and a concentrated ($2 \cdot 10^{-4}$ M) solution of complex **PtCl13** in CH_2Cl_2 , after three Freeze-Pump-Thaw cycles.

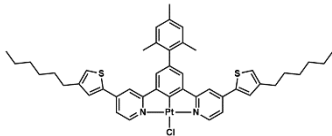
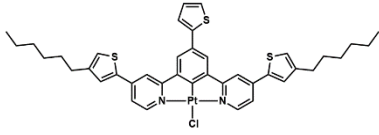
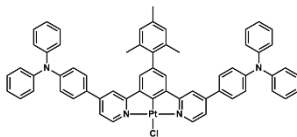
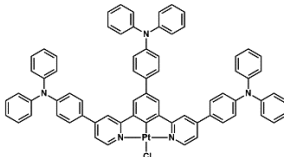
Table 11. Emission maxima for complexes **PtCl8**, **PtCl10**, **PtCl12**, **PtCl13**, for both the monomer and the aggregates.

Complex	$\lambda_{\max, \text{em}} / \text{nm}$ (monomer)	$\lambda_{\max, \text{em}} / \text{nm}$ (aggregates)
	534 568	~752
	554	~738
	548	~725
	560	~705

4.4 Absolute Quantum Yields and lifetimes

In **Table 12** all data about the absolute Quantum Yields are listed, for a dilute and a concentrated dichloromethane solution, both before and after the FPT procedure.

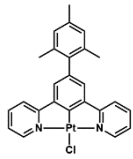
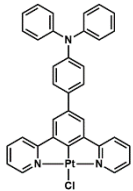
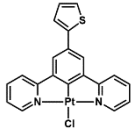
Table 12. Quantum Yield and lifetime values for complexes **PtCl8**, **PtCl10**, **PtCl12**, **PtCl13**.

Complex	c / M	$\text{QY}_{\text{after}} (\text{QY}_{\text{before}})$	$\tau / \mu\text{s}$	$\lambda_{\text{ex}}, \lambda_{\text{em}} / \text{nm}$
	$2.5 \cdot 10^{-6}$	96.4% (2.6%)	24.08	405, 532
			23.73	405, 725
	$1 \cdot 10^{-4}$	50.1% (2.1%)	6.06	405, 532
			6.29	405, 753
	$1 \cdot 10^{-6}$	100% (6.0%)	5.94	405, 553
			6.01	405, 700
	$2.3 \cdot 10^{-4}$	42.5% (4.6%)	1.41	405, 553
			1.51	405, 740
	$2 \cdot 10^{-6}$	89.4% (1.0%)	50.0	424, 511
			50.0	424, 549
	$1 \cdot 10^{-4}$	43.7% (0.8%)	49.8	424, 700
			16.45	424, 549
	$2 \cdot 10^{-6}$	87.9% (5.1%)	6.57	424, 561
			6.42	424, 700
	$2 \cdot 10^{-4}$	70.1% (3.2%)	3.02	424, 561
			2.96	445, 561

4.5 Comparison with related compounds PtCl1, PtCl2 and PtCl6

To make a comparison, data of the related parent NCN-PtCl compounds **PtCl1**, **PtCl2** and **PtCl6** are resumed in **Table 13**.

Table 13. Emission maxima for complexes **PtCl1-PtCl2** and **PtCl6**; data are from reff. [64] and [65] and refer only to monomeric emission.

Complex	$\lambda_{\max, \text{em}} / \text{nm}$ (monomer)	QY _{after} (QY _{before})	$\tau / \mu\text{s}$
	PtCl1 501 534	62% (4.5%)	7.9
	PtCl2 557	29% (-)	9.0
	PtCl6 505 539	54% (1.5%)	20.5

As can be pointed out by the data collected in **Tables 12-13**, the introduction of aromatic substituents on the pyridyl rings causes a red-shift of the emission in the case of the ligands bearing a mesityl and 2-thienyl group.

This shift exceeds 30 nm in the case of **PtCl8** and almost reaches 50 nm for **PtCl12**; a variation of about 50 nm is observed also in the case of complex **PtCl10**, while for **PtCl13** the emission is practically unchanged.

A graphical comparison of the QY values for diluted dichloromethane solutions is presented in **Figure 115**.

In all cases the absolute Quantum Yield of the compound is exceptionally higher than the value of the related complex. The mesityl-bearing complexes **PtCl8** and **PtCl12** undergo an increase from 62% to 96.4% and 89.4%, respectively.

The most remarkable effect is observed for compounds **PtCl2** and **PtCl13**, with a threefold growth of the Quantum Yield (from 29% to 87.9%). Extraordinary is also the increase for complex **PtCl10**, having a thienyl moiety, since the QY passes from 54% to 100%, almost doubling its original value and reaching unit efficiency.

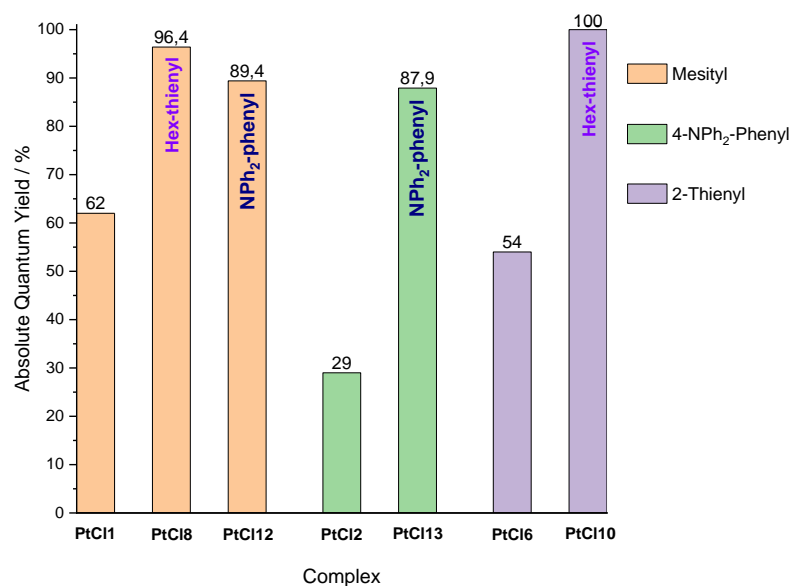


Figure 115. Graphical comparison of the QY values for the studied complexes, referring to diluted solutions.

Considering the lifetimes, no general consideration can be pointed out, since the effect of the introduction of substituents on the pyridines caused different effects. In fact, an important increase of the value is observed in the case of the complexes having a mesityl group on the benzene, with the lifetime passing from 7.9 μs to 24.08 μs and 50.0 μs for **PtCl8** and **PtCl12**, respectively. Moreover, the value for **PtCl10** undergoes a remarkable decrease, going from 20.5 μs to 5.94 μs , while that of **PtCl13** passes from 9.0 μs to 6.57 μs .

All decay graphs can be found in the **Appendix**.

5. Crystal structure of Pt1

Crystals of complex **Pt1** were obtained from the slow evaporation of a CH_2Cl_2 solution of the compound.

Here the complete data and details about the X-ray characterization are reported.

$\text{C}_{32}\text{H}_{26}\text{N}_6\text{SPt}\cdot 0.5\text{CH}_2\text{Cl}_2$: $M = 764.20$ g/mol, monoclinic, $a = 20.869(2)$, $b = 9.272(1)$, $c = 29.834(3)$ Å, $\beta = 92.711(2)$, $V = 5766(2)$ Å³, $T = 200(2)$ K, space group $P2_1/n$ (No. 14), $Z = 8$, $\mu = (\text{Mo-K}\alpha) 5.066$ mm⁻¹; 39 824 reflections (10 463 unique; $R_{\text{int}} = 0.0882$) were collected in the range $2.32^\circ < 2\theta < 50.58^\circ$, using a $0.15 \times 0.06 \times 0.01$ mm³ crystal mounted on a Bruker APEX II CCD diffractometer and using graphite-monochromatized Mo-K α radiation ($\lambda = 0.71073$ Å).

Data sets were corrected for the Lorentz polarization effects and for absorption ($T_{\text{min}} = 0.699$) (SADABS). The structure was solved by direct methods (SIR-92) and was finished by iterative cycles of full-matrix least-squares refinement on F_o^2 and ΔF synthesis using the SHELXL-97 program (the WinGX suite). Hydrogen atoms were located on the ΔF maps and allowed to ride on their carbon atoms. Final R_1 [wR_2] values are 0.0618 [0.1264] on $I > 2\sigma(I)$.

Crystallographic data for **Pt1** have been deposited with the Cambridge Crystallographic Data Centre as supplementary publication n. CCDC 1979249.

Observing the crystal structure of the complex (**Figure 116**), it appears that the asymmetric unit is composed of two independent molecules of **Pt1**, together with half molecule of CH_2Cl_2 . Both π - π and Pt...Pt interactions can be noticed in the structure, with the planes of the aromatic system of the NCN ligand almost parallel. As expected because of its steric hindrance, the mesityl group lies almost perpendicular to the NCN plane, while the phenyl-tetrazole thiolate points away from the metal center.

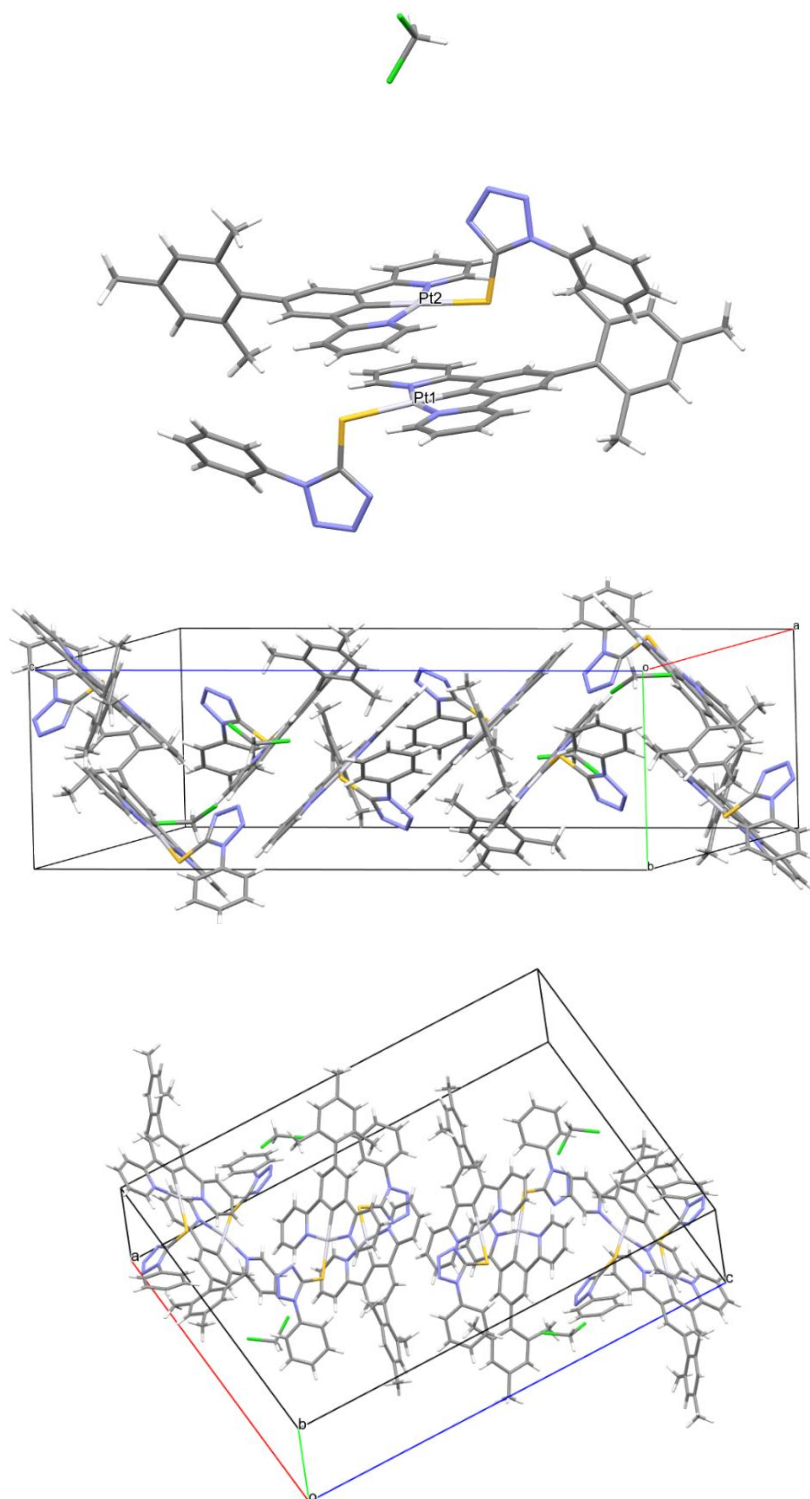


Figure 116. X-ray structure of **Pt1**, with the asymmetric unit and two views of the unit cell.

6. OLEDs produced with the Pt(II) complexes

Among the presented NCN-platinum(II) complexes, compounds **Pt1** and **Pt9** have been employed by dr. Massimo Cocchi (ISOF-CNR, Bologna) for the preparation of some OLED devices.

In this section all data about the OLED fabrication, together with the related spectra and graphs, are reported.

6.1 OLEDs produced with Pt1

Pt1 has been used for the preparation of three OLED devices, having different amount of platinum complex in the Emitting Layer. The composition of the three OLEDs is the following:

- ITO (120 nm) / PEDOT:PSS (40 nm) / **8% wt Pt1** in TCTA (40 nm) / TPBi (30 nm) / LiF (0.5 nm) / Al (100 nm)
- ITO (120 nm) / PEDOT:PSS (40 nm) / **25% wt Pt1** in TCTA (40 nm) / TPBi (30 nm) / LiF (0.5 nm) / Al (100 nm)
- ITO (120 nm) / PEDOT:PSS (40 nm) / **100% Pt1** (40 nm) / TPBi (30 nm) / LiF (0.5 nm) / Al (100 nm)

The layers of **Pt1** were deposited by spin coating (2000 rpm) from a 10 mg mL⁻¹ dichloromethane solution of the complex.

PEDOT:PSS (**Figure 117**) is a conductive polymer made of poly(3,4-ethylenedioxythiophene) and polystyrene sulfonate; TCTA and TPBi were already presented in **Chapter II – Section 2.1** and act as HTL and ETL, respectively.

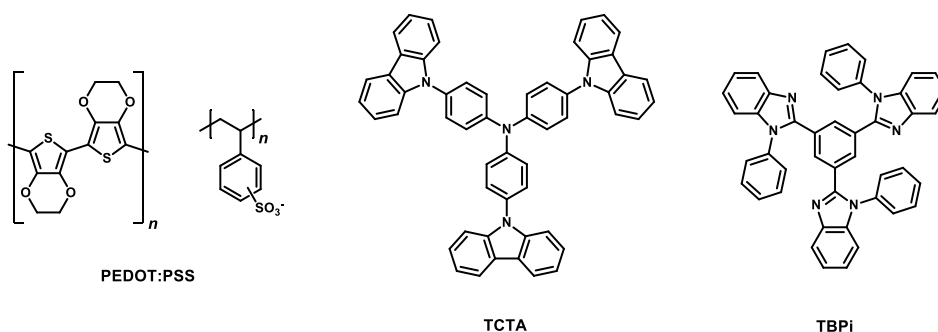


Figure 117. Structure of PEDOT:PSS, TCTA and TBPI.

Figure 118 shows the normalized emission spectra of the three devices produced with **Pt1**. It can be observed that the different amount of complex in the Emitting Layer brings about different emission colors, due to the formation of molecular aggregates when the concentration becomes sufficiently high: while the spectrum of the 8% device corresponds well with that of the monomer (see **Figure 86**), at 25% the monomer coexists with the aggregates and finally at 100% only the aggregates (with their red-shifted emission) are visible.

The CIE coordinates for the three devices are: (0.27, 0.59) for 8%, (0.40, 0.52) for 15% and (0.63, 0.36) for 100%. As shown in the CIE diagram in **Figure 119**, also reporting the real images of the devices, the emission color moves from green to yellow to red, thus providing the possibility to be tuned on the basis of the amount of Pt(II) complex.

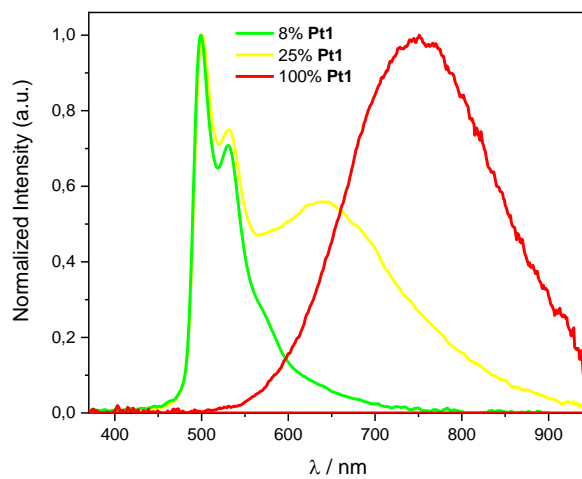


Figure 118. Normalized emission spectra of the three OLEDs produced with complex **Pt1**.

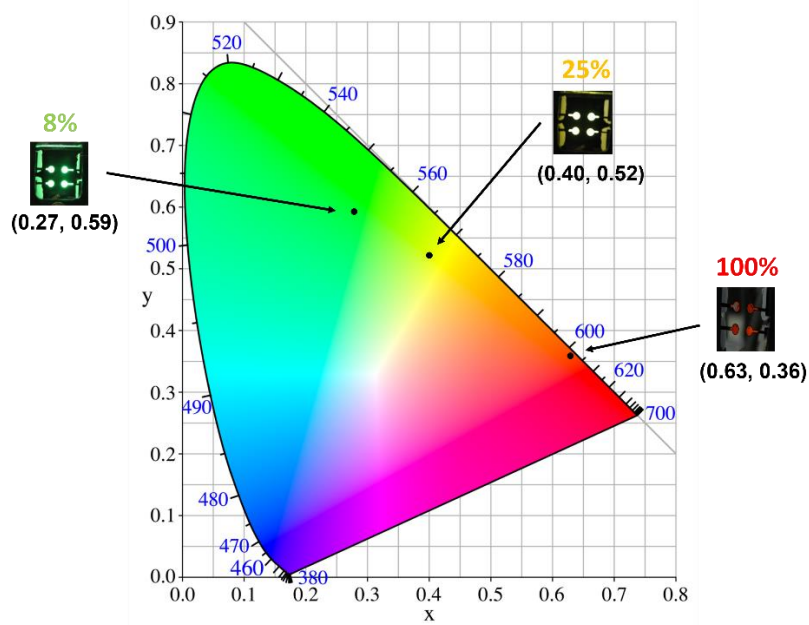


Figure 119. CIE diagram of the emission color of the three OLEDs produced with complex **Pt1**.

Figures 120 and 121 report the graphs relative to *Luminance vs Voltage* and *Efficiency vs Current density* for the OLEDs having 8% and 25% of **Pt1** in the Emitting Layer.

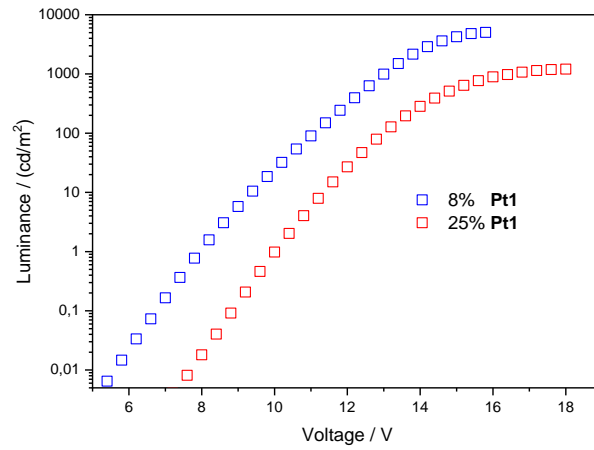


Figure 120. *Luminance vs Voltage* for the OLEDs having 8% and 25% of **Pt1** in the EL.

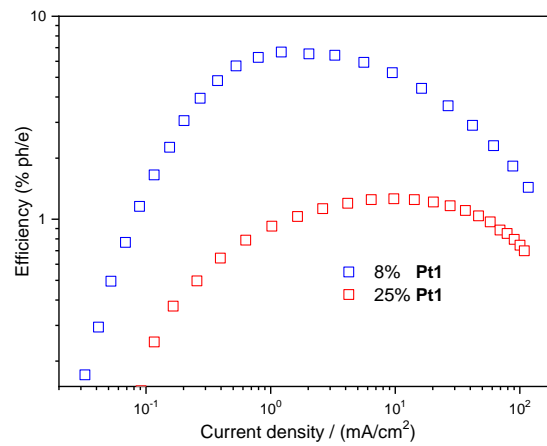


Figure 121. *Efficiency vs Current density* for the OLEDs having 8% and 25% of **Pt1** in the EL.

Figures 122 and 123 report the graphs relative to *Electroluminescence intensity vs Voltage* and *Efficiency vs Current density* for the OLED having 100% of **Pt1** in the Emitting Layer.

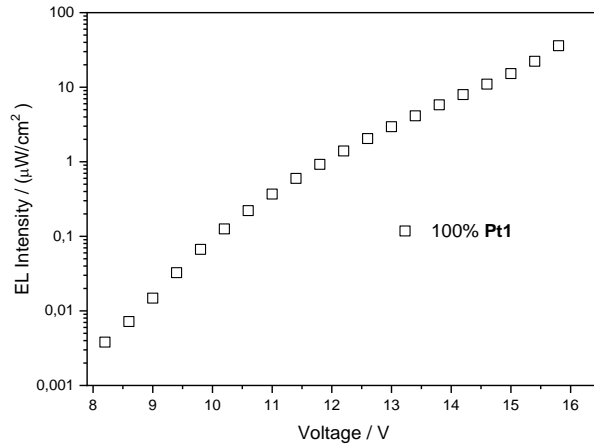


Figure 122. *Electroluminescence intensity vs Voltage* for the OLED having 100% of **Pt1** in the EL.

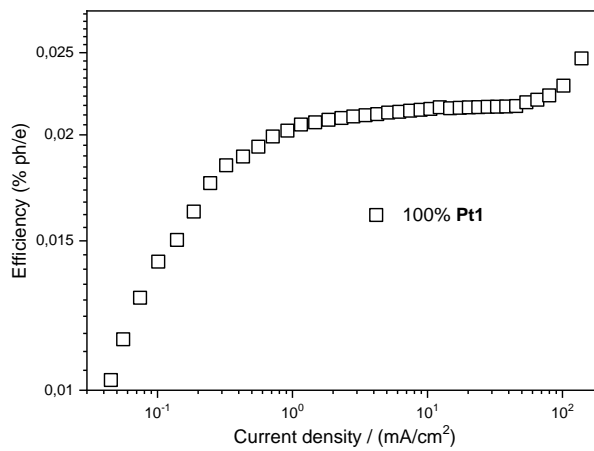


Figure 123. *Efficiency vs Current density* for the OLEDs having 100% of **Pt1** in the EL.

6.2 OLED produced with Pt9

Also compound **Pt9** has been tested as dopant in an OLED device, having the following composition:

- ITO (120 nm) / PEDOT:PSS (40 nm) / **8% wt Pt9** in TCTA (40 nm) / TPBi (30 nm) / LiF (0.5 nm) / Al (100 nm)

The emission spectrum of the OLED having 8% of **Pt9** in the Emitting Layer is reported in **Figure 124**; the emission has CIE coordinates (0.42, 0.52), as shown in **Figure 125**.

Figures 126 and **127** report the graphs relative to *Luminance vs Voltage* and *Efficiency vs Current density* for the OLED having 8% of **Pt9** in the Emitting Layer.

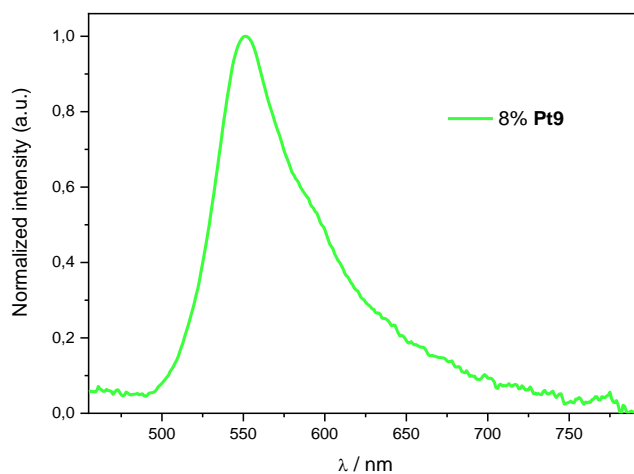


Figure 124. Normalized emission spectrum of the OLED produced with complex **Pt9**.

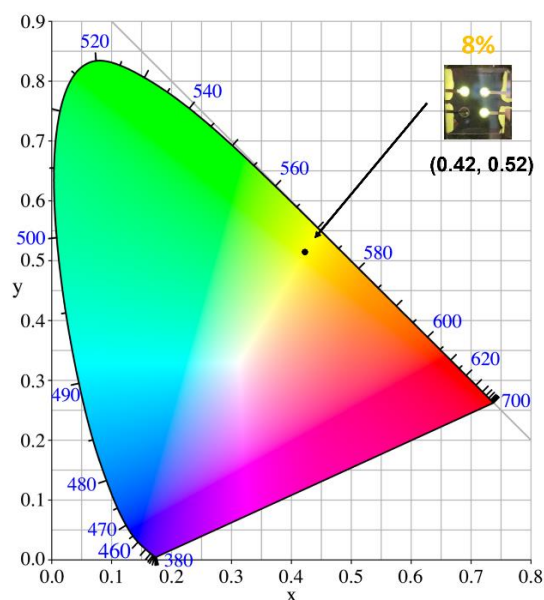


Figure 125. CIE diagram of the emission color of the OLED produced with complex **Pt9**.

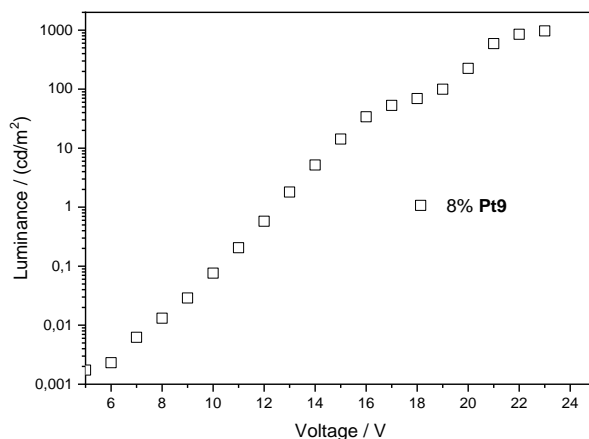


Figure 126. Luminance vs Voltage for the OLED having 8% of **Pt9** in the EL.

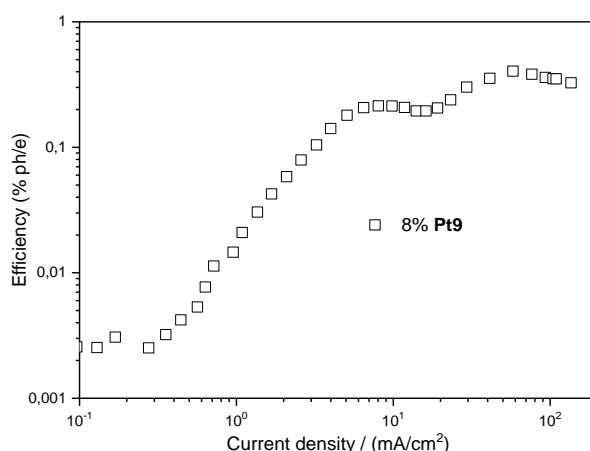


Figure 127. Efficiency vs Current density for the OLED having 8% of **Pt9** in the EL.

6.3 Comments about the prepared OLEDs

As it can be observed from data reported in the graphs, the best results come from the device having only 8% of **Pt1** in the Emissive Layer, this being probably due to the aggregation-caused quenching of the luminescence arising from higher amounts of complex in the organic layers. At that concentration, the Luminance reaches a value of 6000 cd m^{-2} at $\sim 16 \text{ V}$, while the photon/electron Efficiency approaches 7% at a current density of $\sim 1 \text{ mA cm}^{-2}$. By comparing these data with those of more “diluted” EL, it is clear that the even higher concentration of the pure layer of **Pt1** gives rise to a very low Efficiency, being always $< 0.5\%$.

Moving to **Pt9**, the Luminance value reached 1000 cd m^{-2} at a voltage $> 20 \text{ V}$, while the Efficiency remained under 0.5% even at 100 mA cm^{-2} .

At the moment, the aforementioned low efficiencies are undoubtedly the most relevant limitation of such devices; the low Efficiency values and the red-shift of the emission arise from the same phenomenon, *i.e.* the aggregation of complex molecules when their concentration in the organic layer becomes sufficiently high. This drawback could be faced through the proper design of new complexes, always belonging to the NCN-Pt(II) family but able to maintain remarkable QY values avoiding the ease of aggregation.

V – EXPERIMENTAL SECTION

1. General comments

All the commercially available reagents and solvents were used as received from the supplier; all dry solvents were bought and used without further purification.

Air- and water-sensitive reactions were performed in flame-dried glassware under argon atmosphere.

All organic compounds were purified through column flash chromatography on silica gel (Sigma-Aldrich, pore size 60 Å, 230-400 mesh particle size).

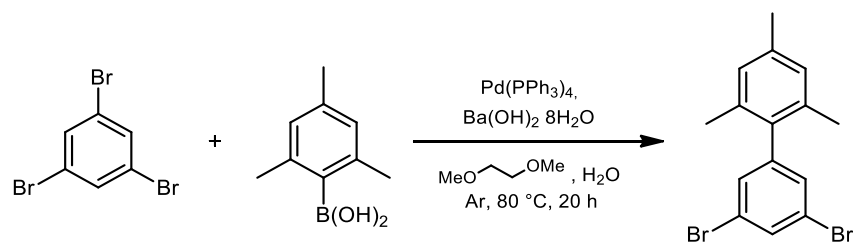
Analytical thin layer chromatography (TLC) was performed on silica gel Al foils (Sigma-Aldrich, fluorescent indicator 254 nm).

When necessary, platinum complexes were purified by recrystallization from pentane/dichloromethane mixture.

The characterization of each intermediate and of the final products was performed recording the NMR spectra on a Bruker AV III 300 MHz or AV III 400 MHz spectrometers. Chemical shifts of ^1H , ^{13}C and ^{19}F NMR spectra are reported in parts per million (ppm) and the coupling constants are measured in Hertz (Hz). Signal multiplicities are listed as singlet (s), d (doublet), t (triplet), quartet (q), multiplet (m).

All registered NMR spectra are reported in the **Appendix**.

1.1 Synthesis of I1



Reagent/Solvent	PM (g/mol)	mmol	Mass	eq	Volume
1,3,5-tribromobenzene	314.80	6.112	1.924 g	1	
mesitylboronic acid	164.01	6.250	1.025 g	1.02	
Pd(PPh ₃) ₄	1155.56	0.181	209 mg	0.03	
Ba(OH) ₂ · 8H ₂ O	315.86	9.150	2.890 g	1.5	
1,2-dimethoxyethane					12 mL
H ₂ O					2.0 mL

Procedure

The reagents were added to the solvents in a Schlenk tube and the mixture was stirred at 80 °C under Ar atmosphere. After 20 h the reaction was cooled to rt, toluene and water were added and the phases were separated. The organic phase was washed with brine (2x) and water (2x), dried over Na₂SO₄ and evaporated at reduced pressure.

The product was purified by flash chromatography on silica gel (eluent: hexane).

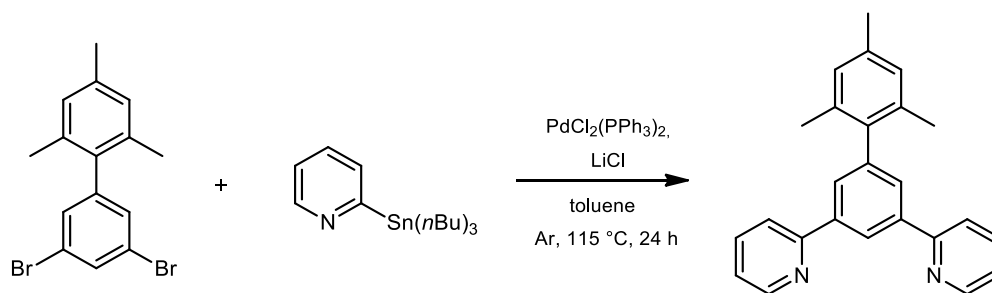
Mass of the product = 1.67 g.

Yield = 77%.

Characterization

¹H-NMR (300 MHz, CDCl₃) δ (ppm): 7.66 (1H, t, J = 1.6 Hz), 7.26 (2H, d, J = 1.6 Hz), 6.94 (2H, s), 2.34 (3H, s), 2.02 (6H, s).

1.2 Synthesis of L1



Reagent/Solvent	PM (g/mol)	mmol	Mass	eq	Volume	Density
I1	354.08	0.565	200 mg	1		
$n\text{Bu}_3\text{Sn-pyridine}$	368.14	1.695	624 mg	3	550 μL	1.14 g/mL
$\text{PdCl}_2(\text{PPh}_3)_2$	701.90	0.017	13 mg	0.03		
LiCl	42.39	5.085	213 mg	9		
dry toluene					2.0 mL	

Procedure

The reagents were added to the solvent in a Schlenk tube and the mixture was stirred at reflux under Ar atmosphere. After 24 h a solution of NaOH (1 M, 7 mL), water and AcOEt were added and the phases were separated. The aqueous phase was extracted with AcOEt (4x), the organic phases were dried over Na_2SO_4 and evaporated.

The product was purified by flash chromatography on silica gel (eluent: from hexane to hexane/AcOEt 9:1).

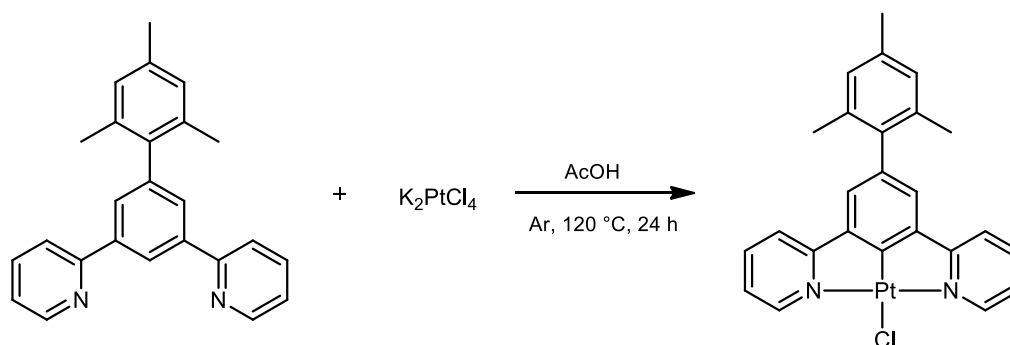
Mass of the product = 116 mg.

Yield = 59%.

Characterization

$^1\text{H-NMR}$ (400 MHz, CDCl_3) δ (ppm): 8.76-8.72 (2H, m), 8.70 (1H, t, $J = 1.7$ Hz), 7.89-7.84 (4H, m), 7.79 (2H, dd, $J = 7.6$ Hz, $J = 8.0$ Hz), 7.30-7.24 (2H, m, under residual CHCl_3), 6.99 (2H, s), 2.37 (3H, s), 2.11 (6H, s).

1.3 Synthesis of PtCl1



Reagent/Solvent	PM (g/mol)	mmol	Mass	eq	Volume
L1	350.46	0.171	60 mg	1	
K_2PtCl_4	415.09	0.205	85 mg	1.2	
glacial AcOH					6.0 mL

Procedure

The reagents were added to the glacial AcOH in a Schlenk tube and the mixture was stirred at reflux under Ar atmosphere. After 24 h the orange precipitate was filtered on a Buchner funnel, washed with MeOH, H₂O, EtOH and Et₂O, and dried.

The product was not furtherly purified.

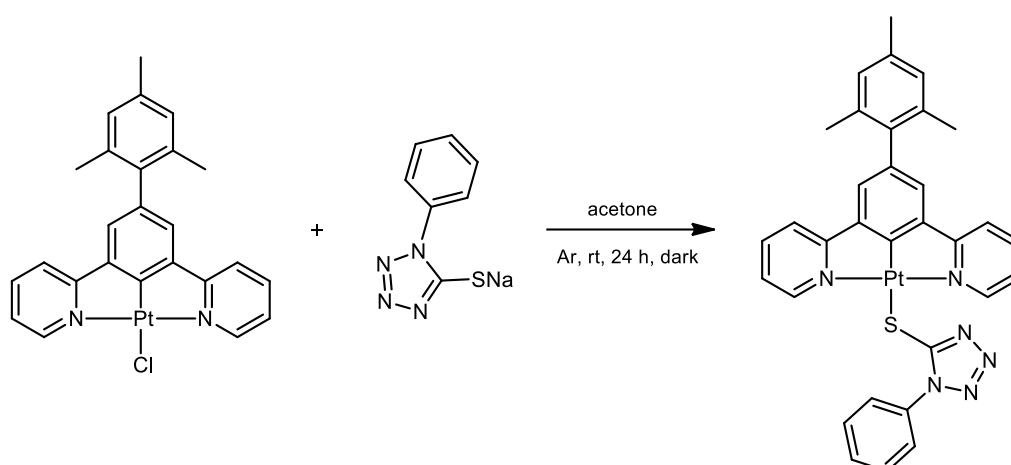
Mass of the product = 45 mg.

Yield = 45%.

Characterization

¹H-NMR (400 MHz, CD₂Cl₂) δ (ppm): 9.34 (2H, d, J = 5.6 Hz, J(¹⁹⁵Pt) = 42 Hz), 8.00 (2H, dd, J = 7.6 Hz, J = 7.7 Hz), 7.72 (2H, d, J = 7.7 Hz), 7.37 (2H, dd, J = 5.6 Hz, J = 7.6 Hz), 2.37 (3H, s), 2.11 (6H, s).

1.4 Synthesis of Pt1



Reagent/Solvent	PM (g/mol)	mmol	Mass	eq	Volume
PtClI	579.98	0.190	110 mg	1	
1-phenyl-1H-tetrazole-5-thiol sodium salt	200.20	2.647	530 mg	14	
acetone					250 mL

Procedure

In a two-necked round-bottom flask the platinum complex and the sodium salt were added to the solvent and the mixture was stirred at rt in the dark under Ar atmosphere. After 24 h the acetone was evaporated at reduced pressure and DCM was added to dissolve the product; the evaporation of the DCM gave the product as an orange solid.

The product was recrystallized from DCM/hexane and dried.

Mass of the product = 129 mg.

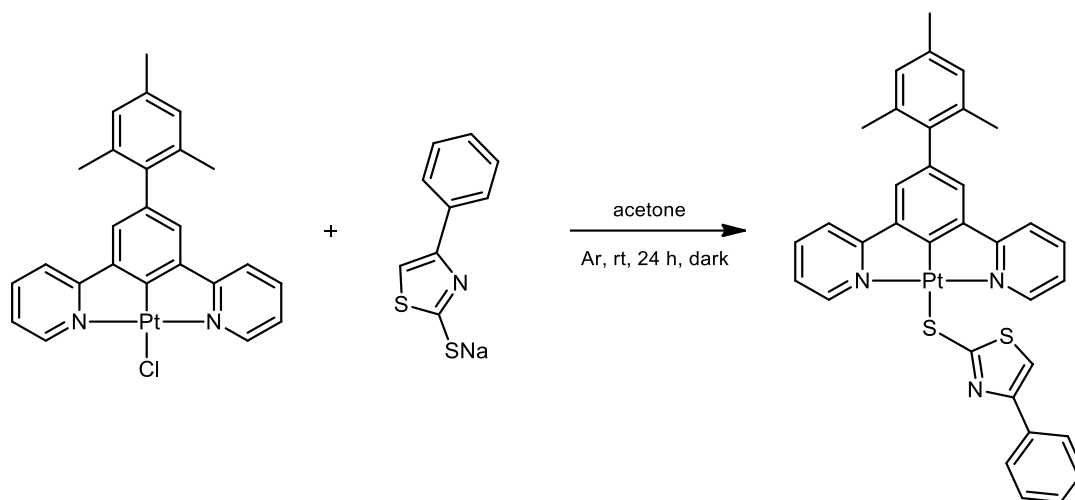
Yield = 94%.

Characterization

$^1\text{H-NMR}$ (400 MHz, CD_2Cl_2) δ (ppm): 9.19 (2H, d, $J = 4.9$ Hz, $J(^{195}\text{Pt}) = 40$ Hz), 7.98 (2H, dd, $J = 7.7$ Hz, $J = 7.9$ Hz), 7.88 (2H, d, $J = 7.6$ Hz), 7.71 (2H, d, $J = 7.7$ Hz), 7.52-7.40 (3H, m), 7.33 (2H, s), 7.26 (2H, dd, $J = 4.9$ Hz, $J = 7.9$ Hz), 2.38 (3H, s), 2.13 (6H, s).

$^{13}\text{C-NMR}$ (100 MHz, CD_2Cl_2) δ (ppm): 153.57, 139.85, 136.37, 129.22, 128.48, 125.53, 124.05, 120.00, 30.06, 20.99.

1.5 Synthesis of Pt2



Reagent/Solvent	PM (g/mol)	mmol	Mass	eq	Volume
PtClI	579.98	0.086	50 mg	1	
4-phenylthiazole-2-thiol sodium salt	215.25	0.859	185 mg	10	
acetone					50 mL

Procedure

In a two-necked round-bottom flask the platinum complex and the sodium salt were added to the solvent and the mixture was stirred at rt in the dark under Ar atmosphere. After 24 h the acetone was evaporated at reduced pressure and DCM was added to dissolve the product; the evaporation of the DCM gave the product as an orange solid.

The product was recrystallized from DCM/hexane and dried.

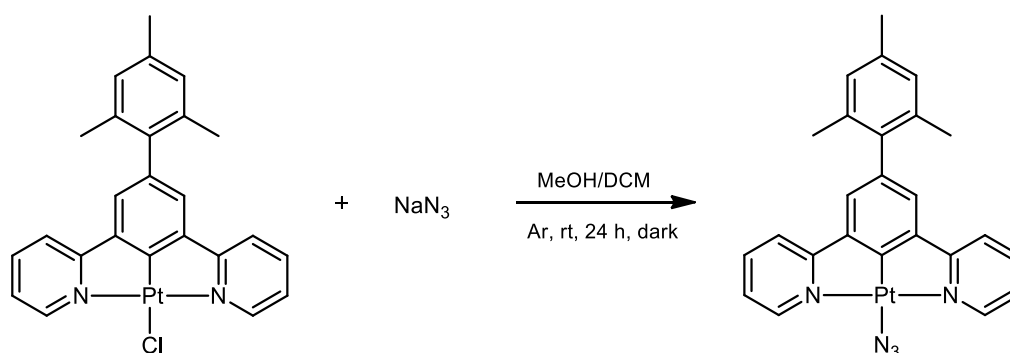
Mass of the product = 51 mg.

Yield = 81%.

Characterization

$^1\text{H-NMR}$ (400 MHz, CD_2Cl_2) δ (ppm): 9.48 (2H, d, $J = 5.6$ Hz, $J(^{195}\text{Pt}) = 44$ Hz), 7.99 (2H, dd, $J = 8.1$ Hz, $J = 8.2$ Hz), 7.88 (2H, d, $J = 7.5$ Hz), 7.74 (2H, d, $J = 7.6$ Hz), 7.43-7.35 (4H, m), 7.34-7.26 (3H, m), 7.05-6.98 (3H, m), 2.38 (3H, s), 2.14 (6H, s).

1.6 Synthesis of Pt3



Reagent/Solvent	PM (g/mol)	mmol	Mass	eq	Volume
PtClI	579.98	0.052	30 mg	1	
NaN_3	65.01	1.034	67 mg	20	
MeOH					4.0 mL
DCM					4.0 mL

Procedure

In a two-necked round-bottom flask a solution of NaN_3 in MeOH was added to a solution of platinum complex in DCM; the orange solution was stirred at rt in the dark under Ar atmosphere. After 24 h the precipitation of the product was observed and MeOH was added to dissolve the NaN_3 in excess; after further 10 minutes of stirring, the solid was filtered on a Buchner funnel, washed with MeOH and Et_2O , and dried.

The product was not furtherly purified.

Mass of the product = 23 mg.

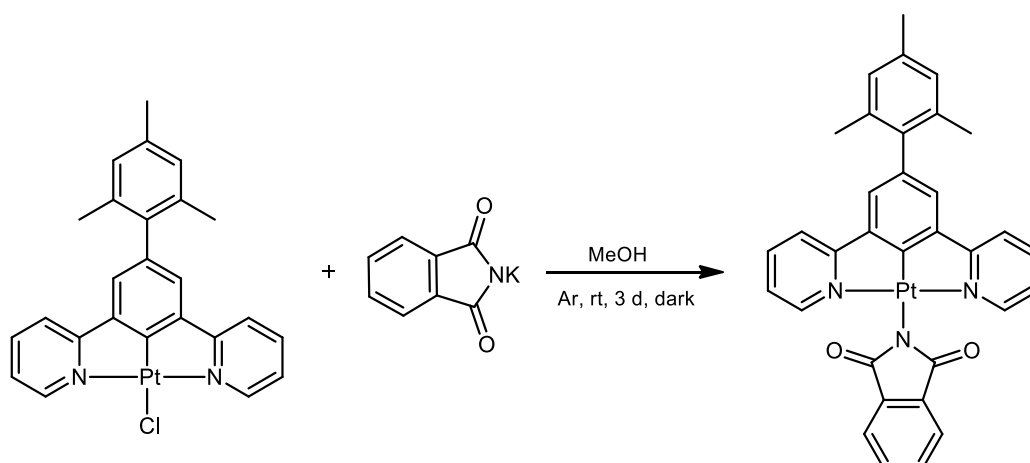
Yield = 75%.

Characterization

$^1\text{H-NMR}$ (400 MHz, CD_2Cl_2) δ (ppm): 8.90 (2H, d, $J = 5.7$ Hz, $J(^{195}\text{Pt}) = 41$ Hz), 8.04 (2H, dd, $J = 7.4$ Hz, $J = 7.8$ Hz), 7.75 (2H, d, $J = 7.8$ Hz), 7.42 (2H, dd, $J = 5.7$ Hz, $J = 7.4$ Hz), 7.32 (2H, s), 7.01 (2H, s), 2.37 (3H, s), 2.11 (6H, s).

$^{13}\text{C-NMR}$ (100 MHz, CD_2Cl_2) δ (ppm): 152.49, 151.09, 139.95, 128.48, 125.64, 123.96, 123.78, 120.13, 21.13, 21.02.

1.7 Synthesis of Pt4



Reagent/Solvent	PM (g/mol)	mmol	Mass	eq	Volume
PtClI	579.98	0.062	36 mg	1	
potassium phthalimide	185.22	0.620	115 mg	10	
MeOH					5 mL

Procedure

In a Schlenk tube the platinum complex and the potassium salt were added to the solvent and the mixture was stirred at rt in the dark under Ar atmosphere. After 72 h the yellow precipitate was filtered on a Buchner funnel, washed with MeOH and Et₂O, and dried.

The product was not furtherly purified.

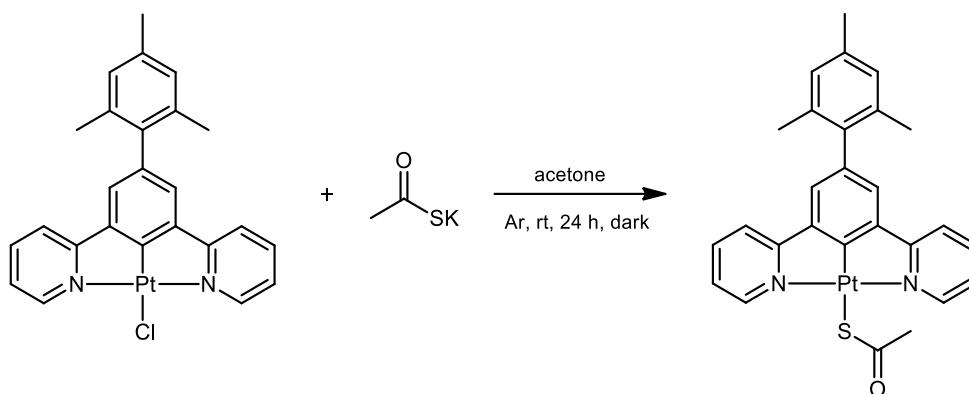
Mass of the product = 25 mg.

Yield = 58%.

Characterization

¹H-NMR (400 MHz, CD₂Cl₂) δ (ppm): 8.90 (2H, d, J = 5.7 Hz, J(¹⁹⁵Pt) = 43 Hz), 7.98 (2H, dd, J = 7.6 Hz, J = 7.8 Hz), 7.82-7.78 (2H, m), 7.74 (2H, d, J = 7.6 Hz), 7.70-7.66 (2H, m), 7.34 (2H, s), 7.22 (2H, dd, J = 5.7 Hz, J = 7.8 Hz), 7.02 (2H, s), 2.38 (3H, s), 2.13 (6H, s).

1.8 Synthesis of Pt5



Reagent/Solvent	PM (g/mol)	mmol	Mass	eq	Volume
PtClI	579.98	0.121	70 mg	1	
AcSK	114.21	1.45	166 mg	12	
acetone					25 mL

Procedure

In a two-necked round-bottom flask the platinum complex was suspended in acetone and potassium thioacetate was added; the mixture was stirred at rt in the dark under Ar atmosphere. After 24 h the dark yellow precipitate was filtered on a Buchner funnel, washed with acetone and Et₂O, and dried.

The product was not furtherly purified.

Mass of the product = 64 mg.

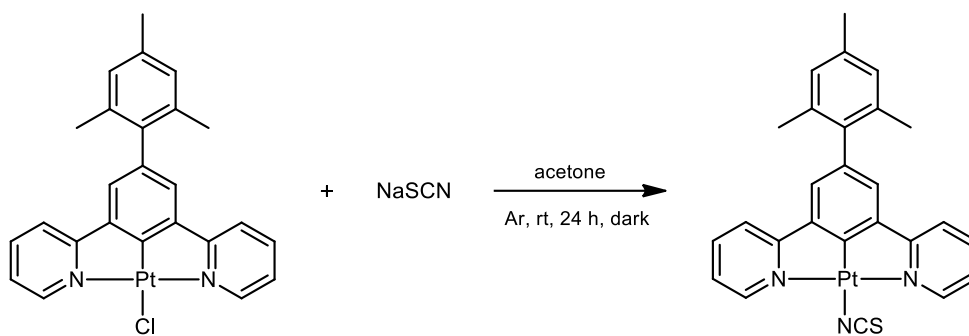
Yield = 86%.

Characterization

¹H NMR (400 MHz, CD₂Cl₂) δ (ppm): 9.34 (2H, d, J = 5.3 Hz, J(¹⁹⁵Pt) = 45 Hz), 7.99 (2H, dd, J = 7.8 Hz, J = 8.8 Hz), 7.71 (d, J = 7.8 Hz), 7.36–7.29 (4H, m), 7.01 (2H, s), 2.57 (3H, s), 2.37 (3H, s), 2.11 (6H, s).

¹³C NMR (100 MHz, CD₂Cl₂) δ (ppm): 154.17, 139.07, 136.14, 128.20, 124.87, 123.52, 119.29, 21-04, 20-84.

1.9 Synthesis of Pt6



Reagent/Solvent	PM (g/mol)	mmol	Mass	eq	Volume
PtClI	579.98	0.074	43 mg	1	
NaSCN	81.07	0,890	72 mg	12	
acetone					15 mL

Procedure

In a two-necked round-bottom flask the platinum complex was suspended in acetone and sodium isothiocyanate was added; the mixture was stirred at rt in the dark under Ar atmosphere. After 24 h the dark green precipitate was filtered on a Buchner funnel, washed with acetone and Et₂O, and dried.

The product was not furtherly purified.

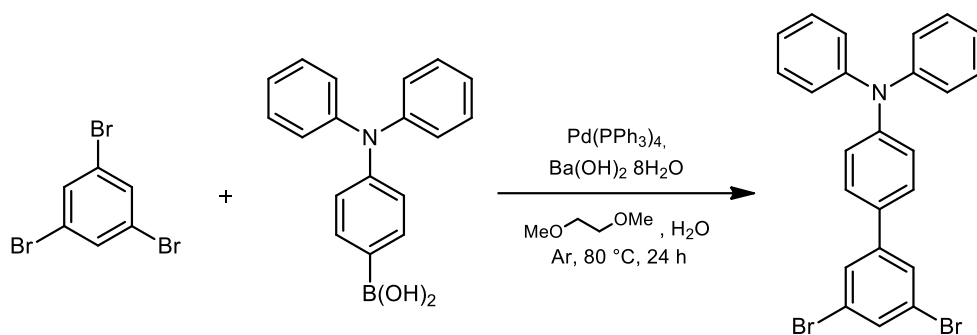
Mass of the product = 33 mg.

Yield = 73%.

Characterization

¹H NMR (400 MHz, CD₂Cl₂) δ (ppm): 8.88 (2H, d, J = 4.9 Hz, J(¹⁹⁵Pt) = 42 Hz), 8.04 (2H, dd, J = 8.0 Hz, J = 8.7 Hz), 7.73 (d, J = 7.8 Hz), 7.41 (2H, dd, J = 6.4 Hz, J = 8.0 Hz), 7.30 (2H, s), 7.01 (2H, s), 2.37 (3H, s), 2.10 (6H, s).

1.10 Synthesis of I2



Reagent/Solvent	PM (g/mol)	mmol	Mass	eq	Volume
1,3,5-tribromobenzene	314.80	1.588	500 mg	1.2	
4-NPh ₂ -phenylboronic acid	289.14	1.325	383 mg	1	
Pd(PPh ₃) ₄	1155.56	0.0432	50 mg	0.03	
Ba(OH) ₂ · 8H ₂ O	315.86	1.975	624 mg	1.5	
1,2-dimethoxyethane					3.0 mL
H ₂ O					0.5 mL

Procedure

The reagents were added to the solvents in a Schlenk tube and the mixture was stirred at 80 °C under Ar atmosphere. After 24 h the reaction was cooled to rt, toluene and water were added and the phases were separated. The organic phase was washed with brine (2x) and water (2x), dried over Na₂SO₄ and evaporated at reduced pressure.

The product was purified by flash chromatography on silica gel (eluent: from hexane to hexane/AcOEt 9:1).

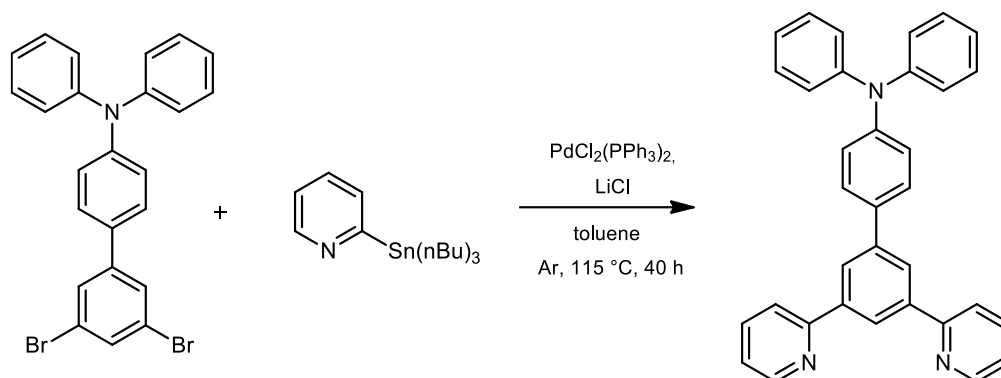
Mass of the product = 435 mg.

Yield = 69%.

Characterization

¹H-NMR (400 MHz, CDCl₃) δ (ppm): 7.64 (2H, d, J = 1.7 Hz), 7.60 (1H, t, J = 1.7 Hz), 7.40 (2H, d, J = 8.7 Hz), 7.31 (4H, t, J = 8.2 Hz), 7.18-7.06 (8H, m).

1.11 Synthesis of L2



Reagent/Solvent	PM (g/mol)	mmol	Mass	eq	Volume	Density
I2	479.21	0.565	190 mg	1		
$n\text{Bu}_3\text{Sn-pyridine}$	368.14	1.695	456 mg	3.1	400 μL	1.14 g/mL
$\text{PdCl}_2(\text{PPh}_3)_2$	701.90	0.017	14 mg	0.05		
LiCl	42.39	5.085	151 mg	9		
dry toluene					2.8 mL	

Procedure

The reagents were added to the solvent in a Schlenk tube and the mixture was stirred at reflux under Ar atmosphere. After 40 h a solution of NaOH (1 M, 5 mL), water and AcOEt were added and the phases were separated. The aqueous phase was extracted with AcOEt (2x), the organic phases were dried over Na_2SO_4 and evaporated.

The product was purified by flash chromatography on silica gel (eluent: hexane/AcOEt 9:1).

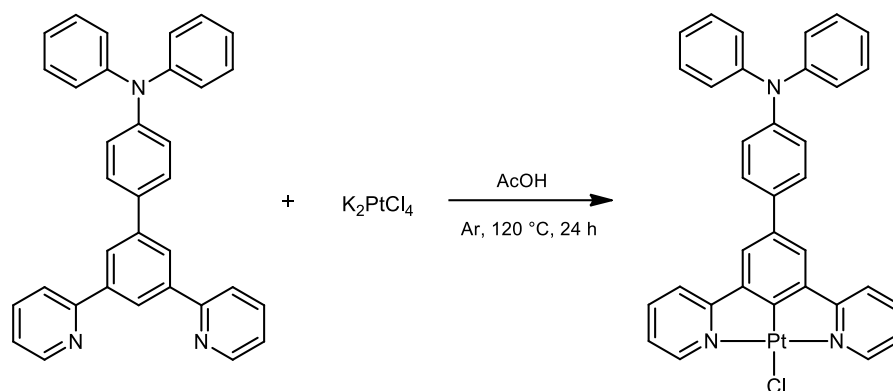
Mass of the product = 118 mg.

Yield = 44%.

Characterization

$^1\text{H-NMR}$ (400 MHz, CD_2Cl_2) δ (ppm): 8.76 (dd, 2H, $J = 4.8\text{ Hz}$, $J =$), 8.67 (t, 1H, $J = 1.6\text{ Hz}$), 8.34 (d, 2H, $J = 1.6\text{ Hz}$), 7.96 (d, 2H, $J = 7.8\text{ Hz}$), 7.86 (2H, dd, $J = 7.8\text{ Hz}$, $J = 8.0\text{ Hz}$), 7.70 (d, 2H, $J = 8.8\text{ Hz}$), 7.36-7.30 (m, 6H), 7.24-7.17 (m, 6H), 7.09 (dd, 2H, $J = 4.8\text{ Hz}$, $J = 8.0\text{ Hz}$).

1.12 Synthesis of PtCl₂



Reagent/Solvent	PM (g/mol)	mmol	Mass	eq	Volume
L2	475.58	0.168	80 mg	1	
K ₂ PtCl ₄	415.09	0.202	84 mg	1.2	
glacial AcOH					5 mL

Procedure

The reagents were added to the glacial AcOH in a Schlenk tube and the mixture was stirred at reflux under Ar atmosphere. After 24 h the reaction was cooled to rt and the orange-yellow precipitate was filtered on a Buchner funnel, washed with H₂O, MeOH and Et₂O, and dried.

The product was not furtherly purified.

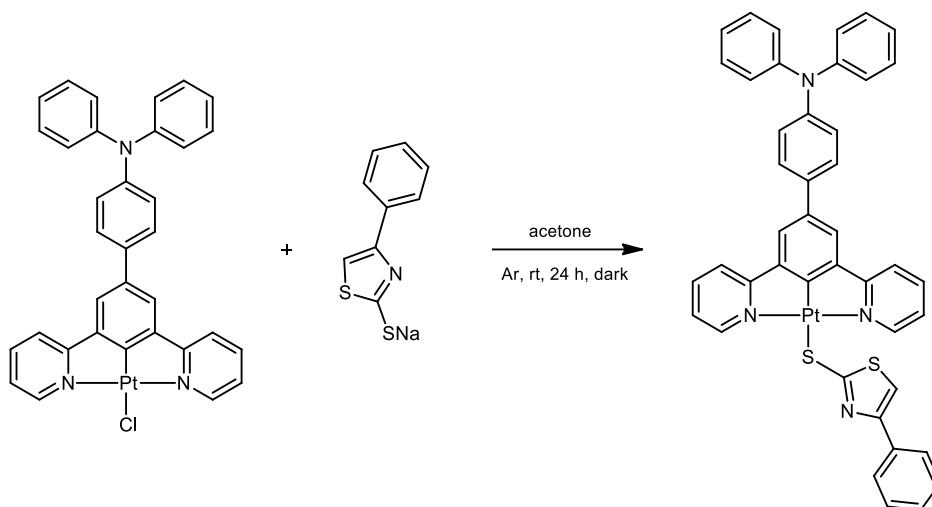
Mass of the product = 91 mg.

Yield = 77%.

Characterization

¹H-NMR (300 MHz, CD₂Cl₂) δ (ppm): 9.35 (2H, d, J = 5.7 Hz, J(¹⁹⁵Pt) = 42 Hz), 8.05 (2H, dd, J = 7.6 Hz, J = 8.5 Hz), 7.85 (2H, d, J = 7.6 Hz), 7.75 (2H, s), 7.61 (2H, d, J = 8.6 Hz), 7.42-7.28 (6H, m), 7.24-7.14 (6H, m), 7.10 (2H, dd, J = 7.3 Hz, J = 8.0 Hz).

1.13 Synthesis of Pt7



Reagent/Solvent	PM (g/mol)	mmol	Mass	eq	Volume
PtCl ₂	705.11	0.057	40 mg	1	
4-phenylthiazole-2-thiol sodium salt	215.25	0.798	172 mg	14	
acetone					60 mL

Procedure

In a two-necked round-bottom flask the platinum complex and the sodium salt were added to the solvent and the mixture was stirred at rt in the dark under Ar atmosphere. After 24 h the acetone was evaporated at reduced pressure and DCM was added to dissolve the product; the sodium salt in excess was filtered through cotton and the evaporation of the DCM gave the product as an orange solid.

The product was not furtherly purified.

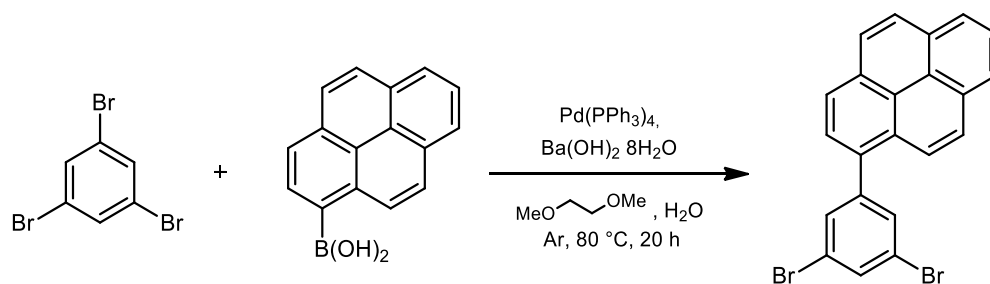
Mass of the product = 31 mg.

Yield = 63%.

Characterization

¹H-NMR (300 MHz, CD₂Cl₂) δ (ppm): 9.45 (2H, d, J = 5.7 Hz, J(¹⁹⁵Pt) = 41 Hz), 8.02 (2H, dd, J = 8.0 Hz, J = 8.4 Hz), 7.91-7.81 (4H, m), 7.79 (2H, s), 7.62 (2H, d, J = 8.6 Hz), 7.44-7.05 (15H, m), 6.99 (1H, s).

1.14 Synthesis of I3



Reagent/Solvent	PM (g/mol)	mmol	Mass	eq	Volume
1,3,5-tribromobenzene	314.80	0.651	205 mg	1	
pyrene-1-boronic acid	246.07	0.650	160 mg	1	
Pd(PPh ₃) ₄	1155.56	0.0199	23 mg	0.03	
Ba(OH) ₂ · 8H ₂ O	315.86	0.969	306 mg	1.5	
1,2-dimethoxyethane					3.0 mL
H ₂ O					0.5 mL

Procedure

The reagents were added to the solvents in a Schlenk tube and the mixture was stirred at 80 °C under Ar atmosphere. After 24 h the reaction was cooled to rt, toluene and water were added and the phases were separated. The organic phase was washed with brine (2x) and water (2x), dried over Na₂SO₄ and evaporated at reduced pressure.

The product was purified by flash chromatography on silica gel (eluent: hexane).

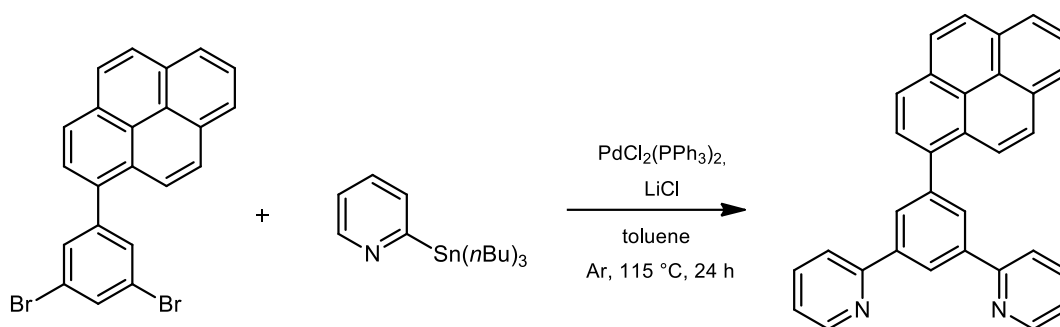
Mass of the product = 145 mg.

Yield = 51%.

Characterization

¹H-NMR (400 MHz, CD₂Cl₂) δ (ppm): 8.32-8.07 (8H, m), 7.98 (1H, d, J = 7.9 Hz), 7.87 (1H, t, J = 1.7 Hz), 7.79 (2H, d, J = 1.7 Hz).

1.15 Synthesis of L3



Reagent/Solvent	PM (g/mol)	mmol	Mass	eq	Volume	Density
I3	354.08	0.280	122 mg	1		
$n\text{Bu}_3\text{Sn-pyridine}$	368.14	0.929	342 mg	3.3	300 μL	1.14 g/mL
$\text{PdCl}_2(\text{PPh}_3)_2$	701.90	0.014	10 mg	0.03		
LiCl	42.39	2.500	106 mg	9		
dry toluene					2.0 mL	

Procedure

The reagents were added to the solvent in a Schlenk tube and the mixture was stirred at reflux under Ar atmosphere. After 24 h a solution of NaOH (1 M, 3.5 mL), water and AcOEt were added and the phases were separated. The aqueous phase was extracted with AcOEt (2x), the organic phases were dried over Na_2SO_4 and evaporated.

The product was purified by flash chromatography on silica gel (eluent: hexane/AcOEt 7:3).

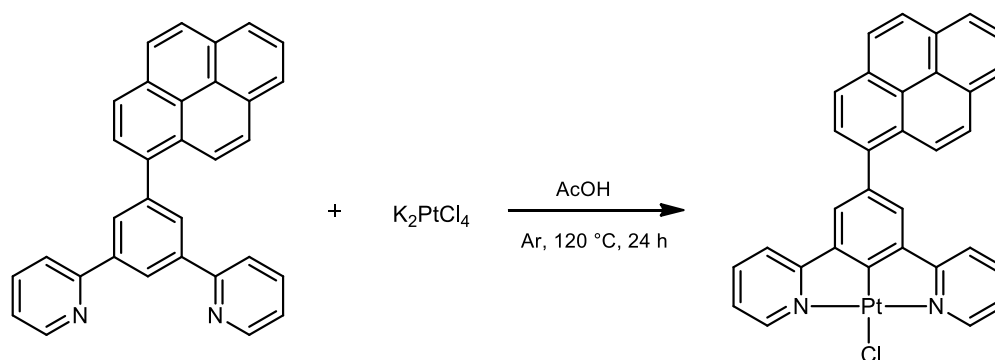
Mass of the product = 99 mg.

Yield = 82%.

Characterization

$^1\text{H-NMR}$ (400 MHz, CD_2Cl_2) δ (ppm): 8.90 (1H, dd, $J = 1.7\text{ Hz}$, $J = 2.0\text{ Hz}$), 8.77 (2H, d, $J = 4.7\text{ Hz}$), 8.38 (2H, d, $J = 1.7\text{ Hz}$), 8.37-8.06 (9H, m), 8.00 (2H, d, $J = 8.1\text{ Hz}$), 7.86 (2H, dd, $J = 7.6\text{ Hz}$, $J = 8.1\text{ Hz}$), 7.34 (2H, dd, $J = 4.7\text{ Hz}$, $J = 7.6\text{ Hz}$).

1.16 Synthesis of PtCl3



Reagent/Solvent	PM (g/mol)	mmol	Mass	eq	Volume
FF141	432.51	0.208	90 mg	1	
K ₂ PtCl ₄	415.09	0.250	104 mg	1.2	
glacial AcOH					7.5 mL

Procedure

The reagents were added to the glacial AcOH in a Schlenk tube and the mixture was stirred at reflux under Ar atmosphere. After 24 h the reaction was cooled to rt and the orange-yellow precipitate was filtered on a Buchner funnel, washed with H₂O, MeOH and Et₂O, and dried.

The product was not furtherly purified.

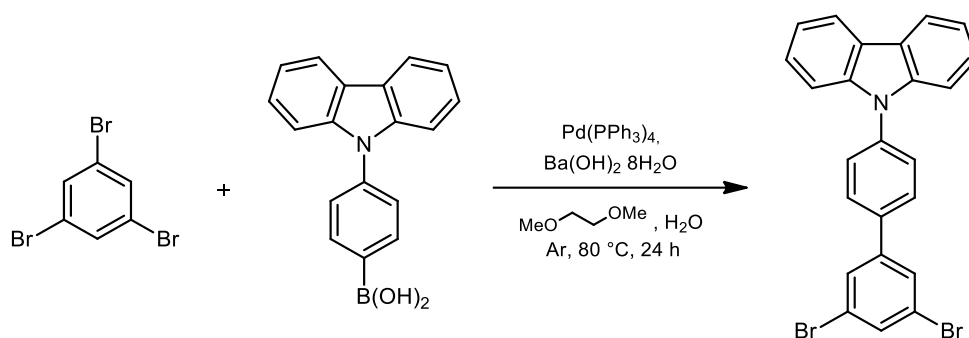
Mass of the product = 106 mg.

Yield = 77%.

Characterization

¹H-NMR (400 MHz, CD₂Cl₂) δ (ppm): 9.40 (2H, d, J = 5.7 Hz, J(¹⁹⁵Pt) = 42 Hz), 8.36-8.07 (9H, m), 8.04 (2H, dd, J = 7.9 Hz, J = 8.3 Hz), 7.86-7.78 (4H, m), 7.42 (2H, dd, J = 5.7 Hz, J = 7.9 Hz).

1.17 Synthesis of I4



Reagent/Solvent	PM (g/mol)	mmol	Mass	Eq	Volume
1,3,5-tribromobenzene	314.80	0.953	300 mg	1.2	
9H-carbazole-9-(4-phenyl)boronic acid pinacol ester	369.26	0.793	293 mg	1	
Pd(PPh ₃) ₄	1155.56	0.024	28 mg	0.03	
Ba(OH) ₂ · 8H ₂ O	315.86	1.190	376 mg	1.5	
1,2-dimethoxyethane					2.0 mL
H ₂ O					0.5 mL

Procedure

The reagents were added to the solvents in a Schlenk tube and the mixture was stirred at 80 °C under Ar atmosphere. After 24 h the reaction was cooled to rt, DCM and water were added and the phases were separated. The aqueous phase was extracted with DCM (2x), dried over Na₂SO₄ and evaporated at reduced pressure.

The product was purified by flash chromatography on silica gel (eluent: from hexane to hexane/AcOEt 95:5).

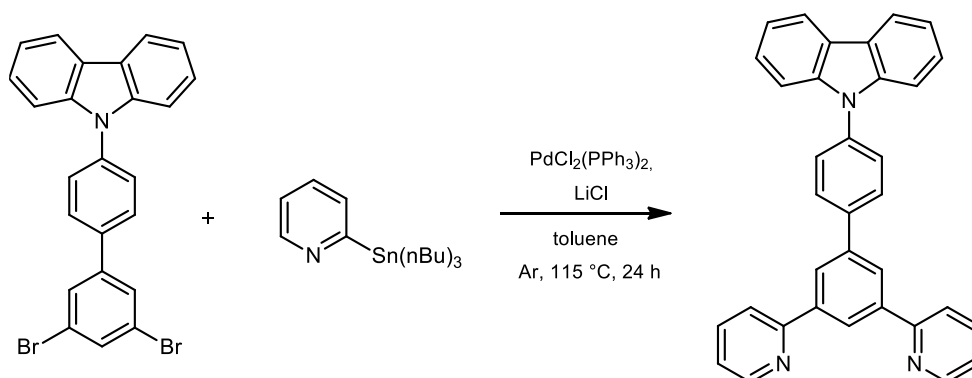
Mass of the product = 228 mg.

Yield = 60%.

Characterization

¹H-NMR (400 MHz, CDCl₃) δ (ppm): 8.18 (2H, d, J = 7.8 Hz), 7.81-7.77 (4H, m), 7.73 (1H, t, J = 1.6 Hz), 7.70 (2H, d, J = 8.5 Hz), 7.50-7.44 (4H, m), 7.34 (2H, dd, J = 6.0 Hz, J = 7.8 Hz).

1.18 Synthesis of L4



Reagent/Solvent	PM (g/mol)	mmol	Mass	eq	Volume	Density
I4	477.19	0.287	137 mg	1		
$n\text{Bu}_3\text{Sn-pyridine}$	368.14	0.861	317 mg	3	278 μL	1.14 g/mL
$\text{Pd}(\text{PPh}_3)_4$	1155.56	0.011	13 mg	0.04		
LiCl	42.39	2.571	109 mg	9		
dry toluene					1.0 mL	

Procedure

The reagents were added to the solvent in a Schlenk tube and the mixture was stirred at reflux under Ar atmosphere. After 24 h water and DCM were added and the phases were separated. The aqueous phase was extracted with DCM (2x), the organic phases were dried over Na_2SO_4 and evaporated.

The product was purified by flash chromatography on silica gel (eluent: hexane/AcOEt 8:2).

Mass of the product = 97 mg.

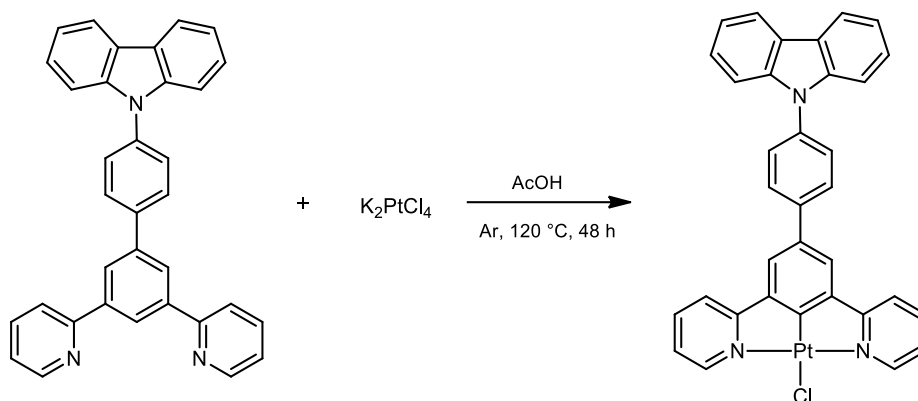
Yield = 71%.

Characterization

$^1\text{H-NMR}$ (400 MHz, CD_2Cl_2) δ (ppm): 8.81 (2H, d, $J = 4.8$ Hz), 8.79 (1H, t, $J = 1.6$ Hz), 8.52 (2H, d, $J = 1.6$ Hz), 8.22 (2H, d, $J = 7.7$ Hz), 8.10 (2H, d, $J = 8.5$ Hz), 8.06 (2H, d, $J = 8.0$ Hz), 7.94 (2H, dd, $J = 7.8$ Hz, $J = 8.4$ Hz), 7.77 (2H, d, $J = 8.4$ Hz), 7.56 (2H, d, $J = 8.2$ Hz), 7.49 (2H, dd, $J = 7.0$ Hz, $J = 8.2$ Hz), 7.40 (2H, dd, $J = 4.8$ Hz, $J = 7.6$ Hz), 7.35 (2H, dd, $J = 7.4$ Hz, $J = 8.0$ Hz).

$^{13}\text{C-NMR}$ (100 MHz, CD_2Cl_2) δ (ppm): 156.41, 149.30, 141.41, 140.85, 140.08, 139.84, 137.42, 137.22, 128.80, 127.31, 126.45, 126.01, 124.78, 123.39, 122.73, 120.94, 120.22, 119.99, 109.83.

1.19 Synthesis of PtCl4



Reagent/Solvent	PM (g/mol)	mmol	Mass	eq	Volume
L4	473.58	0.089	42 mg	1	
K ₂ PtCl ₄	415.09	0.106	44 mg	1.2	
glacial AcOH					1.5 mL

Procedure

The reagents were added to glacial AcOH in a Schlenk tube and the mixture was stirred at reflux under Ar atmosphere. After 48 h the yellow-orange precipitate was filtered on a Buchner funnel, washed with MeOH, H₂O and Et₂O, and dried.

The product was not furtherly purified.

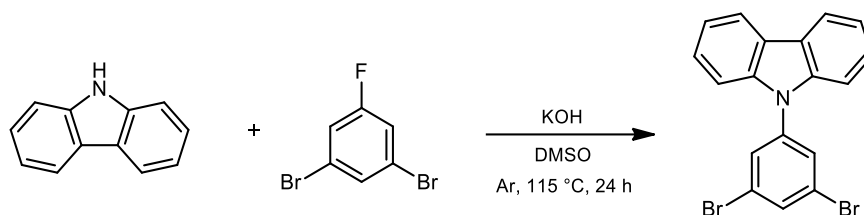
Mass of the product = 52 mg.

Yield = 83%.

Characterization

¹H-NMR (400 MHz, CD₂Cl₂) δ (ppm): 9.38 (2H, d, J = 5.6, J(¹⁹⁵Pt) = 41 Hz), 8.22 (2H, d, J = 7.7 Hz), 8.07 (2H, dd, J = 7.9 Hz, J = 8.7 Hz), 7.98 (2H, d, J = 8.4 Hz), 7.92 (2H, d, J = 7.7 Hz), 7.88 (2H, s), 7.75 (2H, d, J = 8.4 Hz), 7.55 (2H, d, J = 8.2 Hz), 7.50 (2H, dd, J = 7.0 Hz, J = 8.4 Hz), 7.42 (2H, dd, J = 6.0 Hz, J = 7.5 Hz), 7.36 (2H, dd, J = 7.0 Hz, J = 7.9 Hz).

1.20 Synthesis of I5



Reagent/Solvent	PM (g/mol)	mmol	Mass	eq	Volume	Density
carbazole	167.21	1.495	250 mg	1		
1,3-dibromo-5-fluoro benzene	253.91	3.738	949 mg	2.5	470 μ L	2.018 g/mL
KOH	56.11	4.485	252 mg	3		
DMSO					7.5 mL	

Procedure

The reagents were added to the solvent in a Schlenk tube and the mixture was stirred at reflux under Ar atmosphere. After 24 h the solution was cooled to rt, DCM and water were added and the phases were separated. The organic phase was dried over Na_2SO_4 and evaporated.

The product was purified by flash chromatography on silica gel (eluent: hexane).

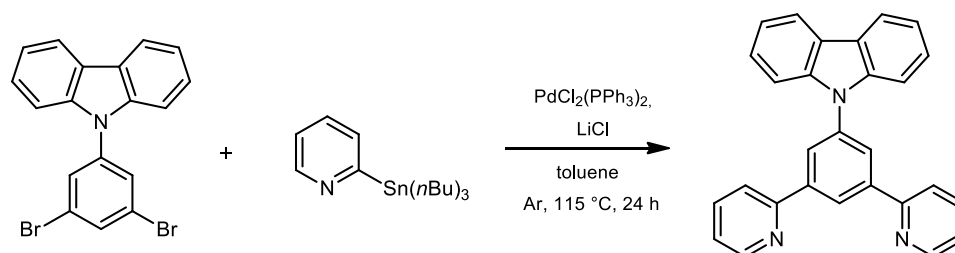
Mass of the product = 281 mg.

Yield = 47%.

Characterization

$^1\text{H-NMR}$ (400 MHz, CDCl_3) δ (ppm): 8.15 (2H, d, $J = 7.8$ Hz), 7.79 (1H, t, $J = 1.7$ Hz), 7.73 (2H, d, $J = 1.7$ Hz), 7.50-7.41 (4H, m), 7.34 (2H, dd, $J = 7.2$ Hz, $J = 7.8$ Hz).

1.21 Synthesis of L5



Reagent/Solvent	PM (g/mol)	mmol	Mass	eq	Volume	Density
I5	401.09	0.499	200 mg	1		
$n\text{Bu}_3\text{Sn-pyridine}$	368.14	1.496	551 mg	3	483 μL	1.14 g/mL
$\text{PdCl}_2(\text{PPh}_3)_2$	701.90	0.030	21 mg	0.06		
LiCl	42.39	4.491	190 mg	9		
dry toluene					1.5 mL	

Procedure

The reagents were added to the solvent in a Schlenk tube and the mixture was stirred at reflux under Ar atmosphere. After 24 h the reaction was cooled to rt, water and AcOEt were added and the phases were separated. The aqueous phase was extracted with AcOEt (2x), the organic phases were dried over Na_2SO_4 and evaporated.

The product was purified by flash chromatography on silica gel (eluent: hexane/AcOEt from 9:1 to 8:2 to 1:1).

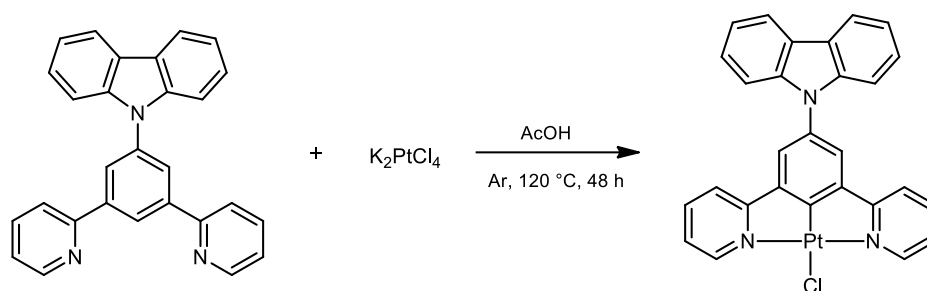
Mass of the product = 92 mg.

Yield = 46%.

Characterization

$^1\text{H-NMR}$ (400 MHz, CD_2Cl_2) δ (ppm): 8.90 (1H, t, $J = 1.6$ Hz), 8.77 (2H, d, $J = 4.7$ Hz), 8.3 (2H, d, $J = 1.6$ Hz), 8.23 (2H, d, $J = 7.5$ Hz), 7.98 (2H, d, $J = 8.0$ Hz), 7.88 (2H, dd, $J = 7.9$ Hz, $J = 8.3$ Hz), 7.58 (2H, d, $J = 8.2$ Hz), 7.48 (2H, dd, $J = 7.4$ Hz, $J = 8.2$ Hz), 7.39-7.33 (4H, m).

1.22 Synthesis of PtCl5



Reagent/Solvent	PM (g/mol)	mmol	Mass	eq	Volume
L5	397.47	0.161	64 mg	1	
K ₂ PtCl ₄	415.09	0.193	80 mg	1.2	
glacial AcOH					1.5 mL

Procedure

The reagents were added to glacial AcOH in a Schlenk tube and the mixture was stirred at reflux under Ar atmosphere. After 48 h the yellow-orange precipitate was filtered on a Buchner funnel, washed with MeOH, H₂O and Et₂O, and dried.

The product was not furtherly purified.

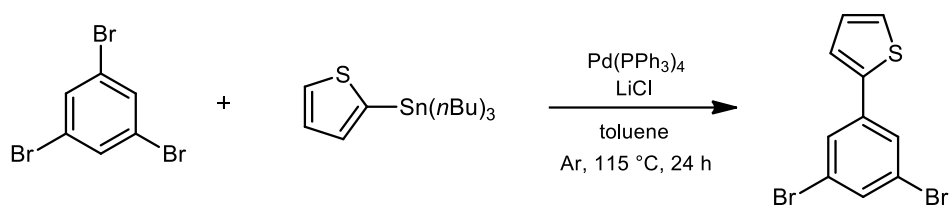
Mass of the product = 86 mg.

Yield = 85%.

Characterization

¹H-NMR (400 MHz, CD₂Cl₂) δ (ppm): 9.42 (2H, d, J = 5.6, J(¹⁹⁵Pt) = 42 Hz), 8.22 (2H, d, J = 7.7 Hz), 8.05 (2H, dd, J = 7.7 Hz, J = 8.8 Hz), 7.76 (2H, d, J = 7.7 Hz), 7.72 (2H, s), 7.51-7.41 (6H, m), 7.35 (2H, dd, J = 7.1 Hz, J = 7.8 Hz).

1.23 Synthesis of I6



Reagent/Solvent	PM (g/mol)	mmol	Mass	eq	Volume	Density
1,3,5-tribromobenzene	314.80	1.439	453 mg	1		
<i>n</i> Bu ₃ Sn-thiophene	373.18	1.572	587 mg	1.1	502 μL	1.17 g/mL
PdCl ₂ (PPh ₃) ₂	701.90	0.070	49 mg	0.05		
LiCl	42.39	7.162	304 mg	5		
dry toluene					2.0 mL	

Procedure

The reagents were added to the solvent in a Schlenk tube and the mixture was stirred at reflux under Ar atmosphere. After 24 h the solution was cooled to rt, the toluene was evaporated at reduced pressure, DCM and water were added and the phases were separated. The organic phase was dried over Na₂SO₄ and evaporated.

The product was purified by flash chromatography on silica gel (eluent: hexane/AcOEt from 8:2 to 6:4).

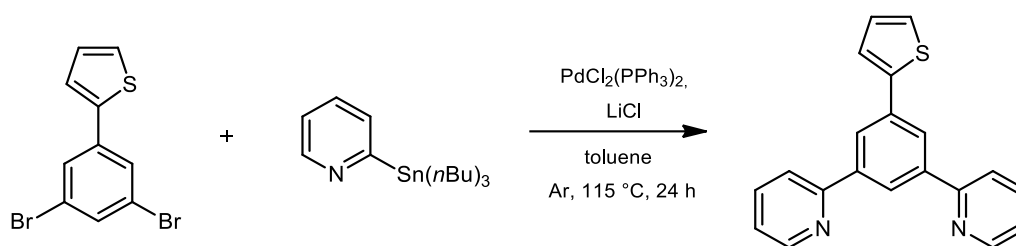
Mass of the product = 224 mg.

Yield = 48%.

Characterization

¹H-NMR (400 MHz, CDCl₃) δ (ppm): 7.69 (2H, s), 7.58 (1H, s), 7.37 (1H, d, J = 5.0 Hz), 7.33 (1H, d, J = 3.4 Hz), 7.11 (1H, dd, J = 3.4 Hz, J = 5.0 Hz).

1.24 Synthesis of L6



Reagent/Solvent	PM (g/mol)	mmol	Mass	eq	Volume	Density
I6	318.03	2.097	667 mg	1		
$n\text{Bu}_3\text{Sn}$ -pyridine	368.14	6.370	2.345 g	3.03	2.0 mL	1.14 g/mL
$\text{PdCl}_2(\text{PPh}_3)_2$	701.90	0.064	45 mg	0.03		
LiCl	42.39	18.919	802 mg	9		
dry toluene					6.5 mL	

Procedure

The reagents were added to the solvent in a Schlenk tube and the mixture was stirred at reflux under Ar atmosphere. After 24 h the reaction was cooled to rt, a solution of NaOH (1 M, 15 mL), water and AcOEt were added and the phases were separated. The aqueous phase was extracted with AcOEt (4x), the organic phases were dried over Na_2SO_4 and evaporated.

The product was purified by flash chromatography on silica gel (eluent: hexane/AcOEt 7:3).

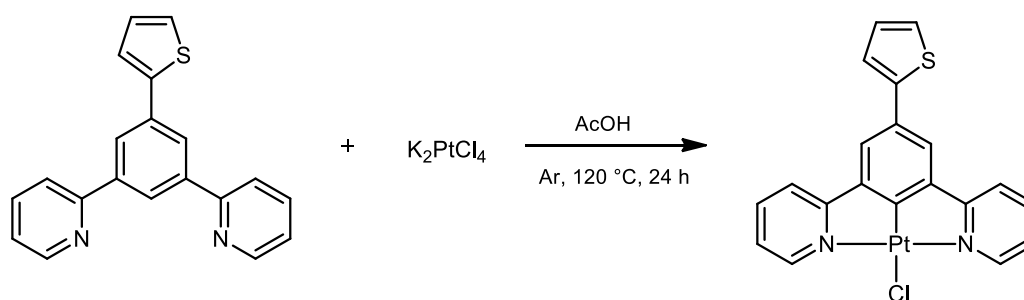
Mass of the product = 489 mg.

Yield = 74%.

Characterization

$^1\text{H-NMR}$ (400 MHz, CDCl_3) δ (ppm): 8.76 (2H, d, $J = 4.8$ Hz), 8.54 (1H, t, $J = 1.5$ Hz), 8.33 (2H, d, $J = 1.5$ Hz), 7.89 (2H, d, $J = 8.0$ Hz), 7.80 (2H, dd, $J = 7.6$ Hz, $J = 8.0$ Hz), 7.53 (1H, d, $J = 3.6$ Hz), 7.34 (1H, d, $J = 5.1$ Hz), 7.28 (2H, dd, $J = 4.8$ Hz, $J = 7.6$ Hz), 7.14 (1H, dd, $J = 3.6$ Hz, $J = 5.1$ Hz).

1.25 Synthesis of PtCl6



Reagent/Solvent	PM (g/mol)	mmol	Mass	eq	Volume
L6	314.41	0.381	120 mg	1	
K_2PtCl_4	415.09	0.458	190 mg	1.2	
glacial AcOH					10 mL

Procedure

The reagents were added to glacial AcOH in a Schlenk tube and the mixture was stirred at reflux under Ar atmosphere. After 24 h the orange precipitate was filtered on a Buchner funnel, washed with MeOH, H₂O, EtOH and Et₂O, and dried.

The product was not furtherly purified.

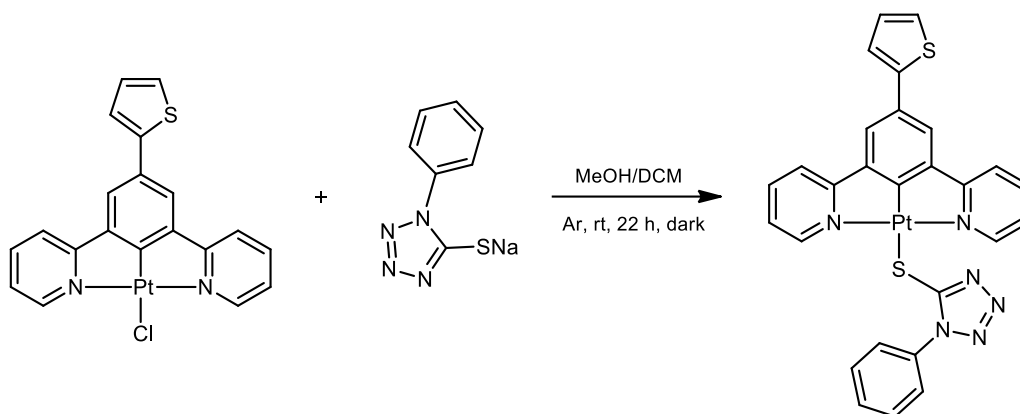
Mass of the product = 140 mg.

Yield = 67%.

Characterization

¹H-NMR (400 MHz, CD₂Cl₂) δ (ppm): 9.33 (2H, d, J = 5.5, J(¹⁹⁵Pt) = 41 Hz), 8.06 (2H, dd, J = 7.8 Hz, J = 8.6 Hz), 7.85 (2H, d, J = 7.8 Hz), 7.78 (2H, s), 7.40 (1H, d, J = 3.5 Hz), 7.43-7.35 (3H, m), 7.17 (1H, dd, J = 3.5 Hz, J = 5.2 Hz).

1.26 Synthesis of Pt8



Reagent/Solvent	PM (g/mol)	mmol	Mass	eq	Volume
PtCl ₆	544.94	0.066	36 mg	1	
1-phenyl-1H-tetrazole-5-thiol sodium salt	200.20	0.799	160 mg	12	
MeOH					6.0 mL
DCM					6.0 mL

Procedure

In a two-necked round-bottom flask a solution of the sodium salt in MeOH was added to a solution of the platinum complex in DCM; the solution became almost black and was stirred at rt in the dark under Ar atmosphere. After 1 h the solution became orange and after 22 h the precipitation of the product was observed; the solid was filtered on a Hirsch funnel, washed with MeOH and Et₂O, and dried.

The product was not furtherly purified.

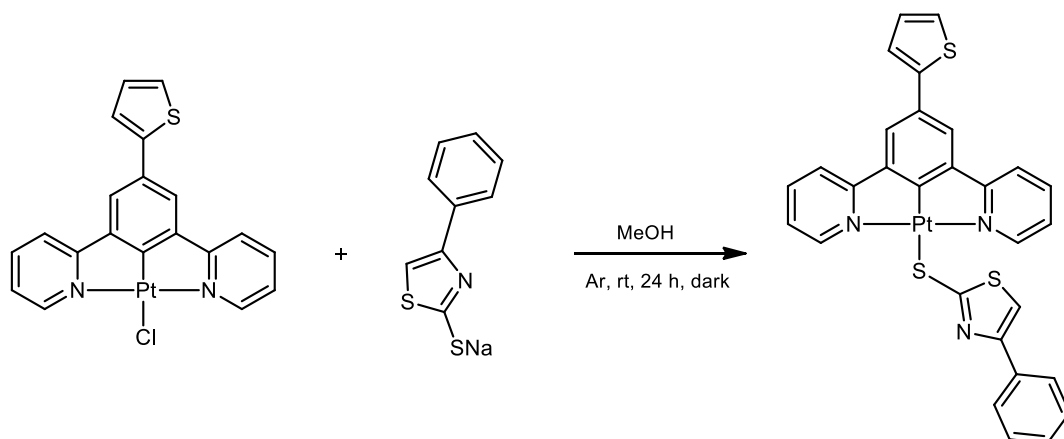
Mass of the product = 22 mg.

Yield = 49%.

Characterization

¹H-NMR (300 MHz, CD₂Cl₂) δ (ppm): 9.19 (2H, m), 8.07-7.99 (2H, m), 7.92-7.77 (5H, m), 7.53-7.42 (3H, m), 7.40 (1H, d, J = 3.7 Hz), 7.33-7.25 (2H, m), 7.20-7.15 (1H, m). For some reason, not for all peaks the multiplicity is clear, and so their J cannot be calculated properly.

1.27 Synthesis of Pt9



Reagent/Solvent	PM (g/mol)	mmol	Mass	eq	Volume
PtCl ₆	543.93	0.055	30 mg	1	
4-phenylthiazole-2-thiol sodium salt	215.27	0.218	47 mg	4	
MeOH					3.0 mL

Procedure

In a two-necked round-bottom flask the platinum complex was added to a solution of the sodium salt in MeOH and the suspension was stirred at rt in the dark under Ar atmosphere. After 24 h an orange precipitate was observed, MeOH was added to dissolve the sodium salt in excess and after 10 minutes of stirring the solid was filtered on a Buchner funnel, washed with MeOH and Et₂O, and dried.

The product was not further purified.

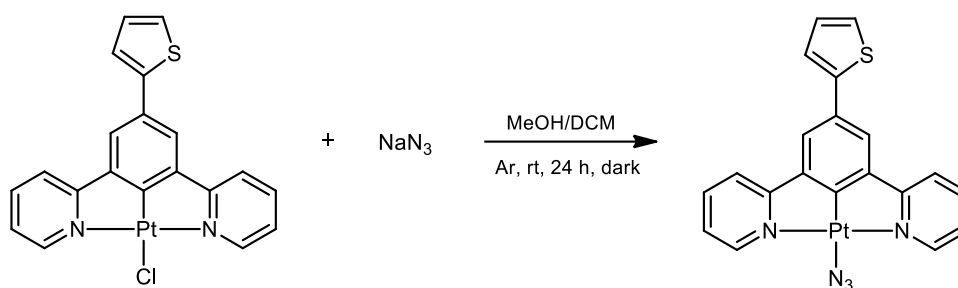
Mass of the product = 35 mg.

Yield = 90%.

Characterization

¹H-NMR (400 MHz, CD₂Cl₂) δ (ppm): 9.41 (2H, d, J = 5.7 Hz, J(¹⁹⁵Pt) = 44 Hz), 8.02 (2H, dd, J = 7.7 Hz, J = 8.6 Hz), 7.90-7.80 (4H, m), 7.78 (2H, s), 7.47 (1H, d, J = 3.5 Hz), 7.42-7.36 (3H, m), 7.20-7.16 (3H, m), 6.99 (1H, s).

1.28 Synthesis of Pt10



Reagent/Solvent	PM (g/mol)	mmol	Mass	eq	Volume
PtCl ₆	544.94	0.038	17 mg	1	
NaN ₃	65.01	0.754	50 mg	20	
MeOH					3.0 mL
DCM					3.0 mL

Procedure

In a Schlenk tube a solution of NaN₃ in MeOH was added to a solution of platinum complex in DCM; almost immediately the solution became dark green, with the precipitation of the product, and the mixture was stirred at rt in the dark under Ar atmosphere. After 24 h water was added to dissolve the NaN₃ in excess and after 5 minutes of stirring the solid was filtered on a Buchner funnel, washed with MeOH and Et₂O, and dried.

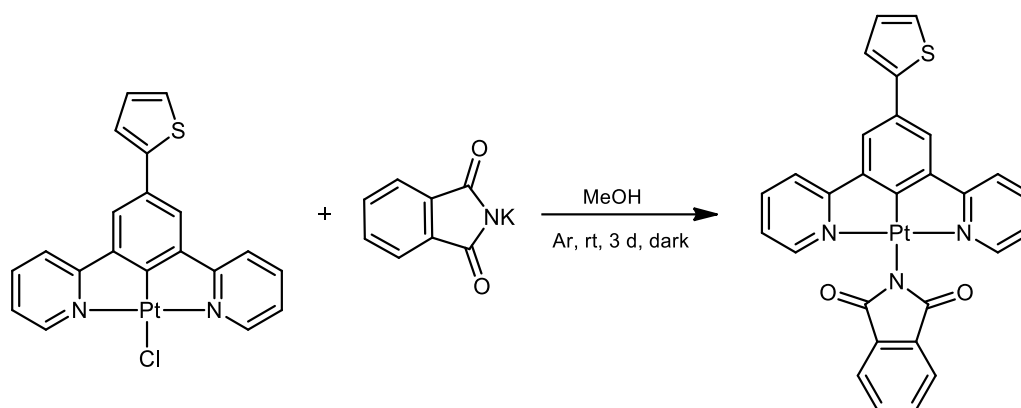
Mass of the product = 17 mg.

Yield = 81%.

Characterization

¹H-NMR (300 MHz, CD₂Cl₂) δ (ppm): 8.83 (2H, d, J = 5.6 Hz, J(¹⁹⁵Pt) = 42 Hz), 8.07 (2H, dd, J = 7.7 Hz, J = 8.8 Hz), 7.85 (2H, d, J = 7.7 Hz), 7.72 (2H, s), 7.47-7.35 (4H, m), 7.17 (1H, dd, J = 3.8 Hz, J = 5.0 Hz).

1.29 Synthesis of Pt11



Reagent/Solvent	PM (g/mol)	mmol	Mass	eq	Volume
PtCl ₆	544.94	0.055	30 mg	1	
potassium phthalimide	185.22	0.550	102 mg	10	
MeOH					4.0 mL

Procedure

In a Schlenk tube the platinum complex and the potassium salt were added to the solvent and the mixture was stirred at rt in the dark under Ar atmosphere. After 72 h the yellow precipitate was filtered on a Buchner funnel, washed with MeOH and Et₂O, and dried.

The product was not furtherly purified.

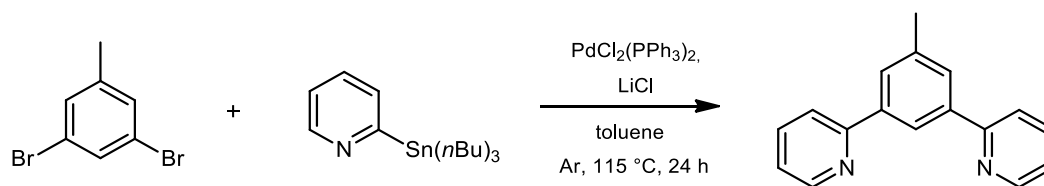
Mass of the product = 18 mg.

Yield = 50%.

Characterization

¹H-NMR (400 MHz, CD₂Cl₂) δ (ppm): 8.49 (2H, d, J = 5.8, J(¹⁹⁵Pt) = 42 Hz), 8.00 (2H, dd, J = 7.5 Hz, J = 7.9 Hz), 7.87 (2H, d, J = 7.5 Hz), 7.83-7.79 (4H, m), 7.71-7.67 (2H, m), 7.47 (1H, dd, J = 1.1 Hz, J = 3.6 Hz), 7.36 (1H, dd, J = 1.1 Hz, J = 5.1 Hz), 7.21 (2H, dd, J = 5.8 Hz, J = 7.9 Hz), 7.14 (1H, dd, J = 3.6 Hz, J = 5.1 Hz).

1.30 Synthesis of L7



Reagent/Solvent	PM (g/mol)	mmol	Mass	eq	Volume	Density
3,5-dibromotoluene	249.96	0.800	200 mg	1		
<i>n</i> Bu ₃ Sn-pyridine	368.14	2.400	884 mg	3	775 μL	1.14 g/mL
PdCl ₂ (PPh ₃) ₂	701.90	0.04	28 mg	0.05		
LiCl	42.39	7.200	305 mg	9		
dry toluene					5.0 mL	

Procedure

The reagents were added to the solvent in a Schlenk tube and the mixture was stirred at reflux under Ar atmosphere. After 24 h a solution of NaOH (1 M, 10 mL), water and AcOEt were added and the phases were separated. The aqueous phase was extracted with AcOEt (3x), the organic phases were dried over Na₂SO₄ and evaporated.

The product was purified by flash chromatography on silica gel (eluent: hexane/AcOEt 7:3).

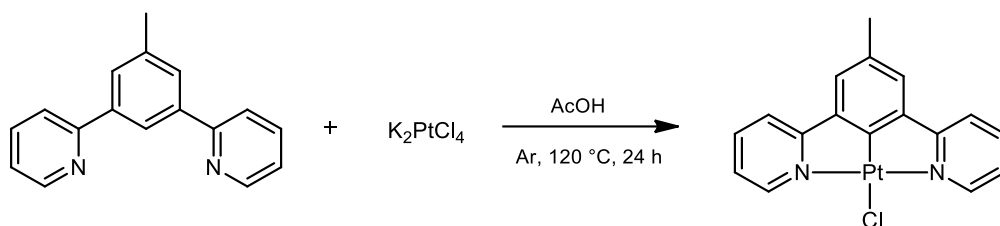
Mass of the product = 138 mg.

Yield = 70%.

Characterization

¹H-NMR (400 MHz, CDCl₃) δ (ppm): 8.72 (2H, d, J = 4.6 Hz), 8.39 (1H, s), 7.91 (2H, s), 7.99-7.79 (6H, m), 7.25 (2H, dd, J = 4.6 Hz, J = 7.4 Hz), 2.53 (3H, s).

1.31 Synthesis of PtCl7



Reagent/Solvent	PM (g/mol)	mmol	Mass	eq	Volume
L7	246.31	0.524	129 mg	1	
K_2PtCl_4	415.09	0.628	260 mg	1.2	
glacial AcOH					8.0 mL

Procedure

The reagents were added to glacial AcOH in a Schlenk tube and the mixture was stirred at reflux under Ar atmosphere. After 24 h some water was added to dissolve the excess K_2PtCl_4 , the yellow precipitate was filtered on a Buchner funnel, washed with H_2O , MeOH and Et_2O , and dried.

The product was not furtherly purified.

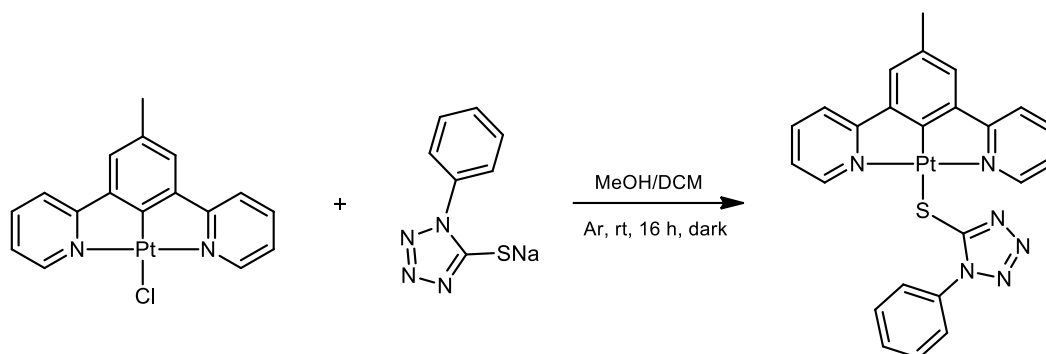
Mass of the product = 229 mg.

Yield = 92%.

Characterization

1H -NMR (400 MHz, CD_2Cl_2) δ (ppm): 9.28 (2H, d, $J = 5.7$ Hz, $J(^{195}Pt) = 42$ Hz), 8.00 (2H, dd, $J = 7.7$ Hz, $J = 8.0$ Hz), 7.73 (2H, d, $J = 8.0$ Hz), 7.37 (2H, s), 7.33 (2H, dd, $J = 5.7$ Hz, $J = 7.7$ Hz), 2.40 (3H, s).

1.32 Synthesis of Pt12



Reagent/Solvent	PM (g/mol)	mmol	Mass	eq	Volume
PtCl7	475,83	0.029	14 mg	1	
1-phenyl-1H-tetrazole-5-thiol sodium salt	200.20	0.589	118 mg	20	
MeOH					3.0 mL
DCM					3.0 mL

Procedure

In a two-necked round-bottom flask a solution of sodium salt in MeOH was added to a solution of platinum complex in DCM; the dark green solution was stirred at rt in the dark under Ar atmosphere. After 1 h the solution became orange and after 22 h the precipitation of the product was observed; MeOH was added to dissolve the sodium salt in excess, after further 10 minutes of stirring the orange solid was filtered on a Hirsch funnel and dried.

The product was not furtherly purified.

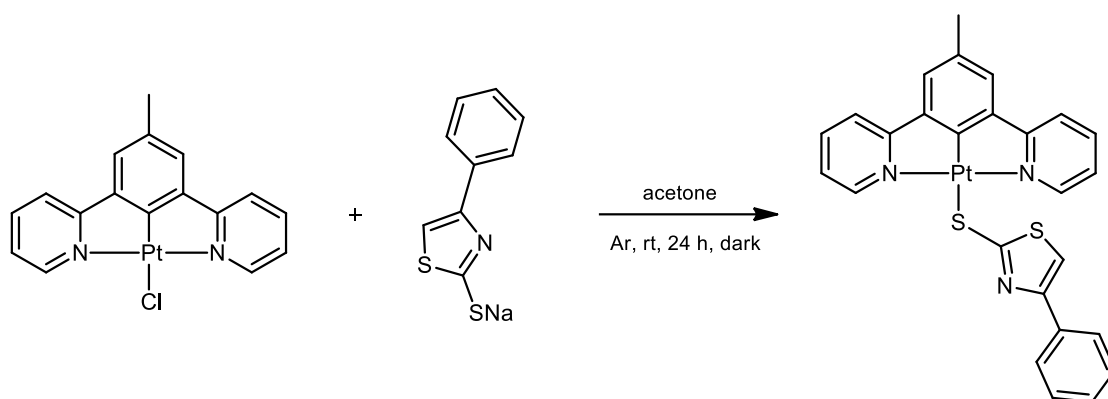
Mass of the product = 17 mg.

Yield = 94%.

Characterization

$^1\text{H-NMR}$ (400 MHz, CD_2Cl_2) δ (ppm): 9.14 (2H, d, $J = 5.7$ Hz, $J(^{195}\text{Pt}) = 41$ Hz), 7.97 (2H, dd, $J = 7.3$ Hz, $J = 7.7$ Hz), 7.88 (2H, d, $J = 7.0$ Hz), 7.73 (2H, d, $J = 7.7$ Hz), 7.53-7.37 (5H, m), 7.23 (2H, m), 2.44 (3H, s).

1.33 Synthesis of Pt13



Reagent/Solvent	PM (g/mol)	mmol	Mass	eq	Volume
PtCl7	475.83	0.210	100 mg	1	
4-phenylthiazole-2-thiol sodium salt	215.25	1.468	316 mg	7	
acetone					100 mL

Procedure

In a two-necked round-bottom flask the platinum complex and the sodium salt were added to the solvent and the mixture was stirred at rt in the dark under Ar atmosphere. After 24 h the acetone was evaporated at reduced pressure and DCM was added to dissolve the product; the sodium salt in excess was filtered through cotton and the evaporation of the DCM gave the product as an orange solid.

The product was not furtherly purified.

Mass of the product = 80 mg.

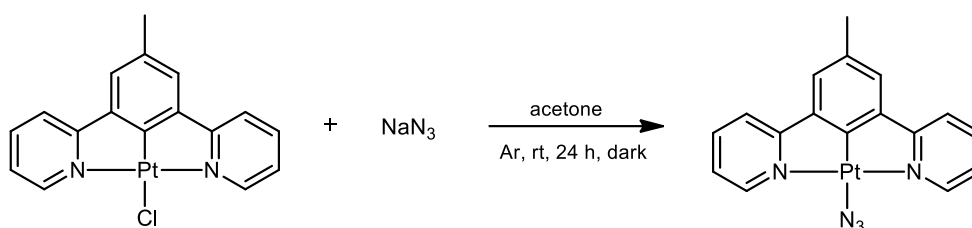
Yield = 60%.

Characterization

$^1\text{H-NMR}$ (400 MHz, CD_2Cl_2) δ (ppm): 9.41 (2H, d, $J = 5.8$ Hz, $J(^{195}\text{Pt}) = 44$ Hz), 7.99 (2H, dd, $J = 7.8$ Hz, $J = 7.2$ Hz), 7.87 (2H, d, $J = 8.7$ Hz), 7.76 (2H, d, $J = 7.9$ Hz), 7.44 (2H, s), 7.39 (2H, dd, $J = 7.3$ Hz, $J = 8.0$ Hz), 7.32-7.23 (3H, m), 6.98 (1H, s), 2.46 (3H, s).

$^{13}\text{C-NMR}$ (100 MHz, CD_2Cl_2) δ (ppm): 153.51, 139.35, 128.41, 127.19, 125.91, 124.87, 123.64, 119.43, 109.84, 21.76.

1.34 Synthesis of Pt14



Reagent/Solvent	PM (g/mol)	mmol	Mass	eq	Volume
PtCl7	475.83	0.168	80 mg	1	
NaN ₃	65.01	2.523	164 mg	14.8	
acetone					250 mL

Procedure

In a two-necked round-bottom flask the platinum complex and the NaN₃ were added to the solvent and the mixture was stirred at rt in the dark under Ar atmosphere. After 24 h the acetone was evaporated at reduced pressure and DCM was added to dissolve the product; the NaN₃ in excess was filtered through cotton and the evaporation of the DCM gave the product as an orange solid.

The product was recrystallized from DCM/pentane and dried.

Mass of the product = 40 mg.

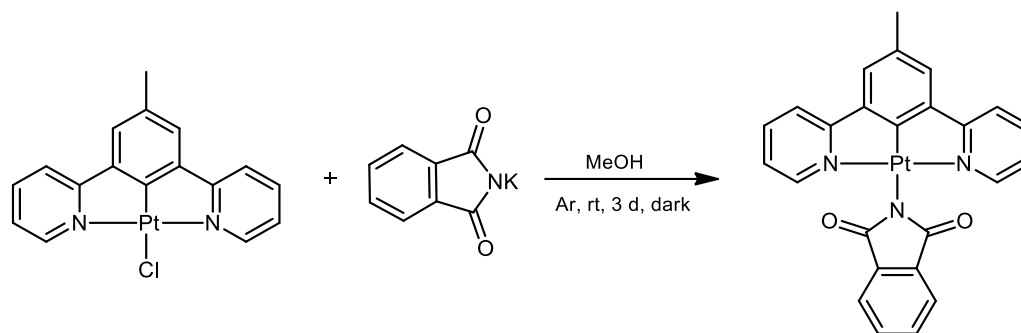
Yield = 49%.

Characterization

¹H-NMR (400 MHz, CD₂Cl₂) δ (ppm): 8.74 (2H, d, J = 5.5 Hz, J(¹⁹⁵Pt) = 42 Hz), 8.00 (2H, dd, J = 7.9 Hz, J = 8.0 Hz), 7.71 (2H, d, J = 8.0 Hz), 7.34 (2H, dd, J = 5.5 Hz, J = 7.9 Hz), 7.29 (2H, s), 2.37 (3H, s).

¹³C-NMR (100 MHz, CD₂Cl₂) δ (ppm): 150.77, 139.52, 125.11, 123.56, 119.80, 22.10.

1.35 Synthesis of Pt15



Reagent/Solvent	PM (g/mol)	mmol	Mass	eq	Volume
PtCl7	475.83	0.063	30 mg	1	
potassium phthalimide	185.22	0.946	175 mg	15	
MeOH					4.0 mL

Procedure

In a Schlenk tube the platinum complex and the potassium salt were added to the solvent and the mixture was stirred at rt in the dark under Ar atmosphere. After 72 h the yellow precipitate was filtered on a Buchner funnel, washed with MeOH and Et₂O, and dried.

The product was not furtherly purified.

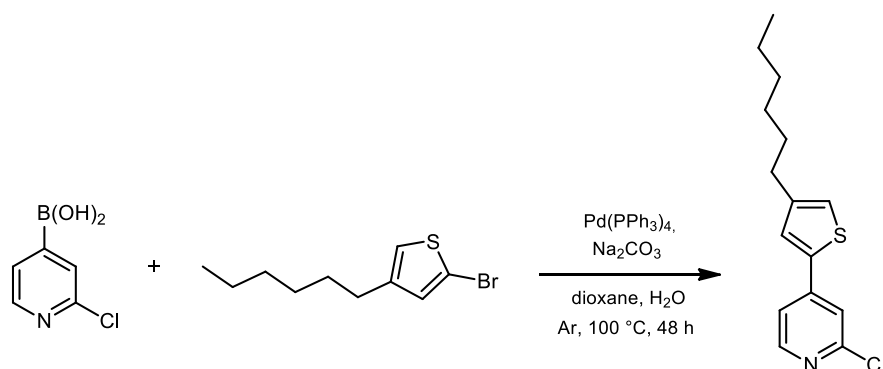
Mass of the product = 15 mg.

Yield = 41%.

Characterization

¹H-NMR (400 MHz, CD₂Cl₂) δ (ppm): 8.47 (2H, d, J = 4.9 Hz, J(¹⁹⁵Pt) = 43 Hz), 7.97 (2H, dd, J = 7.9 Hz, J = 8.0 Hz), 7.82-7.73 (4H, m), 7.70-7.64 (2H, m), 7.42 (2H, s), 7.19 (2H, dd, J = 7.8 Hz, J = 4.9 Hz), 2.44 (3H, s).

1.36 Synthesis of I7



Reagent/Solvent	PM (g/mol)	mmol	Mass	eq	Volume	Density
2-Br-4-hexylthiophene	247.20	2.382	589 mg	1.5	482 μ L	1.222 g/mL
2-Cl-pyridine-4-boronic acid	157.36	1.589	250 mg	1		
Pd(PPh ₃) ₄	1155.56	0.718	83 mg	0.045		
Na ₂ CO ₃	105.99	4.793	508 mg	3		
1,4-dioxane					9.0 mL	
H ₂ O					3.0 mL	

Procedure

The reagents were added to the solvents in a Schlenk tube and the mixture was stirred at reflux under Ar atmosphere. After 48 h water and AcOEt were added and the phases were separated. The organic phase was washed with water (3x), then dried over Na₂SO₄ and evaporated.

The product was purified by flash chromatography on silica gel (eluent: hexane/AcOEt from 9:1 to 8:2).

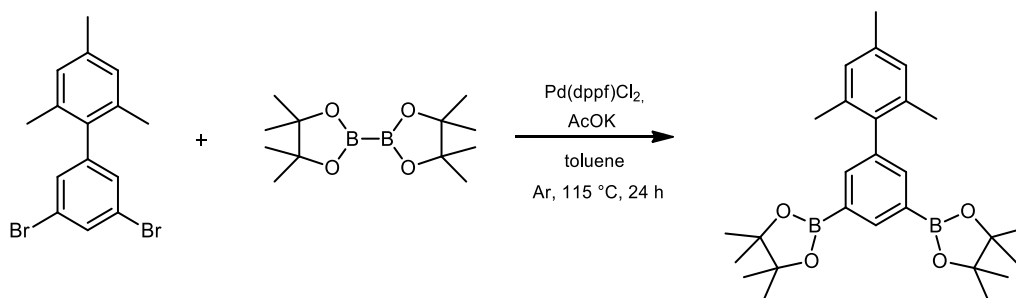
Mass of the product = 265 mg.

Yield = 60%.

Characterization

¹H-NMR (400 MHz, CDCl₃) δ (ppm): 8.35 (1H, d, J = 5.3 Hz), 7.51 (1H, d, J = 1.0 Hz), 7.41-7.36 (2H, m), 7.07 (1H, s), 2.65 (2H, t, J = 7.8 Hz), 1.71-1.61 (2H, m), 1.42-1.28 (6H, m), 0.92 (3H, t, J = 6.8 Hz).

1.37 Synthesis of B1



Reagent/Solvent	PM (g/mol)	mmol	Mass	eq	Volume
I1	352.08	0.860	303 mg	1	
bis(pinacolato) diboron	253.94	1.878	477 mg	2.2	
Pd(dppf)Cl ₂	731.70	0.060	44 mg	0.07	
AcOK	98.14	4.269	419 mg	5	
toluene					3.0 mL

Procedure

The reagents were added to the solvents in a Schlenk tube and the mixture was stirred at reflux under Ar atmosphere. After 24 h the reaction was cooled to rt, AcOEt and water were added and the phases were separated. The organic phase was washed with water (2x) and the aqueous phase was extracted with AcOEt. The organic phases were dried over Na₂SO₄ and evaporated at reduced pressure.

The product was purified by flash chromatography on silica gel (eluent: hexane/AcOEt 9:1).

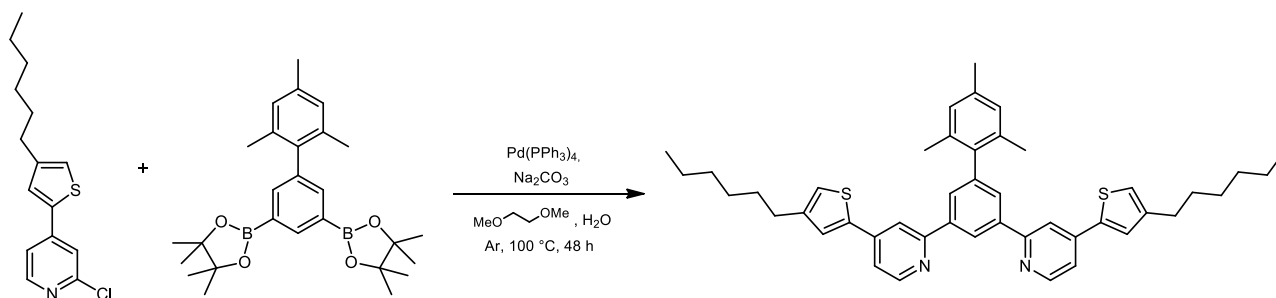
Mass of the product = 217 mg.

Yield = 54%.

Characterization

¹H-NMR (400 MHz, CDCl₃) δ (ppm): 8.25 (1H, t, J = 1.0 Hz), 7.70 (2H, d, J = 1.0 Hz), 6.90 (2H, s), 2.32 (3H, s), 1.99 (6H, s), 1.36 (24H, s).

1.38 Synthesis of L8



Reagent/Solvent	PM (g/mol)	mmol	Mass	eq	Volume
I7	279.83	0.207	58 mg	3	
B1	464.25	0.069	32 mg	1	
Pd(PPh ₃) ₄	1155.56	0,0052	6 mg	0.07	
Na ₂ CO ₃	105.09	0.514	54 mg	7.4	
1,2-dimethoxyethane					1.0 mL
H ₂ O					1.0 mL

Procedure

The reagents were added to the solvents in a Schlenk tube and the mixture was stirred at reflux under Ar atmosphere. After 48 h the reaction was cooled to rt, AcOEt and water were added and the phases were separated. The organic phase was washed with water and the aqueous phase was extracted with AcOEt; the organic phases were dried over Na₂SO₄ and evaporated at reduced pressure.

The product was purified by flash chromatography on silica gel (eluent: hexane/AcOEt 9:1).

Mass of the product = 21 mg.

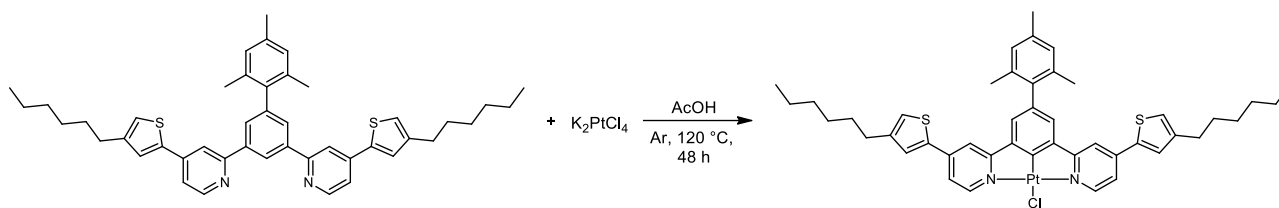
Yield = 45%.

Characterization

¹H-NMR (400 MHz, CD₂Cl₂) δ (ppm): 8.88 (1H, bs), 8.71 (2H, d, J = 5.2 Hz), 8.11 (2H, s), 7.95 (2H, d, J = 1.3 Hz), 7.57 (2H, s), 7.52 (2H, dd, J = 1.3 Hz, J = 5.2 Hz), 7.11 (2H, s), 7.04 (2H, s), 2.69 (4H, t, J = 7.6 Hz), 2.39 (3H, s), 2.15 (6H, s), 1.75-1.67 (4H, m), 1.43-1.32 (12H, m), 0.93 (6H, t, J = 6.8 Hz).

¹³C-NMR (100 MHz, CD₂Cl₂) δ (ppm): 149.52, 128.86, 128.09, 127.46, 124.24, 122.46, 118.56, 116.83, 31.63, 30.44, 30.40, 28.93, 22.59, 20.74, 20.64, 13.81

1.39 Synthesis of PtCl8



Reagent/Solvent	PM (g/mol)	mmol	Mass	eq	Volume
L8	683.02	0.031	21 mg	1	
K ₂ PtCl ₄	415.09	0.036	15 mg	1.2	
glacial AcOH					1.0 mL

Procedure

The ligand and the K₂PtCl₄ were added to the glacial AcOH in a Schlenk tube and the mixture was stirred at reflux under Ar atmosphere. After 48 h the reaction was cooled to rt and water was added to precipitate more product. The orange precipitate was filtered on a Buchner funnel, washed with H₂O, MeOH and Et₂O, and dried.

The product was not furtherly purified.

Mass of the product = 17 mg.

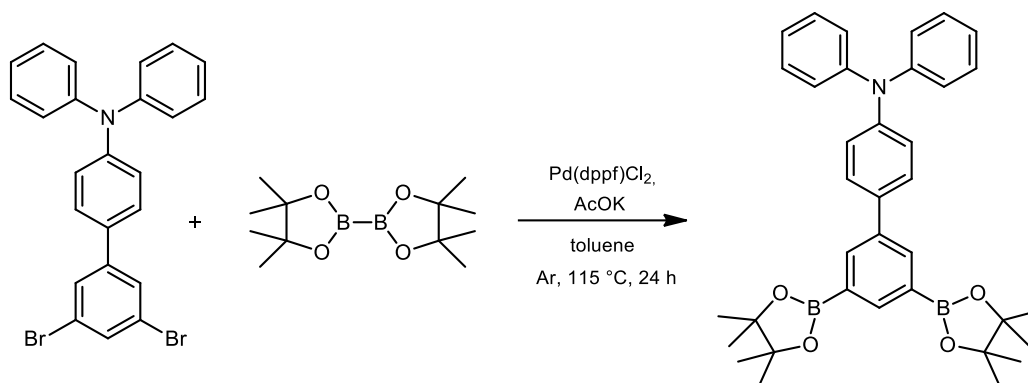
Yield = 61%.

Characterization

¹H-NMR (400 MHz, CD₂Cl₂) δ (ppm): 9.20 (2H, d, J = 6.1 Hz, J(¹⁹⁵Pt) = 40 Hz), 7.86 (2H, d, J = 2.0 Hz), 7.55 (2H, d, J = 1.1 Hz), 7.49 (2H, dd, J = 2.0 Hz, J = 6.1 Hz), 7.41 (2H, s), 7.19 (2H, d, J = 1.1 Hz), 7.04 (2H, s), 2.69 (4H, t, J = 7.6 Hz), 2.39 (3H, s), 2.16 (6H, s), 1.74-1.64 (4H, m), 1.42-1.32 (12H, m), 0.93 (6H, t, J = 6.9 Hz).

¹³C-NMR (100 MHz, CD₂Cl₂) δ (ppm): 151.73, 145.55, 139.24, 136.05, 128.68, 128.05, 125.26, 124.32, 122.59, 118.59, 115.01, 31.61, 30.37, 28.89, 22.57, 20.66, 13.81.

1.40 Synthesis of B2



Reagent/Solvent	PM (g/mol)	mmol	Mass	eq	Volume
I2	479.21	0.357	171 mg	1	
bis(pinacolato) diboron	253.94	0.785	200 mg	2.2	
Pd(dppf)Cl ₂	731.70	0.025	19 mg	0.07	
AcOK	98.14	1.784	175 mg	5	
toluene					1.25 mL

Procedure

The reagents were added to the solvents in a Schlenk tube and the mixture was stirred at reflux under Ar atmosphere. After 24 h the reaction was cooled to rt, AcOEt and water were added and the phases were separated. The aqueous phase was extracted with AcOEt (3x). The organic phase was washed with brine and water, dried over Na₂SO₄ and evaporated at reduced pressure.

The product was purified by flash chromatography on silica gel (eluent: hexane/AcOEt 9:1).

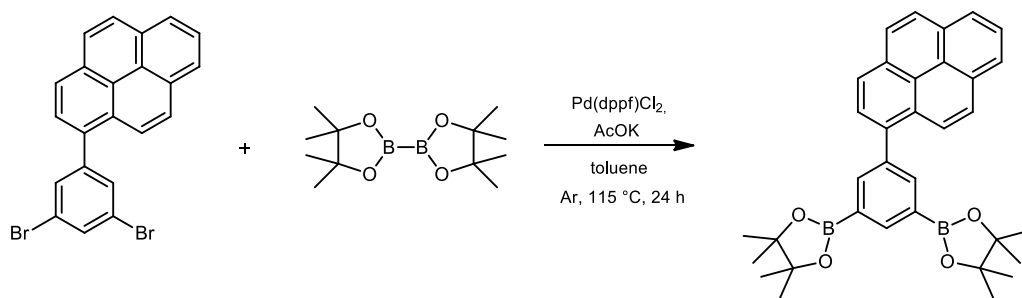
Mass of the product = 117 mg.

Yield = 57%.

Characterization

¹H-NMR (400 MHz, CD₂Cl₂) δ (ppm): 8.12 (1H, bs), 8.09 (2H, d, J = 0.9 Hz), 7.57 (2H, d, J = 8.6 Hz), 7.32 (4H, t, J = 8.4 Hz), 7.18-7.12 (6H, m), 7.07 (2H, t, J = 7.3 Hz), 1.39 (24H, s).

1.41 Synthesis of B3



Reagent/Solvent	PM (g/mol)	mmol	Mass	eq	Volume
I3	436.14	0.314	137 mg	1	
bis(pinacolato) diboron	253.94	0.791	201 mg	2.5	
Pd(dppf)Cl ₂	731.70	0.022	16 mg	0.07	
AcOK	98.14	1.570	154 mg	5	
toluene					2.0 mL

Procedure

The reagents were added to the solvents in a Schlenk tube and the mixture was stirred at reflux under Ar atmosphere. After 24 h the reaction was cooled to rt, AcOEt and water were added and the phases were separated. The organic phase was washed with water (2x) and the aqueous phase was extracted with AcOEt. The organic phases were dried over Na₂SO₄ and evaporated at reduced pressure.

The product was purified by flash chromatography on silica gel (eluent: hexane/AcOEt from 9:1 to 8:2 to 7:3).

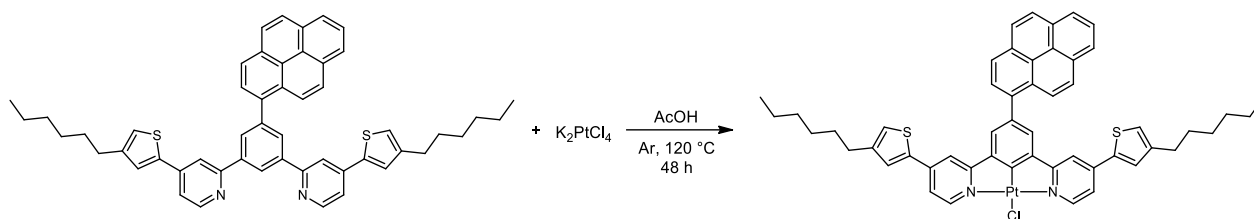
Mass of the product = 103 mg.

Yield = 62%.

Characterization

¹H-NMR (400 MHz, CDCl₃) δ (ppm): 8.42 (1H, bs), 8.25-7.98 (11H, m), 1.38 (24H, s).

1.43 Synthesis of PtCl9



Reagent/Solvent	PM (g/mol)	mmol	Mass	eq	Volume
L9	765.08	0.029	22 mg	1	
K ₂ PtCl ₄	415.09	0.034	15 mg	1.2	
glacial AcOH					1.0 mL

Procedure

The ligand and the K₂PtCl₄ were added to the glacial AcOH in a Schlenk tube and the mixture was stirred at reflux under Ar atmosphere. After 48 h the reaction was cooled to rt and water was added to precipitate more product. The orange precipitate was filtered on a Buchner funnel, washed with H₂O, MeOH and Et₂O, and dried.

The product was not furtherly purified.

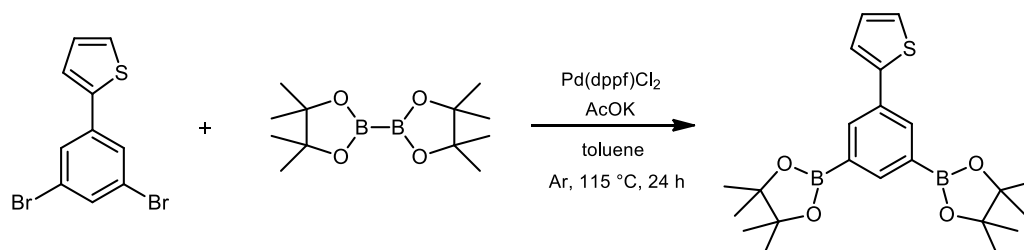
Mass of the product = 15 mg.

Yield = 52%.

Characterization

¹H-NMR (300 MHz, CD₂Cl₂) δ (ppm): 9.26 (2H, d, J = 6.2 Hz, J(¹⁹⁵Pt) = 40 Hz), 8.40-8.23 (5H, m), 8.20-8.06 (4H, m), 7.93 (2H, d, J = 1.8 Hz), 7.88 (2H, s), 7.58-7.51 (4H, m), 7.17 (2H, s), 2.65 (4H, t, J = 7.3 Hz), 1.70-1.60 (4H, m), 1.39-1.26 (12H, m), 0.94-0.84 (6H, m).

1.44 Synthesis of B4



Reagent/Solvent	PM (g/mol)	mmol	Mass	eq	Volume
I6	318.03	0.472	150 mg	1	
bis(pinacolato) diboron	253.94	1.040	264 mg	2.2	
Pd(dppf)Cl ₂	731.70	0.033	24 mg	0.07	
AcOK	98.14	2.364	232 mg	5	
toluene					1.6 mL

Procedure

The reagents were added to the solvents in a Schlenk tube and the mixture was stirred at reflux under Ar atmosphere. After 24 h the reaction was cooled to rt, AcOEt and water were added and the phases were separated. The organic phase was washed with water (3x) and the aqueous phase was extracted with AcOEt (3x). The organic phases were dried over Na₂SO₄ and evaporated at reduced pressure.

The product was purified by flash chromatography on silica gel (eluent: hexane/AcOEt 9:1).

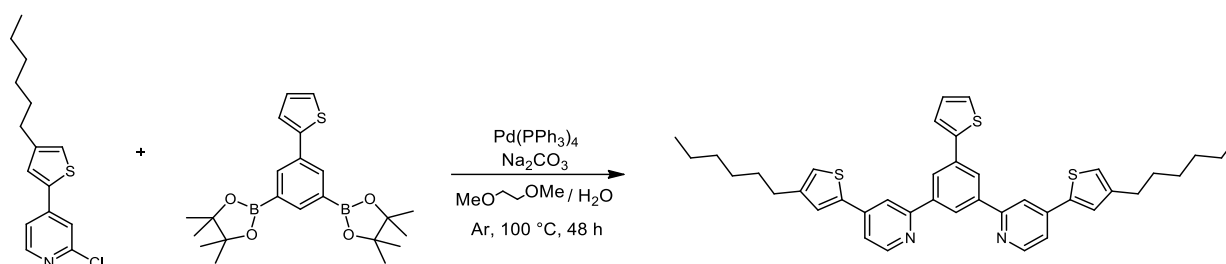
Mass of the product = 43 mg.

Yield = 22%.

Characterization

¹H-NMR (400 MHz, CDCl₃) δ (ppm): 8.21 (1H, t, J = 1.0 Hz), 8.15 (2H, d, J = 1.0 Hz), 7.42 (1H, d, J = 3.6 Hz), 7.29 (1H, d, under residual CHCl₃), 7.09 (1H, dd, J = 3.6 Hz, J = 5.0 Hz).

1.45 Synthesis of L10



Reagent/Solvent	PM (g/mol)	mmol	Mass	eq	Volume
I7	279.83	0.312	87 mg	3	
B4	412.16	0.104	43 mg	1	
Pd(PPh ₃) ₄	1155.56	0,0073	8 mg	0.07	
Na ₂ CO ₃	105.09	0.768	81 mg	7.4	
1,2-dimethoxyethane					1.5 mL
H ₂ O					1.5 mL

Procedure

The reagents were added to the solvents in a Schlenk tube and the mixture was stirred at reflux under Ar atmosphere. After 48 h the reaction was cooled to rt, AcOEt and water were added and the phases were separated. The organic phase was washed with water and the aqueous phase was extracted with AcOEt; the organic phases were dried over Na₂SO₄ and evaporated at reduced pressure.

The product was purified by flash chromatography on silica gel (eluent: hexane/AcOEt 8:2).

Since from a ¹H-NMR in CD₂Cl₂ it was observed that the product was not sufficiently pure, a preparative TLC was carried out (eluent: hexane/AcOEt 9:1).

Mass of the product = 10 mg.

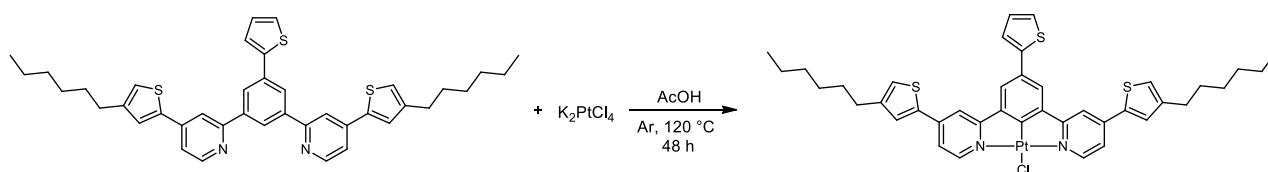
Yield = 15%.

Characterization

¹H-NMR (400 MHz, CD₂Cl₂) δ (ppm): 8.74 (2H, d, J = 5.2 Hz), 8.86 (1H, t, J = 1.5 Hz), 8.42 (2H, d, J = 1.5 Hz), 8.12 (2H, d, J = 0.9 Hz), 7.63 (1H, d, J = 3.6 Hz), 7.58 (2H, d, J = 1,1 Hz), 7.54 (2H, dd, J = 0.9 Hz, J = 5.2 Hz), 7.43 (1H, d, J = 5.1 Hz), 7.21 (1H, dd, J = 3.6 Hz, J = 5.1 Hz), 7.13 (2H, s), 2.71 (4H, t, J = 7.6 Hz), 1.77-1.66 (4H, m), 1.46-1.33 (12H, m), 0.94 (6H, t, J = 7.1 Hz).

¹³C-NMR (100 MHz, CD₂Cl₂) δ (ppm): 156.99, 149.77, 145.14, 143.79, 143.01, 140.55, 140.11, 135.44, 128.19, 127.34, 125.38, 125.27, 124.80, 124.07, 122.41, 118.73, 116.86, 31.65, 30.43, 30.42, 28.96, 22.61, 13.84.

1.46 Synthesis of PtCl10



Reagent/Solvent	PM (g/mol)	mmol	Mass	eq	Volume
L10	646.97	0.015	10 mg	1	
K_2PtCl_4	415.09	0.019	8 mg	1.2	
glacial AcOH					0.5 mL

Procedure

The ligand and the K_2PtCl_4 were added to the glacial AcOH in a Schlenk tube and the mixture was stirred at reflux under Ar atmosphere. After 48 h the reaction was cooled to rt and water was added to precipitate more product. The orange precipitate was filtered on a Buchner funnel, washed with H_2O , MeOH and Et_2O , and dried.

The product was not furtherly purified.

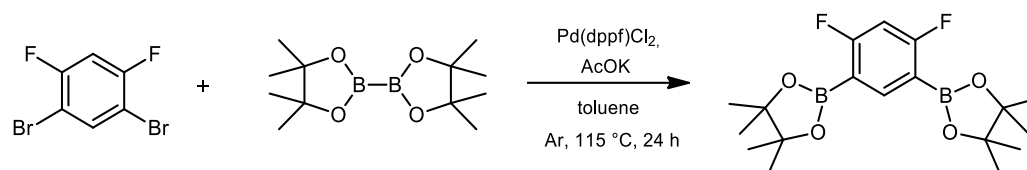
Mass of the product = 8 mg.

Yield = 61%.

Characterization

1H -NMR (400 MHz, CD_2Cl_2) δ (ppm): 9.15 (2H, d, $J = 6.1$ Hz, $J(^{195}Pt) = 39$ Hz), 7.89 (2H, s), 7.81 (2H, s), 7.59 (2H, s), 7.54 (1H, d, $J = 3.5$ Hz), 7.47-7.39 (3H, m), 7.23-7.18 (3H, m), 2.71 (4H, t, $J = 7.7$ Hz), 1.76-1.67 (4H, m), 1.47-1.34 (12H, m), 0.95 (6H, t, $J = 6.7$ Hz).

1.47 Synthesis of B5



Reagent/Solvent	PM (g/mol)	mmol	Mass	eq	Volume
1,3-dibromo-4,6-difluoro benzene	271.88	3.678	1.000 g	1	
bis(pinacolato) diboron	253.94	8.092	2.055 g	2.2	
Pd(dppf)Cl ₂	731.70	0.368	269 mg	0.1	
AcOK	98.14	18.390	1.805 g	5	
toluene					12 mL

Procedure

The reagents were added to the solvents in a Schlenk tube and the mixture was stirred at reflux under Ar atmosphere. After 24 h the reaction was cooled to rt, toluene was added and the solution was filtered through a Celite pad.

The filtered solution was evaporated, and the residue was purified by chromatography on a short silica pad (eluent: hexane/AcOEt 8:2), obtaining a pale yellow solid.

The product was furtherly purified by dissolving it in the minimum amount of pentane and leaving it in the freezer overnight; the crystalized solid was then recovered from the pentane and dried.

Mass of the product = 622 mg.

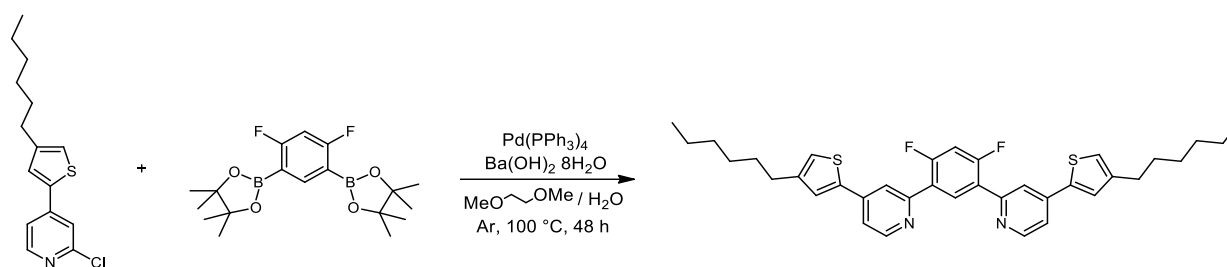
Yield = 63%.

Characterization

¹H-NMR (400 MHz, CDCl₃) δ (ppm): 8.15 (1H, t, J(¹⁹F) = 10.1 Hz), 6.74 (1H, t, J(¹⁹F) = 12.9 Hz), 1.37 (24H, s).

¹⁹F-NMR (MHz, CDCl₃) δ (ppm): -94.15 (s).

1.48 Synthesis of L11



Reagent/Solvent	PM (g/mol)	mmol	Mass	eq	Volume
I7	279.83	0.369	103 mg	3	
B5	366.02	0.123	45 mg	1	
Pd(PPh ₃) ₄	1155.56	0.010	12 mg	0.08	
Ba(OH) ₂ · 8H ₂ O	315.48	0.246	78 mg	2	
1,2-dimethoxyethane					1.0 mL
H ₂ O					0.5 mL

Procedure

The reagents were added to the solvents in a Schlenk tube and the mixture was stirred at reflux under Ar atmosphere. After 48 h the reaction was cooled to rt, AcOEt and water were added and the phases were separated. The organic phase was washed with water and the aqueous phase was extracted with AcOEt; the organic phases were dried over Na₂SO₄ and evaporated at reduced pressure.

The product was purified by flash chromatography on silica gel (eluent: hexane/AcOEt from 9:1 to 8:2 to 7:3).

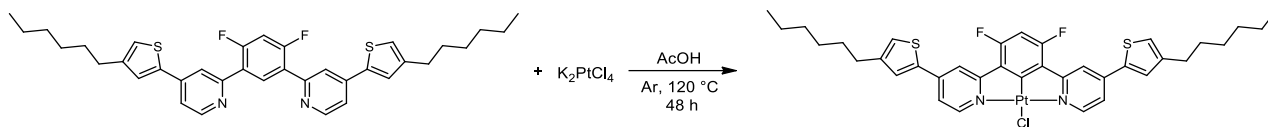
Mass of the product = 22 mg.

Yield = 30%.

Characterization

¹H-NMR (400 MHz, CD₂Cl₂) δ (ppm): 8.69 (2H, d, J = 5.2 Hz), 8.64 (1H, t, J(¹⁹F) = 8.9 Hz), 7.97 (2H, s), 7.46 (2H, d, J = 5.2 Hz), 7.43 (2H, s), 7.10 (1H, t, J(¹⁹F) = 10.6 Hz), 7.05 (2H, s), 2.66 (4H, t, J = 7.6 Hz), 1.73-1.63 (4H, m), 1.43-1.30 (12H, m), 0.92 (6H, t, J = 6.5 Hz).

1.49 Synthesis of PtCl11



Reagent/Solvent	PM (g/mol)	mmol	Mass	eq	Volume
L11	600.83	0.035	21 mg	1	
K_2PtCl_4	415.09	0.043	18 mg	1.2	
glacial AcOH					1.0 mL

Procedure

The ligand and the K_2PtCl_4 were added to the glacial AcOH in a Schlenk tube and the mixture was stirred at reflux under Ar atmosphere. After 48 h the reaction was cooled to rt and water was added to precipitate more product. The orange precipitate was filtered on a Buchner funnel, washed with H_2O , MeOH and Et_2O , and dried.

The product recrystallized by dichloromethane/pentane.

Mass of the product = 13 mg.

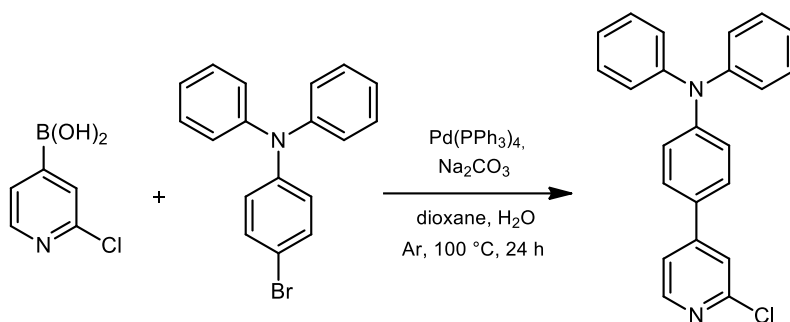
Yield = 45%.

Characterization

1H -NMR (400 MHz, CD_2Cl_2) δ (ppm): 9.21 (2H, d, $J = 6.3$ Hz, $J(^{195}Pt) = 39$ Hz), 8.11 (2H, s), 7.58 (2H, s), 7.50 (2H, d, $J = 6.6$ Hz), 7.23 (2H, s), 6.86 (1H, t, $J(^{19}F) = 11.3$ Hz), 2.71 (4H, t, $J = 7.9$ Hz), 1.75-1.66 (4H, m), 1.41-1.33 (12H, m), 0.97-0.90 (6H, m).

The signals are not clearly visible due to very low solubility of the compound.

1.50 Synthesis of I8



Reagent/Solvent	PM (g/mol)	mmol	Mass	eq	Volume
2-Cl-pyridine-4-boronic acid	157.36	1.28	202 mg	1	
4-Br-triphenylamine	324.22	1.54	500 mg	1.2	
Pd(PPh ₃) ₄	1155.56	0.064	74 mg	0.05	
Na ₂ CO ₃	105.99	3.84	407 mg	3	
1,4-dioxane					9.0 mL
H ₂ O					3.0 mL

Procedure

The reagents were added to the solvents in a Schlenk tube and the mixture was stirred at reflux under Ar atmosphere. After 24 h the reaction was cooled to rt, AcOEt and water were added and the phases were separated. The aqueous phase was extracted with AcOEt. The organic phase was washed with brine and water, dried over Na₂SO₄ and evaporated at reduced pressure.

The product was purified by flash chromatography on silica gel (eluent: hexane/AcOEt 9:1).

Mass of the product = 227 mg.

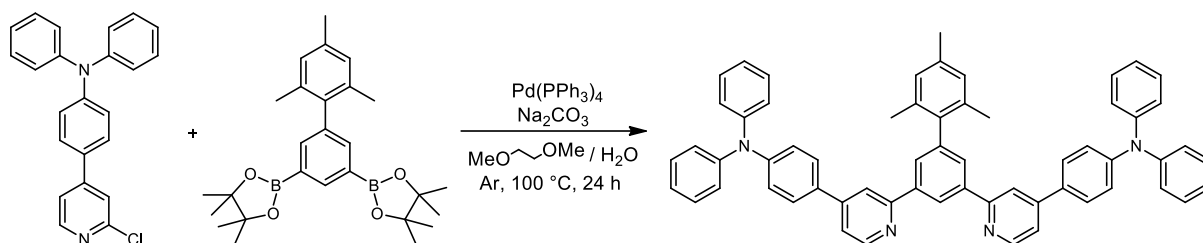
Yield = 50%.

Characterization

¹H-NMR (400 MHz, CD₂Cl₂) δ (ppm): 8.39 (1H, d, J = 5.2 Hz), 7.53-7.48 (3H, m), 7.41 (1H, dd, J = 1.6 Hz, J = 5.3 Hz), 7.36-7.29 (4H, m), 7.19-7.09 (8H, m).

¹³C-NMR (100 MHz, CD₂Cl₂) δ (ppm): 152.13, 150.97, 149.78, 149.57, 147.04, 129.50, 129.23, 127.75, 125.22, 123.91, 122.46, 121.09, 119.63.

1.51 Synthesis of L12



Reagent/Solvent	PM (g/mol)	mmol	Mass	eq	Volume
I8	356.11	0.255	91 mg	3	
B1	464.25	0.084	39 mg	1	
Pd(PPh ₃) ₄	1155.56	0.006	7 mg	0.07	
Na ₂ CO ₃	105.09	0.595	63 mg	7.1	
1,2-dimethoxyethane					1.0 mL
H ₂ O					1.0 mL

Procedure

The reagents were added to the solvents in a Schlenk tube and the mixture was stirred at reflux under Ar atmosphere. After 24 h the reaction was cooled to rt, AcOEt and water were added and the phases were separated. The organic phase was washed with water (2x), dried over Na₂SO₄ and evaporated at reduced pressure.

The product was purified by flash chromatography on silica gel (eluent: hexane/AcOEt 9:1).

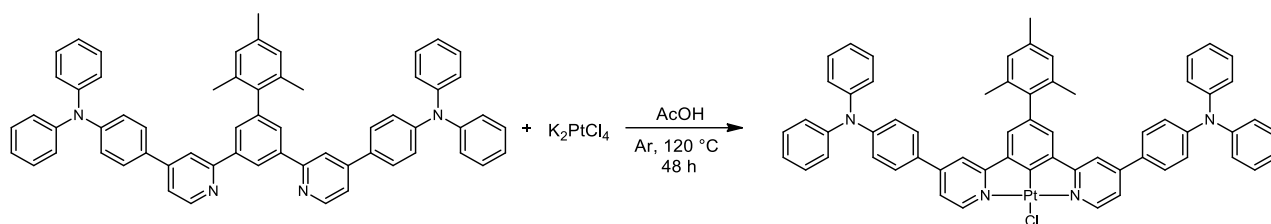
Mass of the product = 40 mg.

Yield = 57%.

Characterization

¹H-NMR (400 MHz, CD₂Cl₂) δ (ppm): 8.90 (1H, bs), 8.74 (2H, d, J = 5.4 Hz), 8.15 (2H, s), 7.97 (2H, d, J = 1.6 Hz), 7.70 (4H, d, J = 8.8 Hz), 7.55 (2H, dd, J = 1.5 Hz, J = 5.2 Hz), 7.38-7.31 (8H, m), 7.21-7.10 (16H, m), 7.02 (2H, s), 2.37 (3H, s), 2.14 (6H, s).

1.52 Synthesis of PtCl12



Reagent/Solvent	PM (g/mol)	mmol	Mass	eq	Volume
L12	837.06	0.017	14 mg	1	
K_2PtCl_4	415.09	0.022	9 mg	1.3	
glacial AcOH					1.0 mL

Procedure

The reagents were added to the glacial AcOH in a Schlenk tube and the mixture was stirred at reflux under Ar atmosphere. After 48 h the reaction was cooled to rt and water was added to precipitate more product. The orange precipitate was filtered on a Buchner funnel, washed with H_2O , MeOH and Et_2O , and dried.

The product was not furtherly purified.

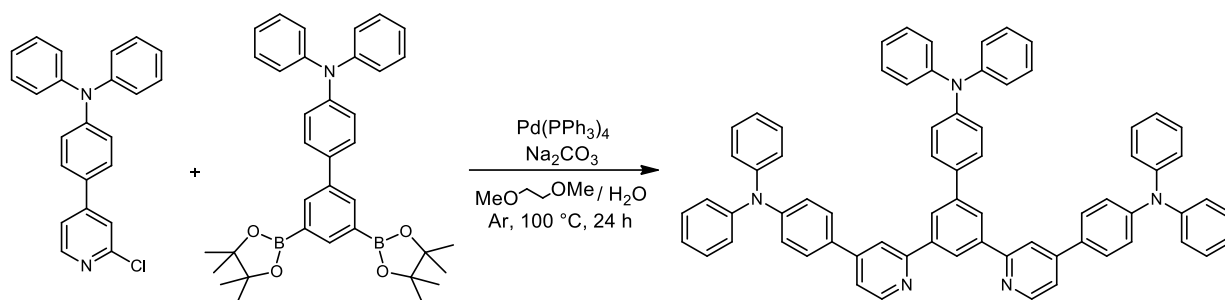
Mass of the product = 16 mg.

Yield = 88%.

Characterization

1H -NMR (400 MHz, CD_2Cl_2) δ (ppm): 9.15 (2H, d, $J = 6.1$ Hz, $J(^{195}Pt) = 40$ Hz), 7.92 (2H, d, $J = 1.8$ Hz), 7.67 (4H, d, $J = 8.8$ Hz), 7.54 (2H, dd, $J = 2.1$ Hz, $J = 6.1$ Hz), 7.40-7.32 (10H, m), 7.21-7.12 (16H, m), 7.01 (2H, s), 2.36 (3H, s), 2.13 (6H, s).

1.53 Synthesis of L13



Reagent/Solvent	PM (g/mol)	mmol	Mass	eq	Volume
I8	356.11	0.510	181 mg	2.5	
B2	573.34	0.204	117 mg	1	
Pd(PPh ₃) ₄	1155.56	0.014	17 mg	0.07	
Na ₂ CO ₃	105.09	1.522	160 mg	7.4	
1,2-dimethoxyethane					3.0 mL
H ₂ O					3.0 mL

Procedure

The reagents were added to the solvents in a Schlenk tube and the mixture was stirred at reflux under Ar atmosphere. After 24 h the reaction was cooled to rt, AcOEt and water were added and the phases were separated. The organic phase was washed with water (2x), dried over Na₂SO₄ and evaporated at reduced pressure.

The product was purified by flash chromatography on silica gel (eluent: hexane/AcOEt 75:25).

Mass of the product = 107 mg.

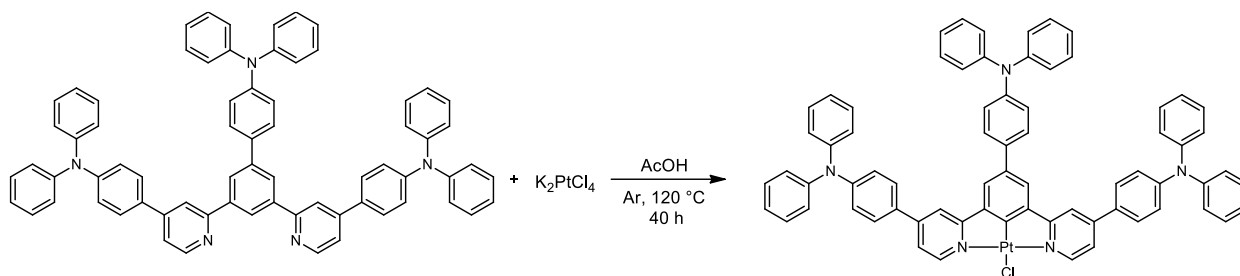
Yield = 55%.

Characterization

¹H-NMR (300 MHz, CD₂Cl₂) δ (ppm): 8.79-8.74 (3H, m), 8.40 (2H, d, J = 1.4 Hz), 8.15 (2H, s), 6.76-6.67 (6H, m), 7.53 (2H, dd, J = 1.4 Hz, J = 5.4 Hz), 7.39-7.29 (12H, m), 7.24-7.06 (24H, m).

¹³C-NMR (75 MHz, CD₂Cl₂) δ (ppm): 157.46, 150.04, 148.98, 148.62, 147.67, 147.55, 147.30, 141.61, 140.55, 134.80, 131.32, 129.39, 129.27, 129.08, 128.03, 127.81, 127.14, 125.82, 124.96, 124.43, 124.09, 123.81, 123.57, 123.01, 122.85, 119.78, 117.97.

1.54 Synthesis of PtCl13



Reagent/Solvent	PM (g/mol)	mmol	Mass	eq	Volume
L13	962.19	0.104	100 mg	1	
K ₂ PtCl ₄	415.09	0.125	52 mg	1.2	
glacial AcOH					2.0 mL

Procedure

The reagents were added to the glacial AcOH in a Schlenk tube and the mixture was stirred at reflux under Ar atmosphere. After 40 h the reaction was cooled to rt and water was added to precipitate more product. The orange precipitate was filtered on a Buchner funnel, washed with H₂O, MeOH and Et₂O, and dried.

The product was not furtherly purified.

Mass of the product = 116 mg.

Yield = 93%.

Characterization

¹H-NMR (400 MHz, CD₂Cl₂) δ (ppm): 9.15 (2H, d, J = 6.1 Hz, J(¹⁹⁵Pt) = 38 Hz), 8.02 (2H, d, J = 1.9 Hz), 7.82 (2H, s), 7.72 (4H, d, J = 8.8 Hz), 7.65 (2H, d, J = 8.6 Hz), 7.55 (2H, dd, J = 1.9 Hz, J = 6.1 Hz), 7.40-7.30 (12H, m), 7.23-7.15 (22H, m), 7.09 (2H, t, J = 7.3 Hz).

VI – CONCLUSIONS

During the doctoral period, my research has been focused on the synthesis and characterization of novel NCN-based platinum(II) complexes, obtaining more than twenty completely new compounds.

These complexes were designed following different strategies:

- A first group of compounds (**PtCl3**, **PtCl4** and **PtCl5**) presents new moieties on the central benzene ring, without any substituents on the pyridines or other species on the Pt(II) center than the simple Cl.
- The complexes belonging to the second group (**Pt1-Pt15**) share the NCN scaffold with their parent compounds **PtCl1**, **PtCl2**, **PtCl6** and **PtCl7**, but bear other ancillary ligands on the metal (thiolates, azide, phthalimide and isothiocyanate).
- Finally, **PtCl8-PtCl13** still have the same -Cl ancillary ligand and substituents on the benzene ring (mesityl, 4-NPh₂-phenyl, 2-thienyl, methyl) of some previously reported compounds, but new groups (*i.e.* 4-hexyl-2-thienyl, 4-NPh₂-phenyl) have been added to the pyridines, to test the effect of an expanded aromatic system.

In this way, new NCN-Pt(II) complexes have been achieved by varying different parts of the 1,3-(di-2-pyridyl)benzene core, to try to develop a relationship between the substituents and the luminescence properties of the final molecules.

Up to now, all complexes have been studied from the UV-Vis absorption point of view, calculating the molar extinction coefficient for all of them; moreover, complexes **Pt1-Pt3**, **Pt5**, **Pt7-Pt10**, **Pt12-Pt14**, **PtCl8**, **PtCl10**, **PtCl12** and **PtCl13** have been fully characterized for their photophysical properties, measuring the excitation and emission spectra, the absolute Quantum Yields and the lifetimes in dichloromethane solutions.

For what concerns the luminescence, some key points have been confirmed:

- Considering the emission of the monomeric species having unsubstituted pyridines, the emission measured from diluted solutions only depends on the substituent on the benzene ring, not being particularly influenced (besides a negligible shift of few nm) by the replacement of the -Cl ligand.
- Regarding the absolute Quantum Yields, the substitution of the chloride is generally helpful to improve the QY values, in many cases causing an important increase up to 90%; this influence is not observed for the lifetimes, which remain in the ranges typical of the parent Pt-Cl compounds.
- The most relevant effects are surely visible for those complexes presenting an expanded aromatic system on the pyridines, since for all of them a very important growth in the QY has been achieved (in the case of **PtCl10** reaching unity), together with a noticeable red-shift of the emission.
- For all complexes, an emission band at lower energies (with maxima in the range 650-750 nm) appears when the concentration is increased; this is due to formation of aggregates and can be seen also from pure layers of compounds in solid-state analysis; nevertheless, the concurrent formation of excimers, participating in the luminescent properties, cannot be excluded.

In the case of **Pt1**, the luminescence has been assessed also for the powders, both at Room and Low Temperature; furthermore, the X-ray crystal structure of the compound has been obtained. Compound **Pt5**, bearing a thioacetate on the Pt center, has been studied non only as powders but also as blend in PMMA matrix at two different concentrations.

Together with **Pt9**, the aforementioned **Pt1** complex has been employed to produce some OLED devices, showing different emission colors on the basis of the amount of compound in the Emitting Layer. These tests can open the way for further strategies of color tuning, designing the device with the proper concentration of complex in order to modulate the emission.

The next thing to do will be surely the study of the remaining complexes, to achieve a complete and clear overview of the photophysical properties of these series of compounds. Moreover, will also be important the testing of the already characterized complexes, both by preparing other OLED devices based on these molecules (to explore the different colors which can be achieved through them) and by applying the synthesized compounds in the biological field, as sensitizers in the bio-imaging of cells and tissues and as active dyes for photodynamic therapies.

To conclude, another important step for the near future can be the synthesis of new members of the NCN-Pt(II) family, in particular following various strategies: i) the substitution of the ancillary -Cl in complexes such as **PtCl8**, **PtCl10**, **PtCl12** and **PtCl13**, to observe the variation in the luminescence arising by the replacement with thiolates or azides, which is in general positive for what concerns the QY values; ii) the use of new thiolates or, in general, new anionic species to replace the chloride ligand; iii) the introduction of new moieties on the pyridines, to confirm the mentioned helpful changes in the properties of such complexes, and to better understand the effect exerted by electron-donor or withdrawing groups, in particular on the emission color.

As a result of the work done up to now, many of the presented and discussed new complexes have become the object of publications, here reported:

1. C. Dragonetti, F. Fagnani, D. Marinotto, A. di Biase, D. Roberto, M. Cocchi, S. Fantacci, A. Colombo
First member of an appealing class of cyclometalated 1,3-di-(2-pyridyl)benzene platinum(II) complexes for solution-processable OLEDs
Journal of Material Chemistry C **2020**, 8, 7873-7881. DOI: 10.1039/d0tc01565b
2. F. Fagnani*, A. Colombo, C. Dragonetti, D. Roberto, D. Marinotto
The intriguing effect of thiolates as co-ligands in platinum(II) complexes bearing a cyclometalated 1,3-di(2-pyridyl)benzene
Inorganica Chimica Acta **2022**, 532, 120744. DOI: 10.1016/j.ica.2021.120744
3. A. Colombo, G. De Soricellis, F. Fagnani, C. Dragonetti, M. Cocchi, B. Carboni, V. Guerchais, D. Marinotto
Introduction of a triphenylamine substituent on pyridyl rings as a springboard for a new appealing brightly luminescent 1,3-di-(2-pyridyl)benzene platinum(II) complex family
Dalton Transactions **2022**, 51, 12161-12169. DOI: 10.1039/d2dt01792j
4. D. Roberto, A. Colombo, C. Dragonetti, F. Fagnani*, M. Cocchi, D. Marinotto
A Novel Class of Cyclometalated Platinum(II) Complexes for Solution-Processable OLEDs
Molecules **2022**, 27, 5171. DOI: 10.3390/molecules27165171

The first paper deals with complex **Pt1**, its crystal structure and the related OLED devices; the second article is about compound **Pt5** and the in-depth photophysical characterization carried out on this complex. In the third paper **PtCl12** and **PtCl13** are presented, together with the study of their luminescence properties, while in the fourth publication the synthesis and the characterization of **Pt2**, **Pt7**, **Pt9** and **Pt13** are reported.

VII – BIBLIOGRAPHY

- [1] A. Jabłoński. Efficiency of Anti-Stokes Fluorescence in Dyes. *Nature* **1933**, 131, 839-840. doi: 10.1038/131839b0
- [2] M. Kasha. Characterization of electronic transitions in complex molecules. *Discussions of the Faraday Society* **1950**, 9, 14-19. doi: 10.1039/DF9500900014
- [3] C.W. Tang, S.A. Vanslyke. Organic electroluminescent diodes. *Applied Physics Letters* **1987**, 51, 913–915. doi: 10.1063/1.98799
- [4] G. Hong, X. Gan, C. Leonhardt, Z. Zhang, J. Seibert, J.M. Busch, S. Bräse. A Brief History of OLEDs – Emitter Development and Industry Milestones. *Advanced Materials* **2021**, 33, 2005630. doi: 10.1002/adma.202005630
- [5] T. Smith, J. Guild. The C.I.E. colorimetric standards and their use. *Transactions of the Optical Society* **1931**, 33, 73-134. doi: 10.1088/1475-4878/33/3/301
- [6] C.M. Che, C.C. Kwok, C.F. Kui, S.L. Lai, K.H. Low. Luminescent Coordination and Organometallic Complexes for OLEDs in *Comprehensive Inorganic Chemistry II (Second Edition): From Elements to Applications*, vol. 8, Elsevier Ltd, **2013**, 607–655. doi: 10.1016/B978-0-08-097774-4.00808-1
- [7] C. Bizzarri, E. Spuling, D.M. Knoll, D. Volz, S. Bräse. Sustainable metal complexes for organic light-emitting diodes (OLEDs). *Coordination Chemistry Reviews* **2018**, 373, 49–82. doi: 10.1016/j.ccr.2017.09.011
- [8] R.C. Evans, P. Douglas, C.J. Winscom. Coordination complexes exhibiting room-temperature phosphorescence: Evaluation of their suitability as triplet emitters in organic light emitting diodes. *Coordination Chemistry Reviews* **2006**, 250, 2093–2126. doi: 10.1016/j.ccr.2006.02.007
- [9] J.A.G. Williams, S. Develay, D.L. Rochester, L. Murphy. Optimising the luminescence of platinum(II) complexes and their application in organic light emitting devices (OLEDs). *Coordination Chemistry Reviews* **2008**, 252, 2596–2611. doi: 10.1016/j.ccr.2008.03.014
- [10] J. Kalinowski, V. Fattori, M. Cocchi, J.A.G. Williams. Light-emitting devices based on organometallic platinum complexes as emitters. *Coordination Chemistry Reviews* **2011**, 255, 2401–2425. doi: 10.1016/j.ccr.2011.01.049
- [11] Y. Ma, H. Zhang, J. Shen, C. Che. Electroluminescence from triplet metal-ligand charge-transfer excited state of transition metal complexes. *Synthetic Metals* **1998**, 94, 245-248. doi: 10.1016/S0379-6779(97)04166-0
- [12] M.A. Baldo, D.F. O'Brien, Y. You, A. Shoustikov, S. Sibley, M.E. Thompson, S.R. Forrest. Highly efficient phosphorescent emission from organic electroluminescent devices. *Nature* **1998**, 395, 151-154. doi: 10.1038/25954

- [13] M.A. Baldo, S. Lamansky, P.E. Burrows, M.E. Thompson, S.R. Forrest. Very high-efficiency green organic light-emitting devices based on electrophosphorescence. *Applied Physics Letters* **1999**, 75, 4–6. doi: 10.1063/1.124258
- [14] S. Lamansky, P. Djurovich, D. Murphy, F. Abdel-Razzaq, H.-E. Lee, C. Adachi, P.E. Burrows, S.R. Forrest, M.E. Thompson. Highly phosphorescent bis-cyclometalated iridium complexes: Synthesis, photophysical characterization, and use in organic light emitting diodes. *Journal of the American Chemical Society* **2001**, 123, 4304–4312. doi: 10.1021/ja003693s
- [15] J. Ding, J. Gao, Y. Cheng, Z. Xie, L. Wang, D. Ma, X. Jing, Wang. Highly efficient green-emitting phosphorescent iridium dendrimers based on carbazole dendrons. *Advanced Functional Materials* **2006**, 16, 575–581. doi: 10.1002/adfm.200500591
- [16] M. Cocchi, D. Virgili, V. Fattori, D.L. Rochester, J.A.G. Williams. N⁴C⁴N-coordinated platinum(II) complexes as phosphorescent emitters in high-performance organic light-emitting devices. *Advanced Functional Materials* **2007**, 17, 285–289. doi: 10.1002/adfm.200600167
- [17] P.-K. Chow, G. Cheng, G.S.M. Tong, W.-P. To, W.-L. Kwong, K.-H. Low, C.-C. Kwok, C. Ma, C.-M. Che. Luminescent pincer platinum(II) complexes with emission quantum yields up to almost unity: Photophysics, photoreductive C-C bond formation, and materials applications. *Angewandte Chemie - International Edition* **2015**, 54, 2084–2089. doi: 10.1002/anie.201408940
- [18] A. Tsuboyama, H. Iwawaki, M. Furugori, T. Mukaide, J. Kamatani, S. Igawa, T. Moriyama, S. Miura, T. Takiguchi, S. Okada, M. Hoshino, K. Ueno. Homoleptic Cyclometalated Iridium Complexes with Highly Efficient Red Phosphorescence and Application to Organic Light-Emitting Diode. *Journal of the American Chemical Society* **2003**, 125, 12971–12979. doi: 10.1021/ja034732d
- [19] M. Cocchi, J. Kalinowski, D. Virgili, J.A.G. Williams. Excimer-based red/near-infrared organic light-emitting diodes with very high quantum efficiency. *Applied Physics Letters* **2008**, 92, 113302. doi: 10.1063/1.2898159
- [20] K.T. Ly, R.-W. Chen-Cheng, H.-W. Lin, Y.-J. Shiau, S.-H. Liu, P.-T. Chou, C.-S. Tsao, Y.-C. Huang, Y. Chi. Near-infrared organic light-emitting diodes with very high external quantum efficiency and radiance. *Nature Photonics* **2016**, 11, 63–68. doi: 10.1038/nphoton.2016.230
- [21] C. Adachi, R.C. Kwong, P. Djurovich, V. Adamovich, M.A. Baldo, M.E. Thompson, S.R. Forrest. Endothermic energy transfer: A mechanism for generating very efficient high-energy phosphorescent emission in organic materials. *Applied Physics Letters* **2001**, 79, 2082–2084. doi: 10.1063/1.1400076
- [22] K.S. Yook, J.Y. Lee. Solution processed deep blue phosphorescent organic light-emitting diodes with over 20% external quantum efficiency. *Organic Electronics* **2011**, 12, 1711–1715. doi: 10.1016/j.orgel.2011.07.004
- [23] H. Shin, Y.H. Ha, H.-G. Kim, R. Kim, S.-K. Kwon, Y.-H. Kim, J.-J. Kim. Controlling Horizontal Dipole Orientation and Emission Spectrum of Ir Complexes by Chemical Design of Ancillary Ligands for Efficient Deep-Blue Organic Light-Emitting Diodes. *Advanced Materials* **2019**, 31, 1808102. doi: 10.1002/adma.201808102

- [24] T. Fleetham, G. Li, L. Wen, J. Li. Efficient 'Pure' blue OLEDs employing tetradentate Pt complexes with a narrow spectral bandwidth. *Advanced Materials* **2014**, 26, 7116–7121. doi: 10.1002/adma.201401759
- [25] S.W. Botchway, M. Charnley, J.W. Haycock, J.A.G. Williams. Time-resolved and two-photon emission imaging microscopy of live cells with inert platinum complexes. *Proceedings of the National Academy of Sciences* **2008**, 105, 16070-16076. doi: 10.1073/pnas.0804071105
- [26] E. Baggaley, I.V. Sazanovich, J.A.G. Williams, J.W. Haycock, S.W. Botchway, J.A. Weinstein. Two-photon phosphorescence lifetime imaging of cells and tissues using a long-lived cyclometallated Npyridyl[^]Cphenyl[^]N pyridyl Pt(II) complex. *RSC Advances* **2014**, 4, 35003–35008. doi: 10.1039/c4ra04489d
- [27] E. Baggaley, S.W. Botchway, J.W. Haycock, H. Morris, I.V. Sazanovich, J.A.G. Williams, J.A. Weinstein. Long-lived metal complexes open up microsecond lifetime imaging microscopy under multiphoton excitation: From FLIM to PLIM and beyond. *Chemical Science* **2014**, 5, 879–886. doi: 10.1039/c3sc51875b
- [28] V. Fernández-Moreira, F.L. Thorp-Greenwood, M.P. Coogan. Application of d⁶ transition metal complexes in fluorescence cell imaging. *Chemical Communications* **2010**, 46, 186–202. doi: 10.1039/b917757d
- [29] K.K.W. Lo, S.P.Y. Li, K.Y. Zhang. Development of luminescent iridium(III) polypyridine complexes as chemical and biological probes. *New Journal of Chemistry* **2011**, 35, 265–287. doi: 10.1039/c0nj00478b
- [30] Q. Zhao, H. Huang, F. Li. Phosphorescent heavy-metal complexes for bioimaging. *Chemical Society Reviews* **2011**, 40, 2508–2524. doi: 10.1039/c0cs00114g
- [31] E. Baggaley, J.A. Weinstein, J.A.G. Williams. Lighting the way to see inside the live cell with luminescent transition metal complexes. *Coordination Chemistry Reviews* **2012**, 256, 1762–1785. doi: 10.1016/j.ccr.2012.03.018
- [32] K.K.W. Lo, A.W.T. Choi, W.H.T. Law. Applications of luminescent inorganic and organometallic transition metal complexes as biomolecular and cellular probes. *Dalton Transactions* **2012**, 41, 6021–6047. doi: 10.1039/c2dt11892k
- [33] K.K.W. Lo. Luminescent Rhenium(I) and Iridium(III) Polypyridine Complexes as Biological Probes, Imaging Reagents, and Photocytotoxic Agents. *Accounts of Chemical Research* **2015**, 48, 2985–2995. doi: 10.1021/acs.accounts.5b00211
- [34] E. Friedman, J.-C. Chambron, J.-P. Sauvage, N.J. Turro, J.K. Barton. Molecular 'Light Switch' for DNA: Ru(bpy)₂(dppz)²⁺. *Journal of the American Chemical Society* **1990**, 112, 4960-4962. doi: 10.1021/ja00168a052
- [35] S.P. Foxon, M.A.H. Alamiry, M.G. Walker, A.J.H.M. Meijer, I.V. Sazanovich, J.A. Weinstein, J.A. Thomas. Photophysical properties and singlet oxygen production by ruthenium(II) complexes of benzo[i]dipyrido[3,2-a:2',3'-c]phenazine: spectroscopic and TD-DFT study. *Journal of Physical Chemistry A* **2009**, 113, 12754–12762. doi: 10.1021/jp906716g

- [36] Y. Sun, L.E. Joyce, N.M. Dickson, C. Turro. Efficient DNA photocleavage by $[\text{Ru}(\text{bpy})_2(\text{dppn})]^{2+}$ with visible light. *Chemical Communications* **2010**, 46, 2426–2428. doi: 10.1039/b925574e
- [37] R.M. Hartshorn, J.K. Barton. Novel Dipyridophenazine Complexes of Ruthenium(II): Exploring Luminescent Reporters of DNA. *Journal of the American Chemical Society* **1992**, 114, 5919–5925. doi: 10.1021/ja00041a002
- [38] M Yu, Q. Zhao, L. Shi, F. Li, Z. Zhou, H. Yang, T. Yi, C. Huang. Cationic iridium(III) complexes for phosphorescence staining in the cytoplasm of living cells. *Chemical Communications* **2008**, 18, 2115–2117. doi: 10.1039/b800939b
- [39] K.K.W. Lo, P.K. Lee, J.S.Y. Lau. Synthesis, characterization, and properties of luminescent organoiridium(III) polypyridine complexes appended with an alkyl chain and their interactions with lipid bilayers, surfactants, and living cells. *Organometallics* **2008**, 27, 2998–3006. doi: 10.1021/om800212t
- [40] P.K.M. Siu, D.L. Ma, C.M. Che. Luminescent cyclometalated platinum(II) complexes with amino acid ligands for protein binding. *Chemical Communications* **2005**, 8, 1025–1027. doi: 10.1039/b414936j
- [41] V.G. Vaidyanathan, B.U. Nair. A platinum(II)-based molecular light switch for proteins. *European Journal of Inorganic Chemistry* **2005**, 18, 3756–3759. doi: 10.1002/ejic.200500335
- [42] W. Dennis E.J.G.J. Dolmans, D. Fukumura, R.K. Jain. Photodynamic therapy for cancer. *Nature Reviews Cancer* **2003**, 3, 375–380. doi: 10.1038/nrc1070
- [43] D. Phillips. The photochemistry of sensitizers for photodynamic therapy. *Pure and Applied Chemistry* **1995**, 67, 117–126. doi: 10.1351/pac199567010117
- [44] D. van Straten, V. Mashayekhi, H.S. de Bruijn, S. Oliveira, D.J. Robinson. Oncologic photodynamic therapy: Basic principles, current clinical status and future directions. *Cancers* **2017**, 9, 19. doi: 10.3390/cancers9020019
- [45] D. Broadwater, H.C.D. Medeiros, R.R. Lunt, S.Y. Lunt. Annual Review of Biomedical Engineering Current Advances in Photoactive Agents for Cancer Imaging and Therapy. *Annual Review of Biomedical Engineering* **2021**, 23, 29–60. doi: 10.1146/annurev-bioeng-122019
- [46] H. Abrahamse, M.R. Hamblin. New photosensitizers for photodynamic therapy. *Biochemical Journal* **2016**, 473, 347–364. doi: 10.1042/BJ20150942
- [47] J. Usuda, H. Kato, T. Okunaka, K. Furukawa, H. Tsutsui, K. Yamada, Y. Suga, H. Honda, Y. Nagatsuka, T. Ohira, M. Tsuboi, T. Hirano. Photodynamic Therapy (PDT) for Lung Cancers. *Journal of Thoracic Oncology* **2006**, 1, 489–493. doi: 10.1016/S1556-0864(15)31616-6
- [48] J. Karges. Clinical Development of Metal Complexes as Photosensitizers for Photodynamic Therapy of Cancer. *Angewandte Chemie - International Edition* **2022**, 61. doi: 10.1002/anie.202112236

- [49] L.K. McKenzie, H.E. Bryant, J.A. Weinstein. Transition metal complexes as photosensitisers in one- and two-photon photodynamic therapy. *Coordination Chemistry Reviews* **2019**, 379, 2–29. doi: 10.1016/j.ccr.2018.03.020
- [50] S. Monro, K.L. Colón, H. Yin, J. Roque III, P. Konda, S. Gujar, R.P. Thummel, L. Lilge, C.G. Cameron, S.A. McFarland. Transition Metal Complexes and Photodynamic Therapy from a Tumor-Centered Approach: Challenges, Opportunities, and Highlights from the Development of TLD1433. *Chemical Reviews* **2019**, 119, 797–828. doi: 10.1021/acs.chemrev.8b00211
- [51] P. Majumdar, X. Yuan, S. Li, B. Le Guennic, J. Ma, C. Zhang, D. Jacquemin, J. Zhao. Cyclometalated Ir(III) complexes with styryl-BODIPY ligands showing near IR absorption/emission: Preparation, study of photophysical properties and application as photodynamic/luminescence imaging materials. *Journal of Materials Chemistry B* **2014**, 2, 2838–2854. doi: 10.1039/c4tb00284a
- [52] R.A. Weersinka, A. Bogaards, M. Gertner, S.R.H. Davidson, K. Zhanga, G. Netcheva, J. Trachtenberg, B.C. Wilson. Techniques for delivery and monitoring of TOOKAD (WST09)-mediated photodynamic therapy of the prostate: Clinical experience and practicalities. *Journal of Photochemistry and Photobiology B: Biology* **2005**, 79, 211–222. doi: 10.1016/j.jphotobiol.2005.01.008
- [53] A. Naik, R. Rubbiani, G. Gasser, B. Spingler. Visible-light-induced annihilation of tumor cells with platinum-porphyrin conjugates. *Angewandte Chemie - International Edition* **2014**, 53, 6938–6941. doi: 10.1002/anie.201400533
- [54] S. Stoccoro, G. Alesso, M.A. Cinellu, G. Minghetti, A. Zucca, M. Manassero, C. Manassero. Reactivity of 1,3-bis(2-pyridyl)benzene, N[^]CH[^]N, with gold(III) chlorides: Salts, adducts and cyclometalated pincer derivatives. Crystal and molecular structures of [HN[^]CH[^]N][AuCl₄], [Au(N[^]C[^]N)Cl][PF₆] and [Au(N[^]C[^]N)Cl(PPh₃)₂][PF₆]. *Dalton Transactions* **2009**, 18, 3467–3477. doi: 10.1039/b822842f
- [55] S.H. Wadman, M. Lutz, D.M. Tooke, A.L. Spek, F. Hartl, R.W.A. Havenith, G.P.M. van Klink, G. van Koten. Consequences of N,C,N'- and C,N,N'-coordination modes on electronic and photophysical properties of cyclometalated aryl ruthenium(II) complexes. *Inorganic Chemistry* **2009**, 48, 1887–1900. doi: 10.1021/ic801595m
- [56] S.H. Wadman, R.W.A. Havenith, M. Lutz, A.L. Spek, G.P.M. van Klink, G. van Koten, "Selective para-halogenation and dimerization of N,C,N'- arylruthenium(II) and -(III) 2,2':6',2''-terpyridine cations. *Journal of the American Chemical Society* **2010**, 132, 1914–1924. doi: 10.1021/ja9073276
- [57] B. Boff, C. Gaiddon, M. Pfeffer. Cancer cell cytotoxicity of cyclometalated compounds obtained with osmium(II) complexes. *Inorganic Chemistry* **2013**, 52, 2705–2715. doi: 10.1021/ic302779q
- [58] A.S. Estrada-Montaña, A.D. Ryabov, A. Gries, C. Gaiddon, R. le Lagadec. Iron(III) Pincer Complexes as a Strategy for Anticancer Studies. *European Journal of Inorganic Chemistry* **2017**, 2017, 1673–1678. doi: 10.1002/ejic.201601350
- [59] Y.S. Wong, M.C. Tang, M. Ng, V.W.W. Yam. Toward the Design of Phosphorescent Emitters of Cyclometalated Earth-Abundant Nickel(II) and Their Supramolecular Study. *Journal of the American Chemical Society* **2020**, 142, 7638–7646. doi: 10.1021/jacs.0c02172

- [60] L. Kletsch, G. Hörner, A. Klein. Cyclometalated Ni(II) Complexes [Ni(N[^]C[^]N)X] of the Tridentate 2,6-di(2-pyridyl)phen-ide Ligand. *Organometallics* **2020**, 39, 2820–2829. doi: 10.1021/acs.organomet.0c00355
- [61] D.J. Cárdenas, A.M. Echavarren, M.C. Ramírez De Arellano. Divergent Behavior of Palladium(II) and Platinum(II) in the Metalation of 1,3-Di(2-pyridyl)benzene. *Organometallics* **1999**, 18, 3337–3341. doi: 10.1021/om990125g
- [62] B. Soro, S. Stoccoro, G. Minghetti, A. Zucca, M.A. Cinellu, S. Gladiali, M. Manassero, M. Sansoni. Synthesis of the first C-2 cyclopalladated derivatives of 1,3-Bis(2-pyridyl)benzene. Crystal structures of [Hg(N-C-N)Cl], [Pd(N-C-N)Cl], and [Pd₂(N-C-N)₂(μ-OAc)]₂[Hg₂Cl₆]. Catalytic activity in the Heck reaction. *Organometallics* **2005**, 24, 53–61. doi: 10.1021/om040102o
- [63] J.A.G. Williams, A. Beeby, E.S. Davies, J.A. Weinstein, C. Wilson. An Alternative Route to Highly Luminescent Platinum(II) Complexes: Cyclometalation with N[^]C[^]N-Coordinating Dipyridylbenzene Ligands. *Inorganic Chemistry* **2003**, 119, 8609. doi: 10.1021/ic035083
- [64] S.J. Farley, D.L. Rochester, A.L. Thompson, J.A.K. Howard, J.A.G. Williams. Controlling emission energy, self-quenching, and excimer formation in highly luminescent N[^]C[^]N-coordinated platinum(II) complexes. *Inorganic Chemistry* **2005**, 44, 9690–9703. doi: 10.1021/ic051049e
- [65] D.L. Rochester, S. Develay, S. Záliš, J.A.G. Williams. Localised to intraligand charge-transfer states in cyclometalated platinum complexes: An experimental and theoretical study into the influence of electron-rich pendants and modulation of excited states by ion binding. *Dalton Transactions* **2009**, 10, 1728–1741. doi: 10.1039/b816375h
- [66] M. Cocchi, J. Kalinowski, V. Fattori, J.A.G. Williams, L. Murphy. Color-variable highly efficient organic electrophosphorescent diodes manipulating molecular exciton and excimer emissions. *Applied Physics Letters* **2009**, 94, 7. doi: 10.1063/1.3086900
- [67] L. Murphy, P. Brulatti, V. Fattori, M. Cocchi, J.A.G. Williams. Blue-shifting the monomer and excimer phosphorescence of tridentate cyclometallated platinum(II) complexes for optimal white-light OLEDs. *Chemical Communications* **2012**, 48, 5817–5819. doi: 10.1039/c2cc31330h
- [68] Z. Wang, E. Turner, V. Mahoney, S. Madakuni, T. Groy, J. Li. Facile synthesis and characterization of phosphorescent Pt(N[^]C[^]N)X complexes. *Inorganic Chemistry* **2010**, 49, 11276–11286. doi: 10.1021/ic100740e
- [69] E. Rossi, L. Murphy, P.L. Brothwood, A. Colombo, C. Dragonetti, D. Roberto, R. Ugo, M. Cocchi, J.A.G. Williams. Cyclometallated platinum(II) complexes of 1,3-di(2-pyridyl)benzenes: Tuning excimer emission from red to near-infrared for NIR-OLEDs. *Journal of Materials Chemistry* **2011**, 21, 15501–15510. doi: 10.1039/c1jm12716k
- [70] V.N. Kozhevnikov, B. Donnio, B. Heinrich, D.W. Bruce. Morphology-driven absorption and emission colour changes in liquid-crystalline, cyclometallated platinum(II) complexes. *Chemical Communications* **2014**, 50, 14191–14193. doi: 10.1039/c4cc06958g

- [71] F. Nisic, A. Colombo, C. Dragonetti, D. Roberto, A. Valore, J.M. Malicka, M. Cocchi, G.R. Freeman, J.A.G. Williams. Platinum(II) complexes with cyclometallated 5- π -delocalized-donor-1,3-di(2-pyridyl)benzene ligands as efficient phosphors for NIR-OLEDs. *Journal of Materials Chemistry C* **2014**, 2, 1791–1800. doi: 10.1039/c3tc32086c
- [72] F. Nisic, E. Cariati, A. Colombo, C. Dragonetti, S. Fantacci, E. Garoni, E. Lucenti, S. Righetto, D. Roberto, J.A.G. Williams. Tuning the dipolar second-order nonlinear optical properties of 5- π -delocalized-donor-1,3-di(2-pyridyl)benzenes, related cyclometallated platinum(II) complexes and methylated salts. *Dalton Transactions* **2017**, 46, 1179–1185. doi: 10.1039/c6dt04359c
- [73] N. Baggi, E. Garoni, A. Colombo, C. Dragonetti, S. Righetto, D. Roberto, J. Boixel, V. Guerchais, S. Fantacci. Design of cyclometallated 5- π -delocalized donor-1,3-di(2-pyridyl)benzene platinum(II) complexes with second-order nonlinear optical properties. *Polyhedron* **2018**, 140, 74–77. doi: 10.1016/j.poly.2017.11.051
- [74] M. Fontani, E. Garoni, A. Colombo, C. Dragonetti, S. Fantacci, H. Doucet, J.-F. Soulé, J. Boixel, V. Guerchais, D. Roberto. Novel cyclometallated 5- π -delocalized donor-1,3-di(2-pyridyl)benzene platinum(II) complexes with good second-order nonlinear optical properties. *Dalton Transactions* **2019**, 48, 202–208. doi: 10.1039/c8dt03622e
- [75] Y.-L. Rao, D. Schoenmakers, Y.-L. Chang, J.-S. Lu, Z.-H. Lu, Y. Kang, S. Wang. Bluish-green BMe₂-functionalized Pt^{II} complexes for high efficiency PhOLEDs: Impact of the BMe₂ location on emission color. *Chemistry - A European Journal* **2012**, 18, 11306–11316. doi: 10.1002/chem.201201255
- [76] E. Baggaley, S.W. Botchway, J.W. Haycock, H. Morris, I.V. Sazanovich, J.A.G. Williams, J.A. Weinstein. Long-lived metal complexes open up microsecond lifetime imaging microscopy under multiphoton excitation: From FLIM to PLIM and beyond. *Chemical Science* **2014**, 5, 879–886. doi: 10.1039/c3sc51875b
- [77] A. Colombo, F. Fiorini, D. Septiadi, C. Dragonetti, F. Nisic, A. Valore, D. Roberto, M. Mauro, L. De Cola. Neutral N⁺C⁻N terdentate luminescent Pt(II) complexes: Their synthesis, photophysical properties, and bio-imaging applications. *Dalton Transactions* **2015**, 44, 8478–8487. doi: 10.1039/c4dt03165b
- [78] T. Chatzisideri, S. Thysiadis, S. Katsamakas, P. Dalezis, I. Sigala, T. Lazarides, E. Nikolakaki, D. Trafalis, O.A. Gederaas, M. Lindgren, V. Sarli. Synthesis and biological evaluation of a Platinum(II)-c(RGDyK) conjugate for integrin-targeted photodynamic therapy. *European Journal of Medicinal Chemistry* **2017**, 141, 221–231. doi: 10.1016/j.ejmech.2017.09.058
- [79] A. Scarpaci, C. Monnereau, N. Hergué, E. Blart, S. Legoupy, F. Odobel, A. Gorfo, J. Pérez-Moreno, K. Clays, I. Asselberghs. Preparation and characterization of second order non-linear optical properties of new ‘push-pull’ platinum complexes. *Dalton Transactions* **2009**, 23, 4538–4546. doi: 10.1039/b900282k
- [80] H. Zhao, E. Garoni, T. Roisnel, A. Colombo, C. Dragonetti, D. Marinotto, S. Righetto, D. Roberto, D. Jacquemin, J. Boixel, V. Guerchais. Photochromic DTE-Substituted-1,3-di(2-pyridyl)benzene Platinum(II) Complexes: Photomodulation of Luminescence and Second-Order Nonlinear Optical Properties. *Inorganic Chemistry* **2018**, 57, 7051–7063. doi: 10.1021/acs.inorgchem.8b00733

- [81] C.J. Lin, Y.H. Liu, S.M. Peng, T. Shinmyozu, J.S. Yang. Excimer-Monomer Photoluminescence Mechanochromism and Vapochromism of Penttiptycene-Containing Cyclometalated Platinum(II) Complexes. *Inorganic Chemistry* **2017**, 56, 4978–4989. doi: 10.1021/acs.inorgchem.7b00009
- [82] C.Y. Lien, Y.F. Hsu, Y.H. Liu, S.M. Peng, T. Shinmyozu, J.S. Yang. Steric Engineering of Cyclometalated Pt(II) Complexes toward High-Contrast Monomer-Excimer-Based Mechanochromic and Vapochromic Luminescence. *Inorganic Chemistry* **2020**, 59, 11584–11594. doi: 10.1021/acs.inorgchem.0c01390
- [83] K. Yamamoto, K. Higuchi, M. Ogawa, H. Sogawa, S. Kuwata, Y. Hayashi, S. Kawauchi, T. Takata. Macrocyclic Metal Complexes Bearing Rigid Polyaromatic Ligands: Synthesis and Catalytic Activity. *Chemistry - An Asian Journal* **2020**, 15, 356–359. doi: 10.1002/asia.201901561
- [84] R. Okamura, T. Wada, K. Aikawa, T. Nagata, K. Tanaka. A platinum-ruthenium dinuclear complex bridged by bis(terpyridyl)xanthene. *Inorganic Chemistry* **2004**, 43, 7210–7217. doi: 10.1021/ic049680n
- [85] S. Develay, J.A.G. Williams. Intramolecular excimers based on rigidly-linked platinum(II) complexes: Intense deep-red triplet luminescence in solution. *Dalton Transactions* **2008**, 34, 4562–4564. doi: 10.1039/b807668e
- [86] W.L. Tong, M.C.W. Chan, S.M. You. Congested cyclometalated platinum(II) ditopic frameworks and their phosphorescent responses to S-containing amino acids. *Organometallics* **2010**, 29, 6377–6383. doi: 10.1021/om1007488
- [87] Z.L. Gong, Y.W. Zhong, J. Yao. Regulation of intra- and intermolecular Pt-Pt and π - π Interactions of a U-shaped diplatinum complex to achieve pseudo-polymorphic emissions in solution and crystalline states. *Journal of Materials Chemistry C* **2017**, 5, 7222–7229. doi: 10.1039/c7tc02282d
- [88] E. Garoni, J. Boixel, V. Dorcet, T. Roisnel, D. Roberto, D. Jacquemin, V. Guerschais. Controlling the emission in flexibly-linked (N[^]C[^]N)platinum dyads. *Dalton Transactions* **2018**, 47, 224–232. doi: 10.1039/c7dt03695g
- [89] E. Rossi, A. Colombo, C. Dragonetti, D. Roberto, R. Ugo, A. Valore, L. Falciola, P. Brulatti, M. Cocchi, J.A.G. Williams. Novel N[^]C[^]N-cyclometallated platinum complexes with acetylide co-ligands as efficient phosphors for OLEDs. *Journal of Materials Chemistry* **2012**, 22, 10650–10655. doi: 10.1039/c2jm16592a
- [90] C.J. Lin, Y.H. Liu, S.M. Peng, T. Shinmyozu, J.S. Yang. Excimer-Monomer Photoluminescence Mechanochromism and Vapochromism of Penttiptycene-Containing Cyclometalated Platinum(II) Complexes. *Inorganic Chemistry* **2017**, 56, 4978–4989. doi: 10.1021/acs.inorgchem.7b00009
- [91] C.Y. Lien, Y.F. Hsu, Y.H. Liu, S.M. Peng, T. Shinmyozu, J.S. Yang. Steric Engineering of Cyclometalated Pt(II) Complexes toward High-Contrast Monomer-Excimer-Based Mechanochromic and Vapochromic Luminescence. *Inorganic Chemistry* **2020**, 59, 11584–11594. doi: 10.1021/acs.inorgchem.0c01390

- [92] Y. Ai, M.H.-Y. Chan, A.K.-W. Chan, M. Ng, Y. Li, V.W.-W. Yam. A platinum(II) molecular hinge with motions visualized by phosphorescence changes. *Proceedings of the National Academy of Sciences* **2019**, 116, 13856–13861. doi:10.1073/pnas.1908034116
- [93] B. Li, Y. Li, M.H.Y. Chan, V.W.W. Yam. Phosphorescent Cyclometalated Platinum(II) Enantiomers with Circularly Polarized Luminescence Properties and Their Assembly Behaviors. *Journal of the American Chemical Society* **2021**, 143, 21676–21684. doi: 10.1021/jacs.1c10943
- [94] Y. Chen, W. Lu, C.M. Che. Luminescent pincer-type cyclometalated platinum(II) complexes with auxiliary isocyanide ligands: Phase-transfer preparation, solvatomorphism, and self-aggregation. *Organometallics* **2013**, 32, 350–353. doi: 10.1021/om300965b
- [95] J. Kuwabara, K. Yamaguchi, K. Yamawaki, T. Yasuda, Y. Nishimura, T. Kanbara. Modulation of the Emission Mode of a Pt(II) Complex via Intermolecular Interactions. *Inorganic Chemistry* **2017**, 56, 8726–8729. doi: 10.1021/acs.inorgchem.7b00880
- [96] K. Yamaguchi, K. Yamawaki, T. Kimura, J. Kuwabara, T. Yasuda, Y. Nishimura, T. Kanbara. Multi-molecular emission of a cationic Pt(II) complex through hydrogen bonding interactions. *Dalton Transactions* **2018**, 47, 4087–4092. doi: 10.1039/c8dt00314a
- [97] W.A. Tarran, G.R. Freeman, L. Murphy, A.M. Benham, R. Katakya, J.A.G. Williams. Platinum(II) complexes of N[^]C[^]N^{^-} coordinating 1,3-bis(2-pyridyl)benzene ligands: Thiolate coligands lead to strong red luminescence from charge-transfer states. *Inorganic Chemistry* **2014**, 53, 5738–5749. doi: 10.1021/ic500555w
- [98] Q. Zheng, S. Borsley, G.S. Nichol, F. Duarte, S.L. Cockroft. The Energetic Significance of Metallophilic Interactions. *Angewandte Chemie - International Edition* **2019**, 58, 12617–12623. doi: 10.1002/anie.201904207
- [99] Q. Zheng, S. Borsley, T. Tu, S.L. Cockroft. Reversible stimuli-responsive chromism of a cyclometallated platinum(II) complex. *Chemical Communications* **2020**, 56, 14705–14708. doi: 10.1039/d0cc06775j
- [100] W. Mróz, C. Botta, U. Giovanella, E. Rossi, A. Colombo, C. Dragonetti, D. Roberto, R. Ugo, A. Valore, J.A.G. Williams. Cyclometallated platinum(II) complexes of 1,3-di(2-pyridyl)benzenes for solution-processable WOLEDs exploiting monomer and excimer phosphorescence. *Journal of Materials Chemistry* **2011**, 21, 8653–8661. doi: 10.1039/c1jm10193e
- [101] E. Rossi, A. Colombo, C. Dragonetti, D. Roberto, F. Demartin, M. Cocchi, P. Brulatti, V. Fattori, J.A.G. Williams. From red to near infra-red OLEDs: The remarkable effect of changing from X = -Cl to -NCS in a cyclometallated [Pt(N[^]C[^]N^{^-})X] complex {N[^]C[^]N^{^-} = 5-mesityl-1,3-di-(2-pyridyl)benzene}. *Chemical Communications* **2012**, 48, 3182–3184. doi: 10.1039/c2cc16399c
- [102] H. Shi, G.J. Clarkson, P.J. Sadler. Dual action photosensitive platinum(II) anticancer prodrugs with photoreleasable azide ligands. *Inorganica Chimica Acta* **2019**, 489, 230–235. doi: 10.1016/j.ica.2019.02.016

- [103] L.M. Cinninger, L.D. Bastatas, Y. Shen, B.J. Holliday, J.D. Slinker. Luminescent properties of a 3,5-diphenylpyrazole bridged Pt(II) dimer. *Dalton Transactions* **2019**, 48, 9684–9691. doi: 10.1039/c9dt00795d
- [104] K. Li, Y. Chen, W. Lu, N. Zhu, C.M. Che. A cyclometalated platinum(II) complex with a pendent pyridyl motif as solid-state luminescent sensor for acidic vapors. *Chemistry - A European Journal* **2011**, 17, 4109–4112. doi: 10.1002/chem.201003606
- [105] H. Sesolis, C.K.M. Chan, G. Gontard, H.L.K. Fu, V.W.W. Yam, H. Amouri. Dinuclear (N[^]C[^]N) Pincer Pt(II) Complexes with Bridged Organometallic Linkers: Synthesis, Structures, Self-Aggregation, and Photophysical Properties. *Organometallics* **2017**, 36, 4794–4801. doi: 10.1021/acs.organomet.7b00680
- [106] K.S. Kisel, A.S. Melnikov, E.V. Grachova, P. Hirva, S. P. Tunik, I.O. Koshevoy. Linking Re^I and Pt^{II} Chromophores with Aminopyridines: A Simple Route to Achieve a Complicated Photophysical Behavior. *Chemistry - A European Journal* **2017**, 23, 11301–11311. doi: 10.1002/chem.201701539
- [107] G. De Soricellis, F. Fagnani, A. Colombo, C. Dragonetti, D. Roberto. Exploring the potential of N[^]C[^]N cyclometalated Pt(II) complexes bearing 1,3-di(2-pyridyl)benzene derivatives for imaging and photodynamic therapy. *Inorganica Chimica Acta* **2022**, 541, 121082. doi: 10.1016/j.ica.2022.121082
- [108] A. Raza, H.E. Colley, E. Baggaley, I.V. Sazanovich, N.H. Green, J.A. Weinstein, S.W. Botchway, S. MacNeil, J.W. Haycock. Oxygen Mapping of Melanoma Spheroids using Small Molecule Platinum Probe and Phosphorescence Lifetime Imaging Microscopy. *Scientific Reports* **2017**, 7. doi: 10.1038/s41598-017-11153-9
- [109] R.E. Doherty, I.V. Sazanovich, L.K. McKenzie, A.S. Stasheuski, R. Coyle, E. Baggaley, S. Bottomley, J.A. Weinstein, H.E. Bryant. Photodynamic killing of cancer cells by a Platinum(II) complex with cyclometallating ligand. *Scientific Reports* **2016**, 6, 22668. doi: 10.1038/srep22668
- [110] M.A. Iqbal, H. Mehmood, J. Lv, R. Hua. Base-promoted SNAR reactions of fluoro- And chloroarenes as a route to N-aryl indoles and carbazoles. *Molecules* **2019**, 24, 1145. doi: 10.3390/molecules24061145
- [111] Y. Lin, X. Yang, Y. Lu, D. Liang, D. Huang. Isothiocyanates as H₂S Donors Triggered by Cysteine: Reaction Mechanism and Structure and Activity Relationship. *Organic Letters* **2019**, 21, 5977–5980. doi: 10.1021/acs.orglett.9b02117
- [112] L. Petri, P.A. Szijj, A. Kelemen, T. Imre, A. Gömöry, M.T.W. Lee, K. Hegedűs, P. Ábrányi-Balogh, V. Chudasama, G. Miklós Keserű. Cysteine specific bioconjugation with benzyl isothiocyanates. *RSC Advances* **2020**, 10, 14928–14936. doi: 10.1039/d0ra02934c
- [113] H.I.A. Phillips, L. Ronconi, P.J. Sadler. Photoinduced Reactions of *cis,trans,cis*- [Pt^{IV}(N₃)₂(OH)₂(NH₃)₂] with 1-methylimidazole. *Chemistry - A European Journal* **2009**, 15, 1588–1596. doi: 10.1002/chem.200802206
- [114] C.A. Wootton, C. Sanchez-Cano, A.F. Lopez-Clavijo, E. Shaili, M.P. Barrow, P.J. Sadler, P.B. O'Connor. Sequence-dependent attack on peptides by photoactivated platinum anticancer complexes. *Chemical Science* **2018**, 9, 2733–2739. doi: 10.1039/c7sc05135b

- [115] J.S. Butler, J.A. Woods, N.J. Farrer, M.E. Newton, P.J. Sadler. Tryptophan switch for a photoactivated platinum anticancer complex. *Journal of the American Chemical Society* **2012**, 134, 16508–16511. doi: 10.1021/ja3074159
- [116] K. Peng, V. Mawamba, E. Schulz, M. Löhr, C. Hagemann, U. Schatzschneider. IClick Reactions of Square-Planar Palladium(II) and Platinum(II) Azido Complexes with Electron-Poor Alkynes: Metal-Dependent Preference for N1 vs N2 Triazolate Coordination and Kinetic Studies with ¹H and ¹⁹F NMR Spectroscopy. *Inorganic Chemistry* **2019**, 58, 11508–11521. doi: 10.1021/acs.inorgchem.9b01304
- [117] K. Peng, D. Moreth, U. Schatzschneider. CNN Coordination Accelerates the iClick Reaction of Square-Planar Palladium(II) and Platinum(II) Azido Complexes with Electron-Poor Alkynes and Enables Cycloaddition with Terminal Alkynes. *Organometallics* **2021**, 40, 2584–2593. doi: 10.1021/acs.organomet.1c00293

APPENDIX

In this section all NMR spectra and lifetimes graphs are reported.

For all intermediates, boronic esters, NCN ligands and Pt(II) complexes, the ^1H NMR spectra have been registered; when possible, also the ^{13}C and ^{19}F NMR spectra were obtained.

NMR spectra were recorded on a Bruker AV III 300 MHz or AV III 400 MHz spectrometers, using deuterated chloroform (CDCl_3) or dichloromethane (CD_2Cl_2) as solvents.

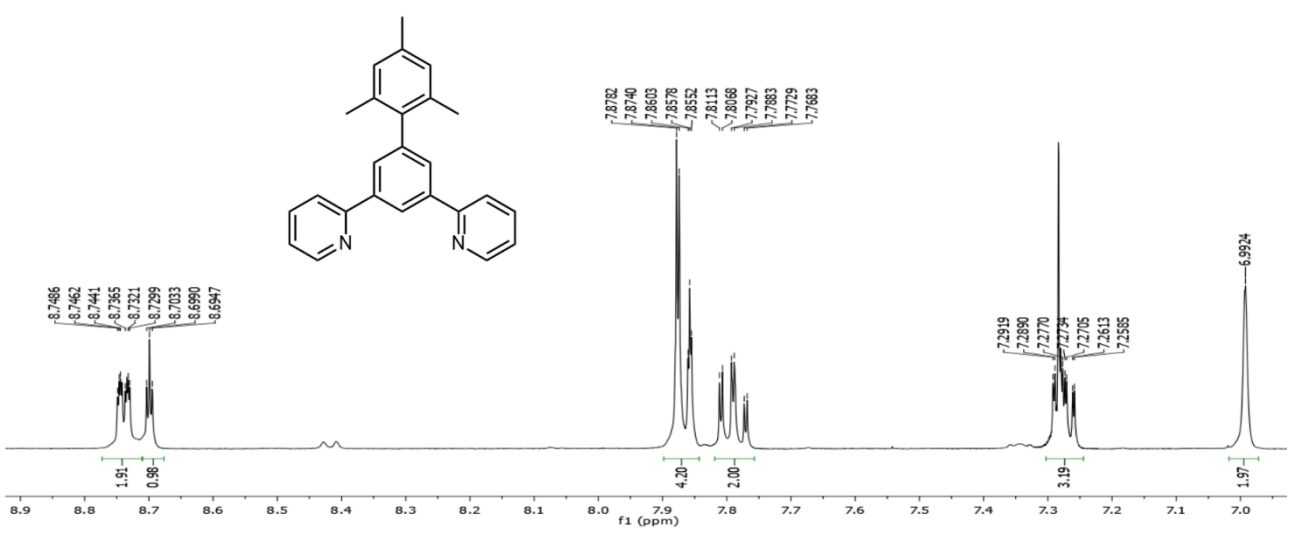
All spectra are already listed in the Experimental Section (**Chapter V**), as part of the characterization carried out on the synthesized compounds. Chemical shifts of ^1H , ^{13}C and ^{19}F NMR spectra are reported in parts per million (ppm) and the coupling constants are measured in Hertz (Hz). Signal multiplicities are listed as singlet (s), d (doublet), t (triplet), quartet (q), multiplet (m).

For most compounds having aromatic signals, the aromatic region is shown on expanded scale for clarity.

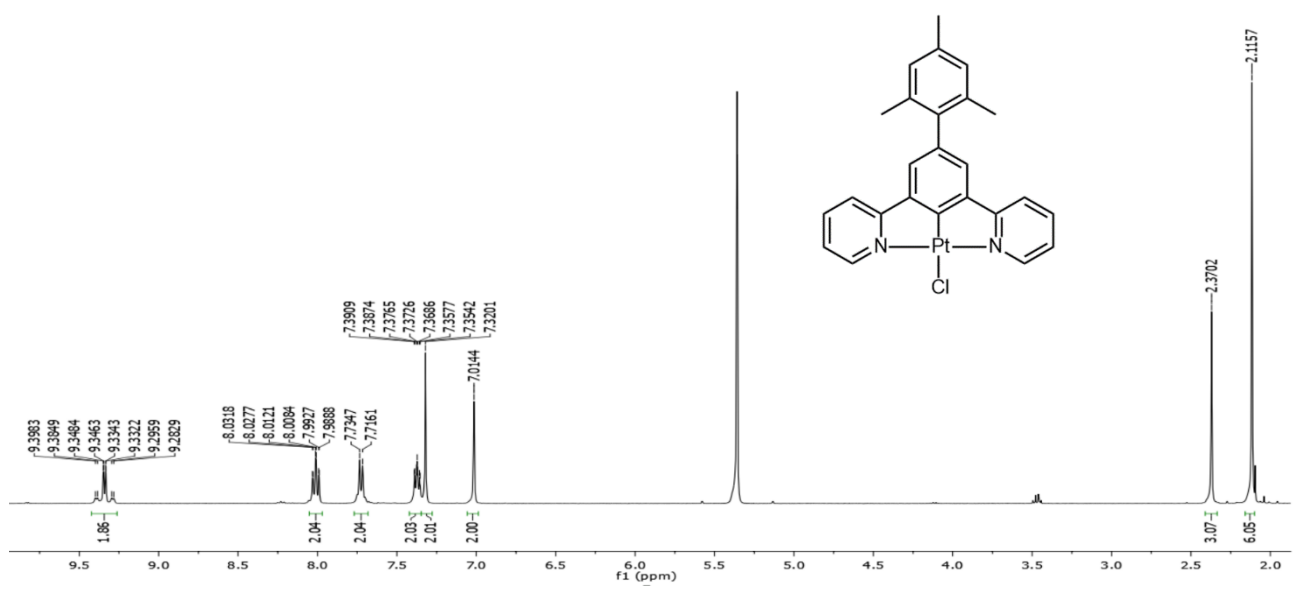
Concerning the lifetime measurements, all details about the employed technique, the instrument and the applied mathematical procedure have already been provided in **Chapter IV – Section 1.4**.

All graphs report the excitation and emission wavelengths together with the percentages relative to the different contributions in the case of multi-exponential decays.

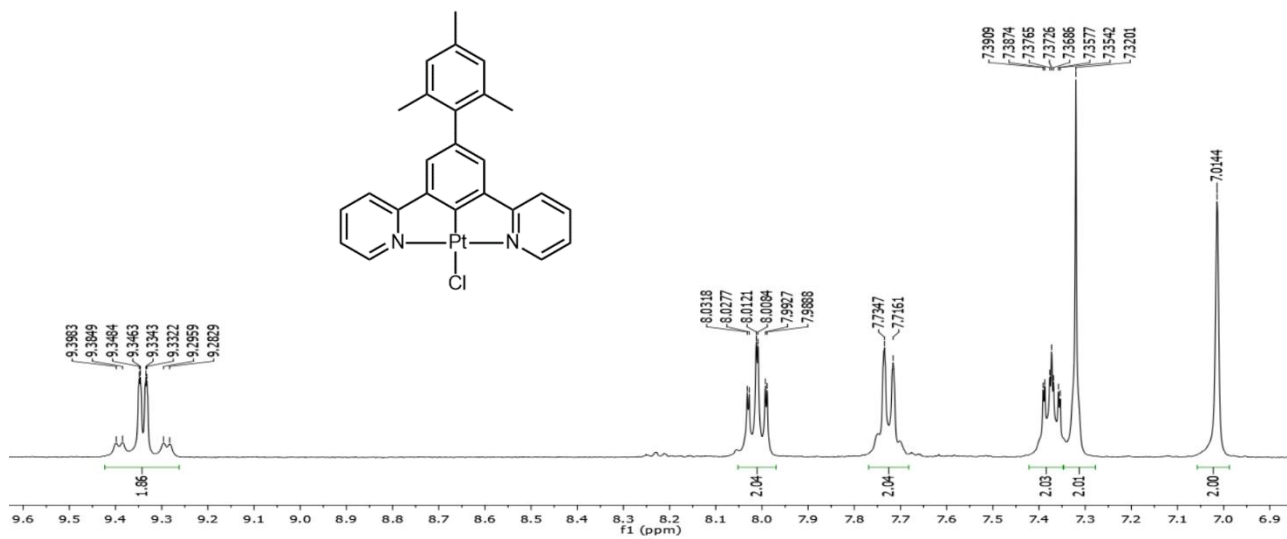
L1 - aromatic region



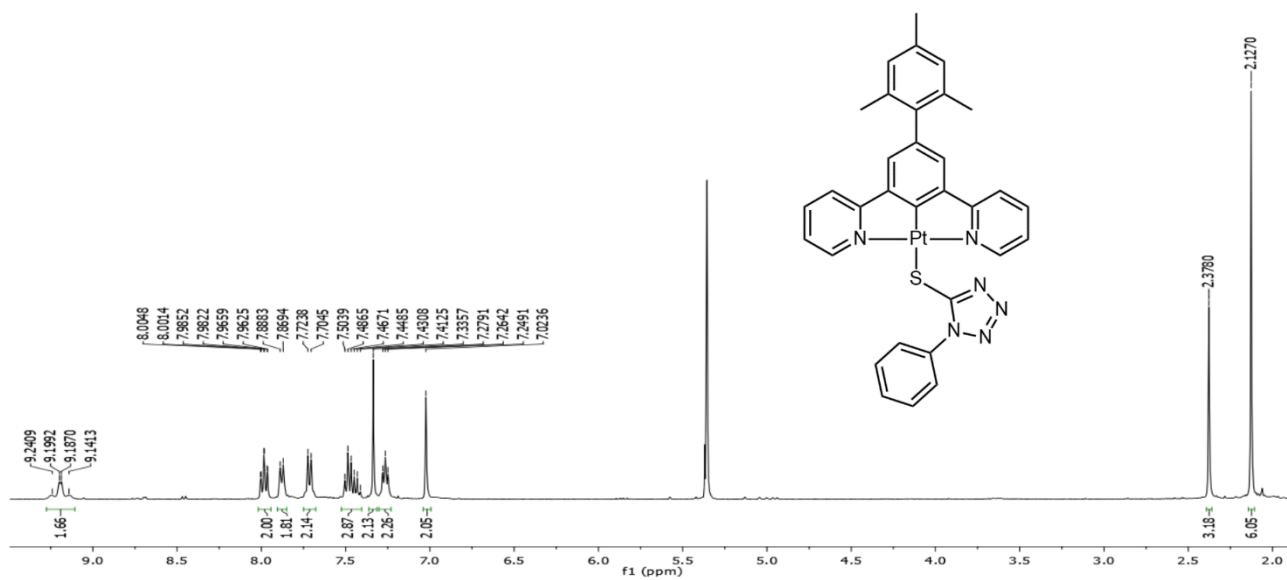
PtCl1



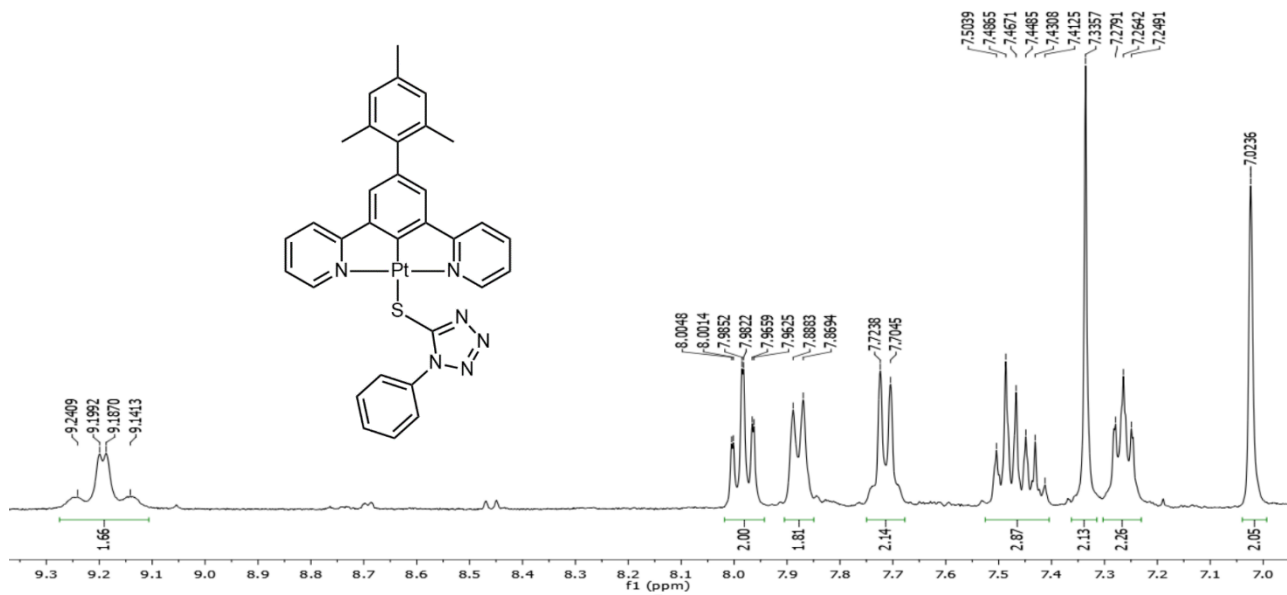
PtCl1 – aromatic region



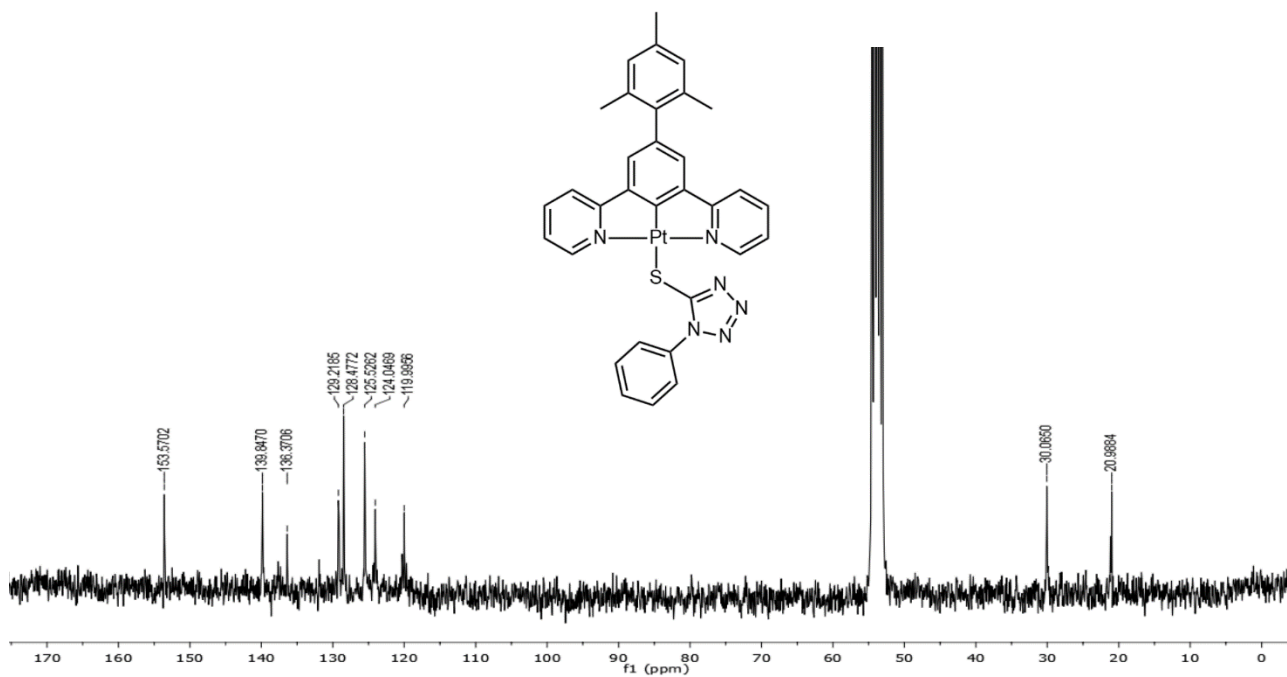
Pt1



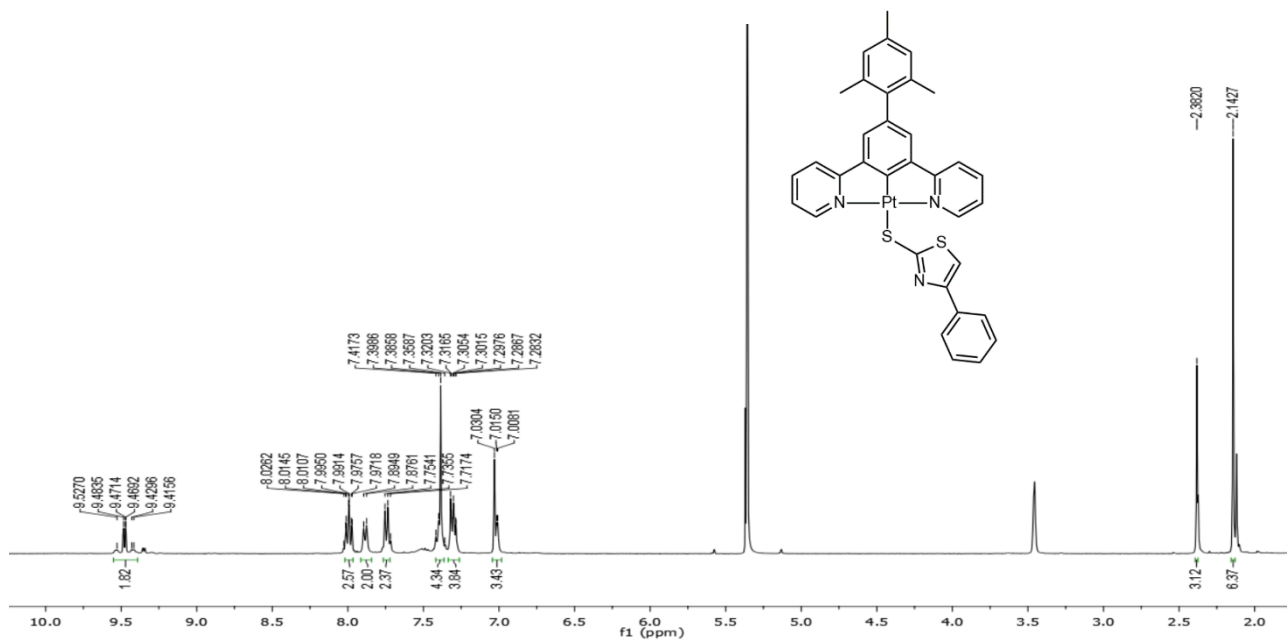
Pt1 – aromatic region



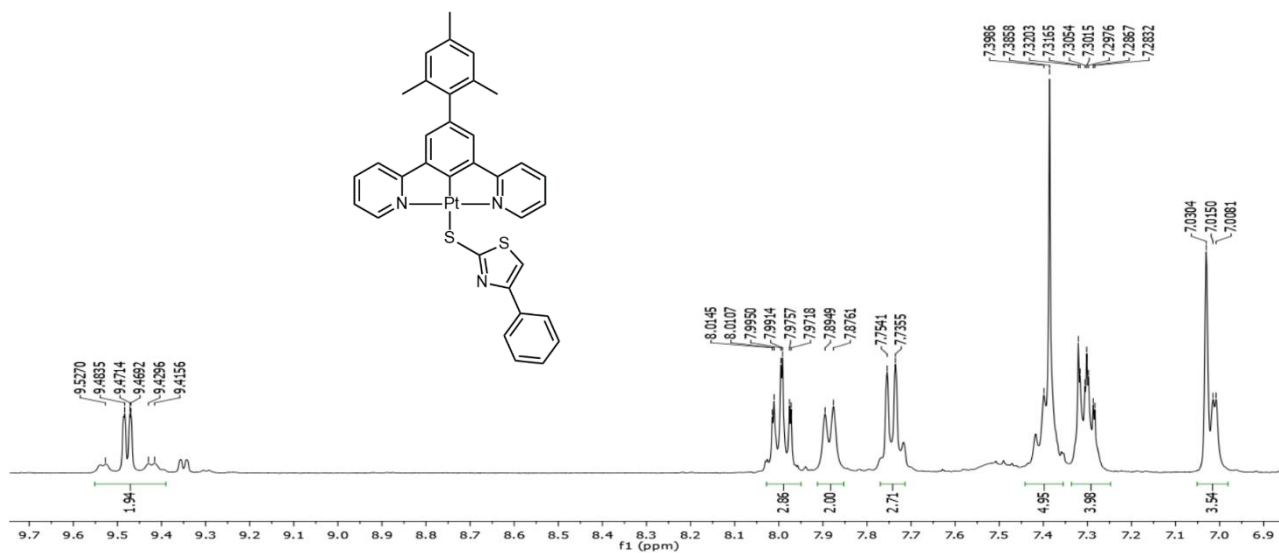
Pt1 – ¹³C NMR



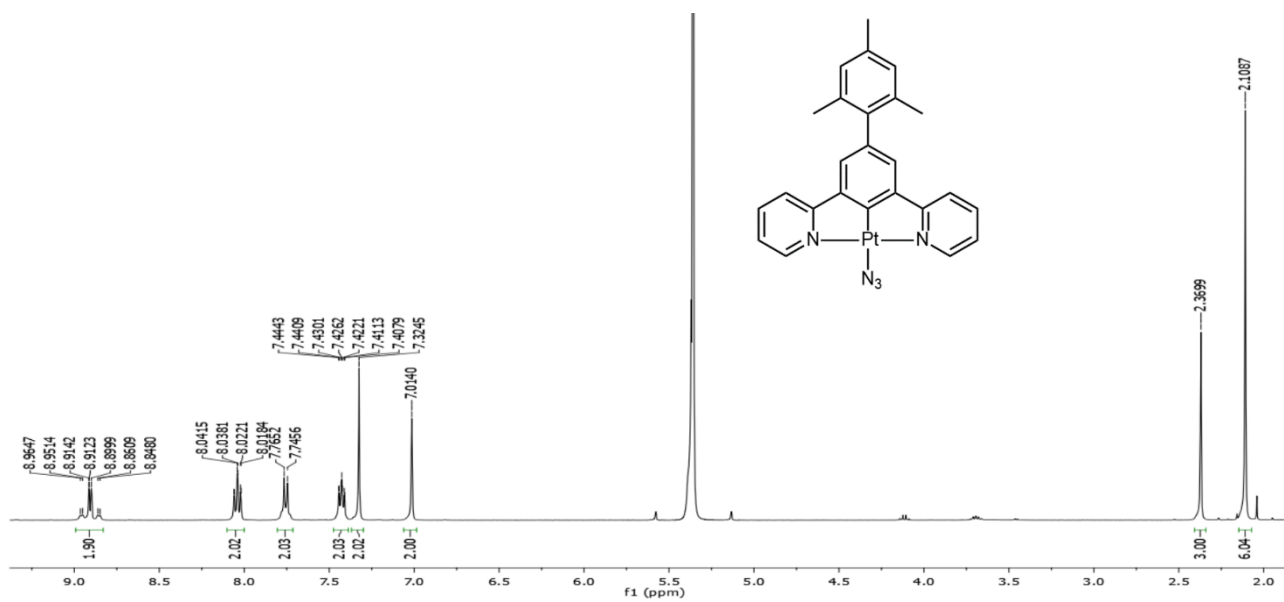
Pt2



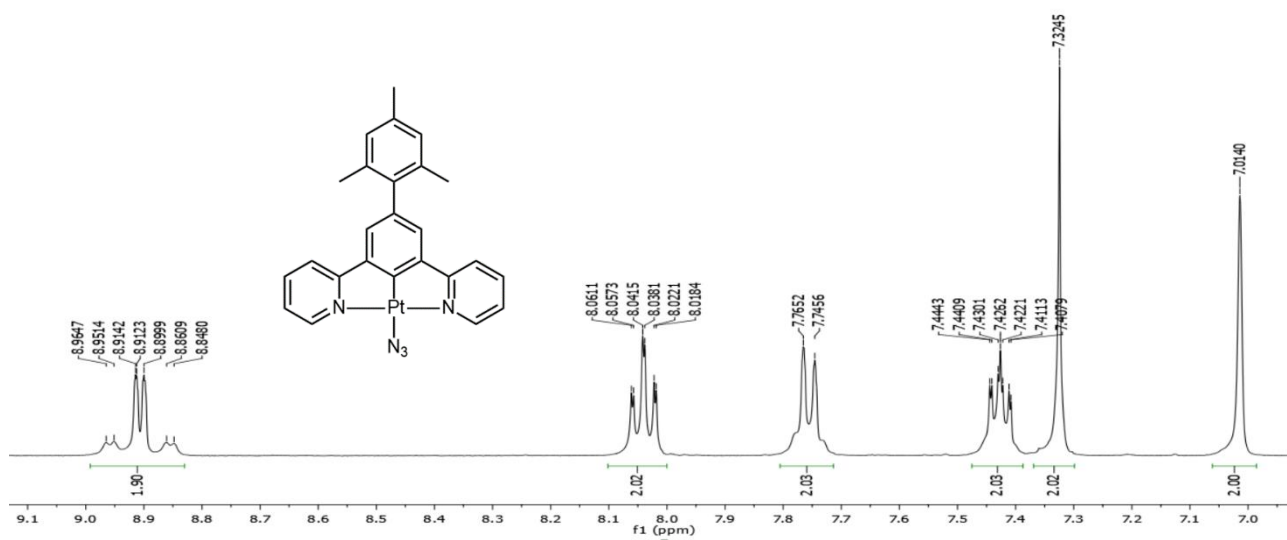
Pt2 - aromatic region



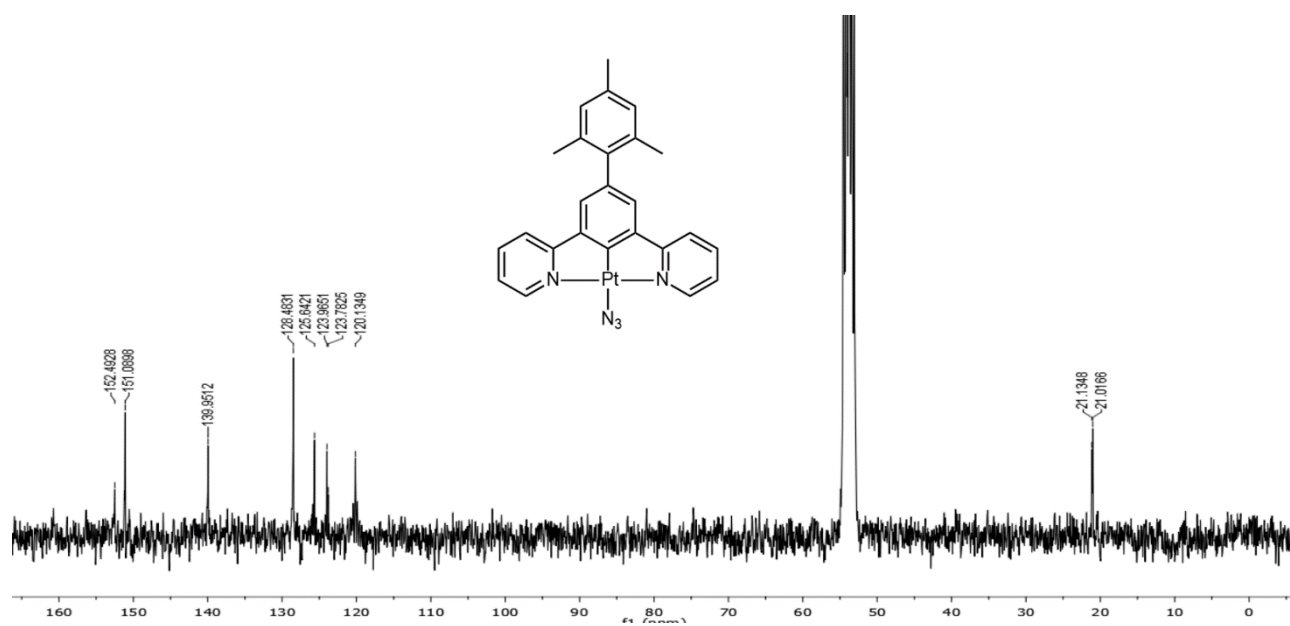
Pt3



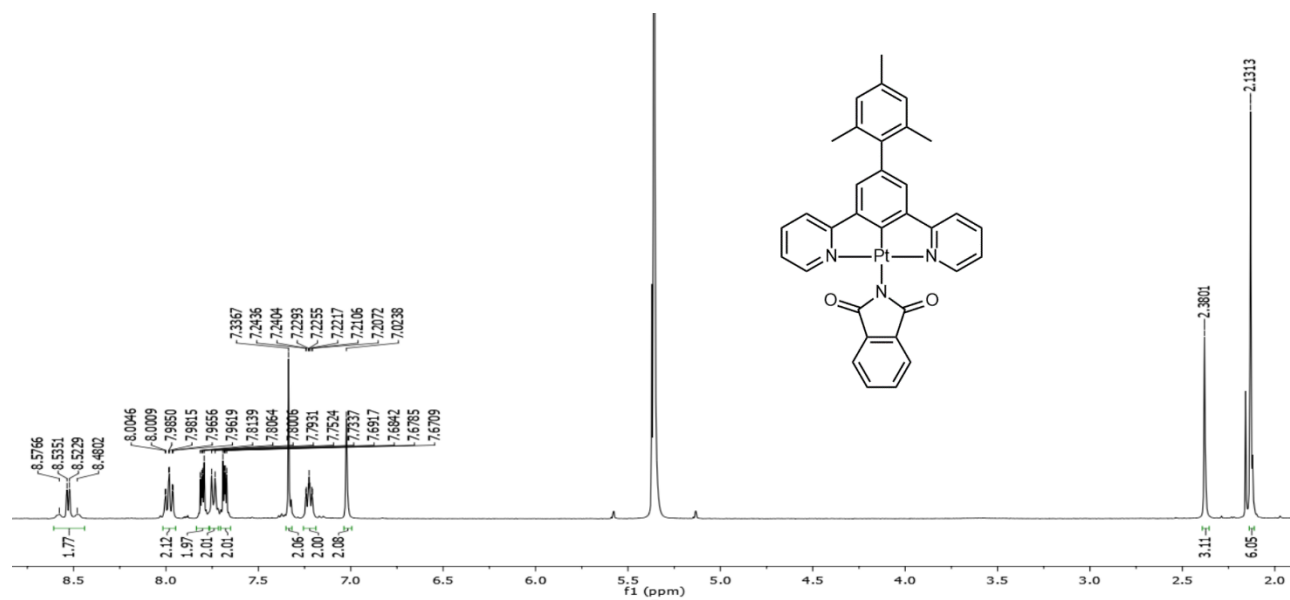
Pt3 – aromatic region



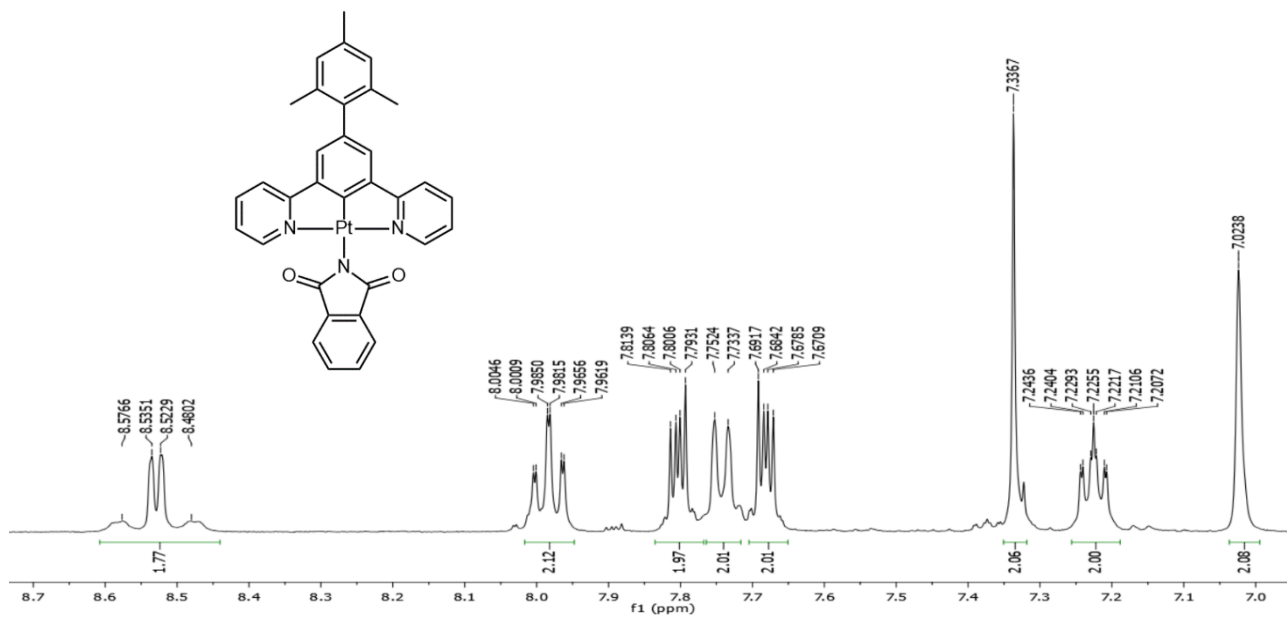
Pt3 - ¹³C NMR



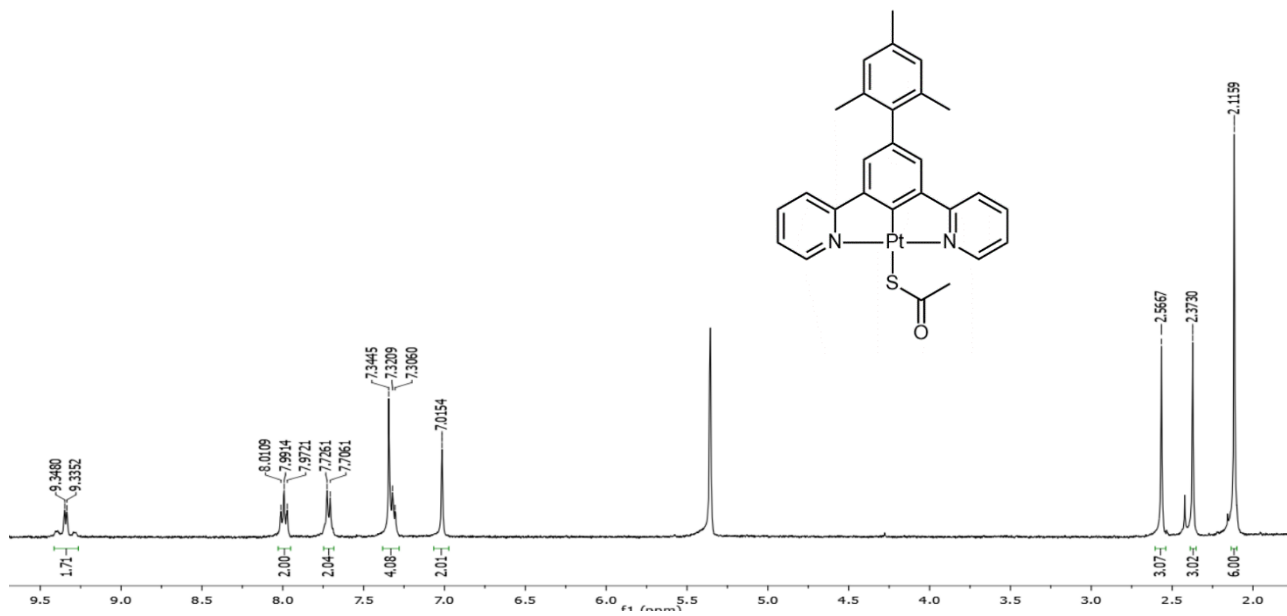
Pt4



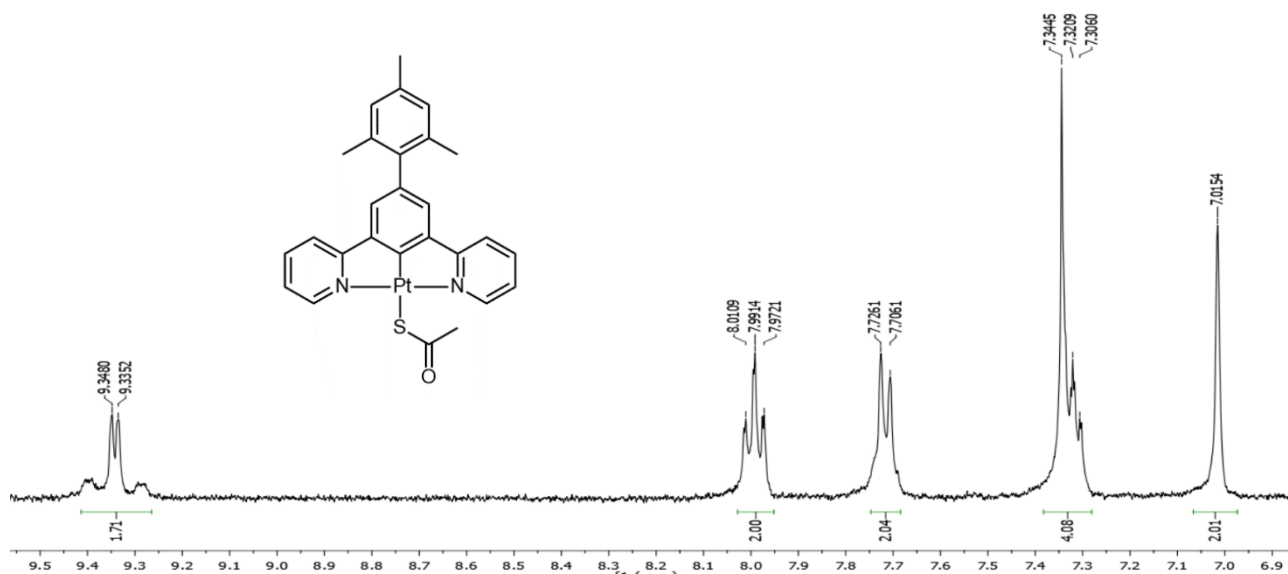
Pt4 – aromatic region



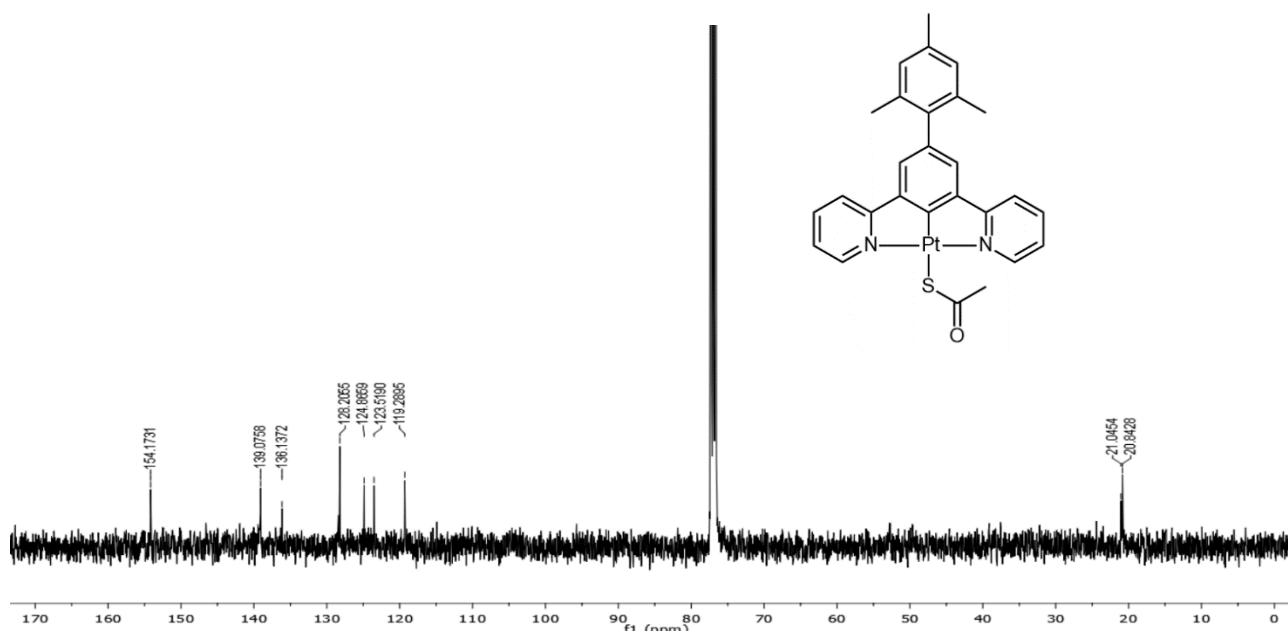
Pt5



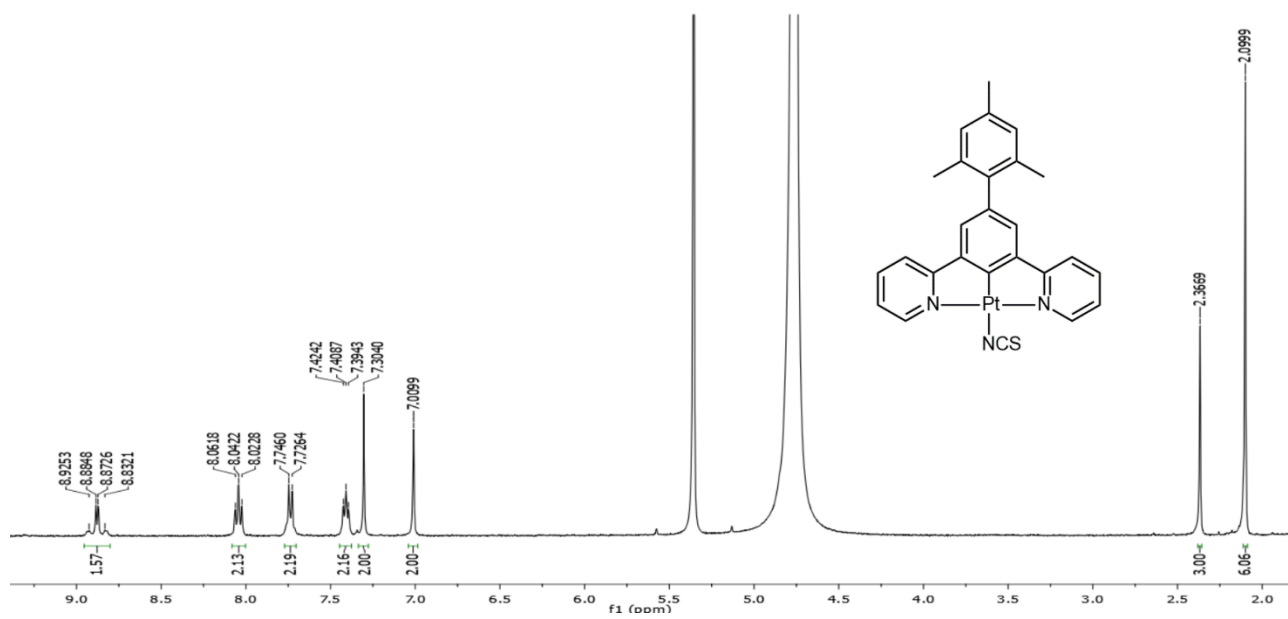
Pt5 – aromatic region



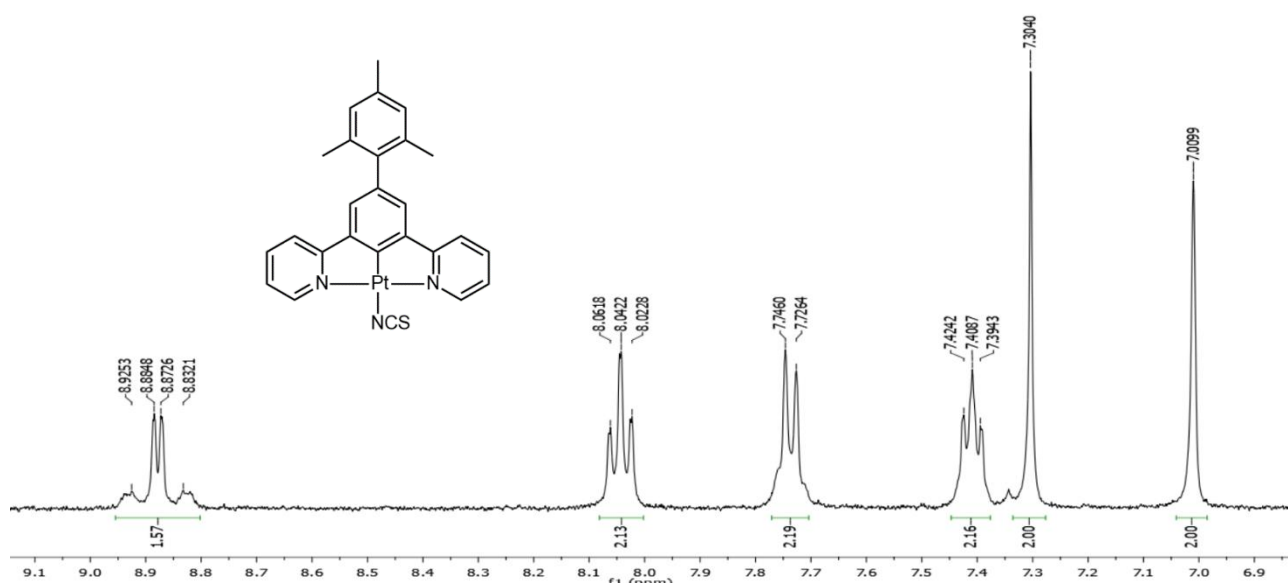
Pt5 – ¹³C NMR



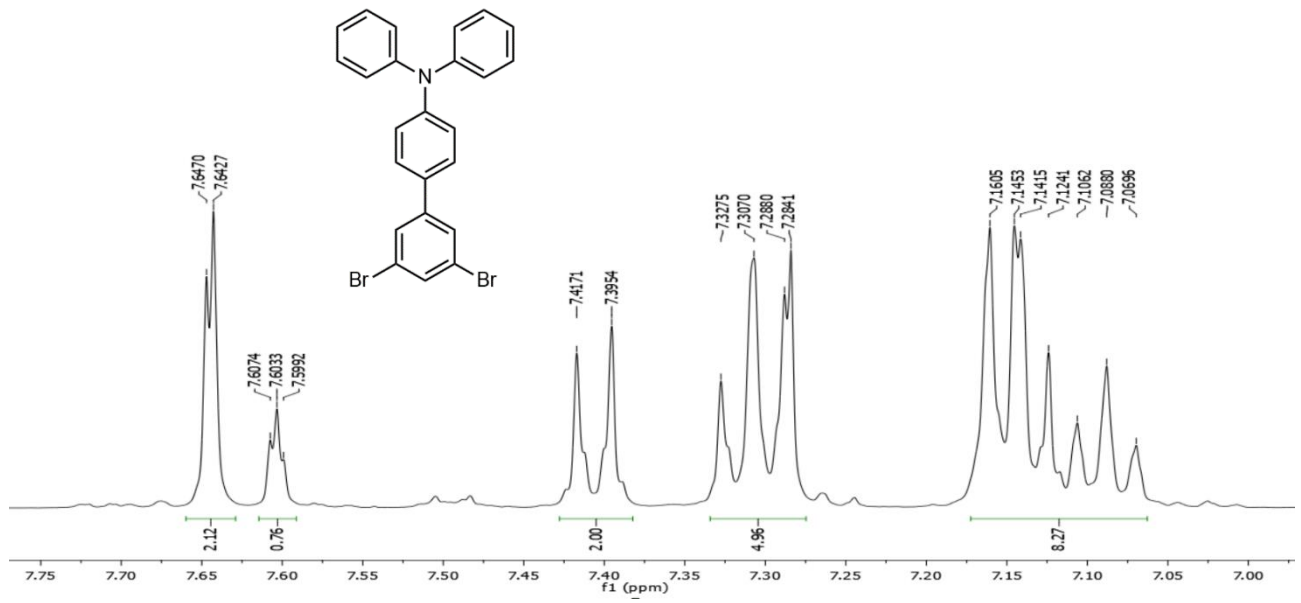
Pt6



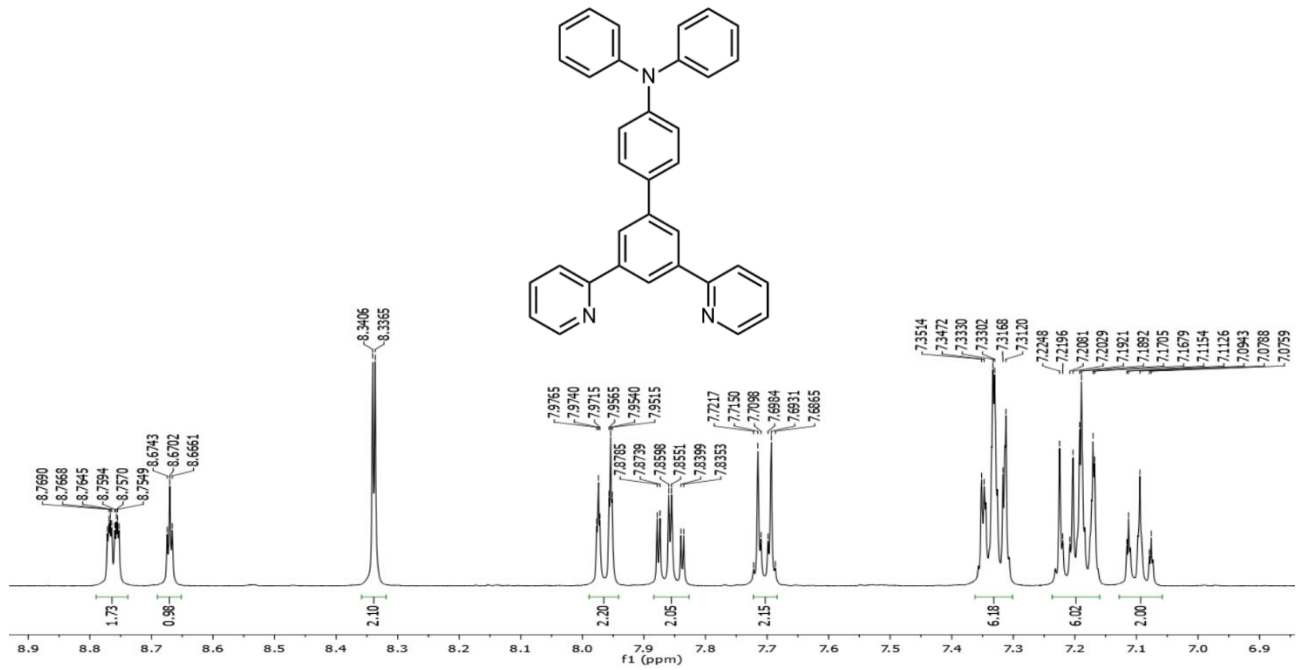
Pt6 - aromatic region



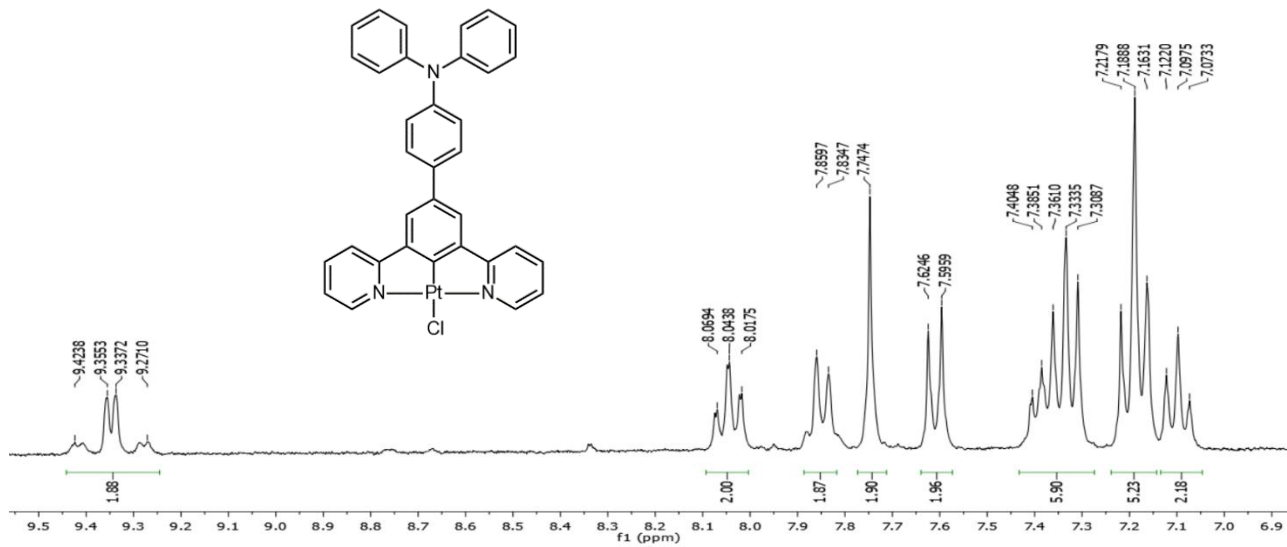
I2



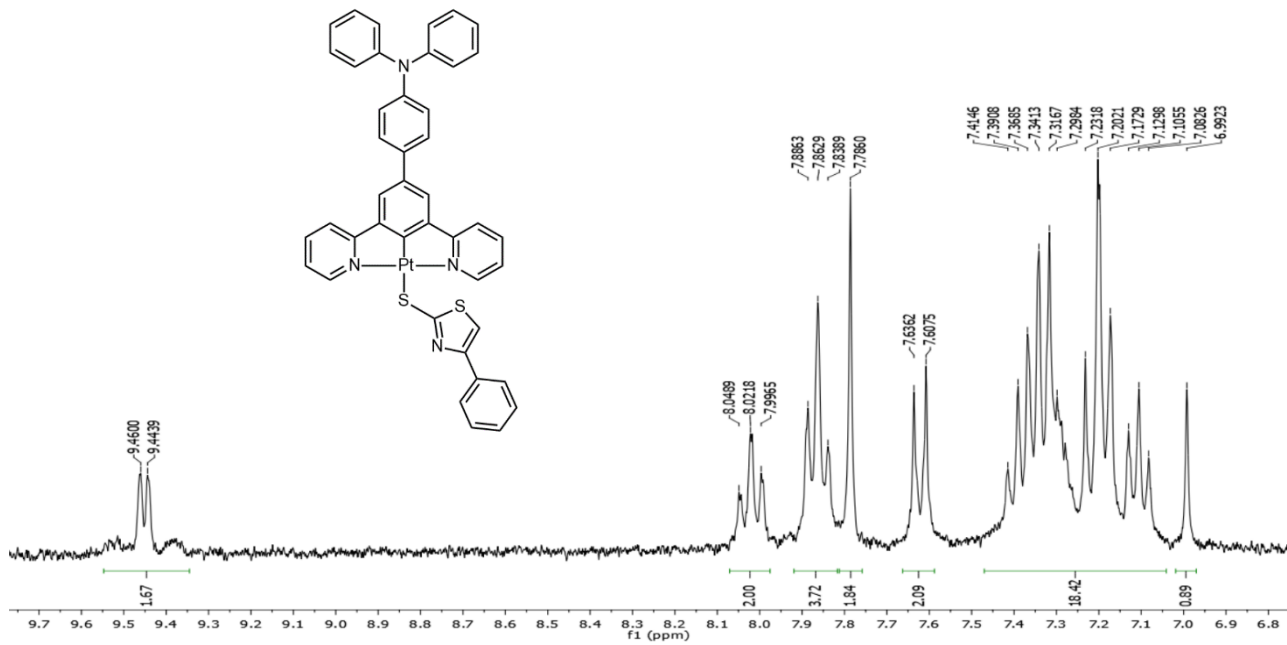
L2



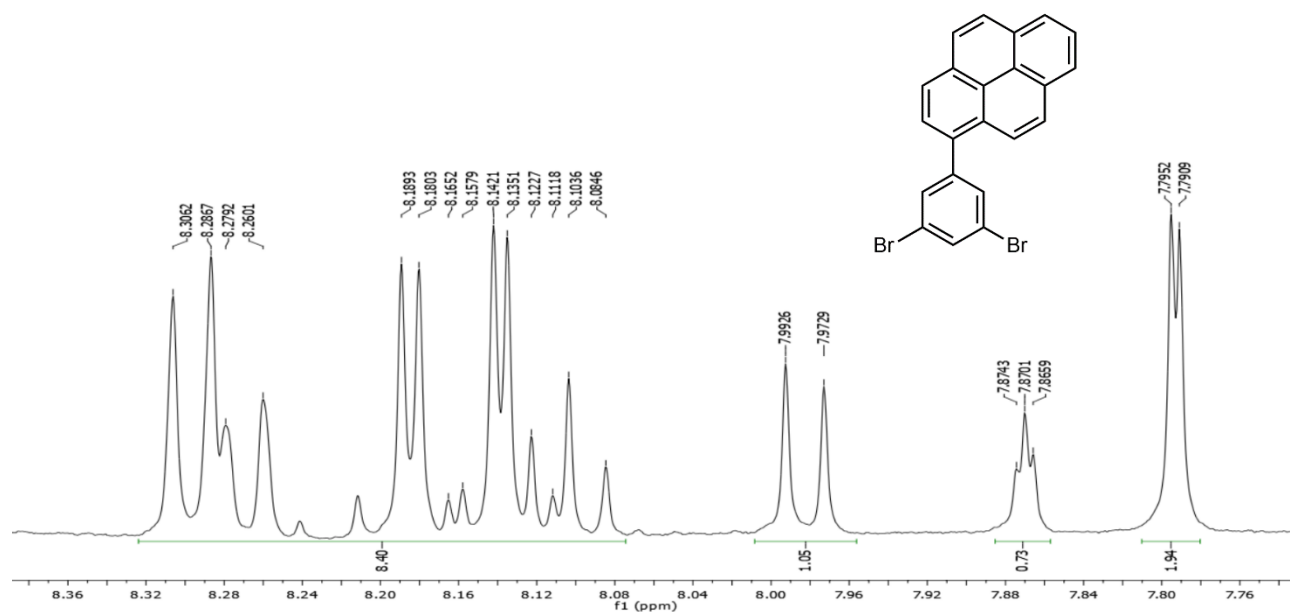
PtCl2



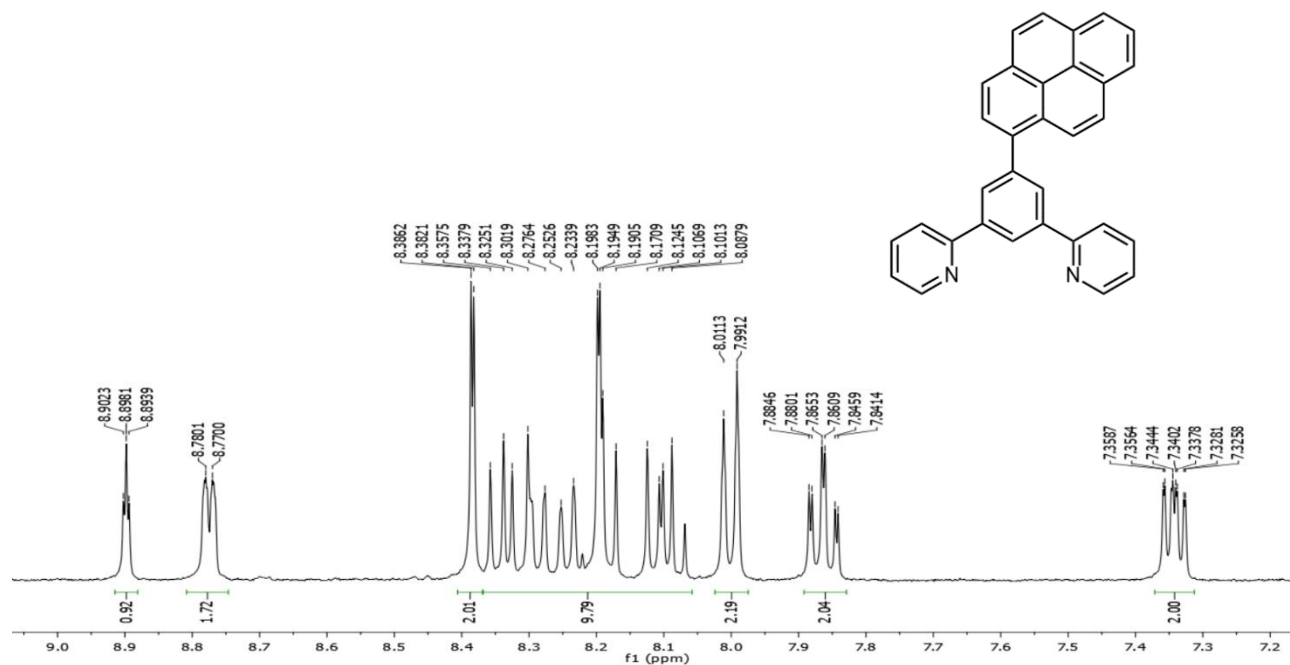
Pt7



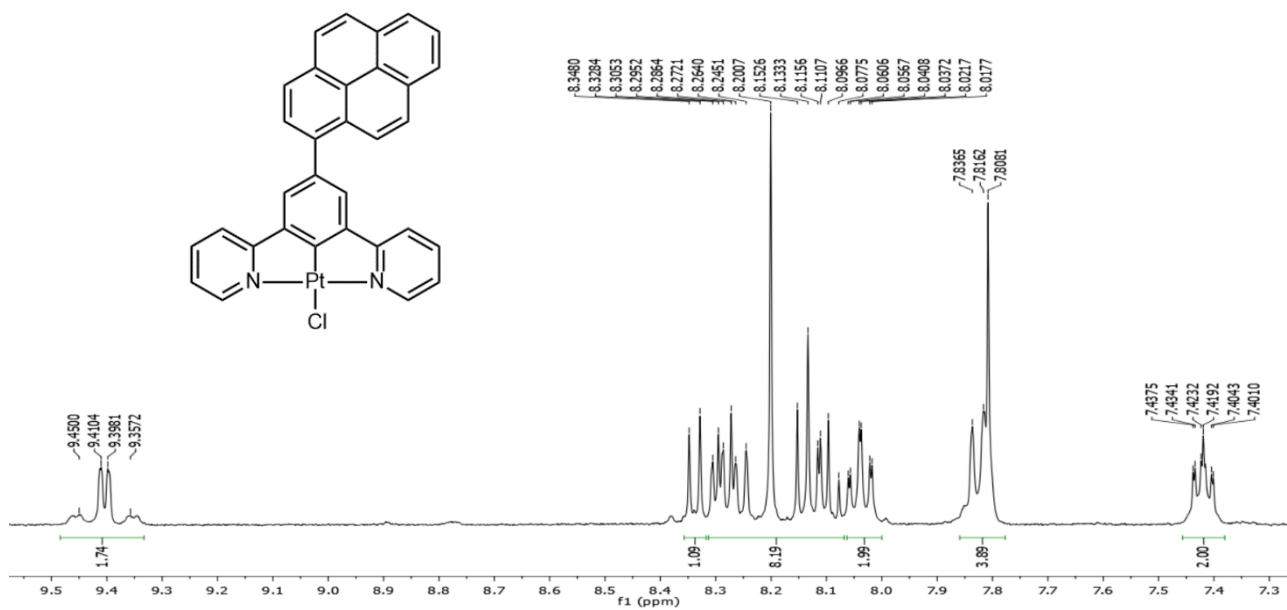
I3



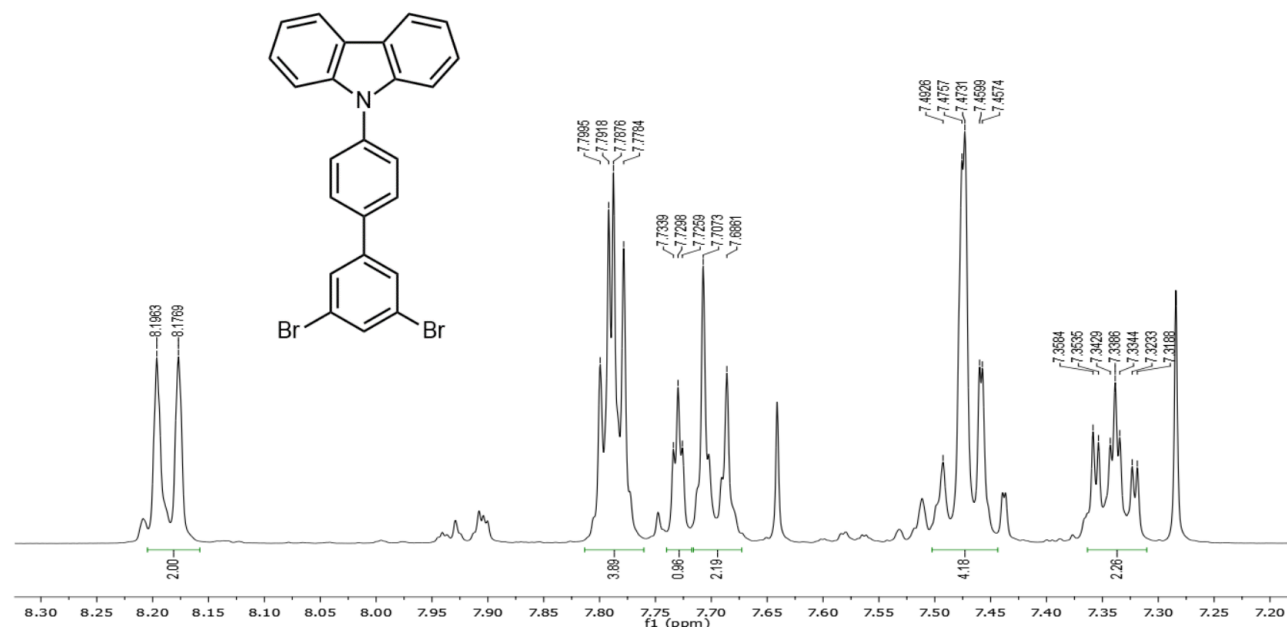
L3



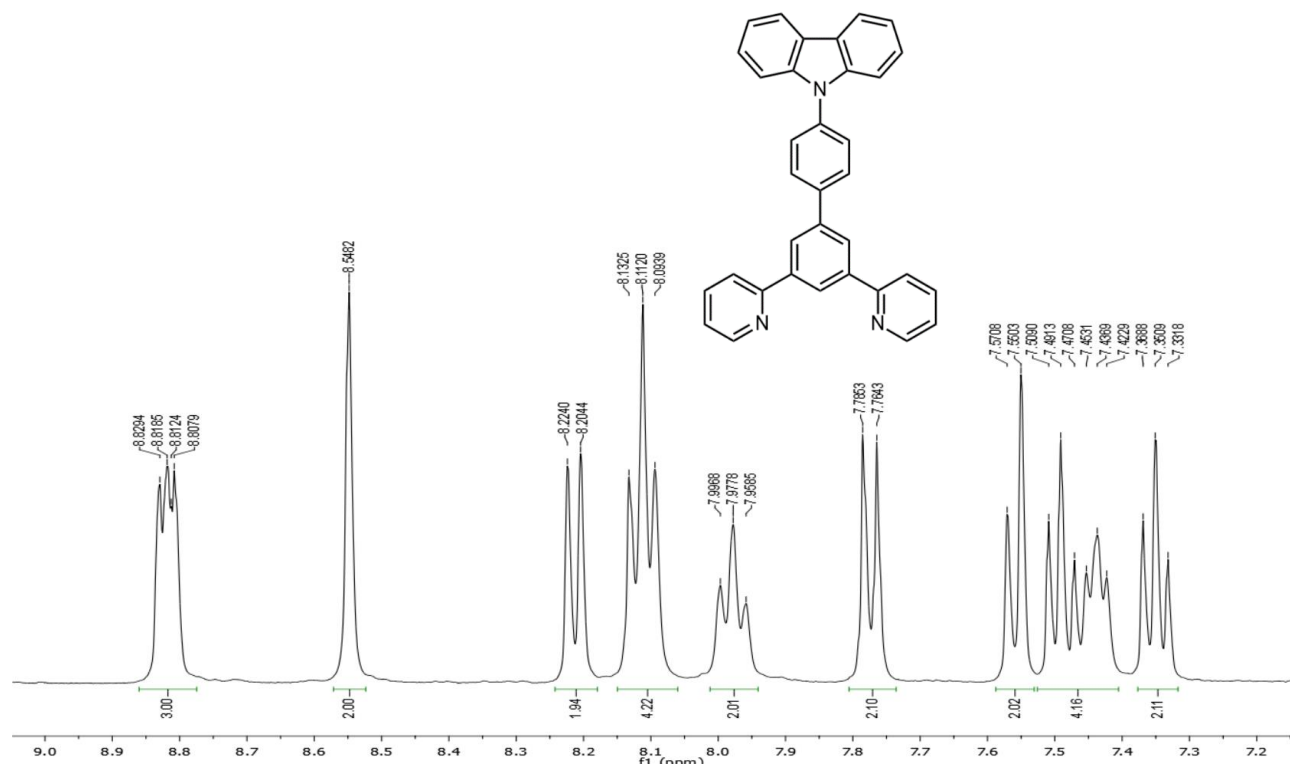
PtCl3



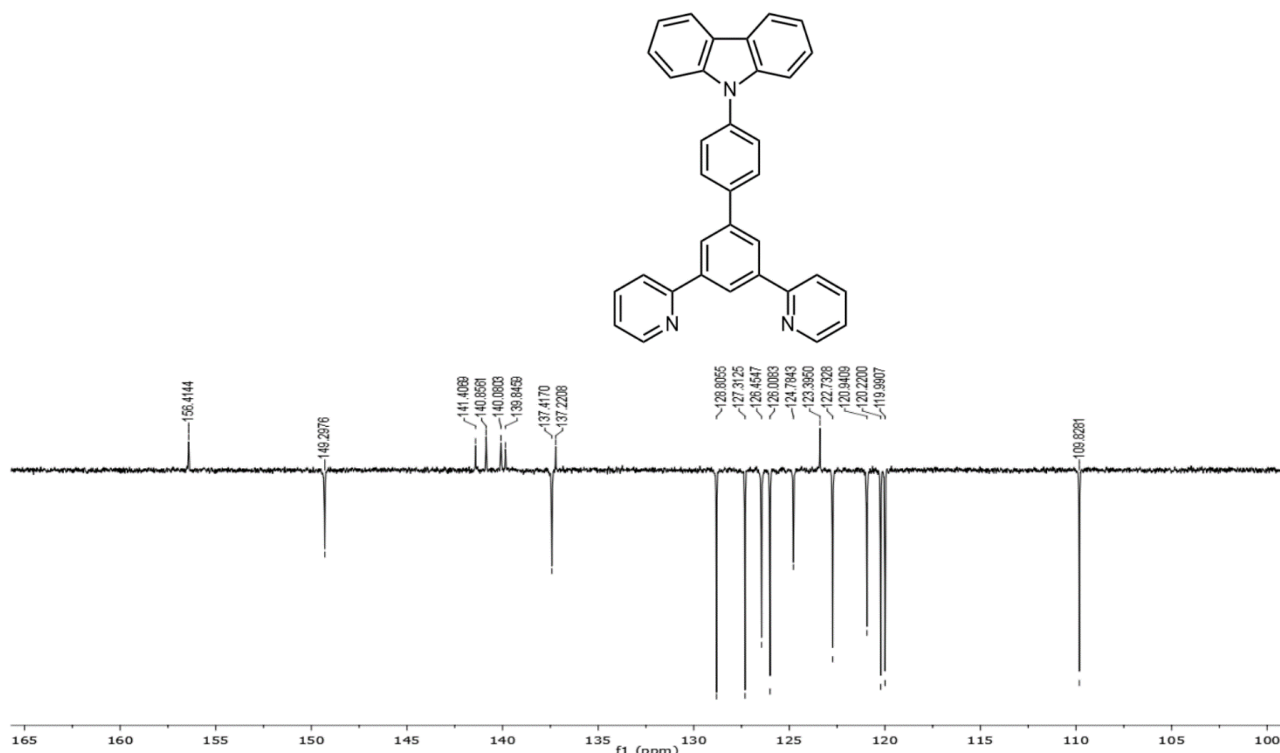
I4



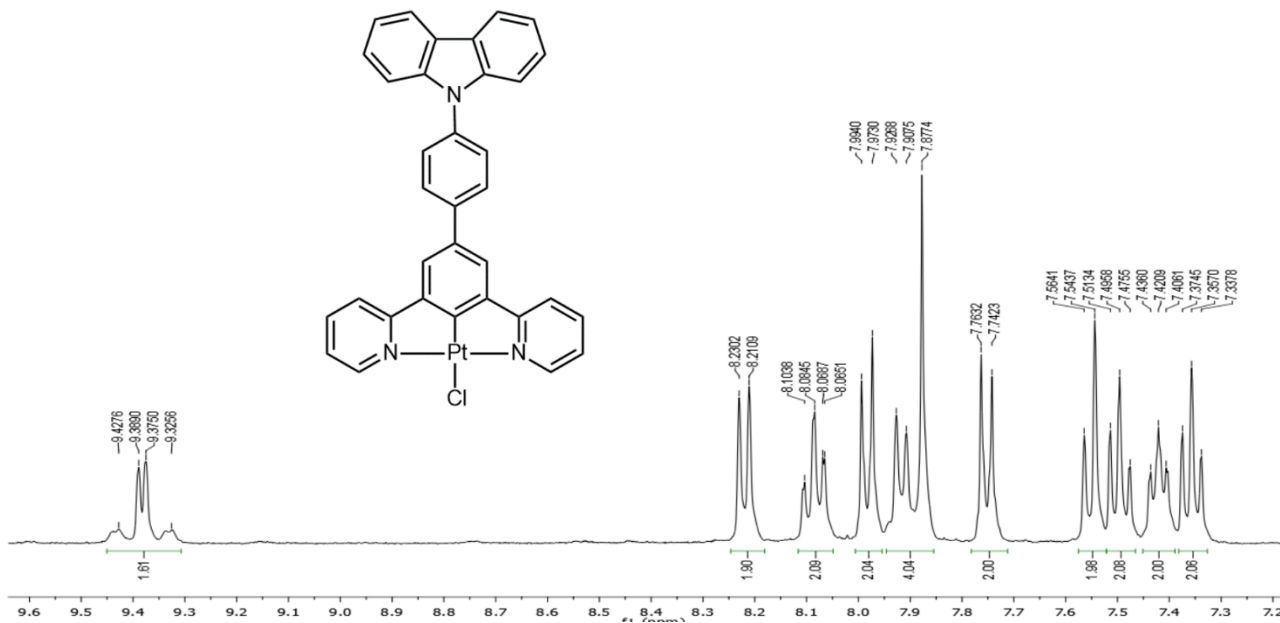
L4



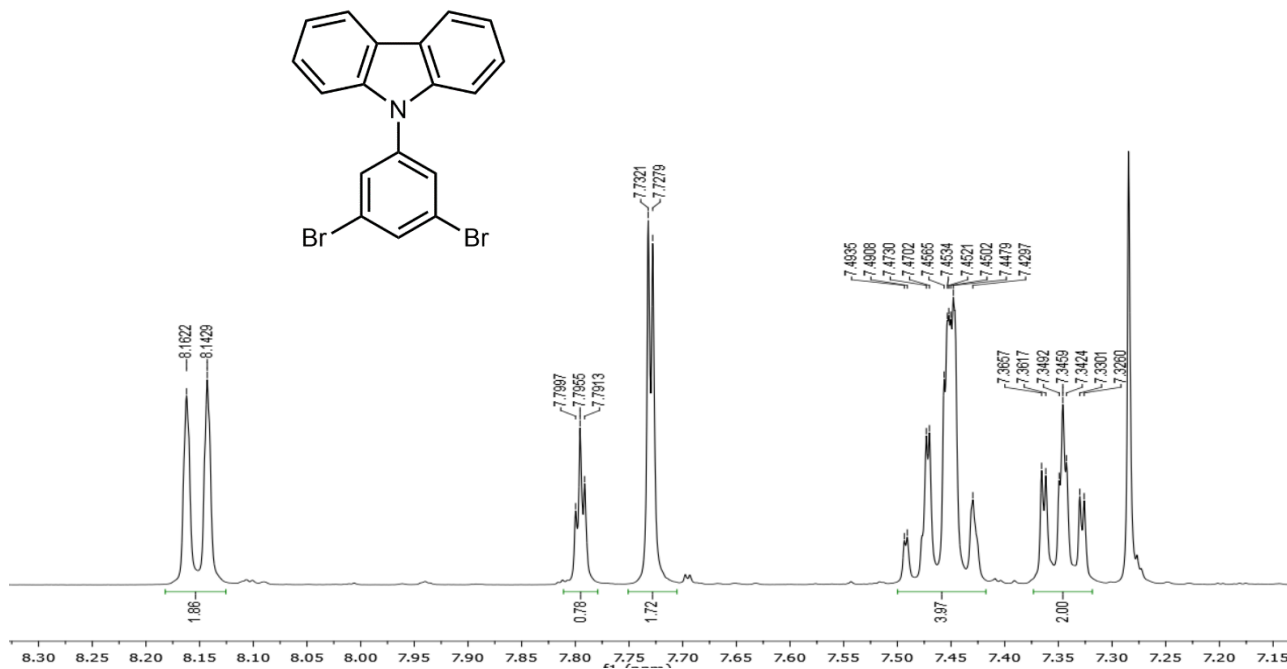
L4 - ¹³C NMR



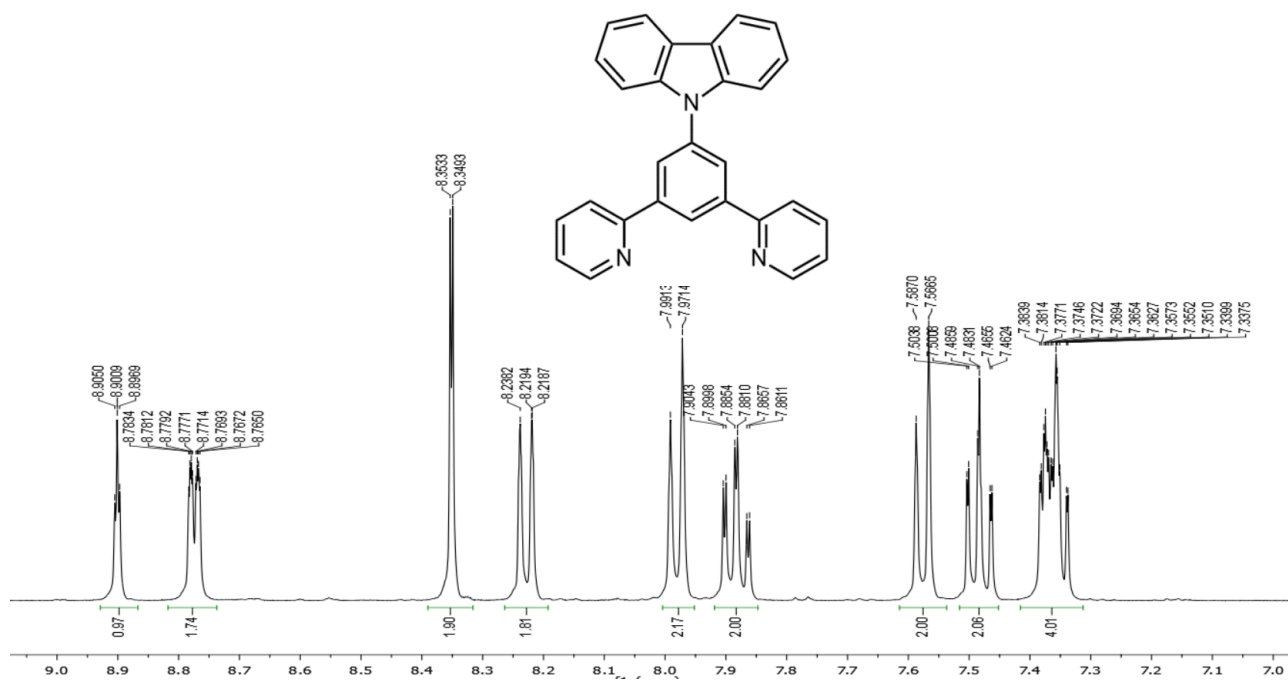
PtCl4



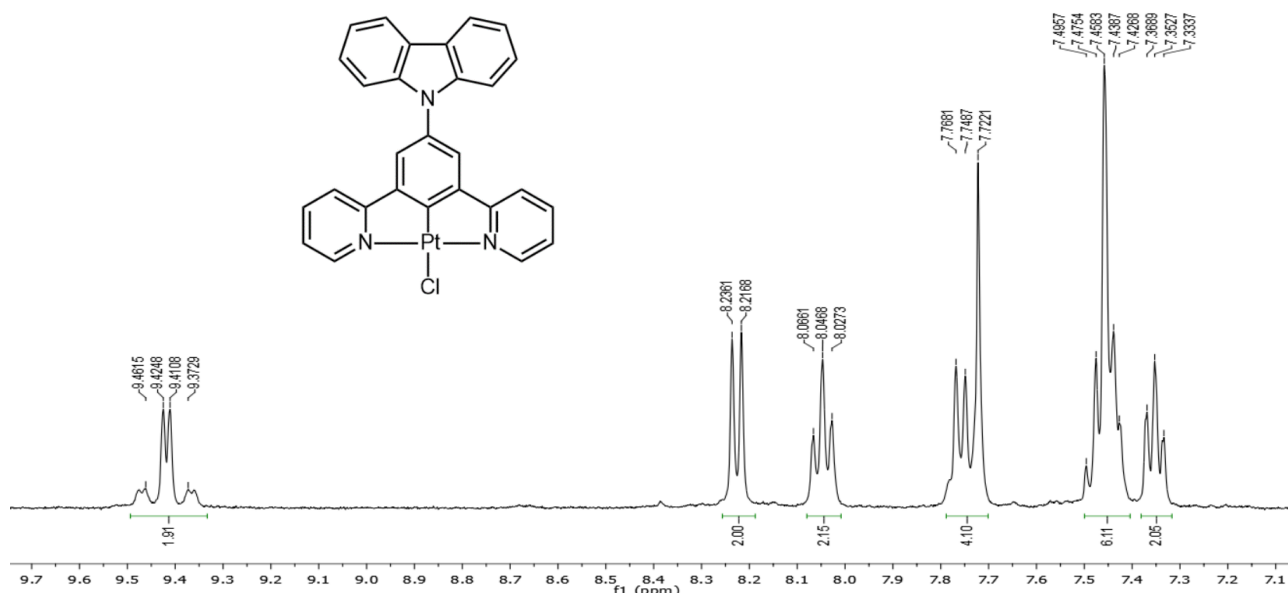
I5



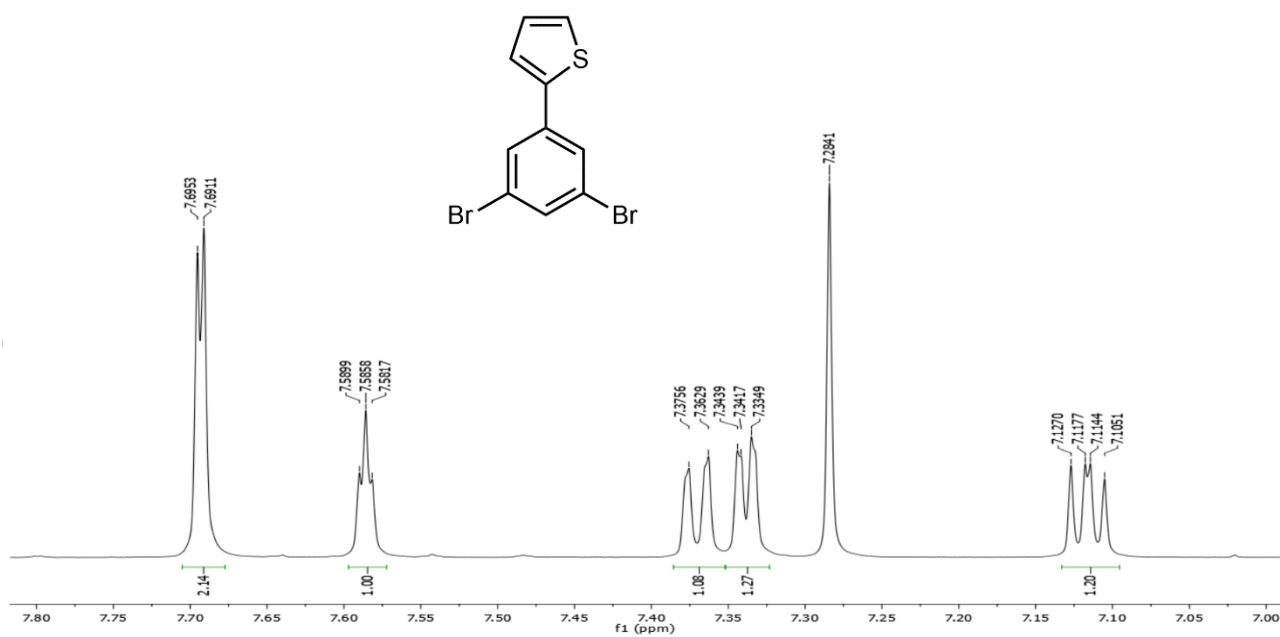
L5



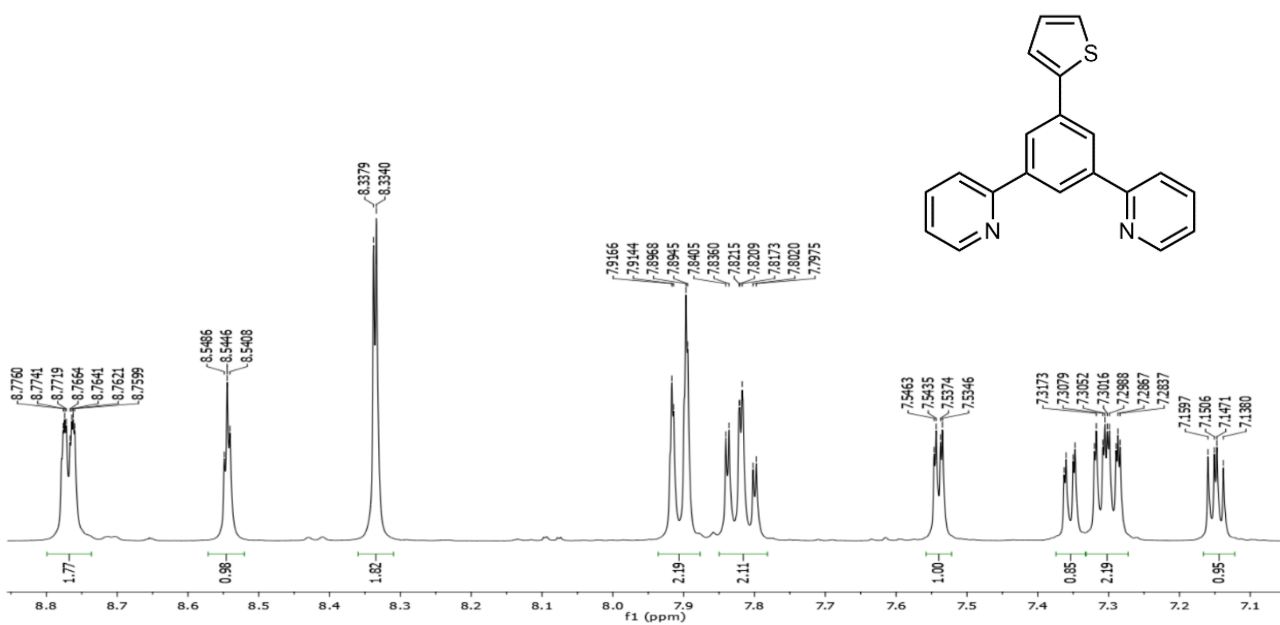
PtCl5



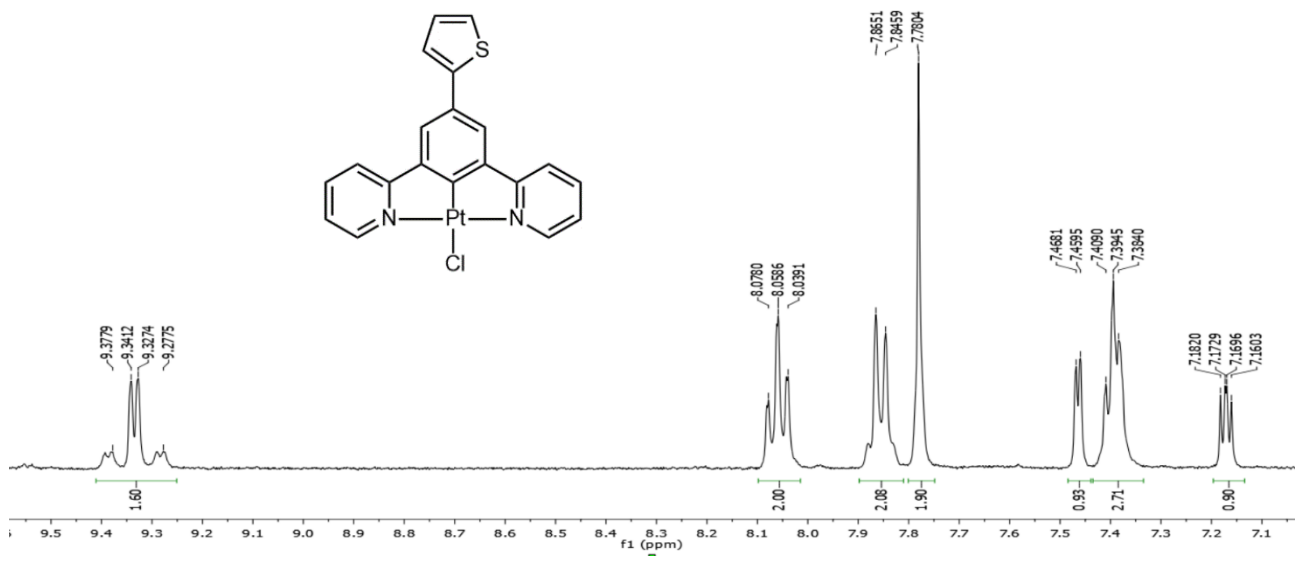
I6



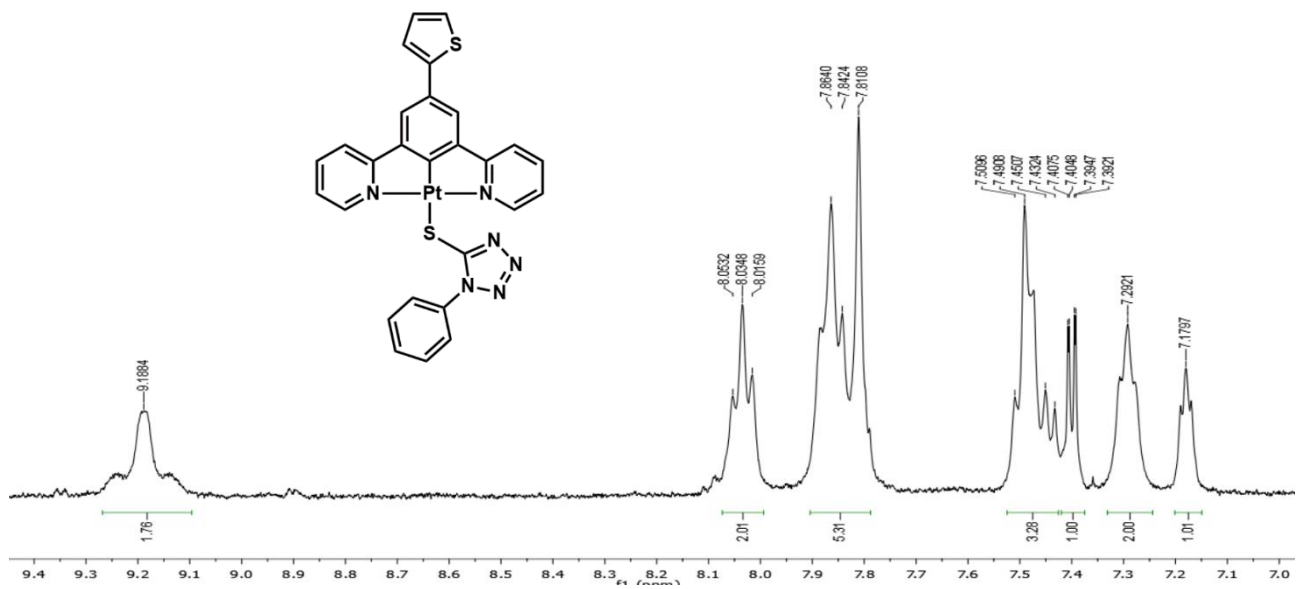
L6



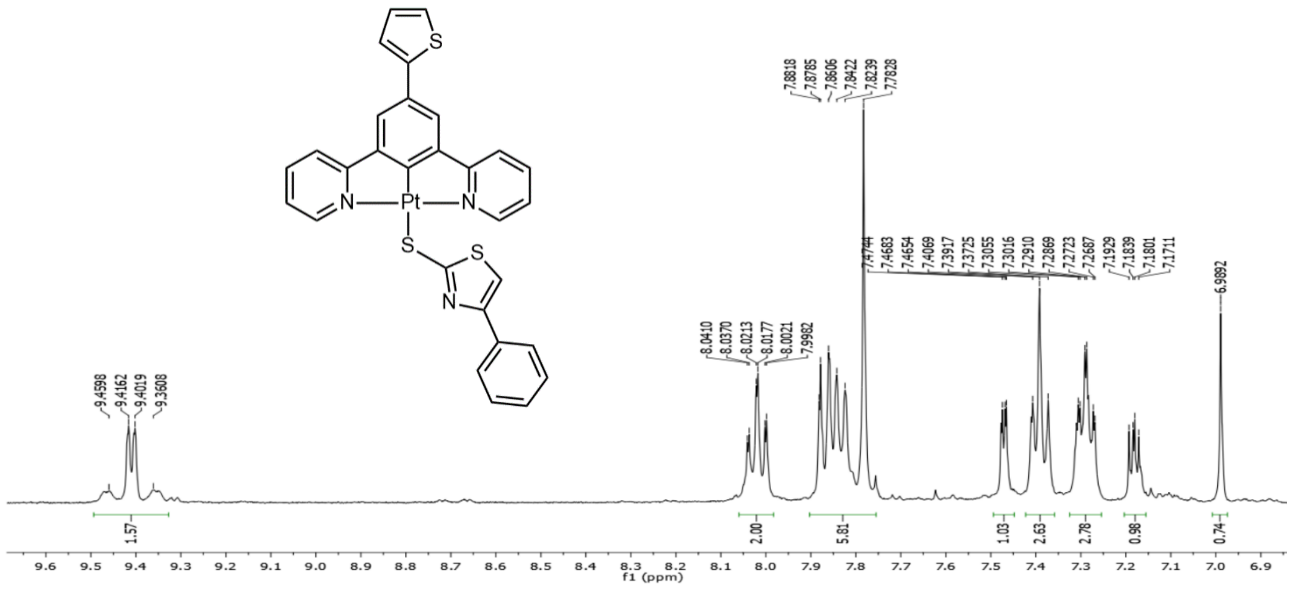
PtCl6



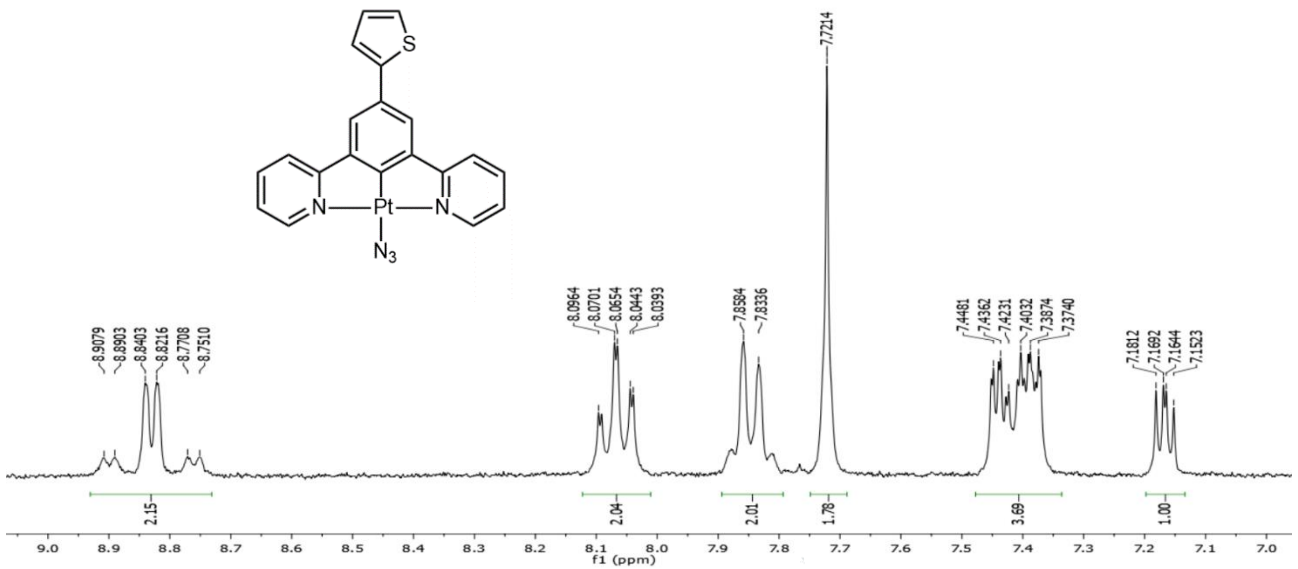
Pt8



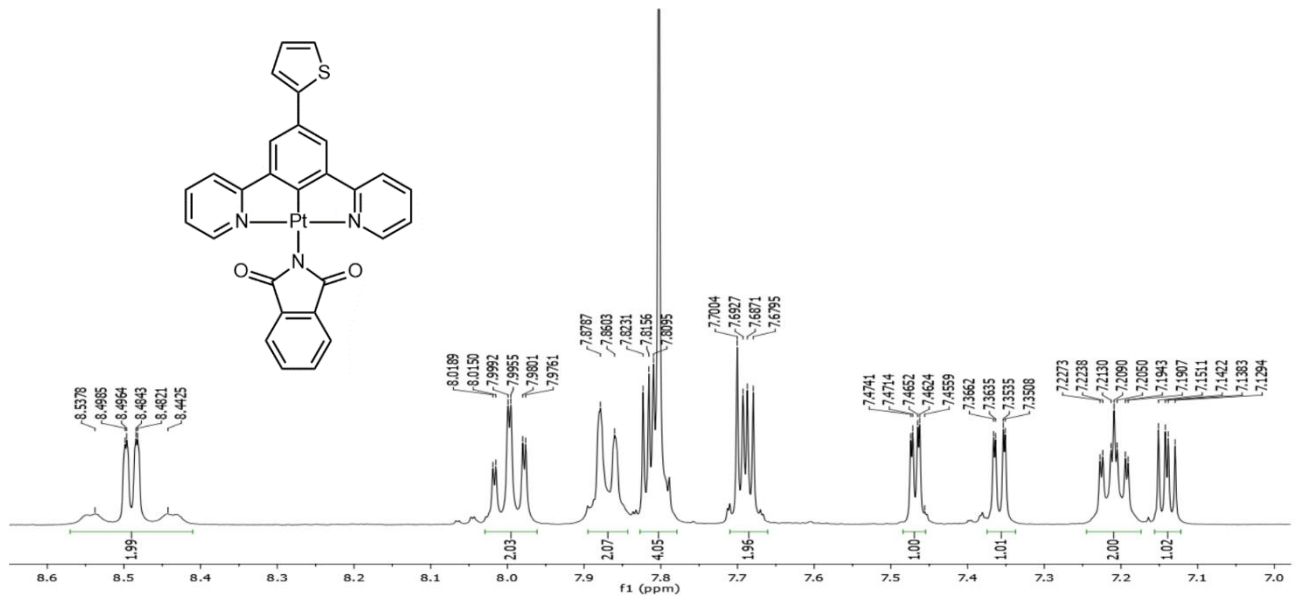
Pt9



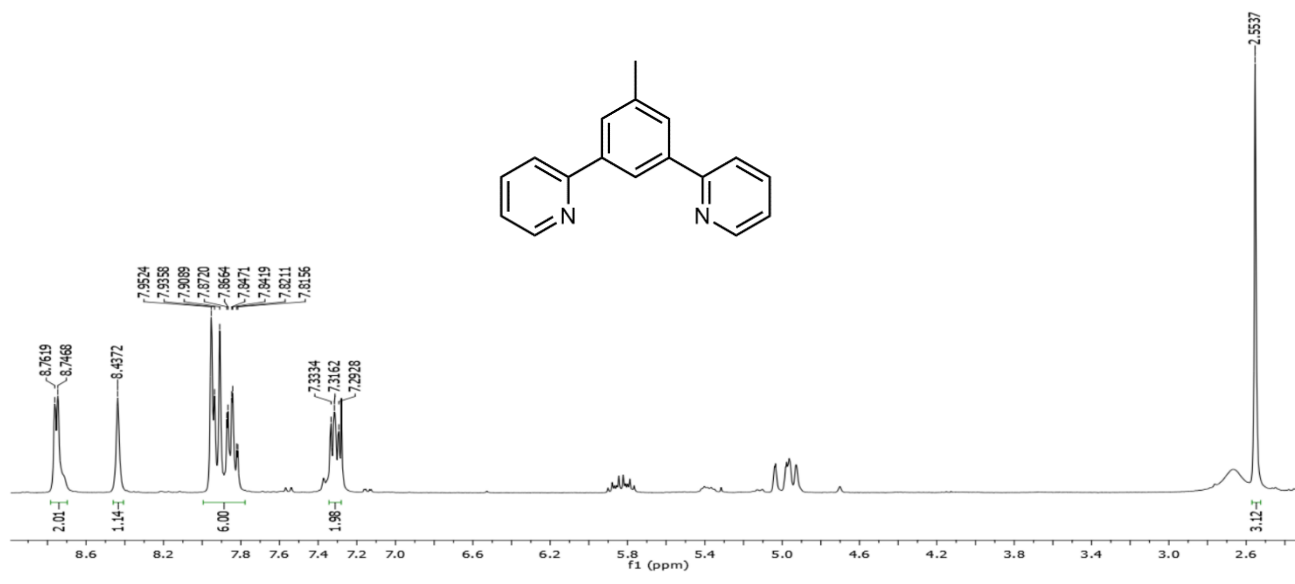
Pt10



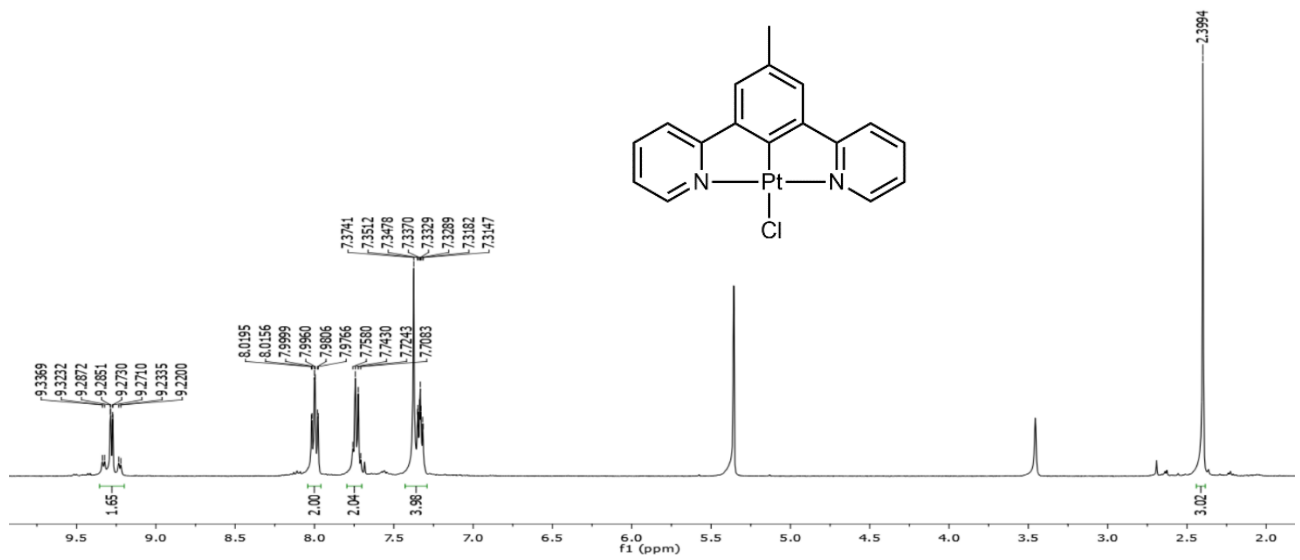
Pt11



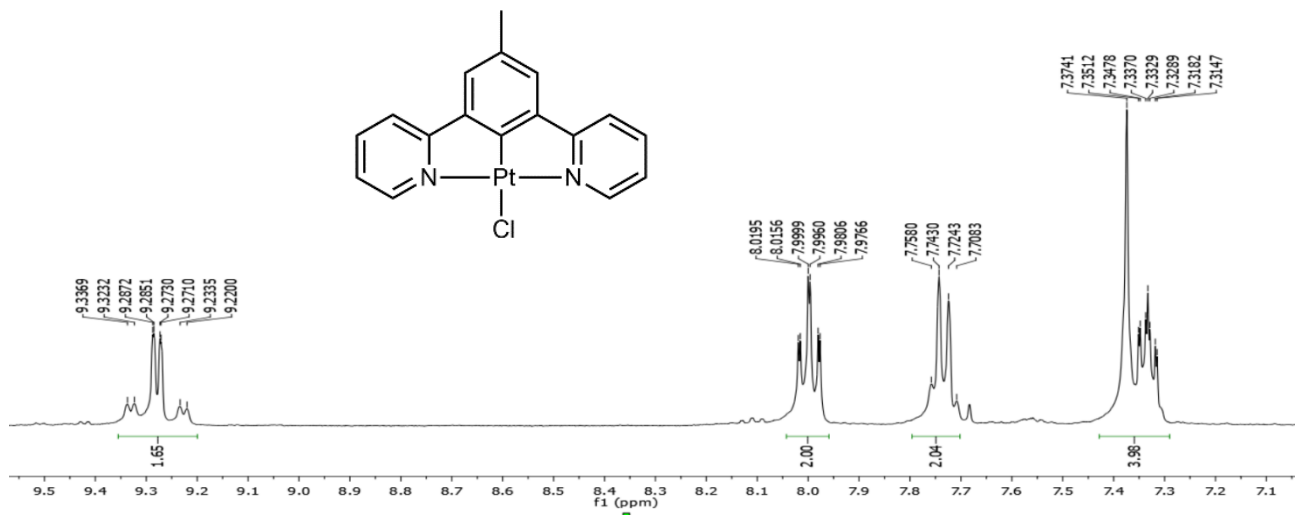
L7



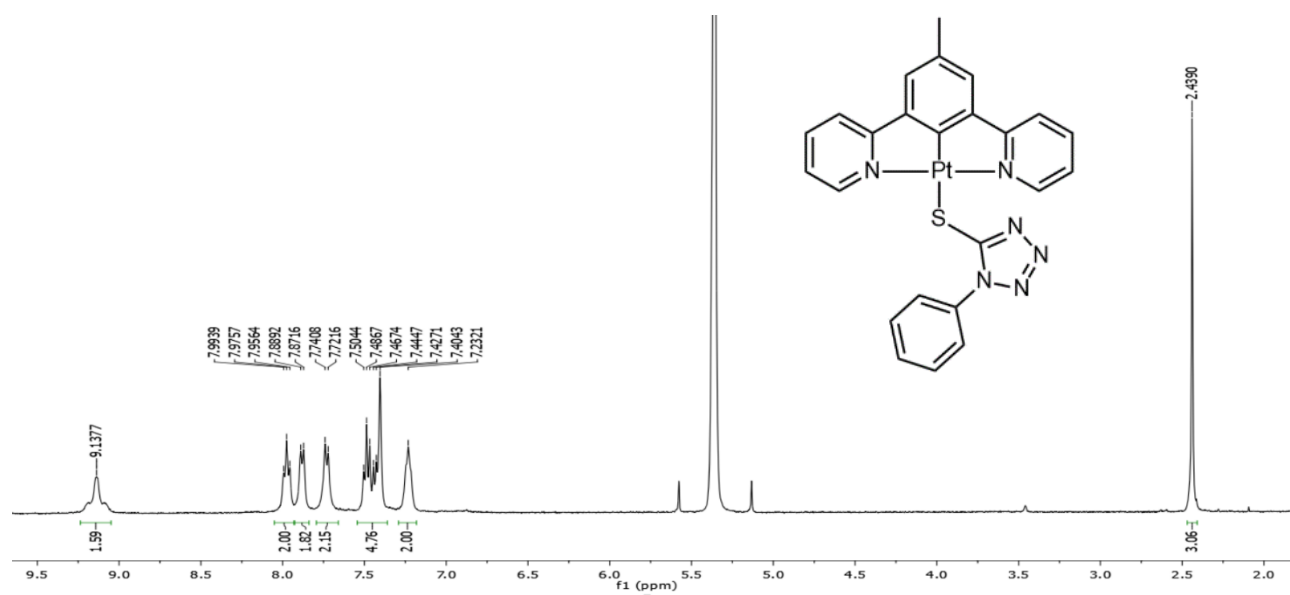
PtCl7



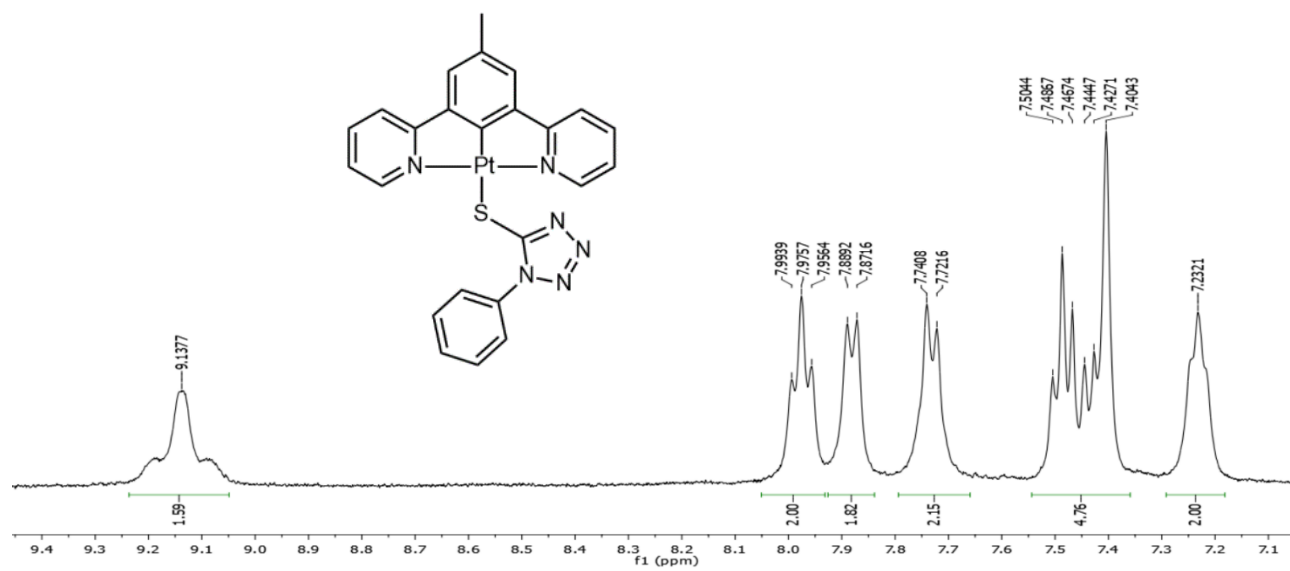
PtCl7 – aromatic region



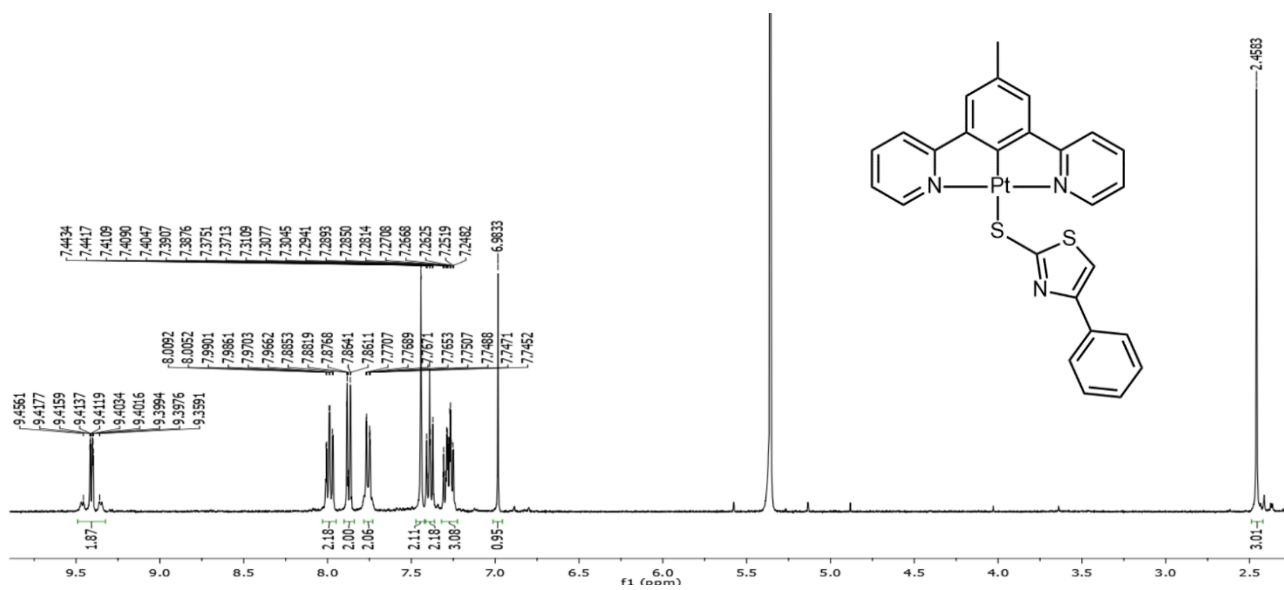
Pt12



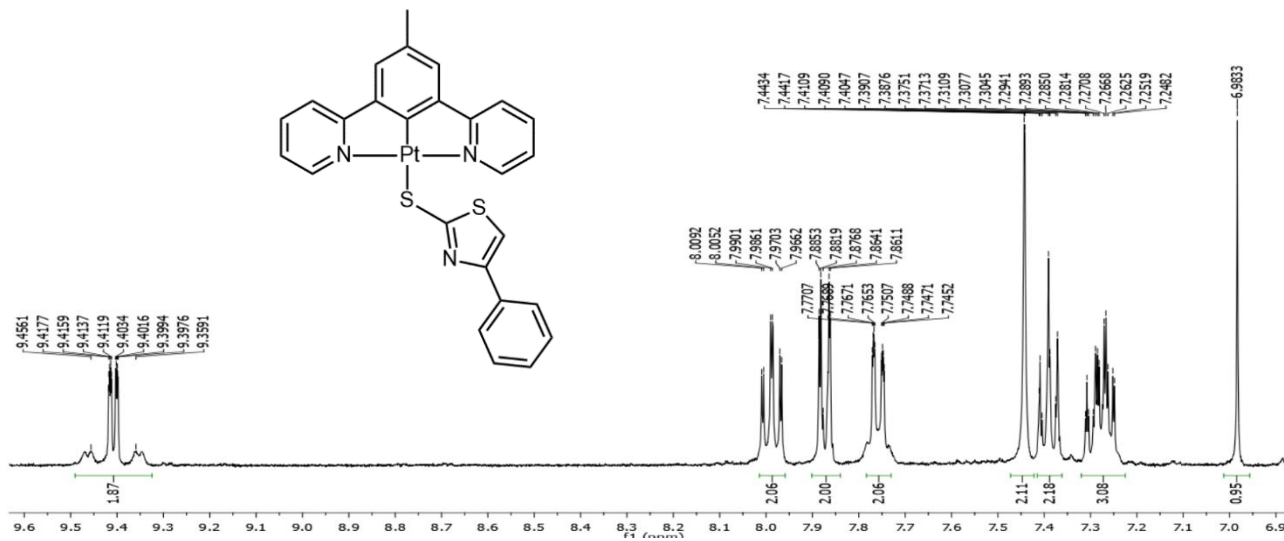
Pt12 - aromatic region



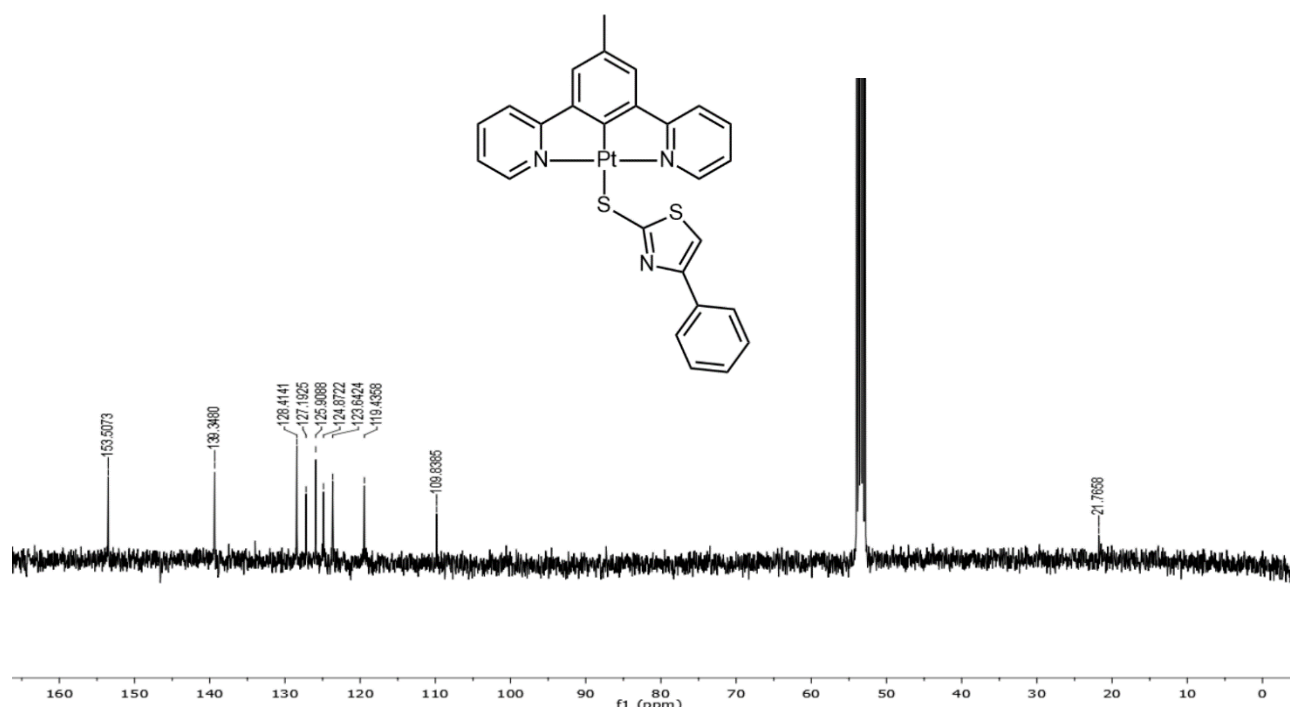
Pt13



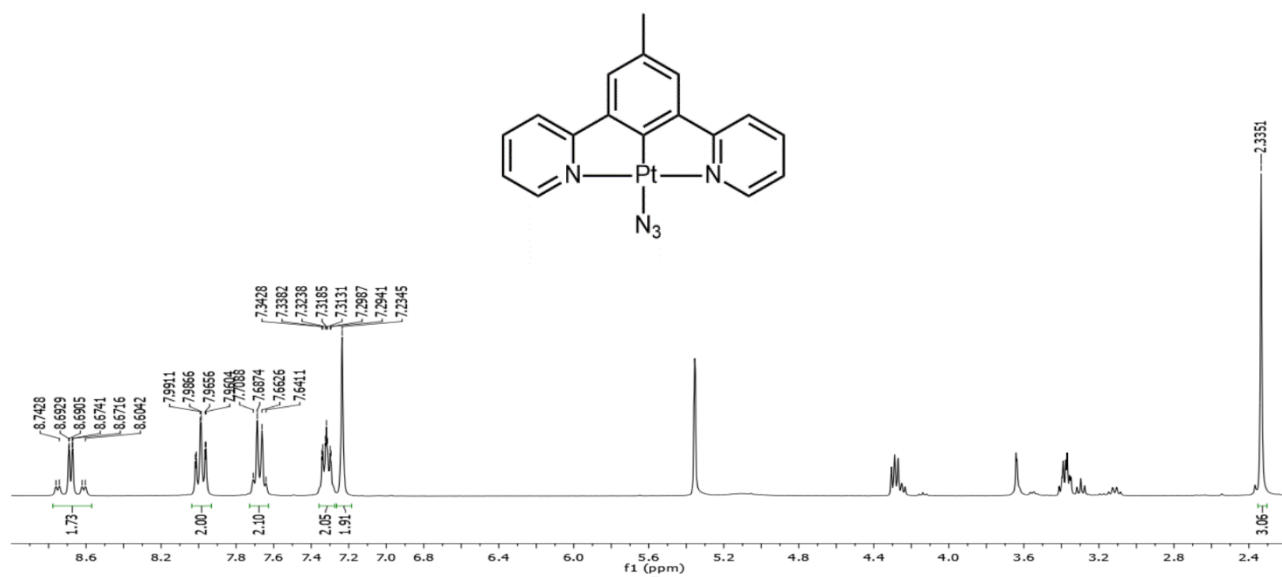
Pt13 - aromatic region



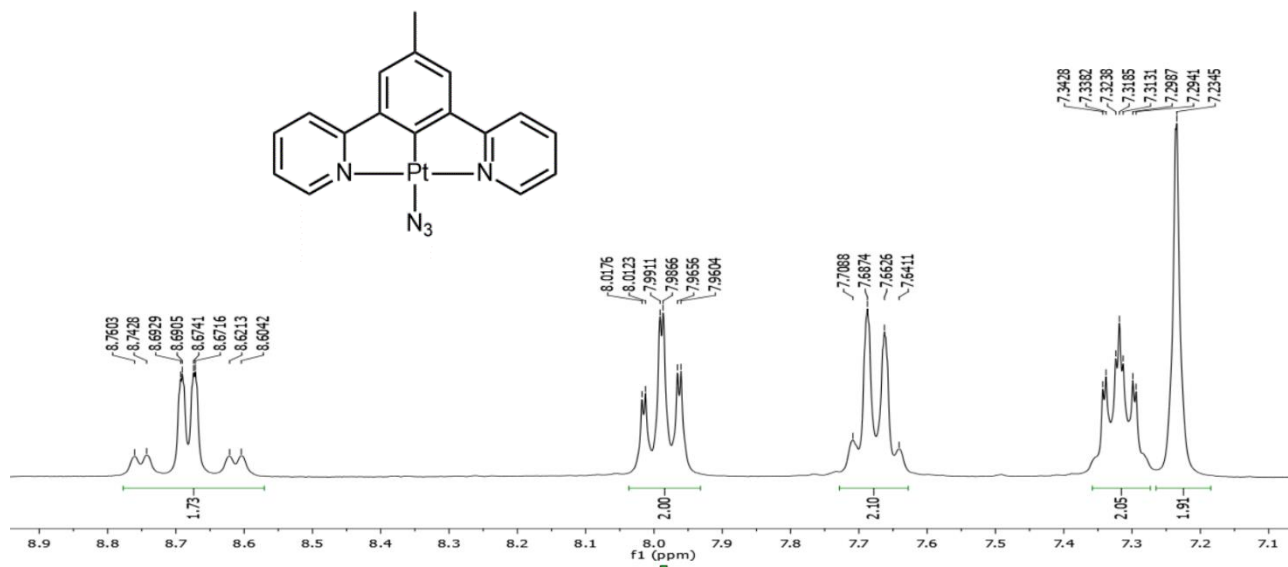
Pt13 - ¹³C NMR



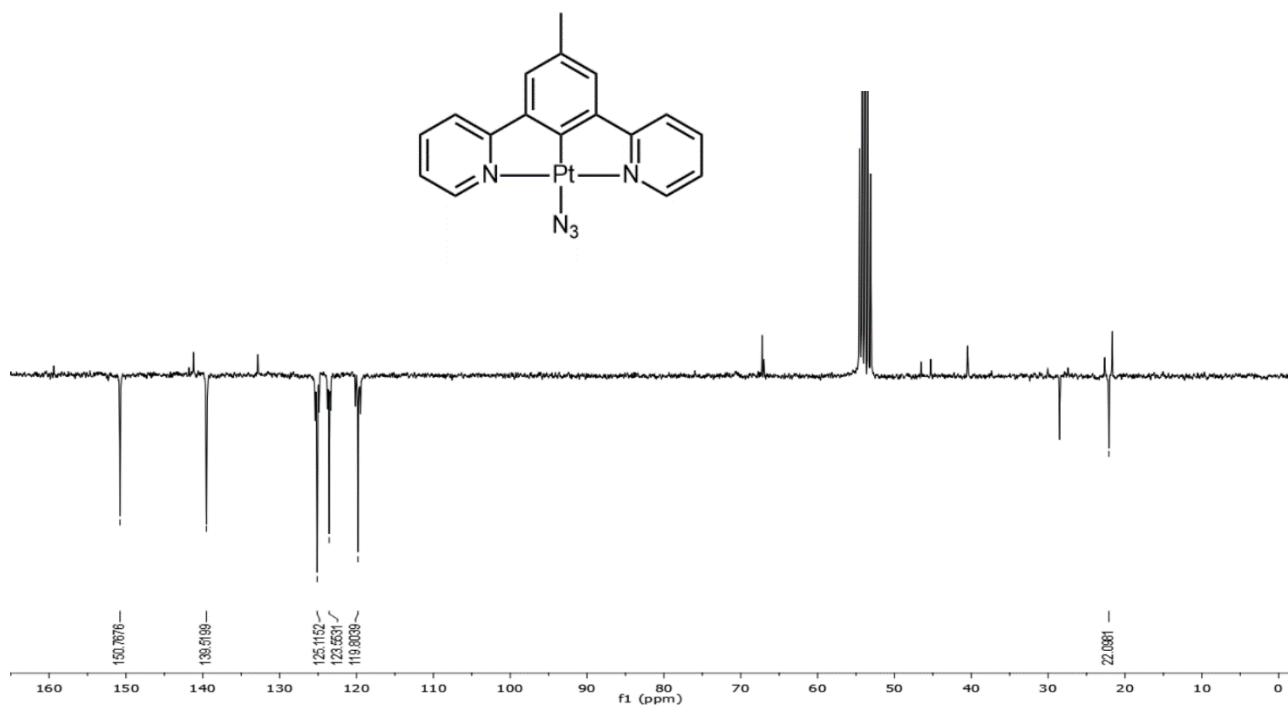
Pt14



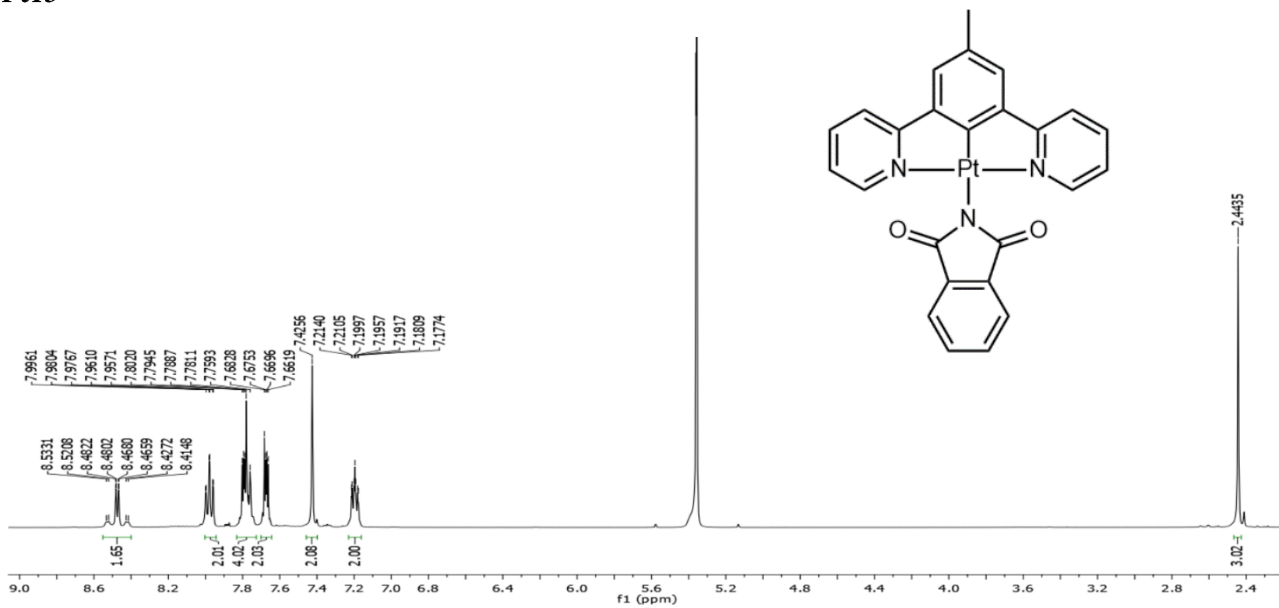
Pt14 – aromatic region



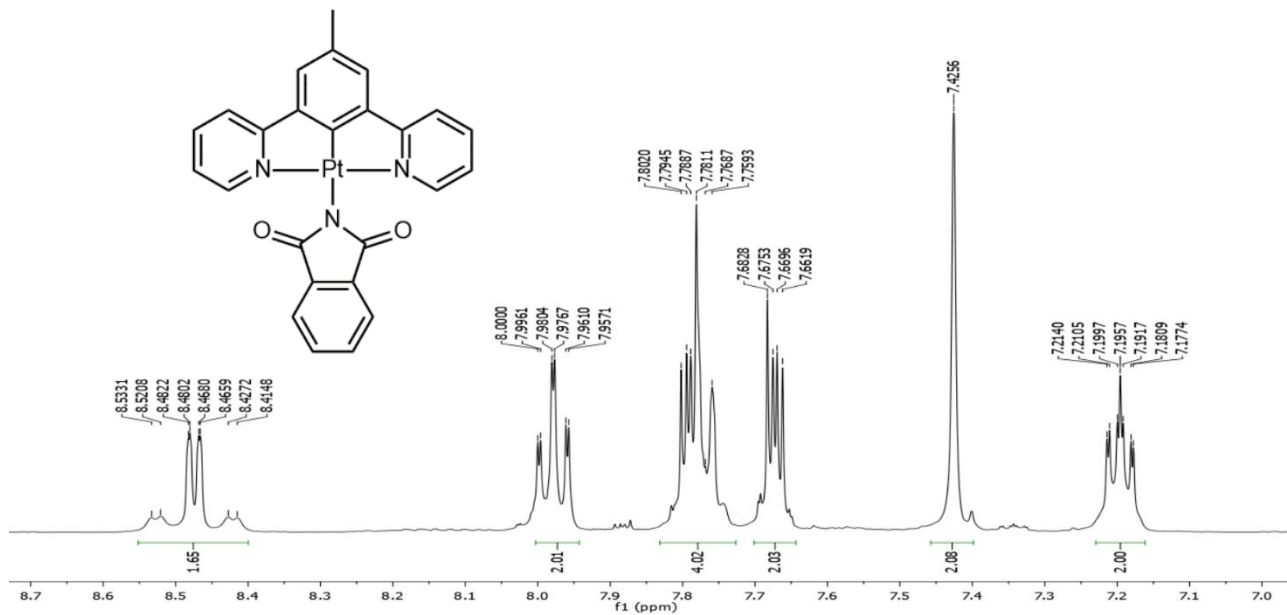
Pt14 – ¹³C NMR



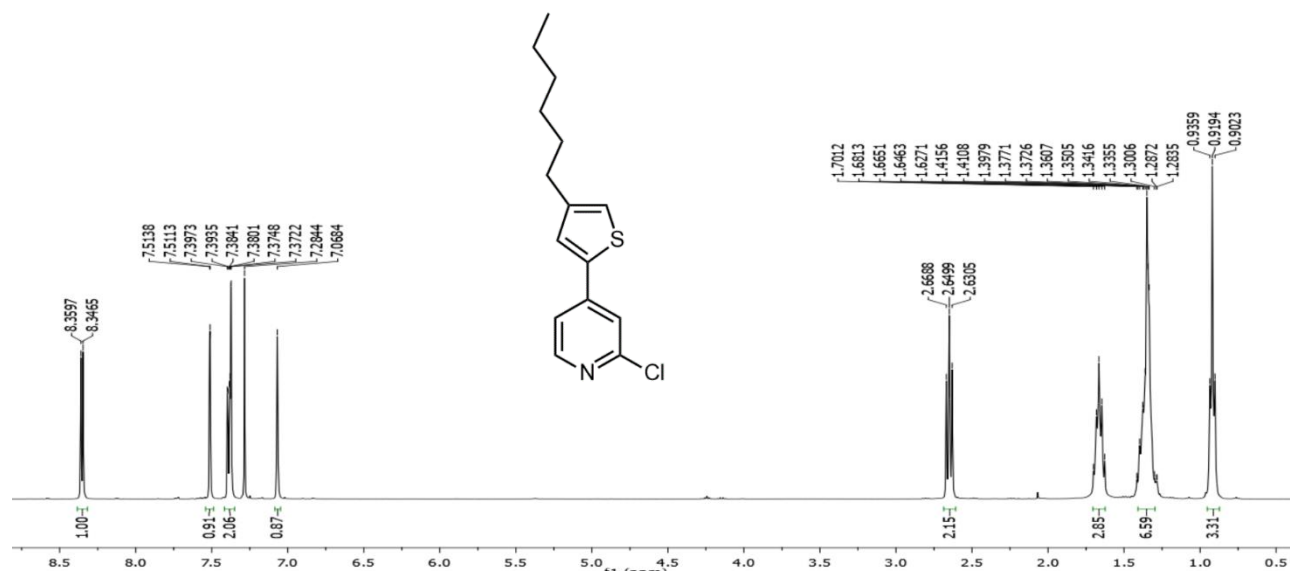
Pt15



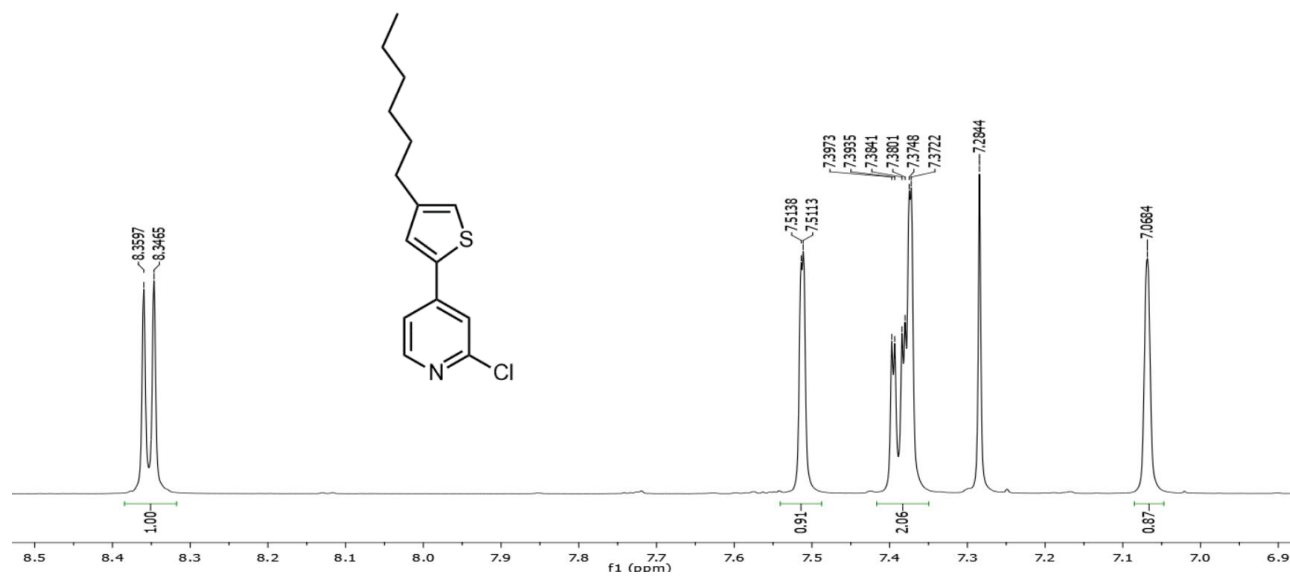
Pt15 – aromatic region



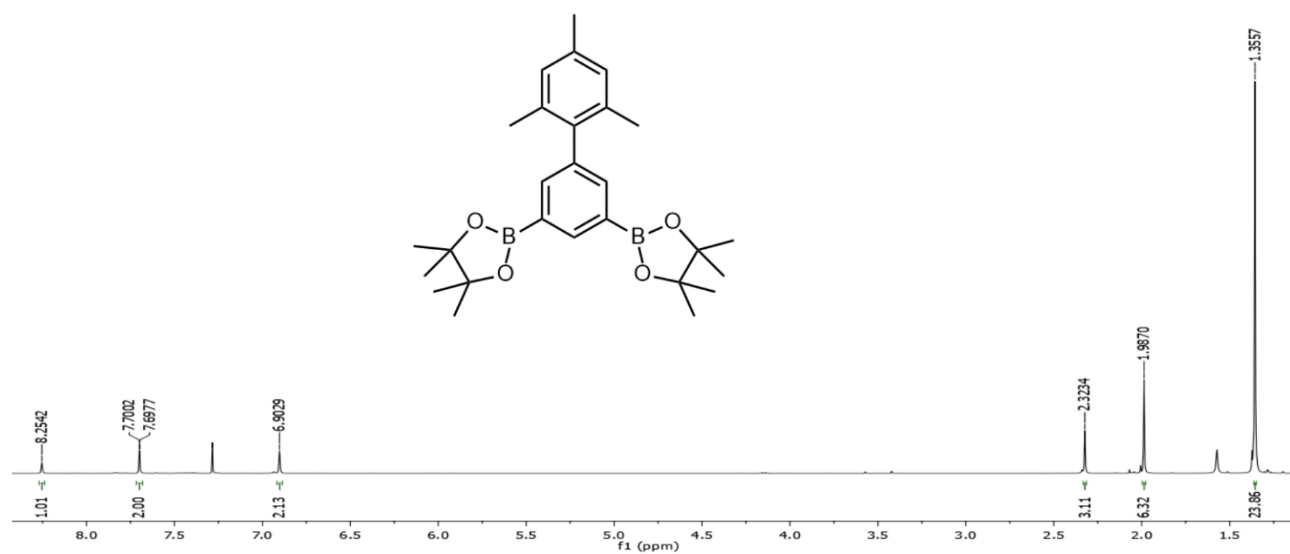
I7



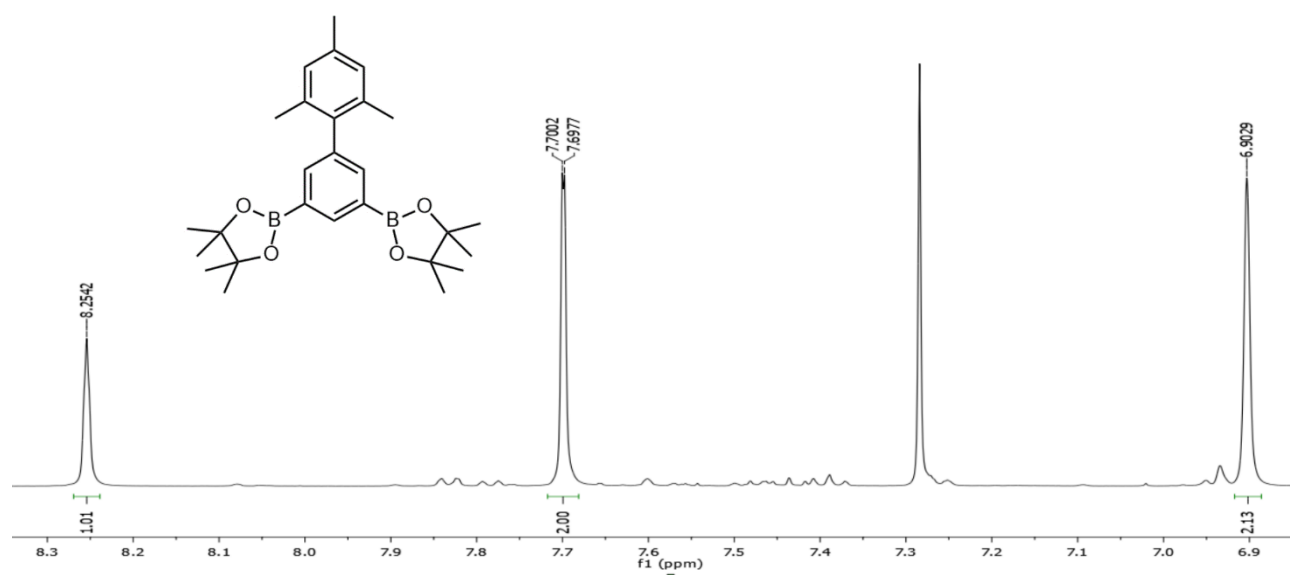
I7 - aromatic region



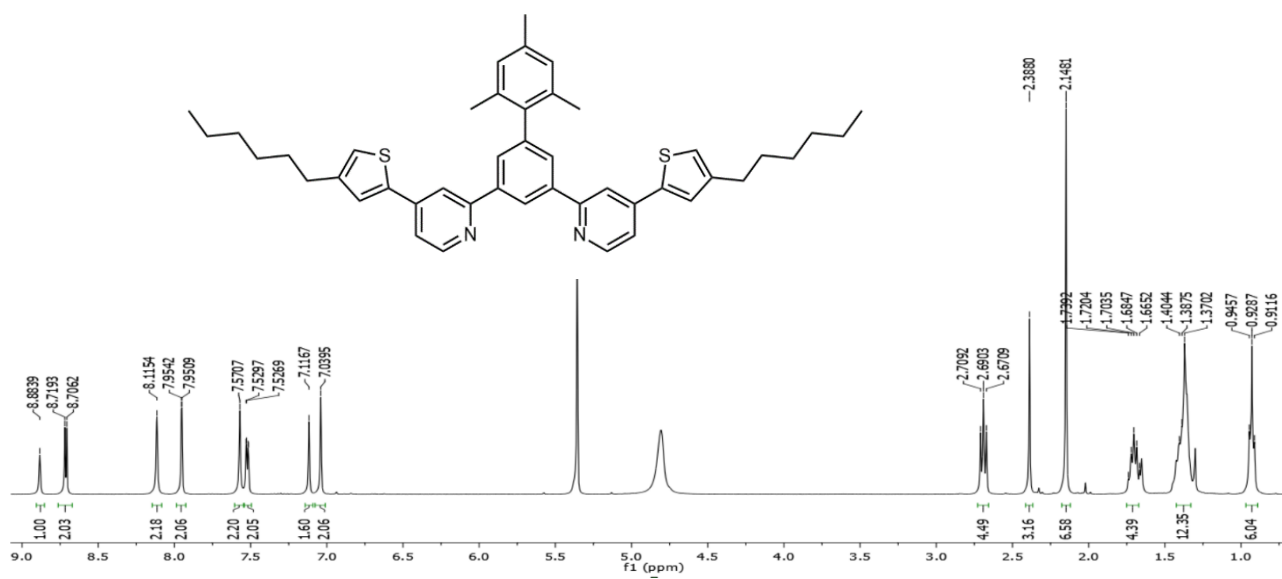
B1



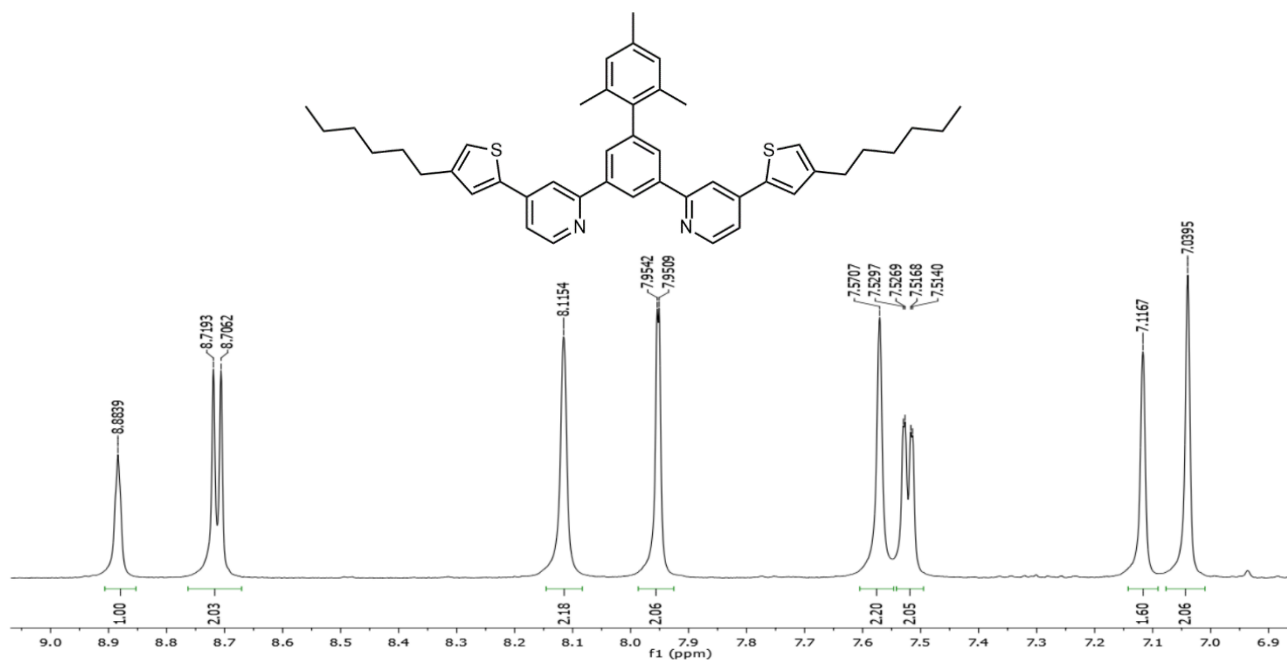
B1 - aromatic region



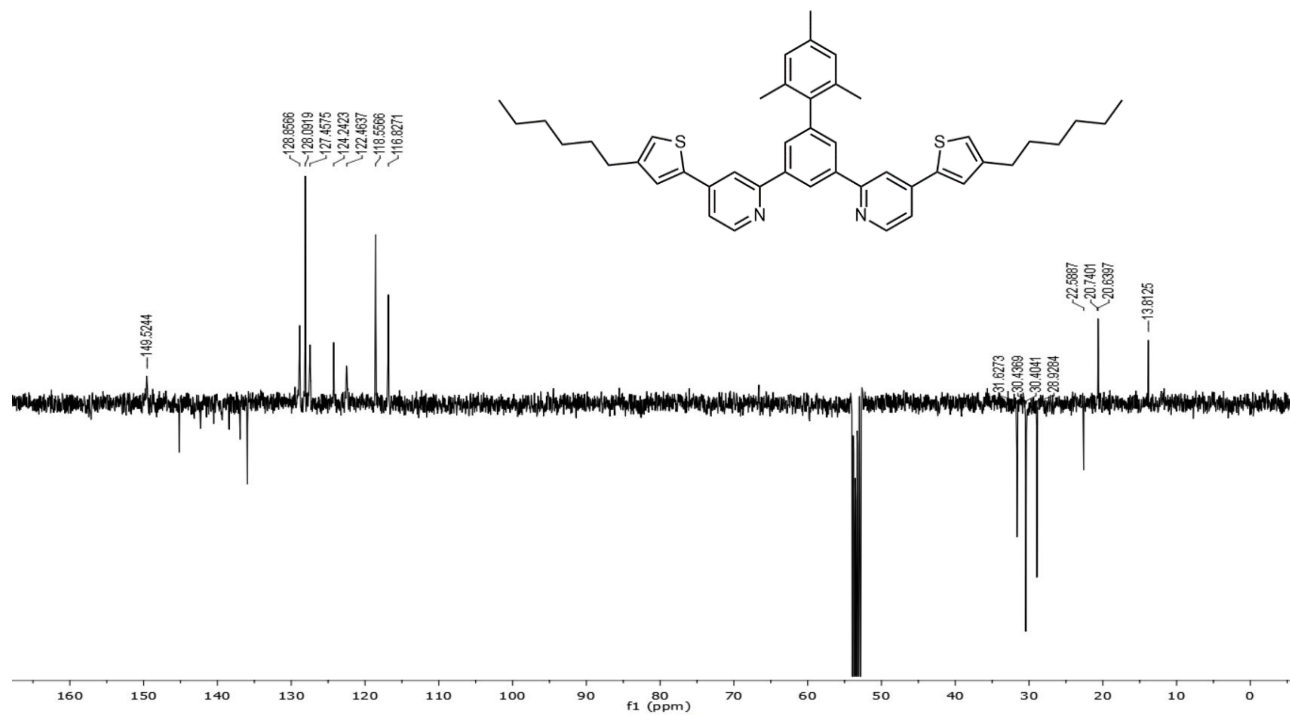
L8



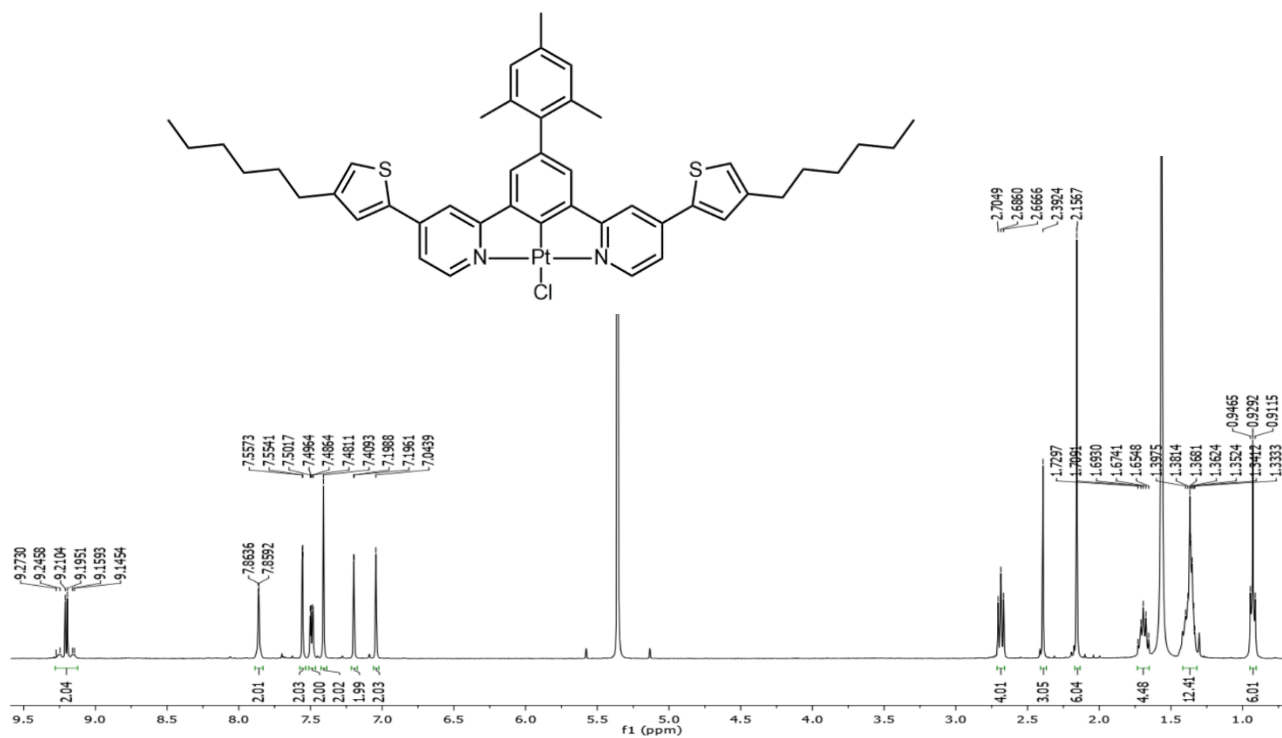
L8 – aromatic region



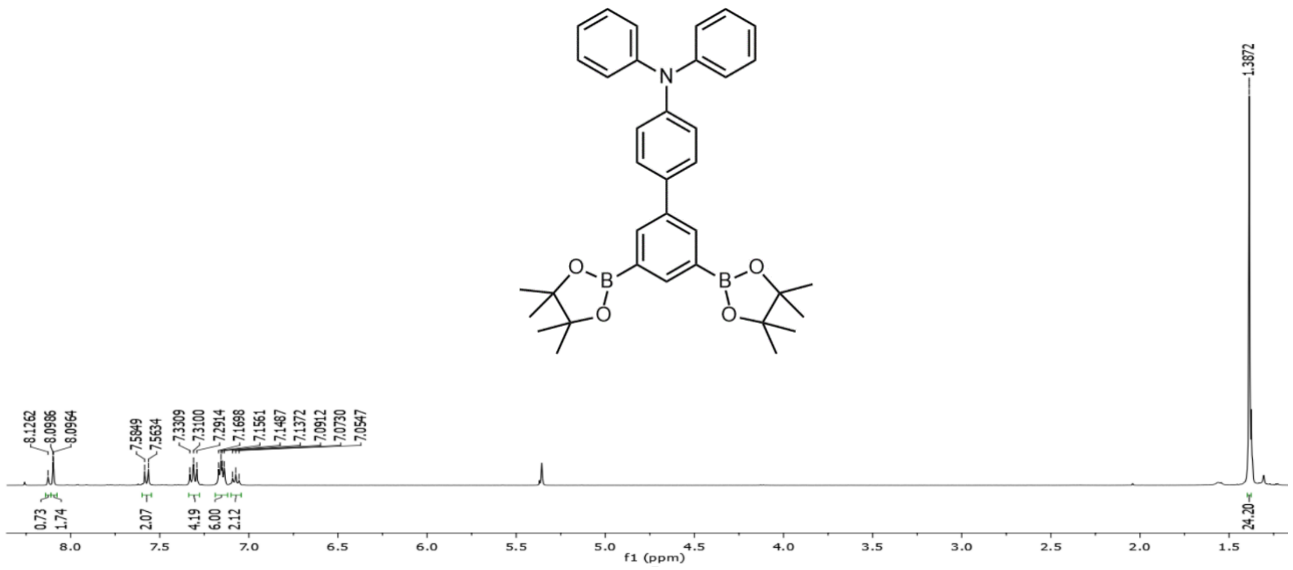
L9 - ¹³C NMR



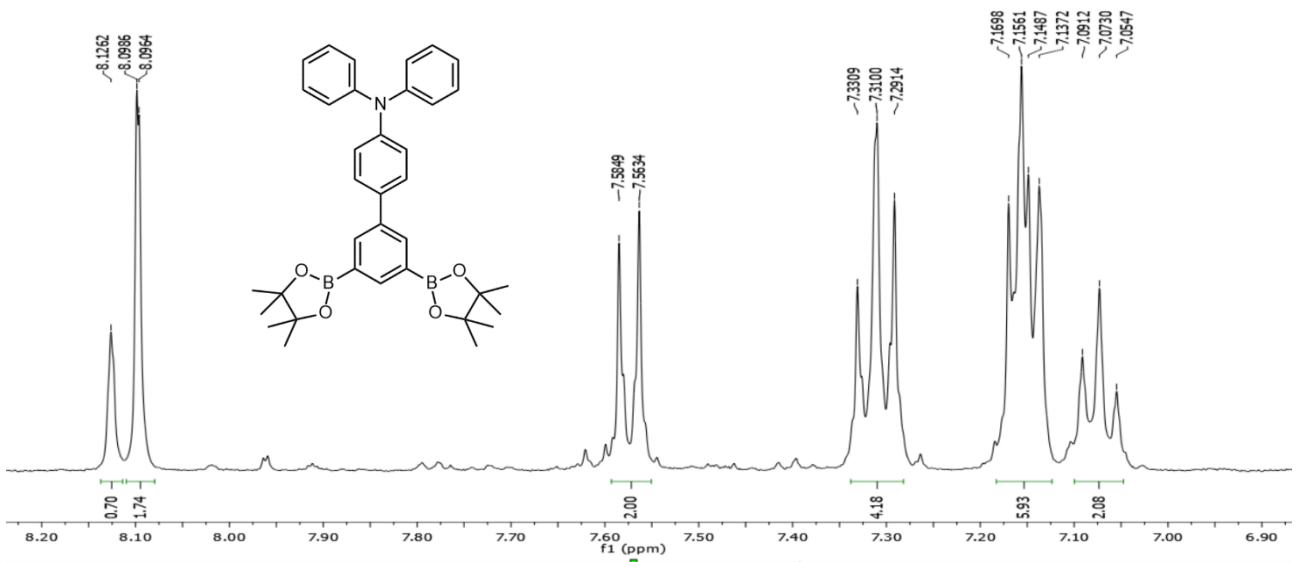
PtCl8



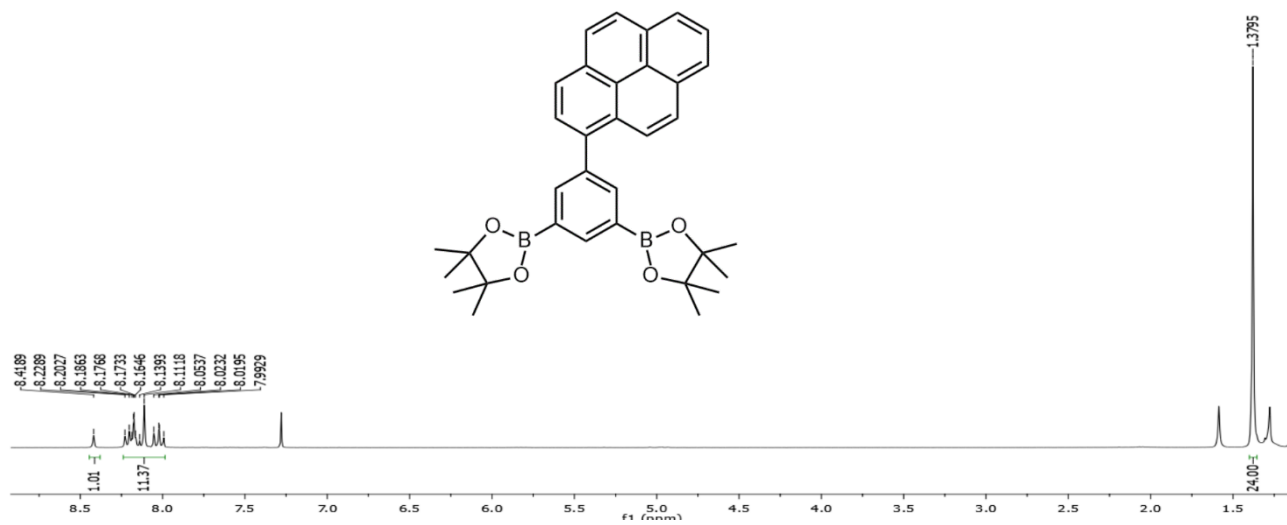
B2



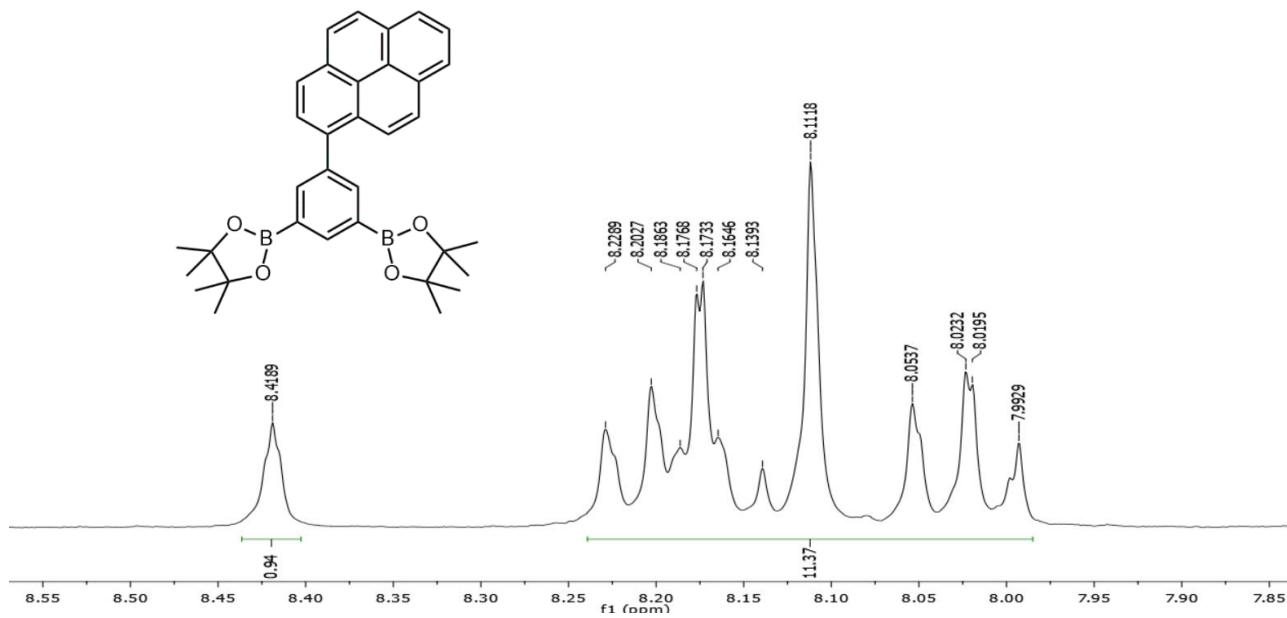
B2 - aromatic region



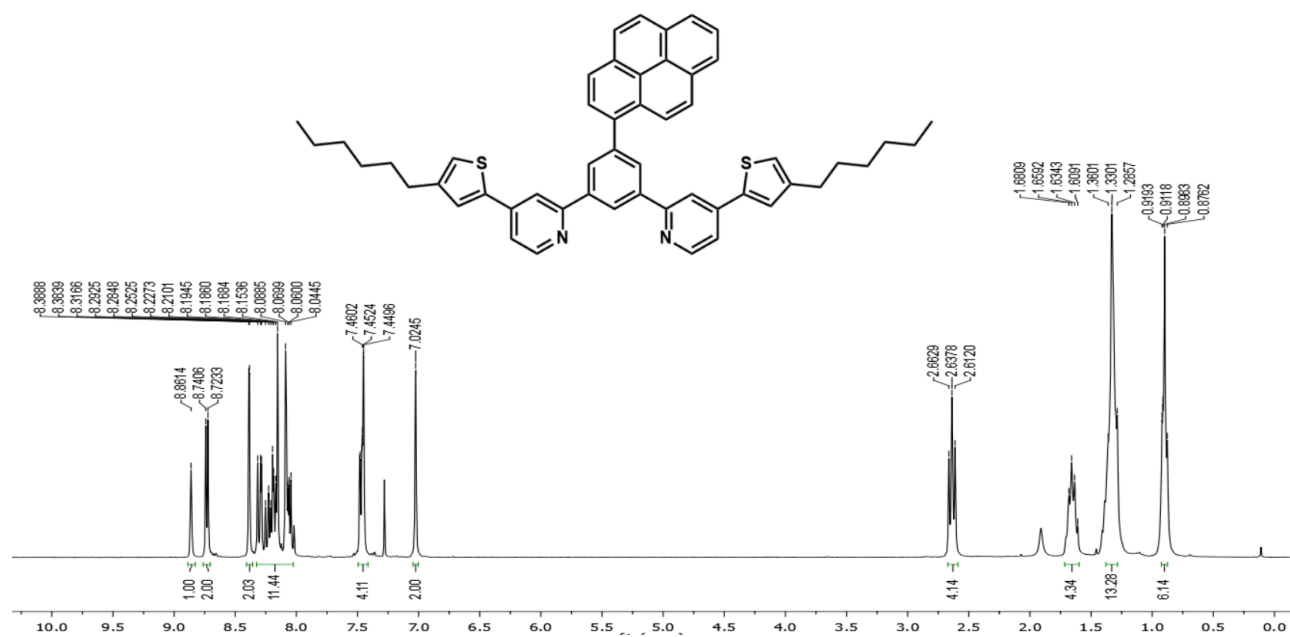
B3



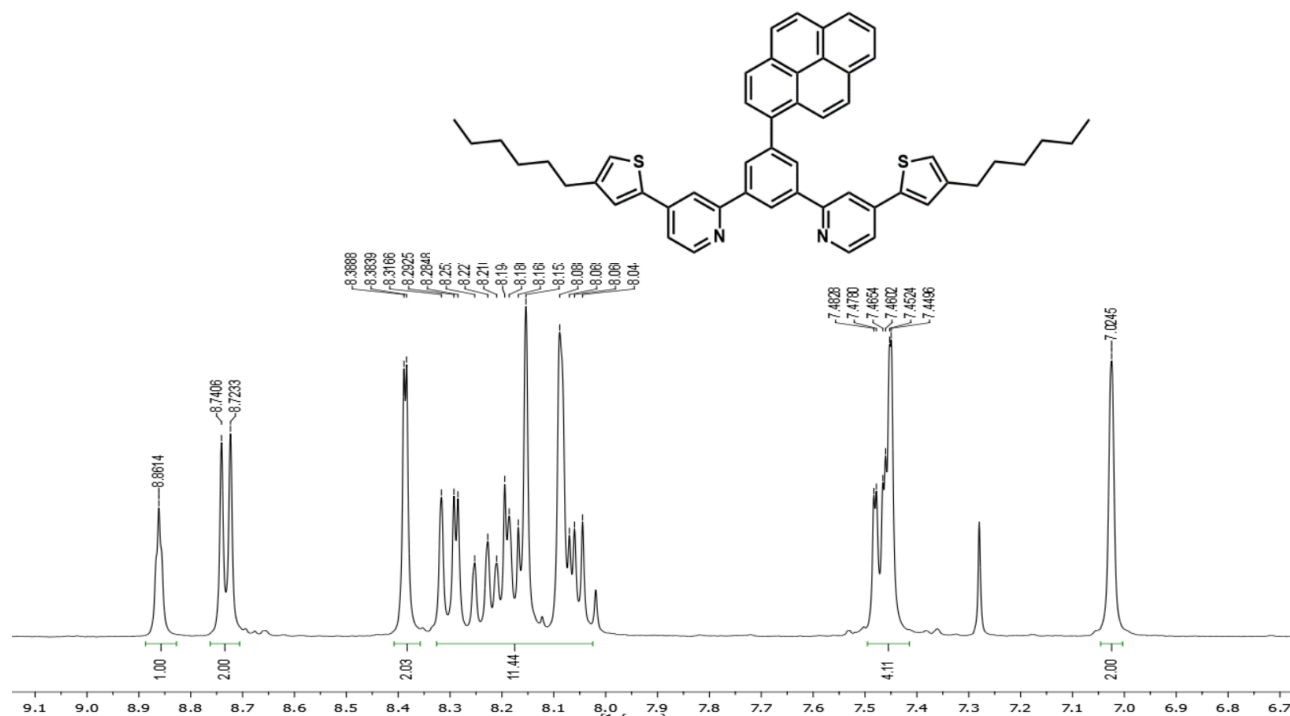
B3 – aromatic region



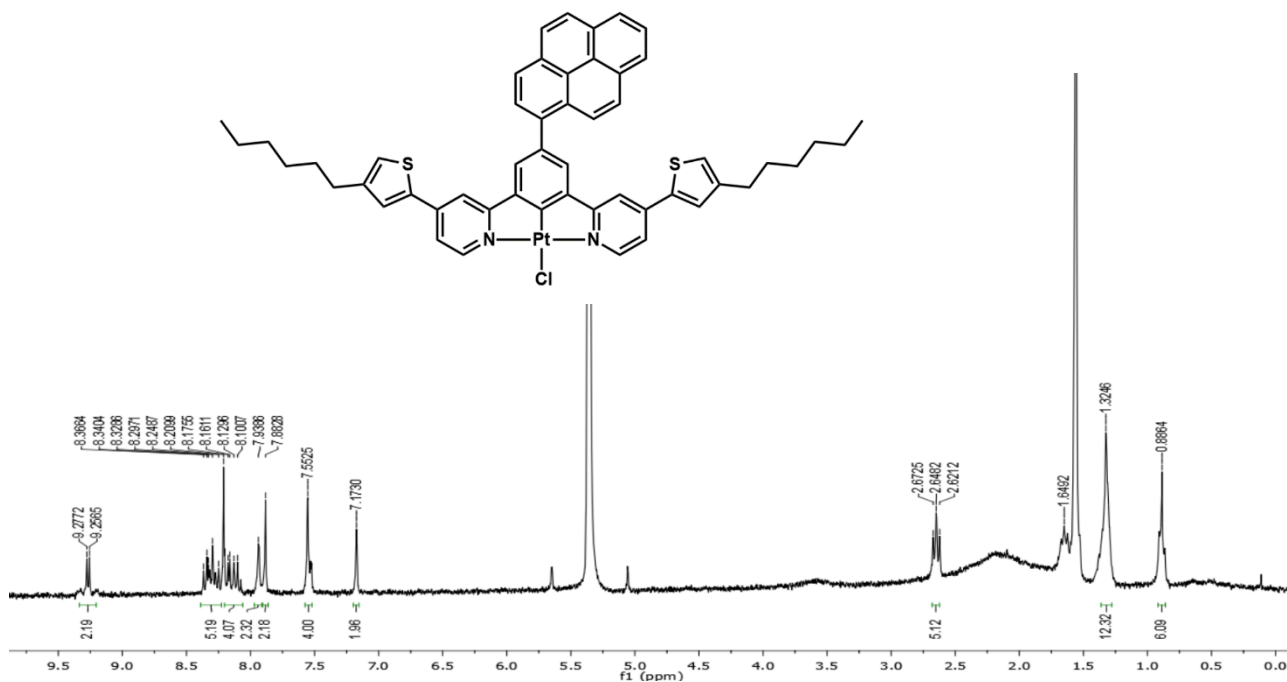
L9



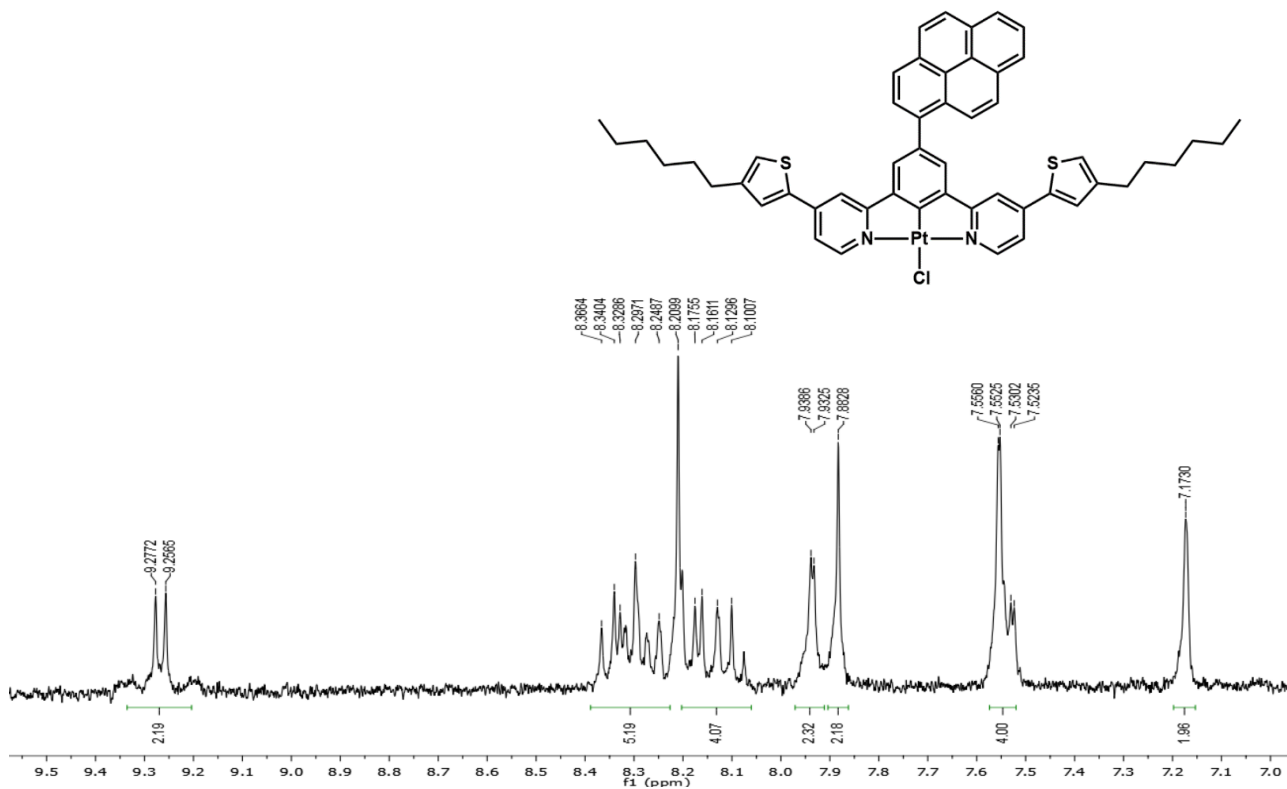
L9 – aromatic region



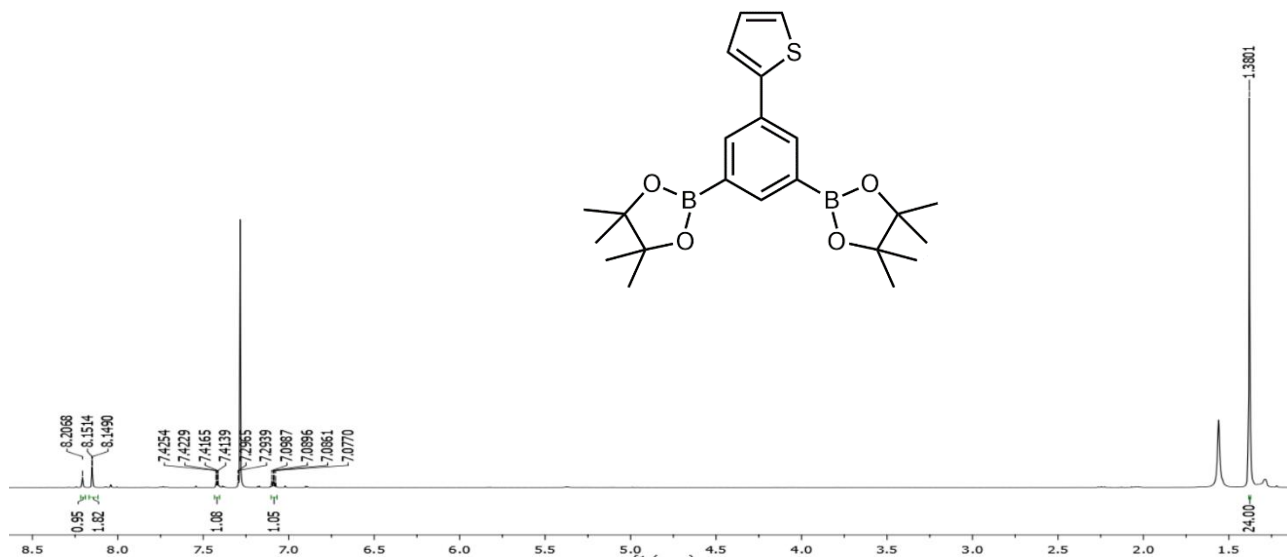
PtCl9



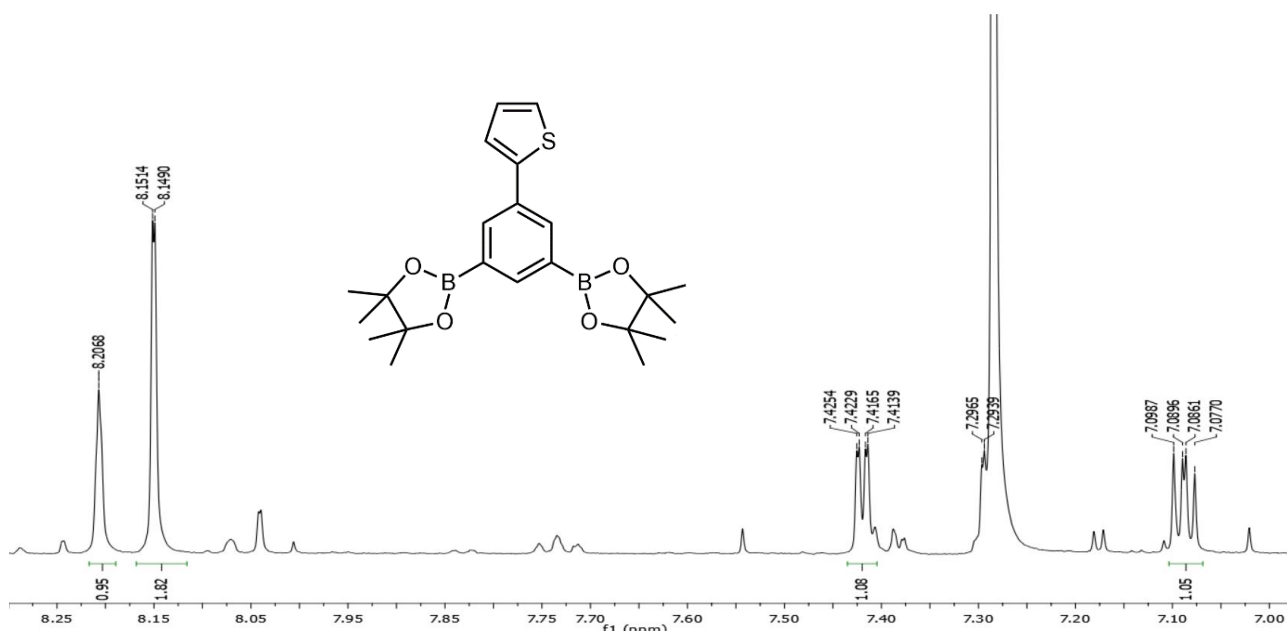
PtCl9 – aromatic region



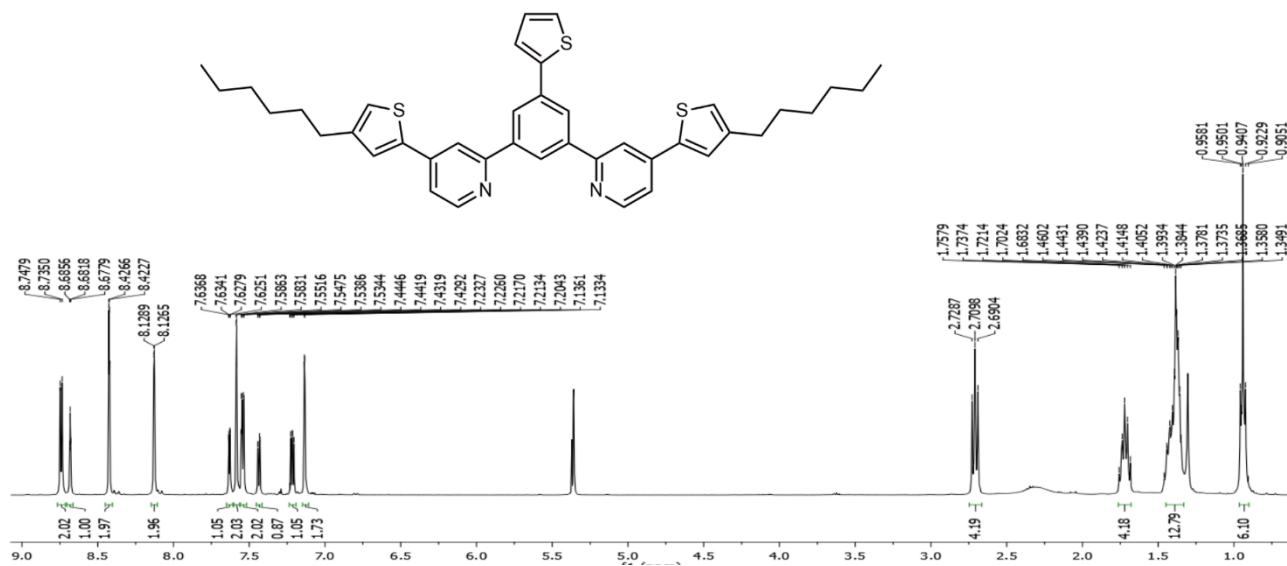
B4



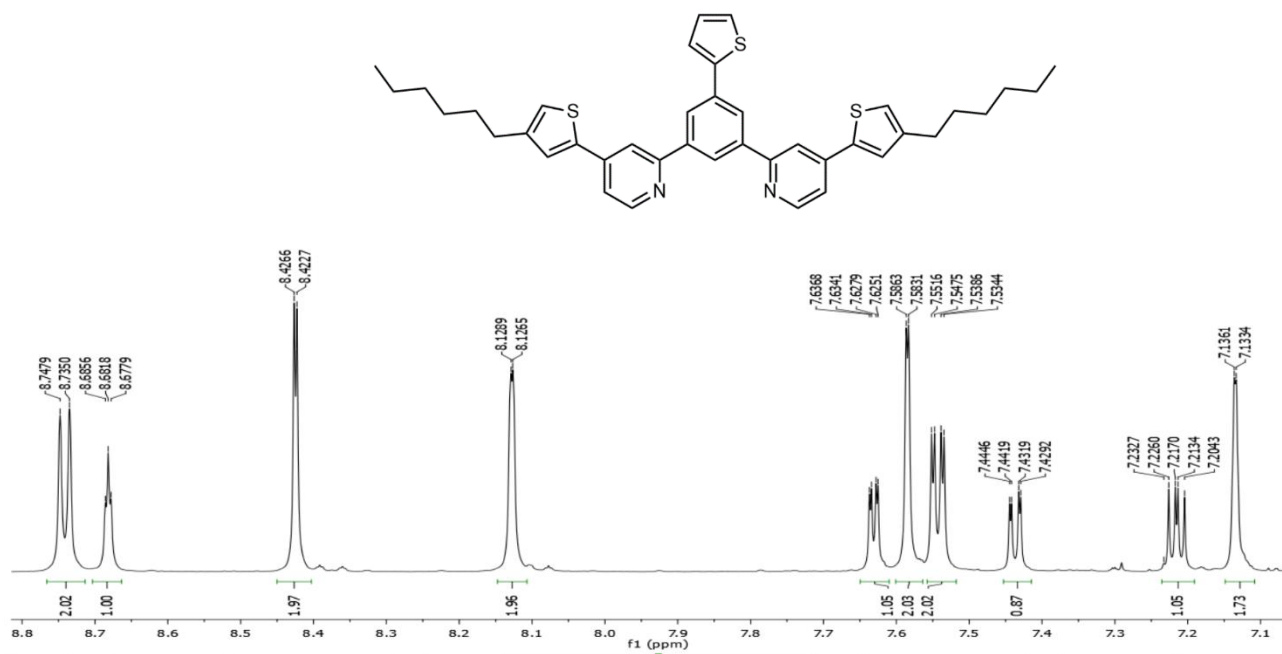
B4 - aromatic region



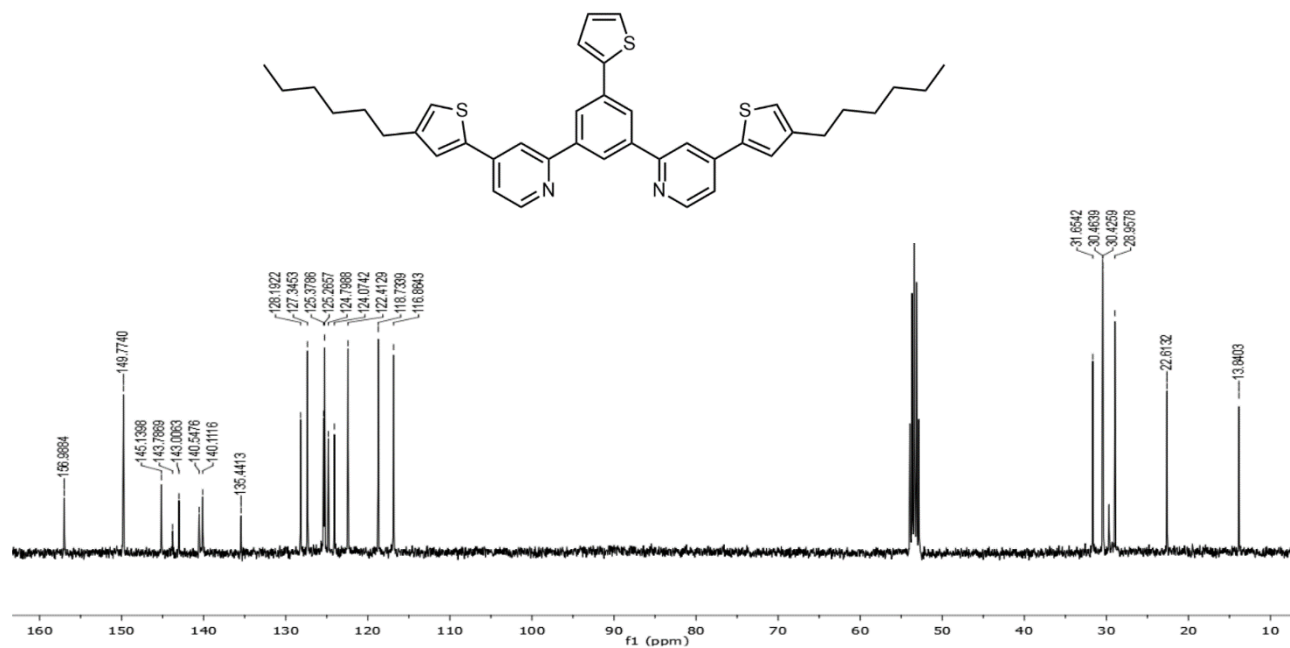
L10



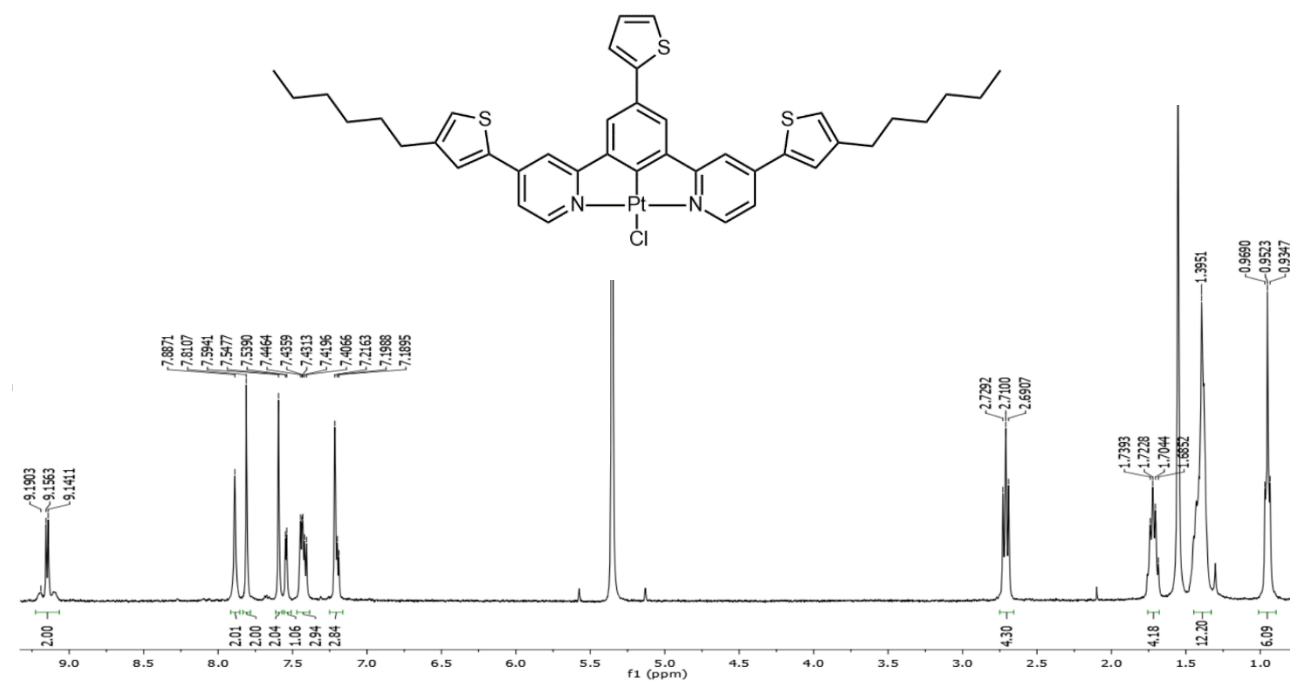
L10 – aromatic region



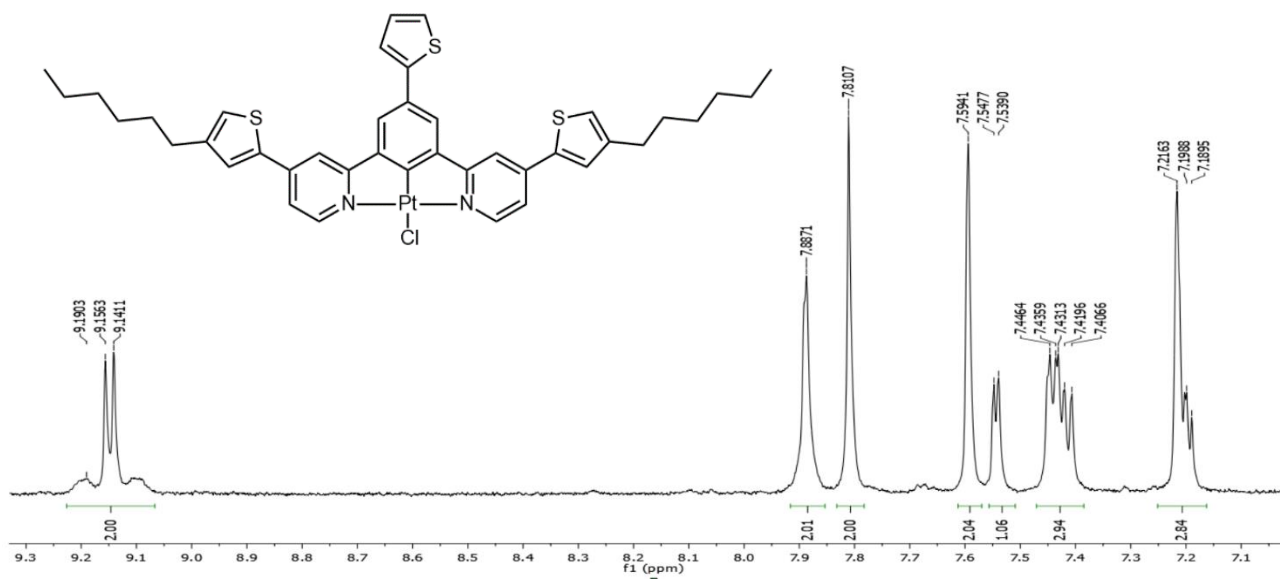
L10 - ¹³C NMR



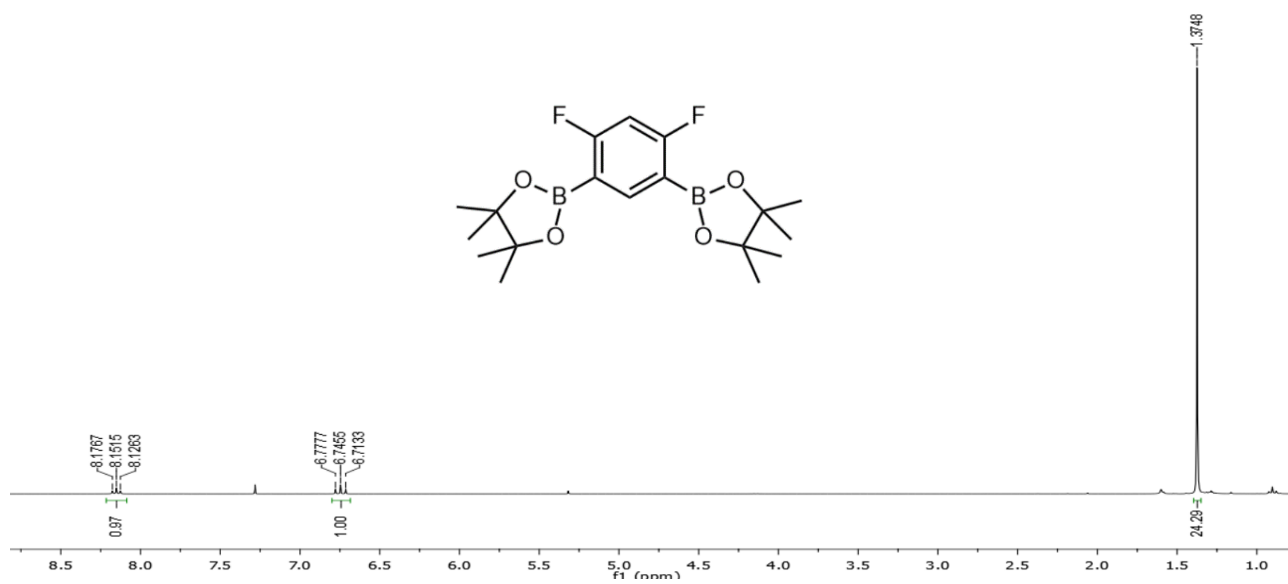
PtCl10



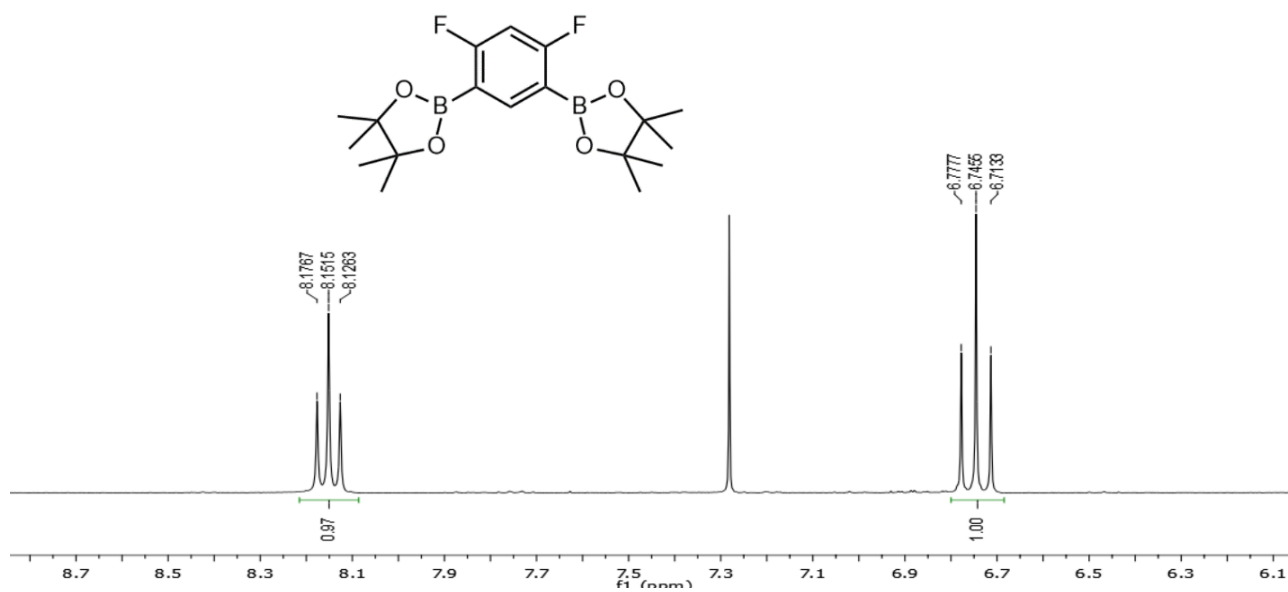
PtCl10 – aromatic region



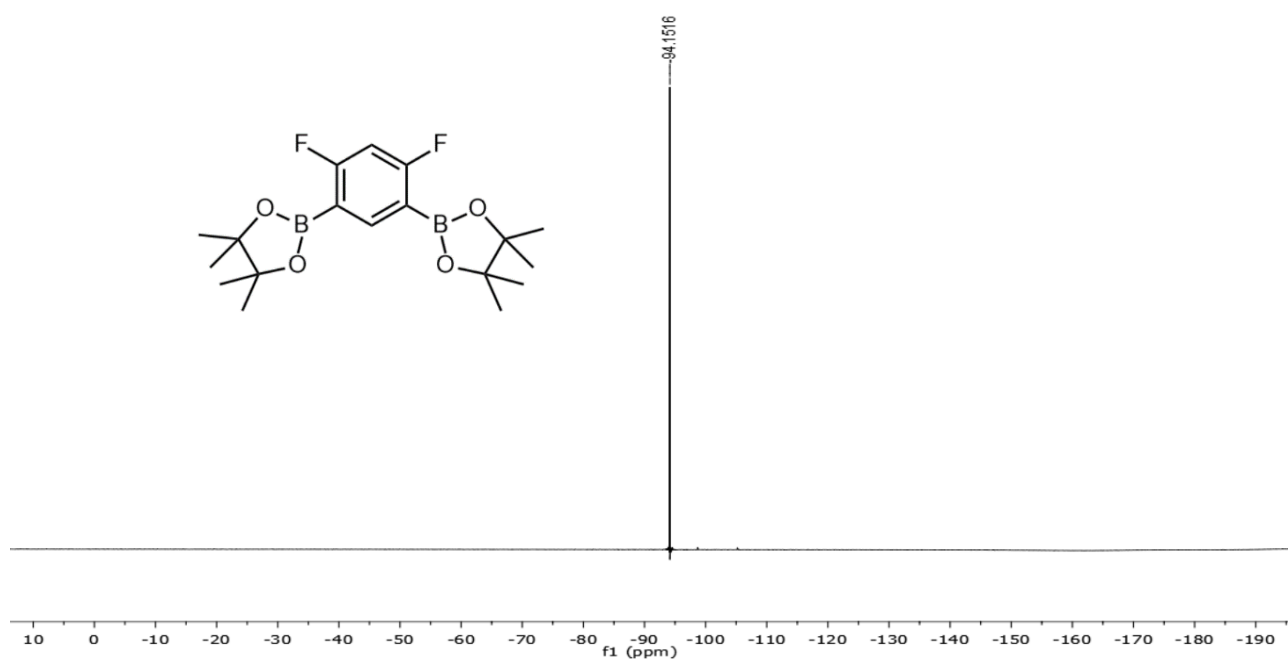
B4



B4 - aromatic region



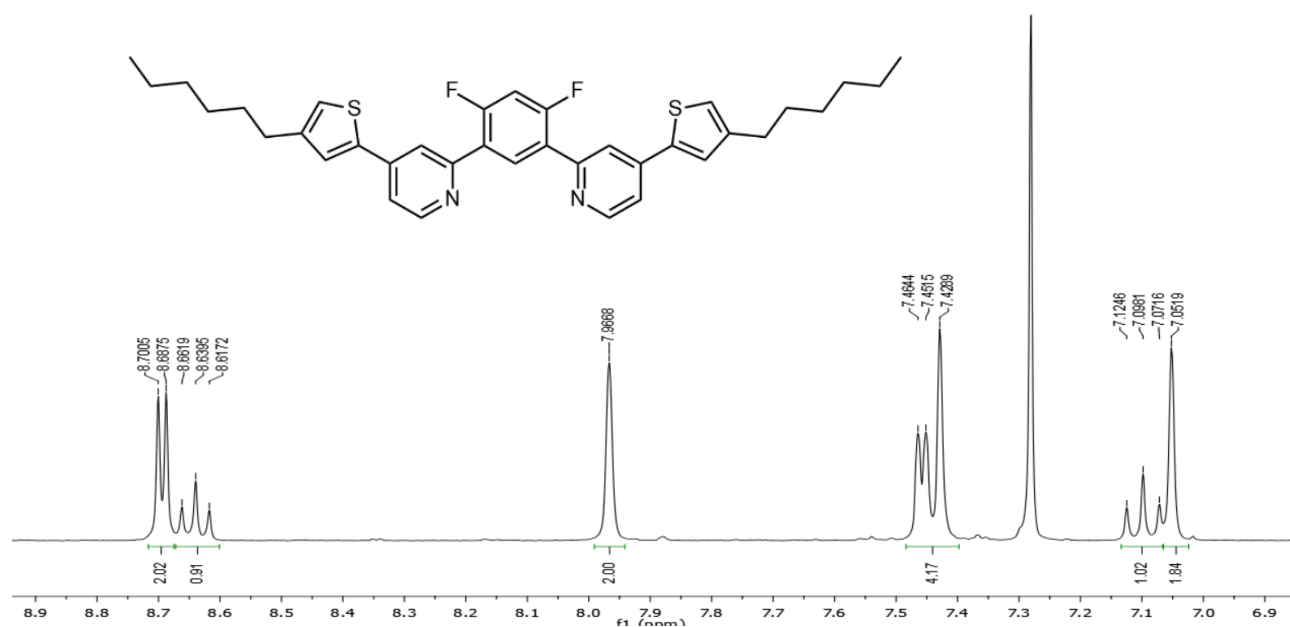
B4 - ¹⁹F NMR



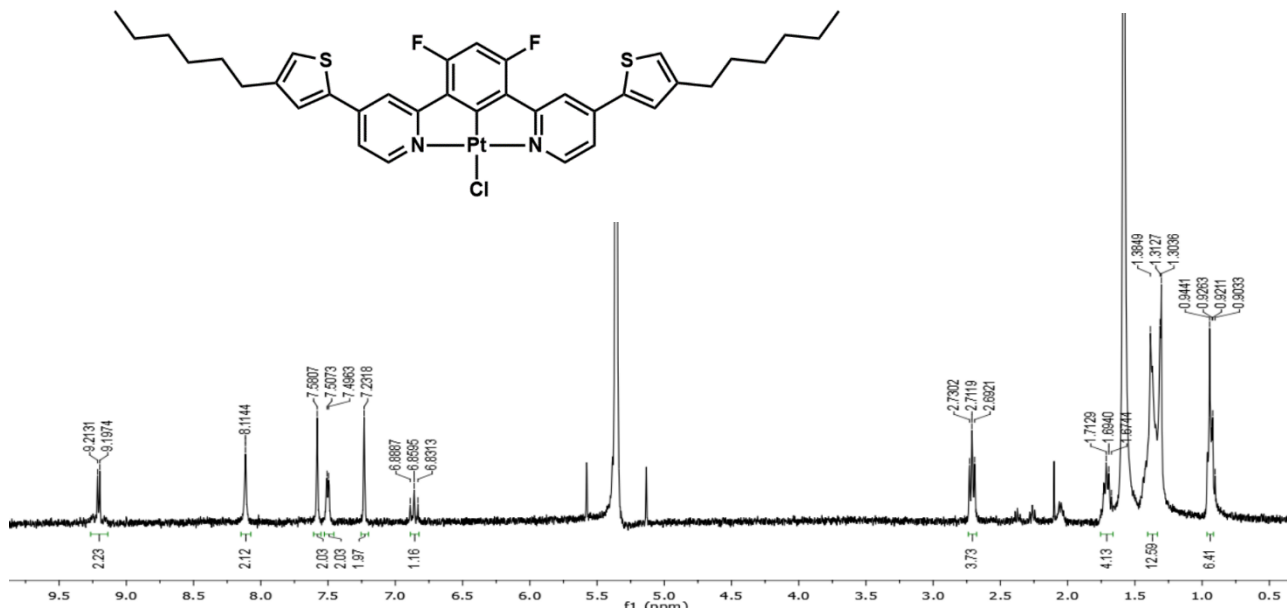
L11



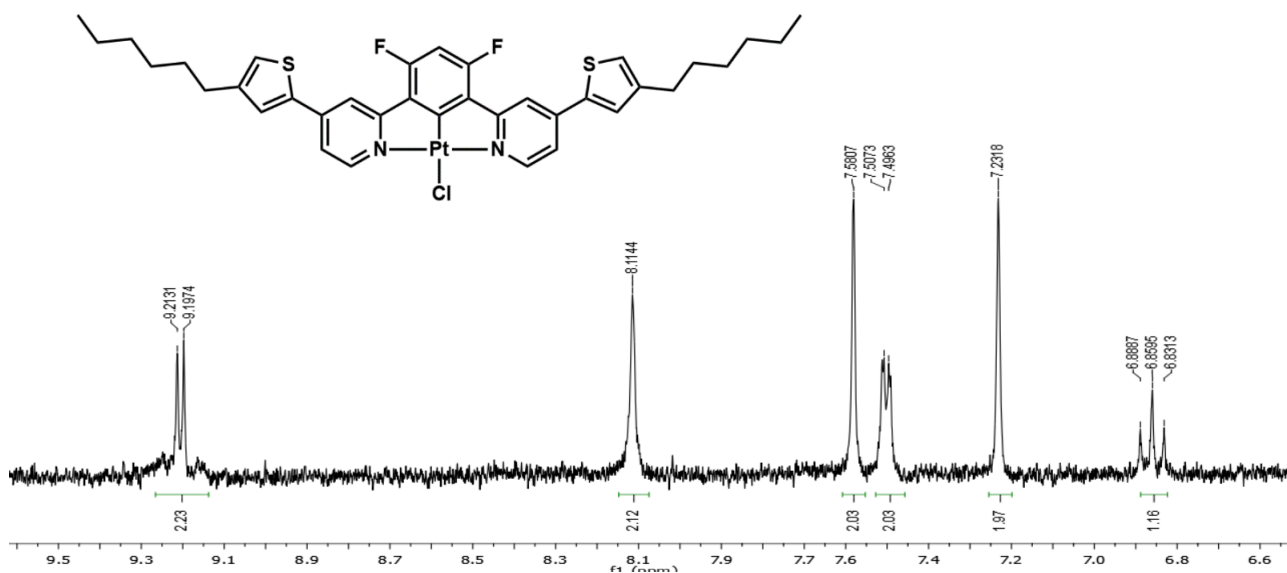
L11 – aromatic region



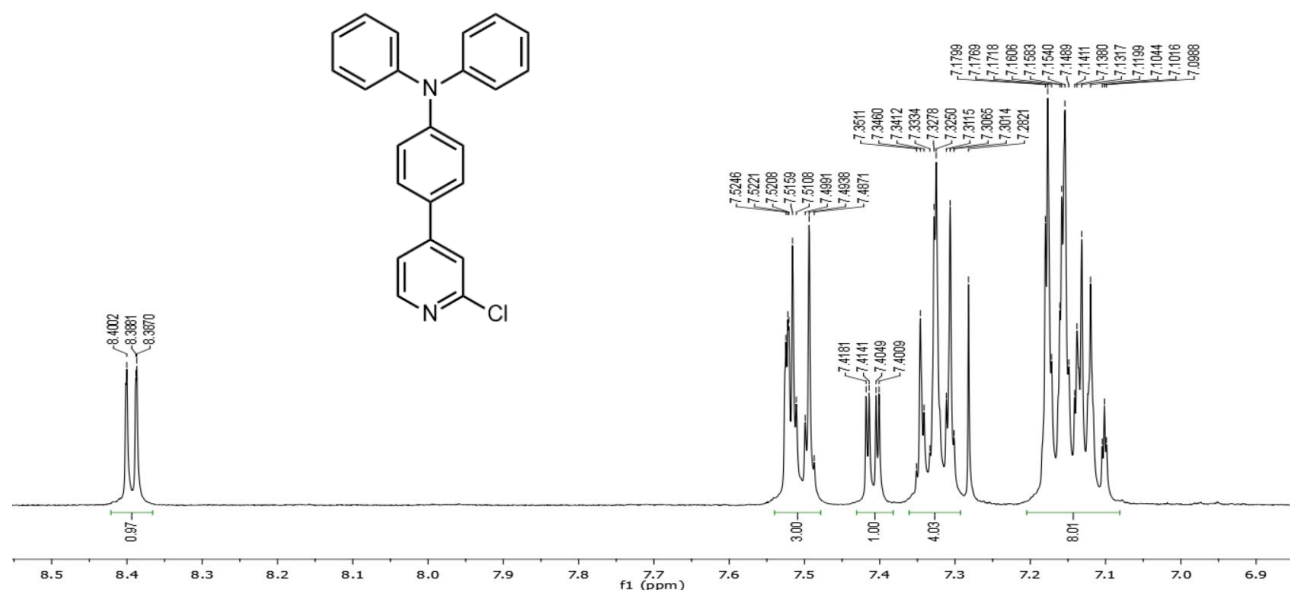
PtCl11



PtCl11 - aromatic region



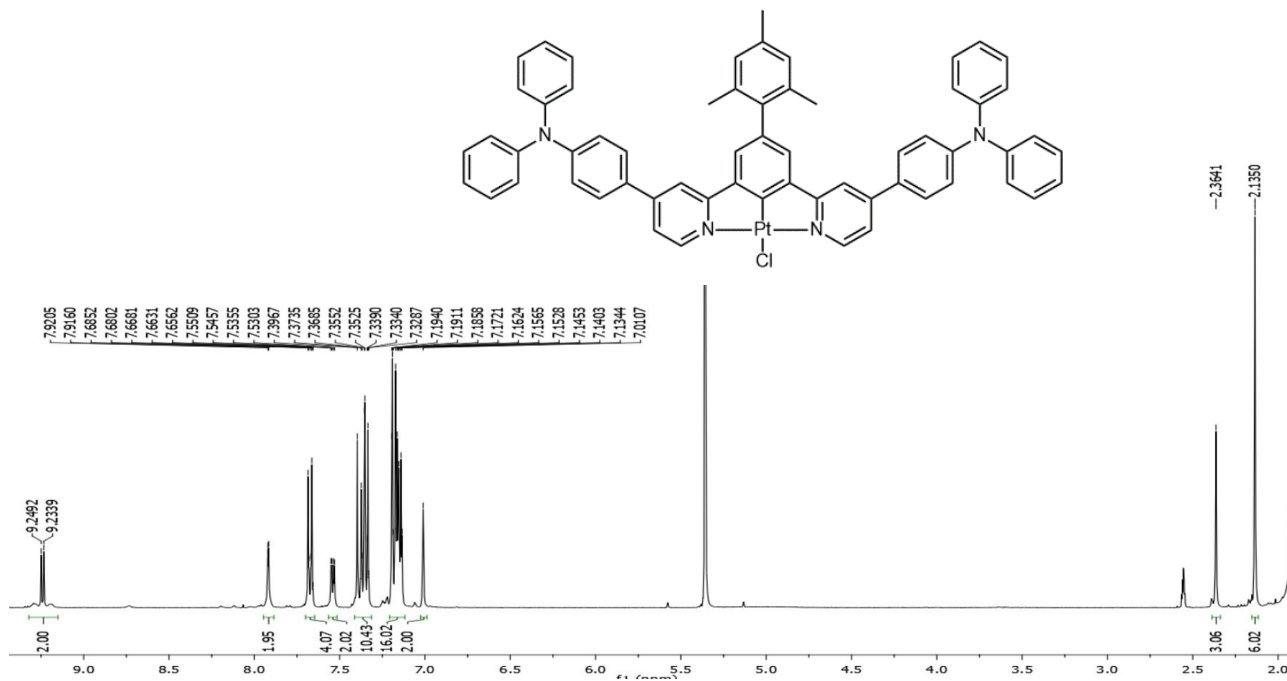
I8



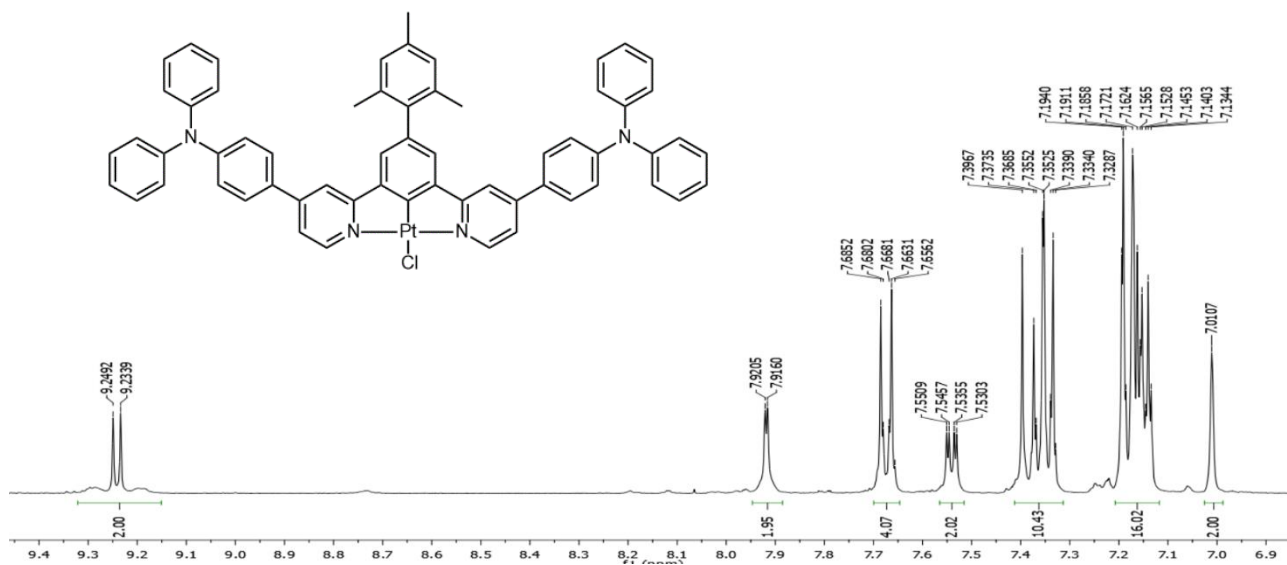
I8 - ¹³C NMR



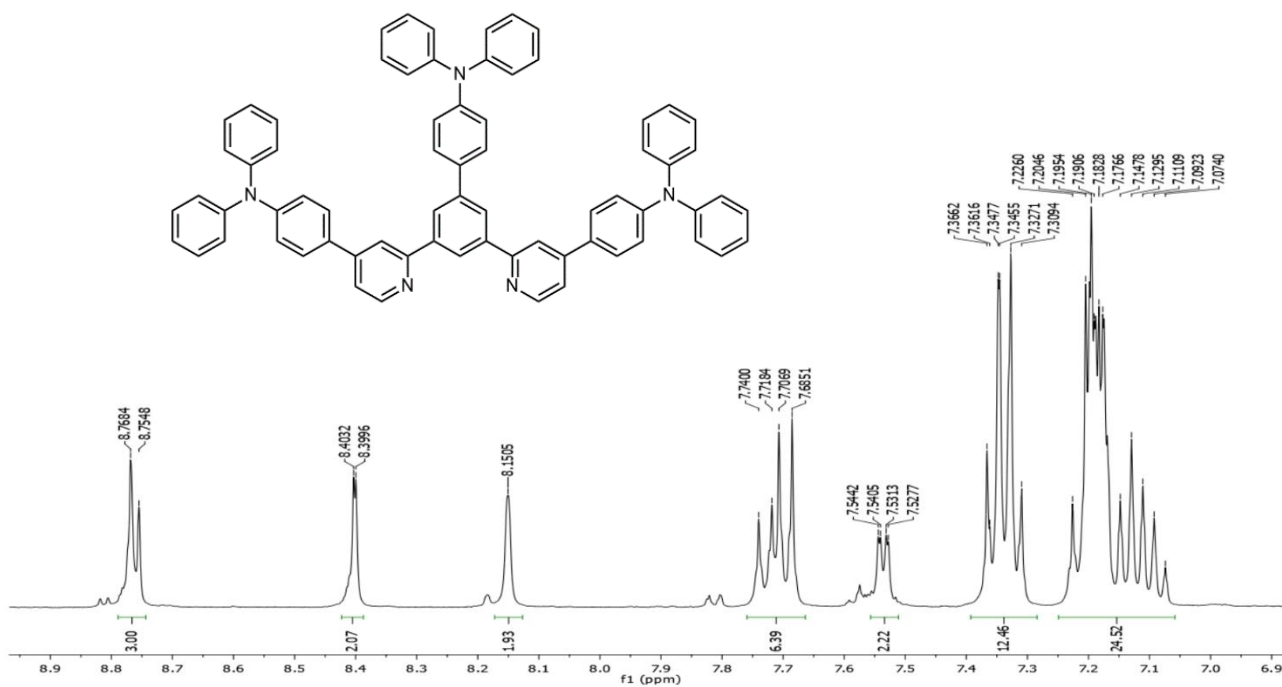
PtCl12



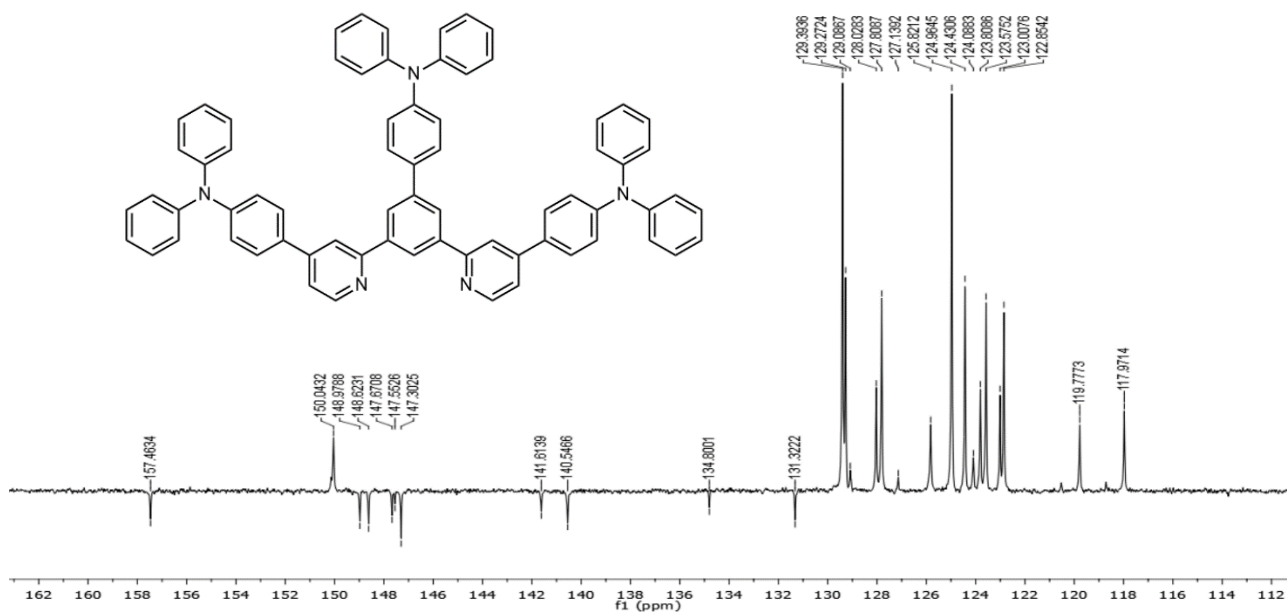
PtCl12 – aromatic region



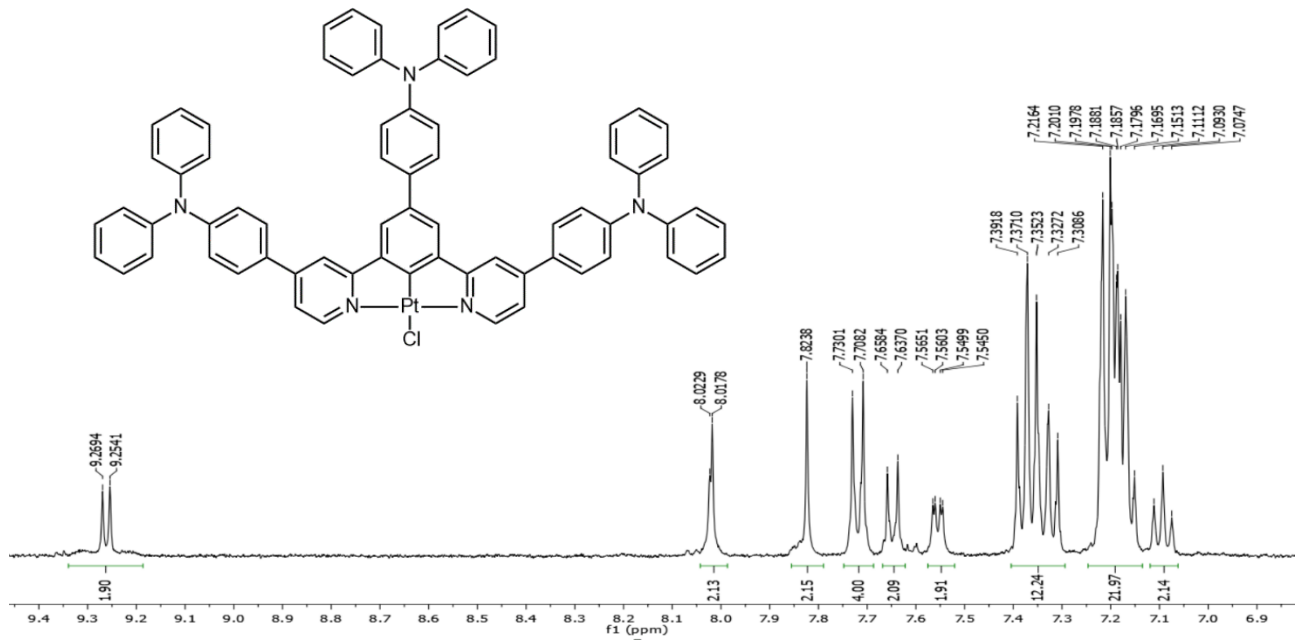
L13



L13 – ¹³C NMR

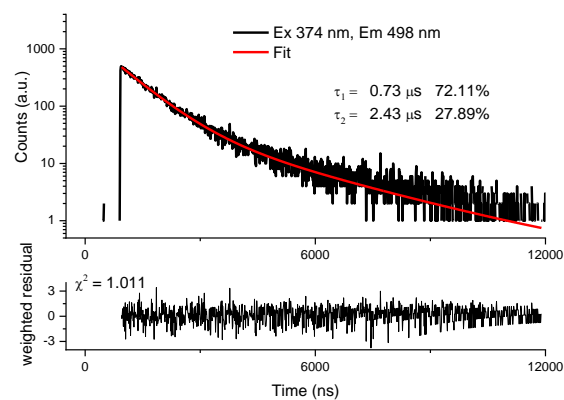
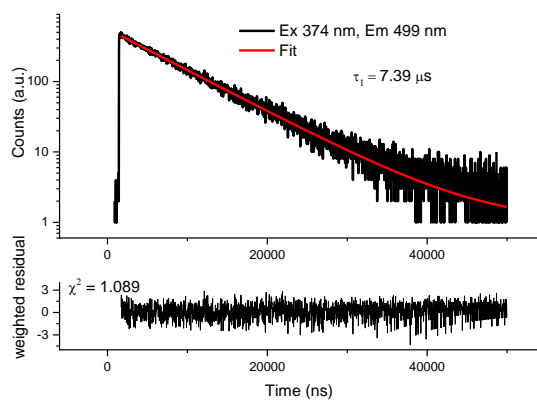


PtCl13

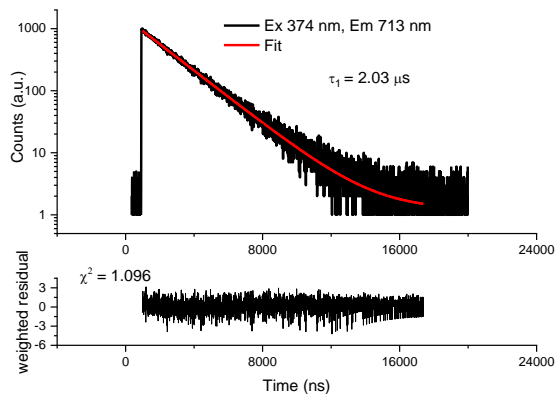
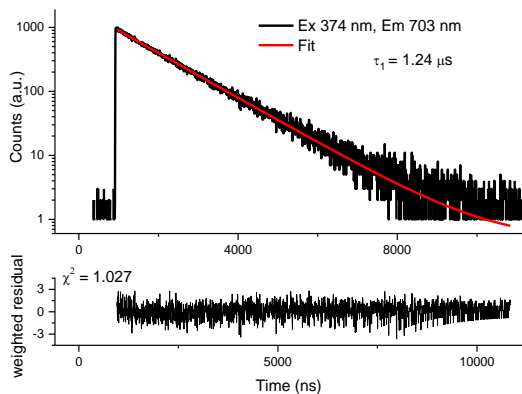


Lifetime measurements

Lifetimes of Pt1

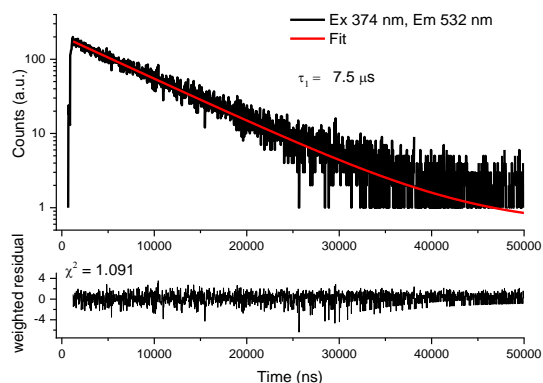
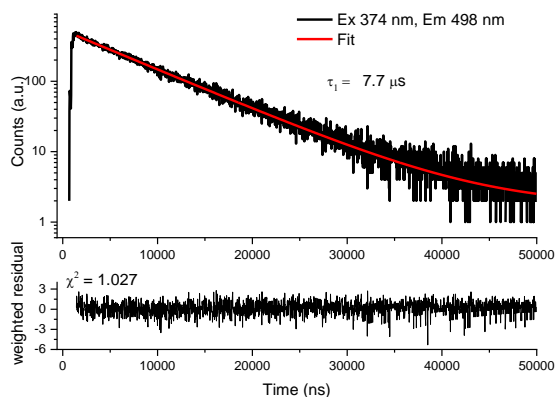


Lifetime measurements of a dilute ($1 \cdot 10^{-6}$ M, on the left) and of a concentrated ($2 \cdot 10^{-4}$ M, on the right) dichloromethane solution of **Pt1**.

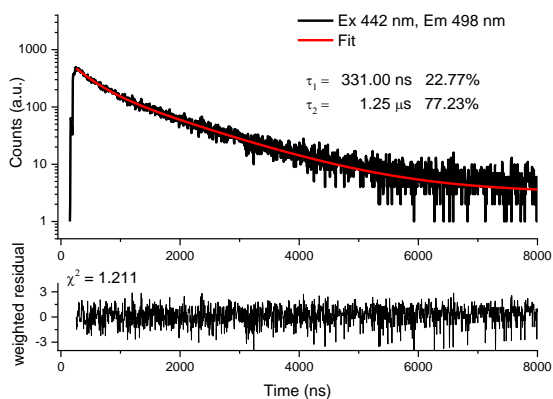
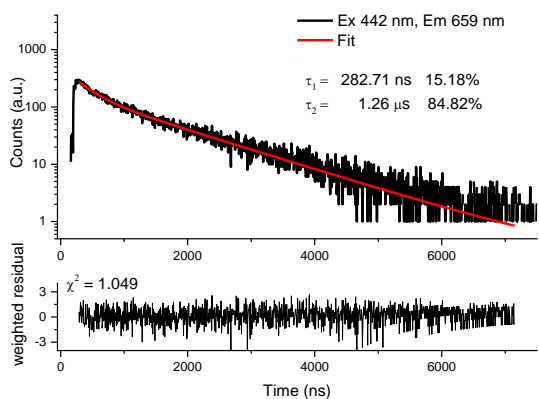
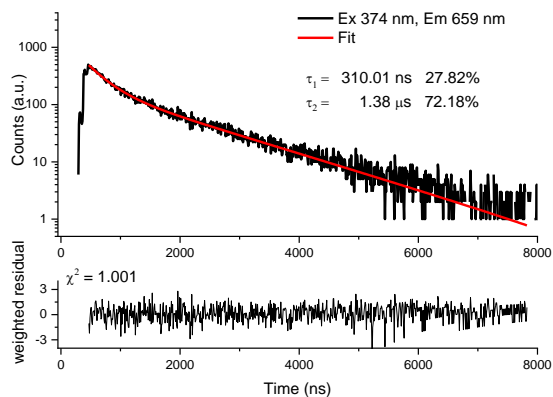
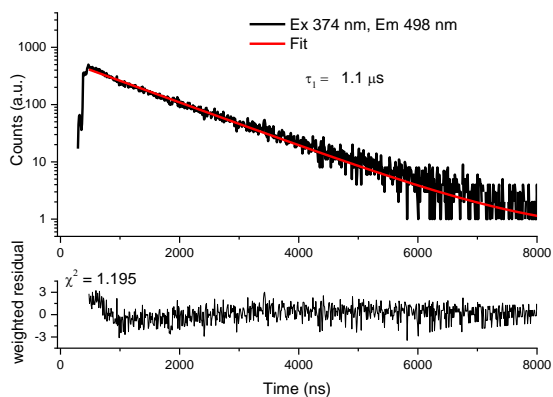


Lifetime measurements of the powders of complex **Pt1**, at Room (on the left) and at Low (on the right) Temperature.

Lifetimes of Pt2

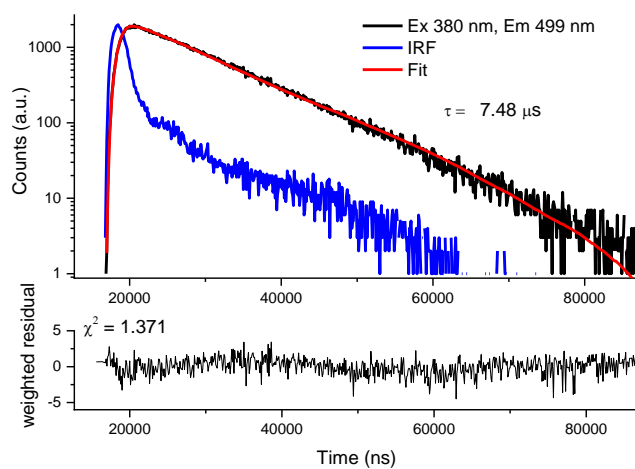


Lifetime measurements of a dilute ($1 \cdot 10^{-6}$ M) dichloromethane solution of Pt2.

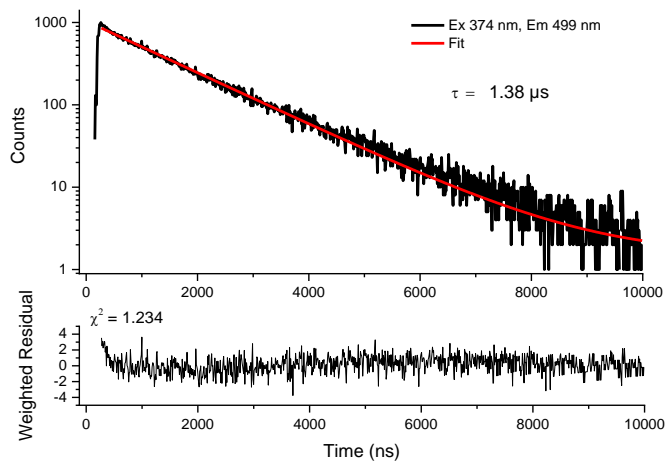


Lifetime measurements of a concentrated ($2 \cdot 10^{-4}$ M) dichloromethane solution of Pt2.

Lifetimes of Pt3

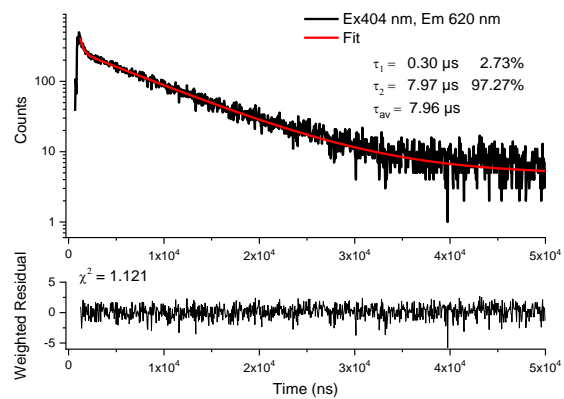
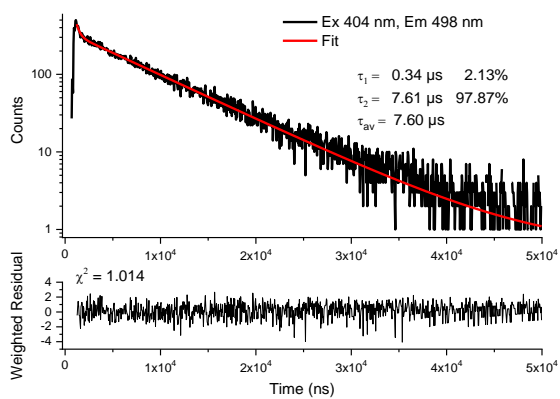


Lifetime measurements of a dilute ($3.5 \cdot 10^{-6}$ M) dichloromethane solution of **Pt3**.

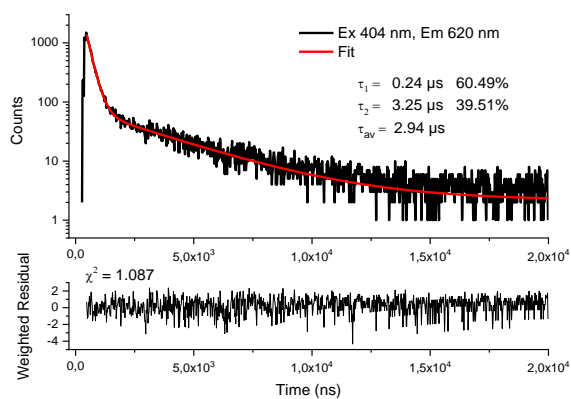
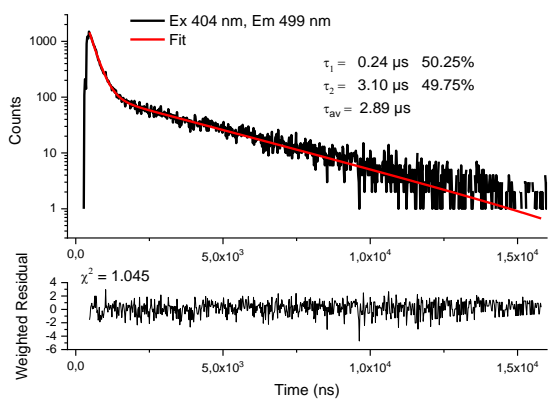


Lifetime measurements of a concentrated ($2 \cdot 10^{-4}$ M) dichloromethane solution of **Pt3**.

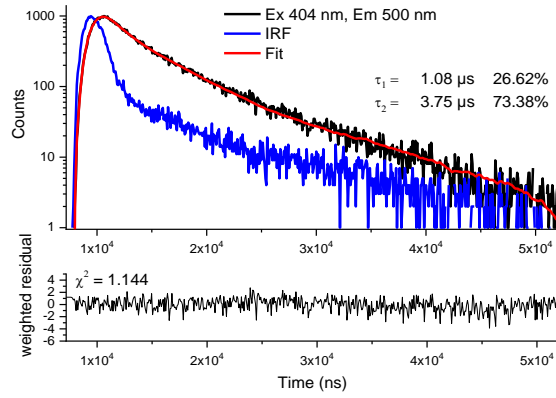
Lifetimes of Pt5



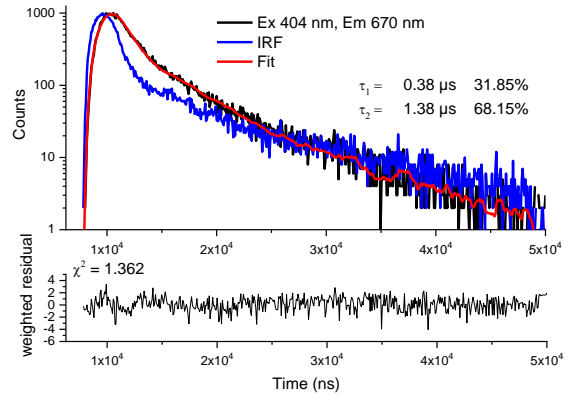
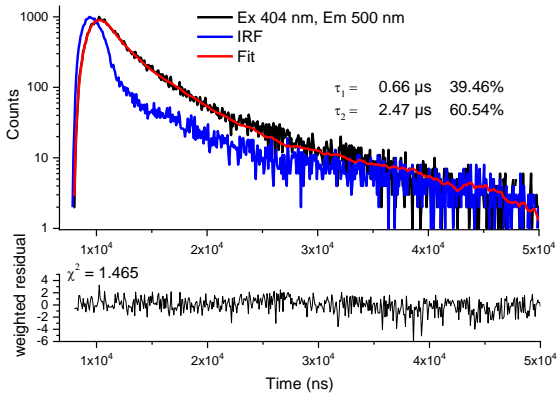
Lifetime measurements of a dilute ($5 \cdot 10^{-6}$ M) dichloromethane solution of **Pt5**.



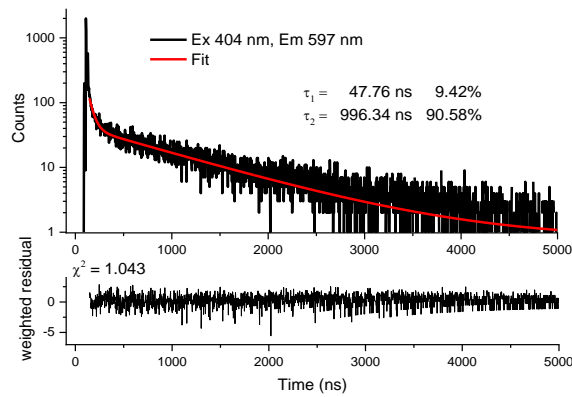
Lifetime measurements of a concentrated ($2 \cdot 10^{-4}$ M) dichloromethane solution of **Pt5**.



Lifetime measurement of a 7.5% w/w film of **Pt5** in PMMA.

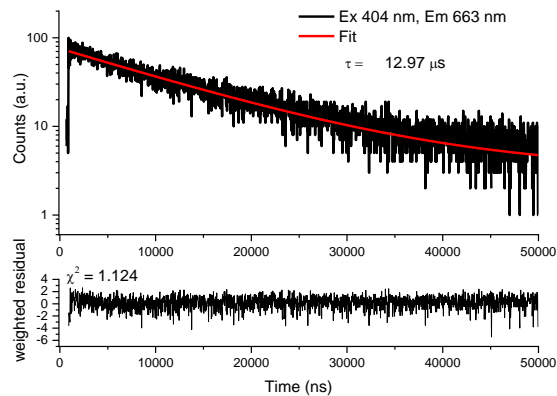
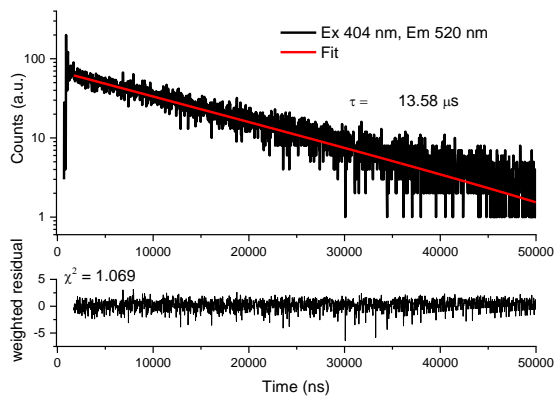


Lifetime measurements of a 15% w/w film of **Pt5** in PMMA.

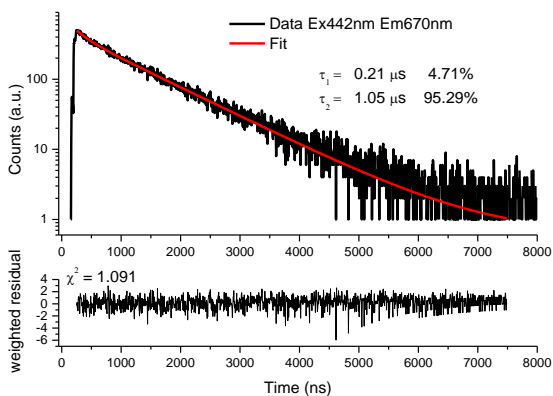
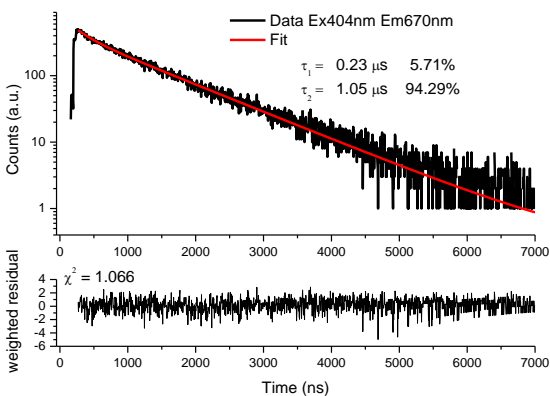
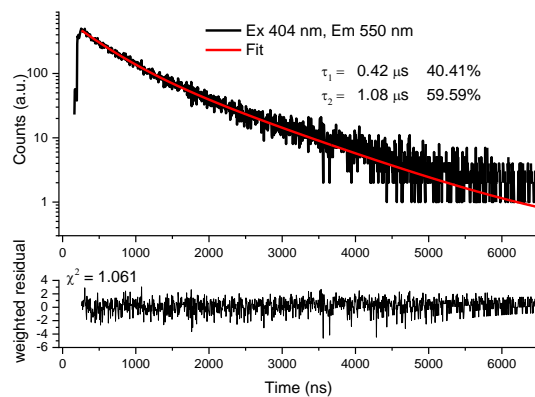
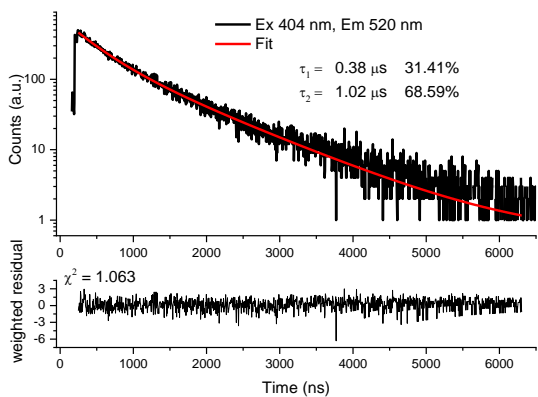


Lifetime measurement of **Pt5** as powder.

Lifetimes of Pt7

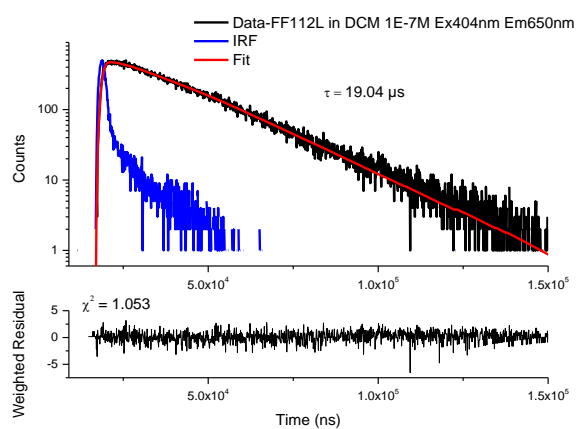
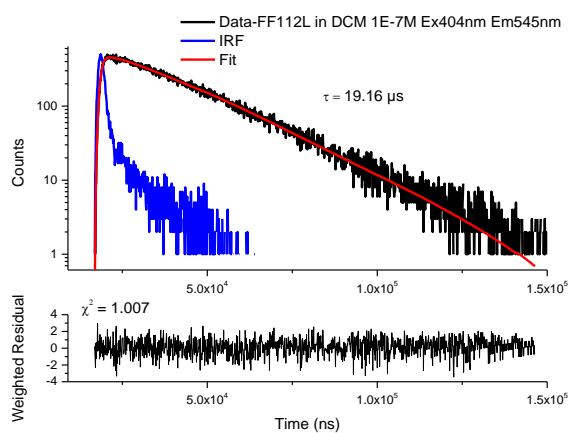


Lifetime measurements of a dilute ($1 \cdot 10^{-6}$ M) dichloromethane solution of Pt7.

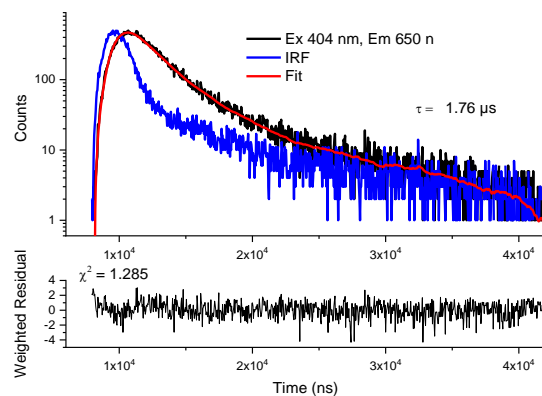
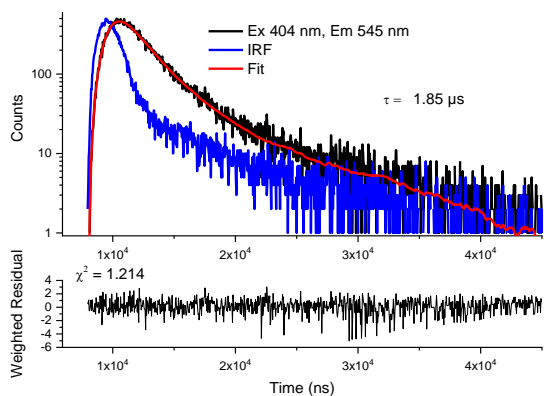


Lifetime measurements of a concentrated ($2 \cdot 10^{-4}$ M) dichloromethane solution of Pt7.

Lifetimes of Pt8

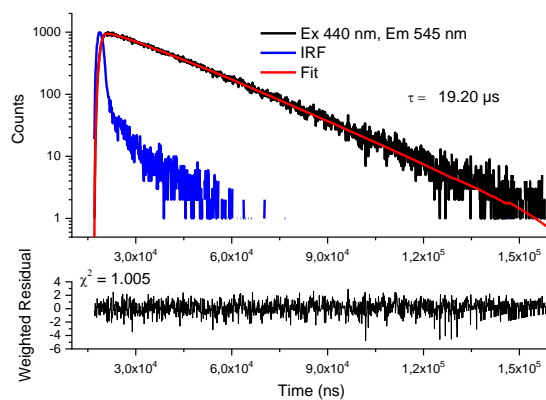
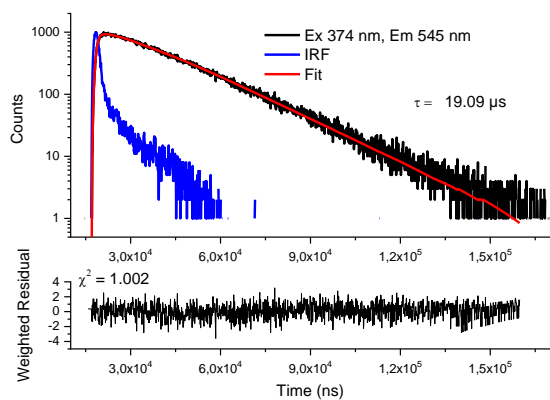


Lifetime measurements of a diluted ($1 \cdot 10^{-7}$ M) dichloromethane solution of **Pt8**.

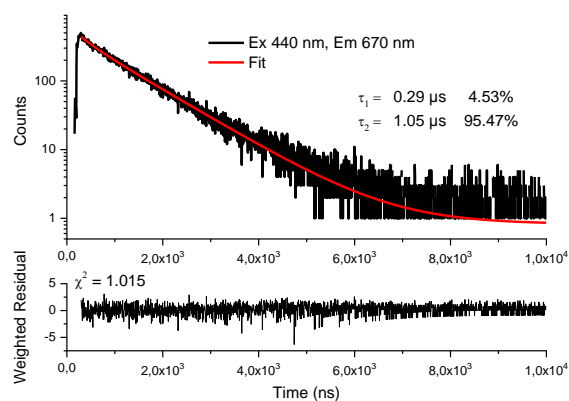
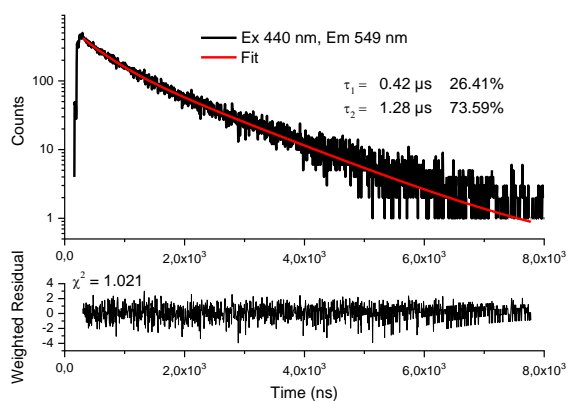


Lifetime measurements of a concentrated ($2 \cdot 10^{-4}$ M) dichloromethane solution of **Pt8**.

Lifetimes of Pt9

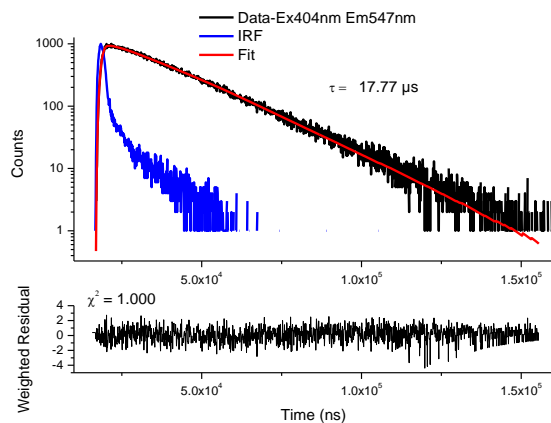
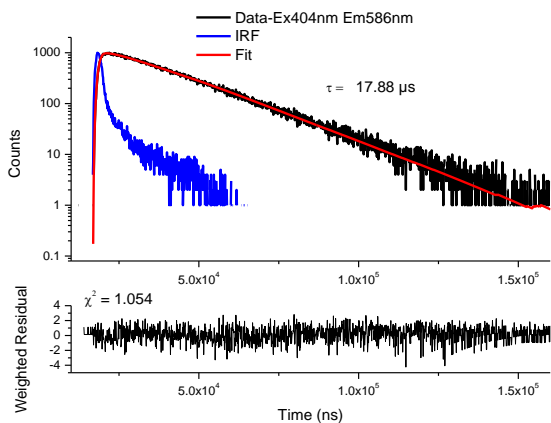


Lifetime measurements of a dilute ($1 \cdot 10^{-6}$ M) dichloromethane solution of **Pt9**.

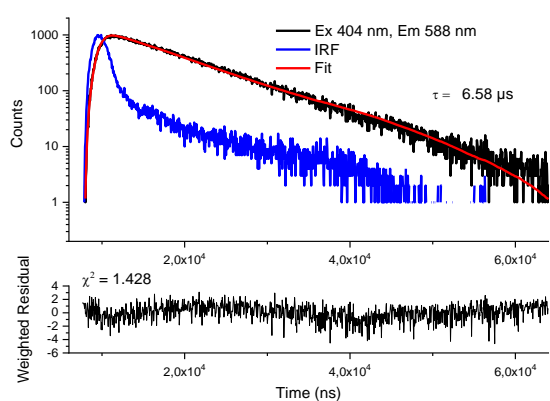
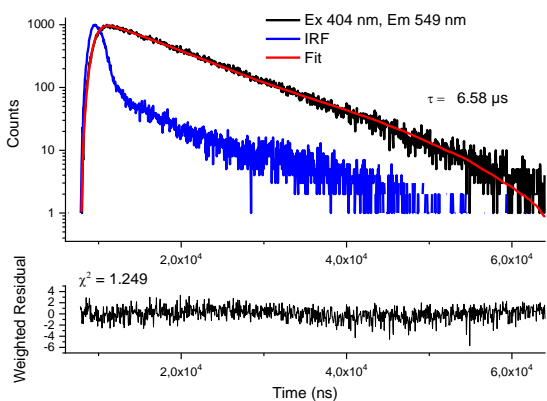


Lifetime measurements of a concentrated ($2 \cdot 10^{-4}$ M) dichloromethane solution of **Pt9**.

Lifetimes of Pt10

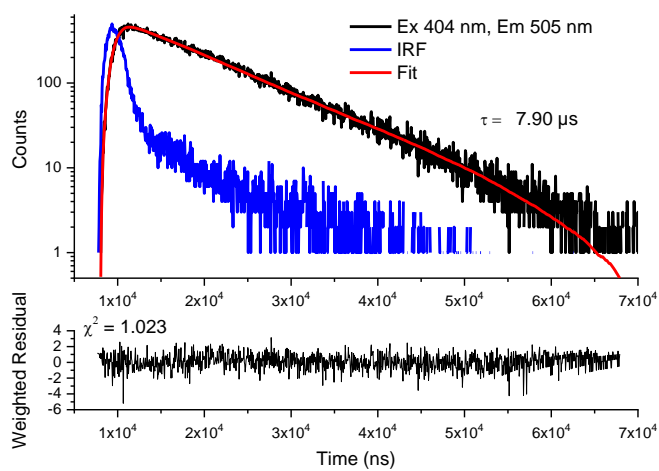


Lifetime measurements of a dilute ($2 \cdot 10^{-6}$ M) dichloromethane solution of Pt10.

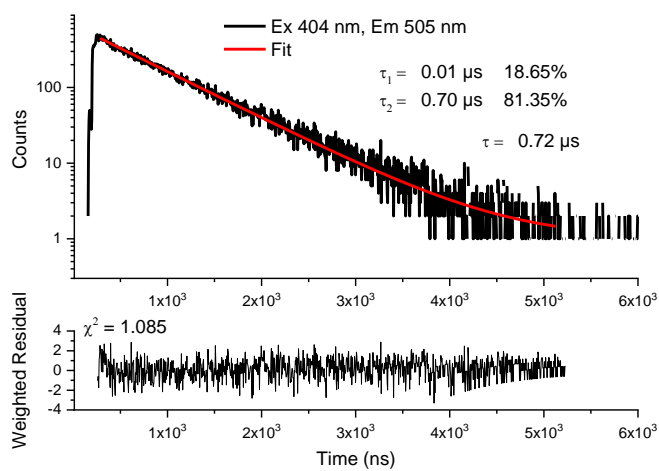


Lifetime measurements of a concentrated ($6 \cdot 10^{-5}$ M) dichloromethane solution of Pt10.

Lifetimes of Pt12

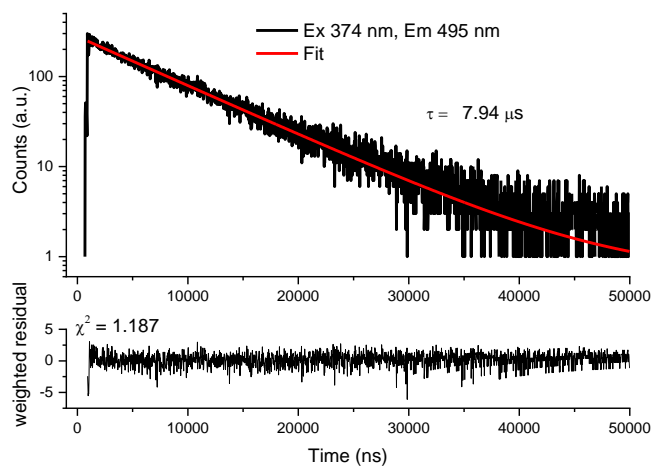


Lifetime measurement of a dilute ($1 \cdot 10^{-6}$ M) dichloromethane solution of **Pt12**.

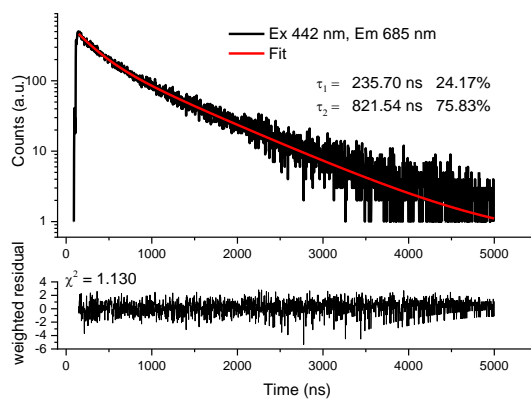
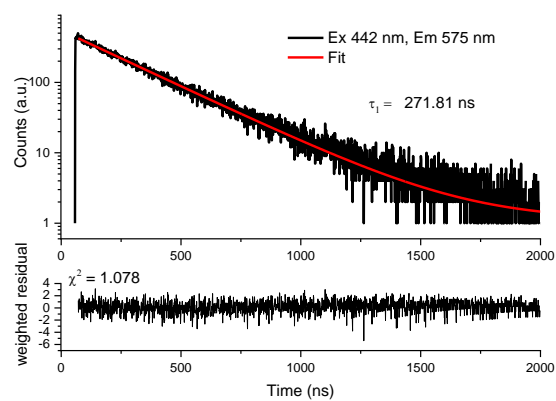
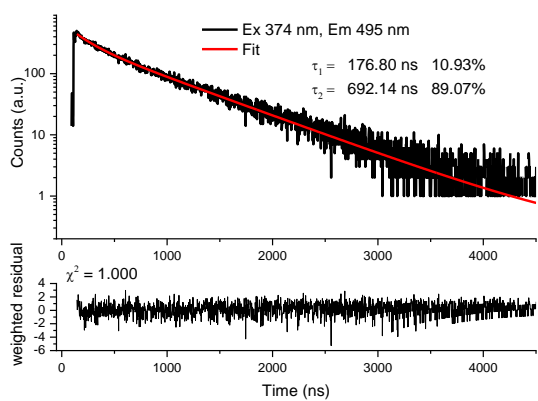


Lifetime measurement of a concentrated ($2 \cdot 10^{-4}$ M) dichloromethane solution of **Pt12**.

Lifetimes of Pt13

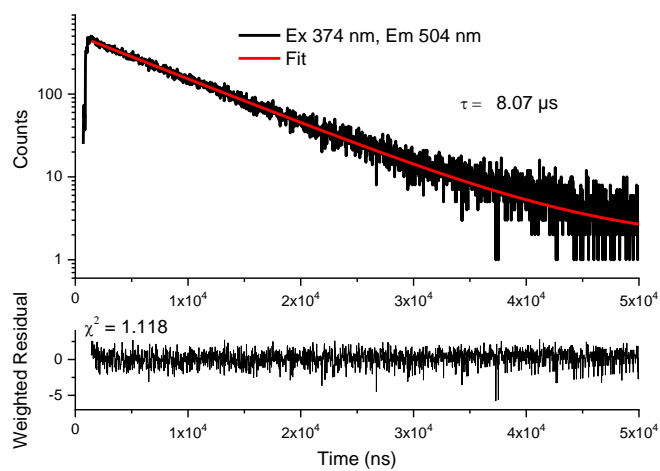


Lifetime measurement of a dilute ($1 \cdot 10^{-6}$ M) dichloromethane solution of **Pt13**.

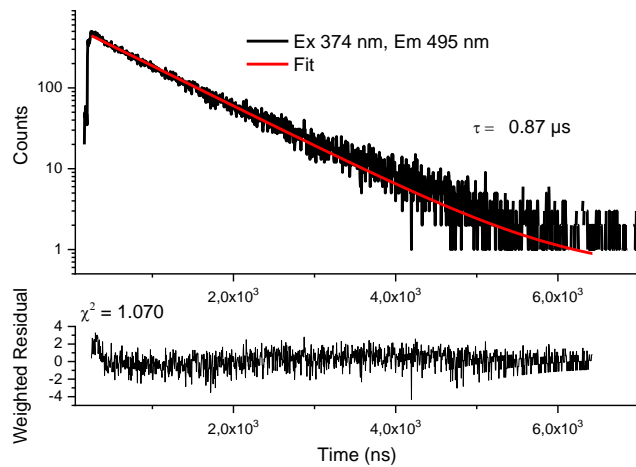


Lifetime measurements of a concentrated ($2 \cdot 10^{-4}$ M) dichloromethane solution of **Pt13**.

Lifetimes of Pt14

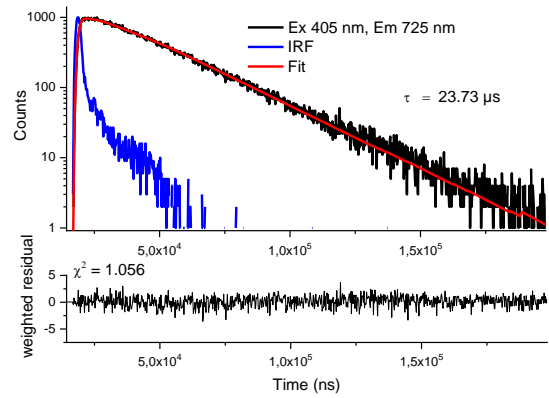
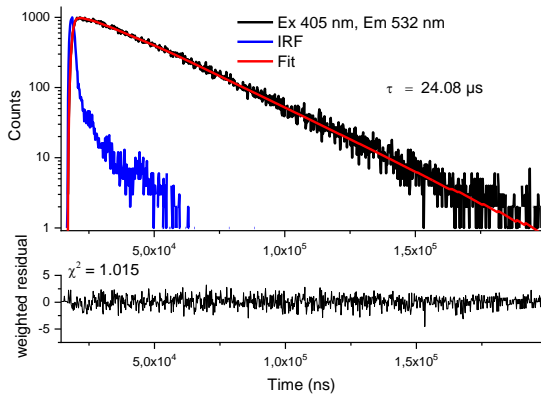


Lifetime measurement of a dilute ($1 \cdot 10^{-6}$ M) dichloromethane solution of **Pt14**.

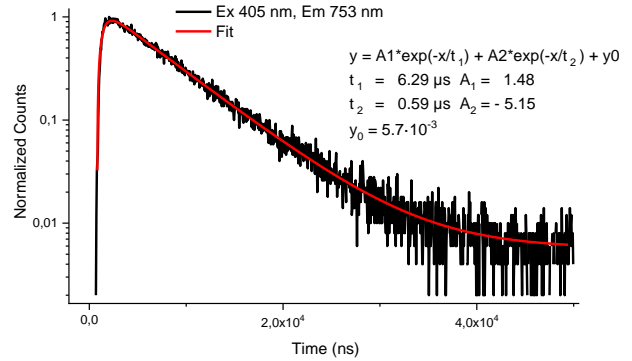
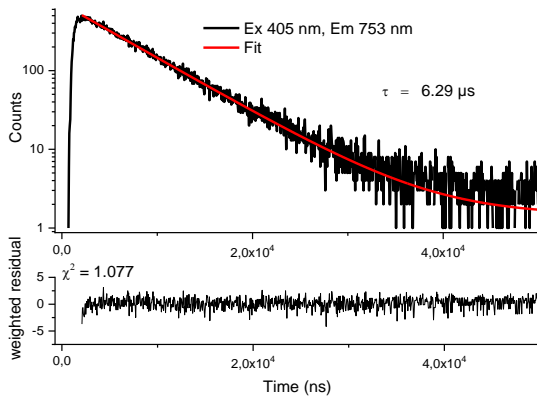


Lifetime measurement of a concentrated ($2 \cdot 10^{-4}$ M) dichloromethane solution of **Pt14**.

Lifetimes of PtCl₈

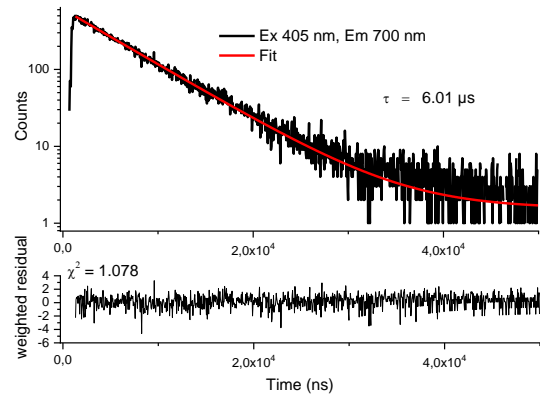
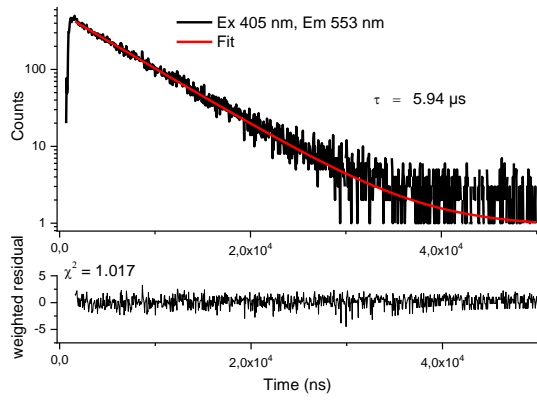


Lifetime measurements of a dilute ($2.5 \cdot 10^{-6}$ M) dichloromethane solution of PtCl₈.

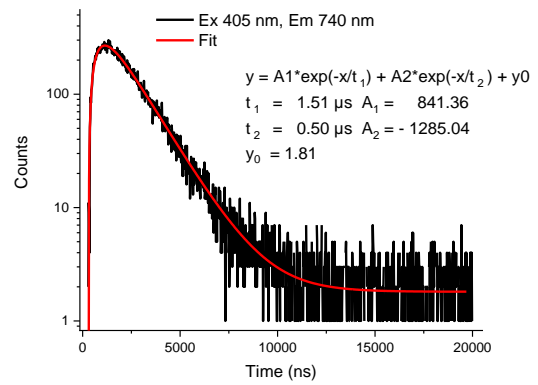
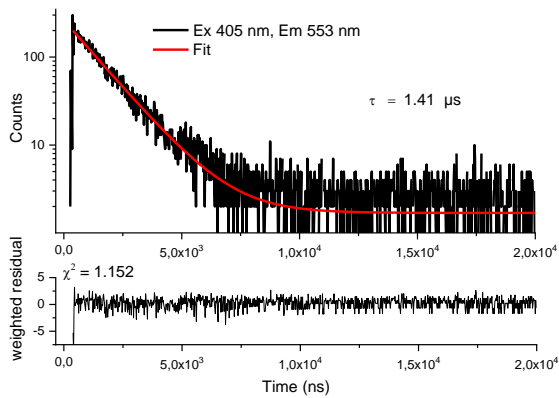


Lifetime measurements of a concentrated ($1 \cdot 10^{-4}$ M) dichloromethane solution of PtCl₈.

Lifetimes of PtCl10

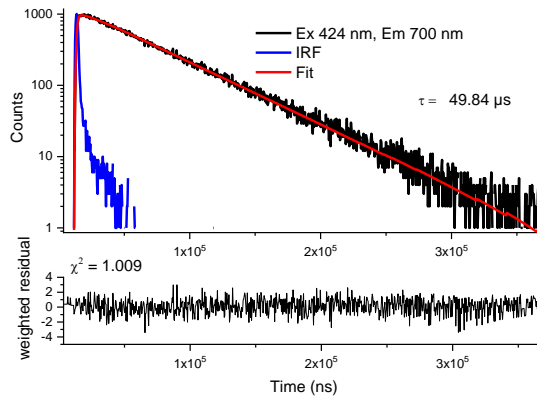
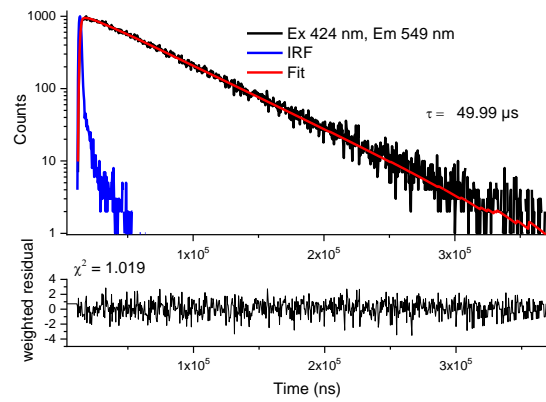
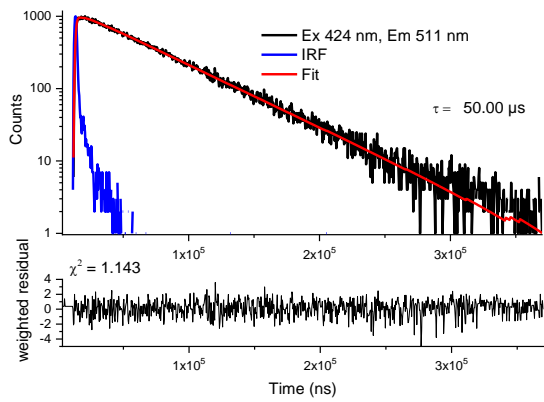


Lifetime measurements of a dilute ($2.5 \cdot 10^{-6}$ M) dichloromethane solution of PtCl10.

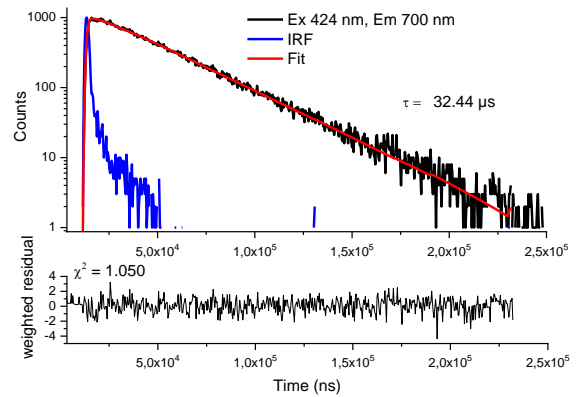
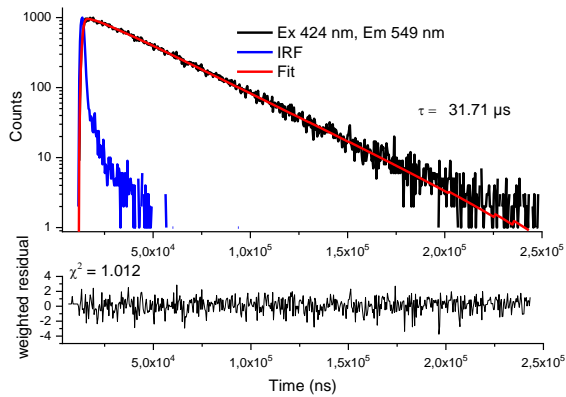


Lifetime measurements of a concentrated ($2.3 \cdot 10^{-4}$ M) dichloromethane solution of PtCl10.

Lifetimes of PtCl12

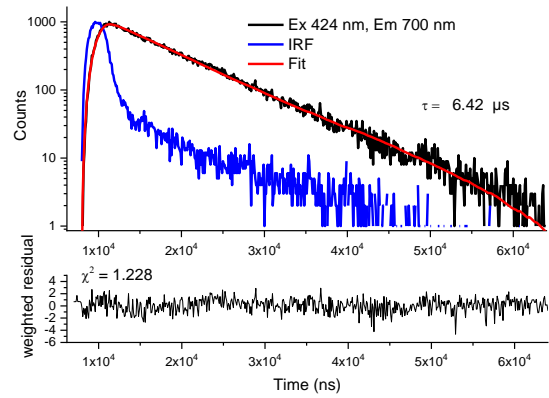
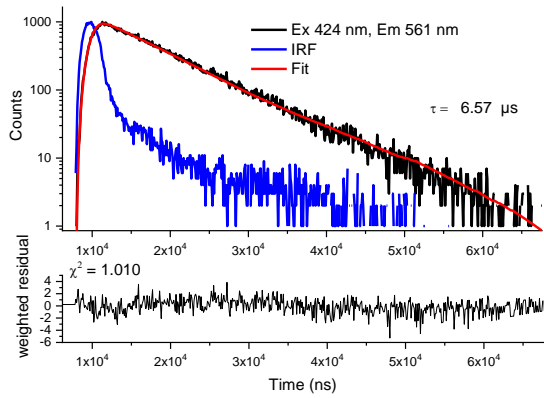


Lifetime measurements of a dilute ($2 \cdot 10^{-6}$ M) dichloromethane solution of PtCl12.

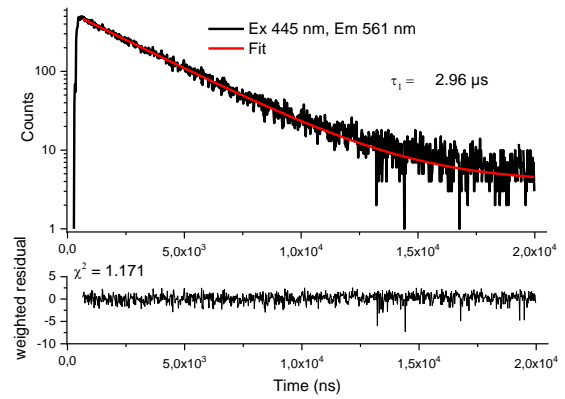
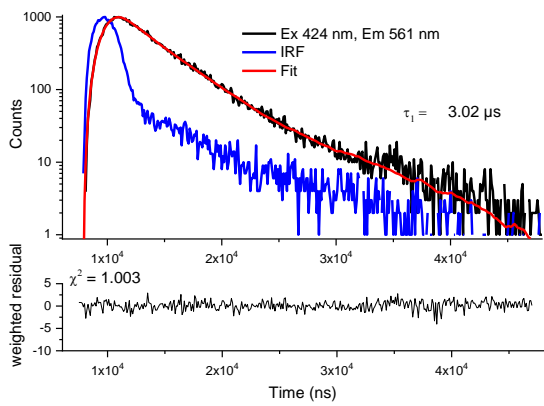


Lifetime measurements of a concentrated ($1 \cdot 10^{-4}$ M) dichloromethane solution of PtCl12.

Lifetimes of PtCl13



Lifetime measurements of a dilute ($2 \cdot 10^{-6}$ M) dichloromethane solution of PtCl13.



Lifetime measurements of a concentrated ($2 \cdot 10^{-4}$ M) dichloromethane solution of PtCl13.

